Distribution Category:
Magnetic Fusion Energy Systems
(UC-424)

ANL/FPP/TM-287

ITER/US/95/IV MAT 10

U.S. CONTRIBUTION 1994 SUMMARY REPORT

TASK T12: COMPATIBILITY AND IRRADIATION TESTING OF VANADIUM ALLOYS

Compiled by
D. L. Smith

CONTRIBUTORS:

ARGONNE NATIONAL LABORATORY

D. E. Busch
H. M. Chung
R. W. Clark
J. Gazda
R. Haglund
A. G. Hins
T.F. Kassner
E. E. Keppler
K. H. Leong
B. Loomis
K. Natesan
L. Neimark
L. Nowicki
D. L. Rink
D. L. Smith
W. K. Soppet
R. V. Strain
H.-C. Tsai

OAK RIDGE NATIONAL LABORATORY

D. J. Alexander
R. B. Dinwiddie
B. Gieseke
G. M. Goodwin
M. L. Grossbeck
A. N. Gubbi
J. L. King
W. D. Porter
W. A. Simpson
C. O. Stevens

PACIFIC NORTHWEST LABORATORY

M. L. Hamilton
R. H. Jones
H. Li

March 1995

Work supported by the Office of Fusion Energy,
U.S. Department of Energy, under
Contract W-31-109-Eng-38

Executive Summary

1994 ITER Summary Report on Task T12: Compatibility and Irradiation Testing of Vanadium Alloys

Vanadium alloys exhibit important advantages as a candidate structural material for fusion first wall/blanket applications. These advantages include fabricability, favorable safety and environmental features, high temperature and high wall load capability, and long lifetime under irradiation. Vanadium alloys with (3-5)% chromium and (3-5)% titanium appear to offer the best combination of properties for first wall/blanket applications. A V-4Cr-4Ti alloy is recommended as the reference composition for the ITER application. This report provides a summary of the R&D conducted during 1994 in support of the ITER Engineering Design Activity. Progress is reported for Vanadium Alloy Production (Section A), Welding (Section B), Physical Properties (Section C), Baseline Mechanical Properties (Section D), Corrosion/Compatibility (Section E), Neutron Irradiation Effects (Section F), Helium Transmutation Effects on Irradiated Alloys (Section G) and the Status of Irradiation Experiments (Section H).

A 500-kg heat of V-4Cr-4Ti (Heat #832665), an alloy identified previously as the most promising vanadium–based candidate alloy for application in fusion reactor structural components, has been produced. The ingot was produced by multiple vacuum–arc melting using screened high–quality raw materials of vanadium, chromium, and titanium. Several long bars ≈64 mm in thickness and ≈200 mm in width were extruded from the ingot, and plates and sheets of various thicknesses ranging from 1.0 to 29.2 mm were fabricated successfully from the extruded bars. The chemical composition of the ingot and the secondary fabrication procedures, specified on the basis of the experience and knowledge gained from fabrication, testing, and microstructural characterization of a laboratory–scale heat, were found to be satisfactory. Charpy–impact tests showed that mechanical properties of the production–scale heat are as good as those of the laboratory–scale heat. This demonstrates a method of reliable fabrication of industrial–scale heats of V–4Cr–4Ti that exhibit excellent properties.

Impact properties were determined on a new 15-kg laboratory heat of V-5Cr-5Ti alloy (Heat #T87), fabricated by the same procedures as those used to produce the 500-kg production-scale heat of V-4Cr-4Ti, to identify optimal annealing procedure of the alloy. Charpy-impact tests were conducted on one-third-size specimens because low-temperature (<0°C) impact properties have been known to be most sensitive to the structure and quality of V-(4-5)Cr-(4-5)Ti alloy class. After final annealing at ≈1000°C for 1 h in high-quality vacuum, the laboratory heat V-5Cr-5Ti exhibited impact properties as excellent as those of the production-scale heat V-4Cr-4Ti; i.e., DBTT < -200°C and absorbed energies of 10-16 J. This demonstrates that when annealed at common optimal condition of 1000°C for 1 h, the V-(4-5)Cr-(4-5)Ti alloy class exhibit excellent impact toughness and a significant tolerance to minor variations in alloying element composition.

Four 15 kg heats with variations in Cr and Ti concentration have been procured in various plate and sheet thicknesses. Measurements of recovery and recrystallization kinetics, precipitation behavior, and Charpy impact properties are in progress to compare properties with the behavior of the primary alloy composition V-4Cr-4Ti. In the fully recrystallized condition, the impact properties of the V-6Cr-3Ti alloy (Heat #T92) are

inferior to those of the 500 kg heat of V-4Cr-4Ti. However, properties comparable to those of the V-4Cr-4Ti can be obtained for the V-6Cr-3Ti when tested in a partially-recrystallized condition.

The weldability and weldment properties of a V-5Cr-5Ti alloy (#BL-63) have been evaluated. Results for the Sigmajig test of the vanadium alloy were similar to the cracking resistance of stainless steels, and indicates hot-cracking is unlikely to be a problem. Subsize Charpy test results for GTA weld metal in the as-welded condition have shown a significant reduction in toughness compared to the base metal. The weld metal toughness properties were restored to approximately that of the base metal after exposure to a PWHT 950°C. The subsize Charpy toughness results for the EB weld metal from this same heat of vanadium alloy has shown significant improvement in properties compared to the GTA weld metal and the base metal. Further testing and analysis will be conducted to more fully characterize the properties of weld metal for each welding process and to develop a basic understanding of the cause of the toughness decrease in the GTA welds.

Laser welding is potentially advantageous because of its flexibility and the reduced amount of material affected by the weld. Lasers do not require a vacuum (as does electron beam welders) and the welds they produce have large depth-to-width ratios. Results of scoping tests using a small, pulsed laser (50 joule, YAG laser) indicated that lasers could produce successful welds in vanadium alloy (V-5%Cr-5%Ti) (#BL-63) sheet (1-mm thick) when the fusion zone was isolated from air. The pulsed laser required an isolating chamber filled with inert gas to produce welds that did not contain cracks and showed only minor hardness increases. Successful bead-on-plate welds have been made to depths of about 4-mm using a 6 kW continuous CO_2 laser with argon purging.

Using a V-5Cr-5Ti alloy (#BL-63), in a fully-annealed condition, a series of physical property measurements have been completed including linear thermal expansion, specific heat, thermal conductivity and the primary elastic constraints. These data agree with previous data on vanadium and vanadium alloys and have been submitted to the ITER Materials Property Data Handbook.

A 500-kg heat of V-4Cr-4Ti (#832665), an alloy identified previously as the primary vanadium–base candidate alloy for application as fusion reactor structural components, has been produced successfully. Impact tests were conducted at –196°C to 150°C on 1/3–size Charpy specimens of the scale–up heat in as–rolled condition and after annealing for 1 h at 950, 1000, and 1050°C in high–quality vacuum. The annealed material remained ductile at all test temperatures; the ductile–brittle transition temperature (DBTT) was lower than –200°C. The upper–shelf energy of the production–scale heat was similar to that of the laboratory–scale (≈30–kg) heat of V–4Cr–4Ti (#BL-47) investigated previously. Effect of annealing temperature was not significant; however, annealing at 1000°C for 1 h not only produces best impact properties but also ensures a sufficient tolerance to effect of temperature inhomogeneity expected when annealing large components. Effect of notch geometry was also investigated on the production heat. When annealed properly (e.g., at 1000°C for 1 h), impact properties were not sensitive to notch geometry (45°–notch, root radius 0.25 mm; and 30°–notch, root radius 0.08 mm).

Up–to–date results on impact properties of unirradiated V, V–Ti, V-Cr-Ti and V–Ti–Si alloys are presented and reviewed in this paper, with an emphasis on the most promising class of alloys, i.e., V–(4–5)Cr–(3–5)Ti containing 400–1000 wppm Si. Database on impact energy and ductile–brittle transition temperature (DBTT) has been established from Charpy impact tests on small laboratory as well as production–scale heats. DBTT is influenced most significantly by Cr contents and, to a lesser extent, by Ti contents of the alloys. When combined contents of Cr and Ti were ≤10 wt.%, V–Cr–Ti alloys exhibit excellent impact properties, i.e., DBTT<–200°C and upper shelf energies of ≈120–140 J/cm^2. Impact properties of the production–scale heat of the U.S. reference alloy V–4Cr–4Ti were as good as those of the laboratory–scale heats. Optimal impact properties of the reference alloy were obtained after annealing the as–rolled products at 1000°C–1050°C for 1–2 h in high–quality vacuum.

Fracture toughness and impact tests were performed on a V-5Cr-5Ti alloy (#BL-63). Specimens annealed at 1125°C for 1 h and furnace cooled in a vacuum of 1.33 x 10^{-5} Pa were brittle at room temperature (RT) and experienced a mixture of intergranular and cleavage fracture. Fracture toughness (J_{1Q}) at RT was 52 kJ/m^2 and the impact fracture energy (IFE) was 6 J. The IFE at -100°C was only 1 J. While specimens exhibited high fracture toughness at 100°C (J_{IQ} is 485 kJ/m^2), fracture was a mixture of dimple and intergranular failure, with intergranular fracture making up 40% of the total fracture surface. This alloy is the only case where extensive intergranular fracture has been observed. The ductile to brittle transition temperature (DBTT) was estimated to be about 20°C. When some specimens were given an additional annealing at 890°C for 24 h, they became very ductile at RT and fractured by microvoid coalescence. The J_{IQ} value increased from 52 kJ/m^2 to ~1100 kJ/m^2. The impact test failed to fracture specimens at RT due to a large amount of plastic deformation.

The current focus of the U.S. program of research on these alloys is on the V-(3-6)Cr-(3-6)Ti alloys containing 400–1000 wppm Si. Experimental results on baseline tensile properties of V–Cr–Ti alloys measured at 23°–700°C are determined with an emphasis on the tensile properties of the U.S. reference alloy V–4Cr–4Ti. The reference alloy was found to exhibit excellent tensile properties up to 700°C.

Thermal creep rates and stress-rupture life of V-4Cr-4Ti (#BL-47) and V-9Cr-5Ti (#BL-43) alloys were determined at 600°C. The impurity composition and microstructural characteristics of creep-tested specimens were analyzed and correlated with the measured creep properties. The results of these tests show that V-4Cr-4Ti, which contains impurity compositions typical of a commercially fabricated vanadium-based alloy, exhibits creep strength substantially superior to that of V-20Ti, HT-9, or Type 316 stainless steel. The V-9Cr-5Ti alloy exhibits creep strength somewhat higher than that of V-4Cr-4Ti.

The results of in-vacuum low cycle fatigue tests are presented for unirradiated V-5Cr-5Ti (#BL 63) tested at temperature (25, 250, and 400°C). In high vacuum, the fatigue results show a trend of increasing cyclic life with increasing temperature between 25 and 400°C. From the limited data available, life at 250°C averages 1.7 times that at 25°C, and at 400°C, life averages 3.2 times that at room temperature. Like the environmental effects at 25°C, the effect of temperature seems to be a function of strain range at each temperature. The results indicate that V-5Cr-5Ti has better resistance to fatigue than 316-SS in the temperature range of 25 to 400°C. A comparison of the fatigue data generated in rough and high vacuums shows that a pronounced environmental

degradation of the fatigue properties exists in this alloy at room temperature. Fatigue life was reduced by as much as 84% for the impure environment. Cyclic stress range data and SEM observations suggest that this reduction is due to a combination of increases in rates of crack initiation and subsequent crack growth. The relative contribution of *each* difference is dependent upon the strain range.

Candidate structural materials are being evaluated for their compatibility, interstitial-element transfer, and corrosion in liquid alkali-metal systems such as lithium and NaK. Type 316 stainless steel and V-5Cr-5Ti (#BL 63) coupon specimens with and without prealuminizing treatment have been exposed to NaK and lithium environments of commercial purity for times up to 3768 h at temperatures between 300 and 400°C. The corrosion rates of the V-alloy in lithium are very low at these temperatures.

Oxidation studies were conducted on V-5Cr-5Ti alloy (#BL 63) specimens at 500°C in an air environment. The oxidation rates calculated from measurements of thermogravimetric testing are 10, 17, and 25 μm/y at 400, 450 and 500°C, respectively. Uniaxial tensile specimens were oxidized for several time periods in air at 500°C and subsequently tensile-tested at 500°C in air. The hardened layer in each of these oxidized specimens was confined to 75 μm after 1000 h exposure at 500°C. The influence of the 1000-h oxidation is to increase the ultimate tensile strength of the alloy by ≈10% while decreasing the tensile rupture strain from 0.23 to 0.14.

Swelling behavior and microstructural evolution of V-Ti, V-Cr-Ti, and V-Ti-Si alloys were investigated after irradiation at 420-600°C up to 114 dpa. The alloys exhibited swelling maxima between 30 and 80 dpa and swelling decreased on irradiation to higher dpa. This is in contrast to the monotonically increasing swelling of binary alloys that contain Fe, Ni, Cr, Mo, W, and Si. Precipitation of dense Ti_5Si_3 promotes good resistance to swelling of the Ti-containing alloys, and it was concluded that Ti of >3 wt.% and 400-1000 wppm Si are necessary to effectively suppress swelling. Swelling was minimal in V-4Cr-4Ti, identified as the most promising alloy based on good mechanical properties and superior resistance to irradiation embrittlement.

Microstructural evolution of V-4Cr-4Ti (#BL-47) was characterized after irradiation in a lithium environment in the Fast Flux Test Facility (FFTF) (a sodium-cooled fast reactor located in Richland, Washington) at 420, 520, and 600°C to 24-34 dpa. The primary feature of microstructural evolution during irradiation at 520 and 600°C was high-density formation of ultrafine Ti_5Si_3 precipitates and short dislocations. For irradiation at 420°C, precipitation of Ti_5Si_3 was negligible, and "black-dot" defects and dislocations were observed in significantly higher densities. In spite of their extremely high densities, neither the "black-dot" defects nor Ti_5Si_3 precipitates are overly detrimental to ductility and toughness of the alloy, yet they very effectively suppress irradiation-induced swelling. Therefore, these features, normally observed in V-base alloys containing Ti and Si, are considered stable. Unstable microstructural modifications that are likely to degrade mechanical properties significantly were not observed, e.g., irradiation-induced formation of fine oxides, carbides, nitrides, or Cr-rich clusters.

Experimental results have been obtained on the effects of neutron irradiation on tensile properties of selected candidate alloys after irradiation at 400°C–600°C in lithium in fast fission reactors to displacement damages of up to ≈120 displacement per atom

(dpa). Effects of irradiation temperature and dose on yield and ultimate tensile strengths and uniform and total elongations are given for tensile test temperatures of 25°C, 420°C, 500°, and 600°C. Results on the higher Cr(9-14%) alloys indicate a saturation of the increase in yield strengths and reduction in total elongation at 20-40 dpa. The uniform elongation of the reference V-4Cr-4Ti (#BL-47) alloy remained above 8% after irradiation to 28-34 dpa at 420, 500 and 600°C.

Up–to–date results on the effects of neutron irradiation on the impact properties and fracture behavior of V, V–Ti, V-Cr-Ti and V–Ti–Si alloys are presented, with an emphasis on the behavior of the U.S. reference alloys V–4Cr–4Ti containing 500–1000 wppm Si. Database on impact energy and ductile–brittle transition temperature (DBTT) has been established from Charpy impact tests of one–third–size specimens irradiated at 420°C–600°C up to ≈50 dpa in lithium environment in fast fission reactors. To supplement the Charpy impact tests fracture behavior was also characterized by quantitative SEM fractography on miniature tensile and disk specimens that were irradiated to similar conditions and fractured at –196°C to 200°C by multiple bending. For similar irradiation conditions irradiation–induced increase in DBTT was influenced most significantly by Cr content, indicating that irradiation–induced clustering of Cr atoms takes place in high–Cr (Cr ≥ 7 wt.%) alloys. When combined contents of Cr and Ti were ≤10 wt.%, effects of neutron irradiation on impact properties and fracture behavior were negligible. For example, from the Charpy–impact and multiple–bend tests there was no indication of irradiation–induced embrittlement for V–5Ti, V–3Ti–1Si and the U.S. reference alloy V–4Cr–4Ti after irradiation to ≈34 dpa at 420°C to 600°C, and only ductile fracture was observed for temperatures as low as –196°C.

Combined effects of dynamically charged helium and neutron damage on density change, void distribution, and microstructural evolution of V–4Cr–4Ti alloy (#BL-47) have been determined after irradiation to 18–31 dpa at 425–600°C in the DHCE, and the results compared with those from a non–DHCE in which helium generation was negligible. For specimens irradiated to ≈18–31 dpa at 500–600°C with a helium generation rate of 0.4–4.2 appm He/dpa, only a few helium bubbles were observed at the interface of grain matrices and some of the Ti(O,N,C) precipitates, and no microvoids or helium bubbles were observed either in grain matrices or near grain boundaries. Under these conditions, dynamically produced helium atoms seem to be trapped in the grain matrix without significant bubble nucleation or growth, and in accordance with this, density changes from DHCE and non–DHCE (negligible helium generation) were similar for comparable fluence and irradiation temperature. Only for specimens irradiated to ≈31 dpa at 425°C, when helium was generated at a rate of 0.4–0.8 appm helium/dpa, were diffuse helium bubbles observed in limited regions of grain matrices and near ≈15% of the grain boundaries in densities significantly lower than those in the extensive coalescence of helium bubbles typical of other alloys irradiated in tritium–trick experiments. Density changes of specimens irradiated at 425°C in the DHCE were significantly higher than those from non–DHCE irradiation. Microstructural evolution in V–4Cr–4Ti was similar for DHCE and non–DHCE except for helium bubble number density and distribution. As in non–DHCE, the irradiation–induced precipitation of ultrafine Ti_5Si_3 was observed for DHCE at >500°C but not at 425°C.

In the present Dynamic Helium Charging Experiment (DHCE), helium was produced uniformly in the specimen at linear rates of ≈0.4 to 4.2 appm helium/dpa by the decay of tritium during irradiation to 18–31 dpa at 425–600°C in the Li-filled DHCE capsules in the

Fast Flux Test Facility. The results of postirradiation tests of tensile properties of V-4Cr-4Ti (#BL-47) are presented. Effects of helium on tensile strength and ductility were insignificant after irradiation and testing at >420°C. Contrary to initial expectation, room–temperature ductilities of DHCE specimens were higher than those of non–DHCE specimens (in which there was negligible helium generation), whereas strengths were lower, indicating that different types of hardening centers are produced during DHCE and non–DHCE irradiation. In strong contrast to tritium–trick experiments in which dense coalescence of helium bubbles is produced on grain boundaries in the absence of displacement damage, no intergranular fracture was observed in any tensile specimens irradiated in the DHCE.

In the DHCE, helium was produced uniformly in tensile and TEM specimens at linear rates ranging from ≈0.4 to 4.2 appm helium/dpa by the decay of tritium during irradiation to 18–31 dpa at 425–600°C in Li-filled DHCE capsules in the Fast Flux Test Facility. Ductile–brittle transition behavior of V–4Cr–4Ti (#BL-47) was determined from multiple–bending tests (at –196°C to 50°C) and quantitative SEM fractography on TEM disks (0.3–mm thick) and broken tensile specimens (1.0–mm thick). No brittle behavior was observed at temperatures >–150°C, and predominantly brittle–cleavage fracture morphologies were observed only at –196°C in some specimens irradiated to 31 dpa at 425°C during DHCE. Ductile–brittle transition temperatures (DBTTs) were –200°C to –175°C for both types of specimens. No intergranular fracture was observed in the bend–tested specimens irradiated in the DHCE.

To obtain early irradiation performance data on the new 500-kg production heat of the V-4Cr-4Ti (#832665) material, an experiment, X530, was expeditiously designed and assembled and irradiated in EBR-II at 375-400°C. Charpy, compact tension, tensile and TEM specimens with different thermal mechanical treatments (TMTs), were enclosed in two capsules and irradiated in the last run of EBR-II, Run 170, from August 9 through September 27. For comparison, specimens from some of the previous heats were also included in the test. The accrued exposure was 35 effective full power days, yielding a peak damage of ≈4 dpa in the specimens. The irradiation is now complete and the vehicle is awaiting to be discharged from EBR-II for postirradiation disassembly.

Seven DHCE capsules containing vanadium-alloy specimens were irradiated in the MOTA-2B vehicle in FFTF to ≈20-29 dpa. In this and the previous reporting periods, equipment and procedures were developed at Argonne National Laboratory-East to disassemble these capsules. All seven capsules have been disassembled. Effluence of tritium into the cell exhaust was <2% of the total inventory. No contamination incidents occurred during the DHCE disassembly work. Initial testing of the retrieved specimens has been conducted.

1994 ITER R&D Summary Reports
Task 12

12A VANADIUM ALLOY PROCUREMENT

12A1: Production Heat of V-4Cr-4Ti

FABRICATION OF PRODUCTION-SCALE HEAT OF V-4Cr-4Ti 11
by H. M. Chung, H.-C. Tsai and D. L. Smith
(Argonne National Laboratory)

12A2: Laboratory-Scale Heats of Vanadium Alloys

FABRICATION AND PROPERTIES OF LABORATORY-SCALE HEAT OF V-5Cr-5Ti 17
by H. M. Chung, L. Nowicki, and D. L. Smith
(Argonne National Laboratory)

12A3: FABRICATION AND PROPERTIES OF COMPOSITIONAL VARIANTS OF VANADIUM ALLOYS 23
by M. L. Grossbeck, D. J. Alexander, and A.N. Gubbi
(Oak Ridge National Laboratory)

12B WELDING OF VANADIUM ALLOYS

12B1: GTA and EB Weldments

WELDING DEVELOPMENT FOR V-Cr-Ti ALLOYS. 31
by J. L. King, G. M. Goodwin, M. L. Grossbeck, and
D. J. Alexander (Oak Ridge National Laboratory)

12B2: Laser Welds

DEVELOPMENT OF LASER WELDING TECHNIQUES FOR VANADIUM ALLOYS 37
by R. Strain, K. H. Leong, E . E. Keppler and D. L. Smith
(Argonne National Laboratory)

12C PHYSICAL PROPERTIES OF VANADIUM ALLOYS

12C1: DETERMINATION OF THERMOPHYSICAL PROPERTIES OF V-5Cr-5Ti 41
by W. D. Porter, R. B. Dinwiddie, W. A. Simpson, and
M. L. Grossbeck (Oak Ridge National Laboratory)

12D BASELINE MECHANICAL PROPERTIES

12D1: IMPACT PROPERTIES OF PRODUCTION HEAT OF V-4Cr-4Ti 53
by H. M. Chung, L. Nowicki and D. L. Smith (Argonne National Laboratory)

12D2: BASELINE IMPACT PROPERTIES OF VANADIUM ALLOYS . . 61
by H. M. Chung, B. A. Loomis and D. L. Smith (Argonne National Laboratory)

12D3: FRACTURE PROPERTIES OF V-5Cr-5Ti ALLOY 69
by H. Li, M. L. Hamilton and R. H. Jones (Pacific Northwest Laboratory)

12D4: BASELINE TENSILE PROPERTIES OF V-Cr-Ti ALLOYS 79
by B. A. Loomis, H. M. Chung, and D. L. Smith (Argonne National Laboratory)

12D5: THERMAL CREEP PROPERTIES OF VANADIUM-BASE ALLOYS. 87
by H. M. Chung, B. A. Loomis, and D. L. Smith (Argonne National Laboratory)

12D6: FATIGUE BEHAVIOR OF UNIRRADIATED V-5Cr-5Ti. 95
by B. Gieseke, C. O. Stevens, and M. L. Grossbeck (Oak Ridge National Laboratory)

12E CORROSION/COMPATIBILITY OF VANADIUM ALLOYS

12E1: Compatibility in Lithium

COMPATIBILITY OF STRUCTURAL MATERIALS IN LIQUID ALKALI METALS. 107
by K. Natesan, D. L. Rink, R. Haglund, and R. W. Clark (Argonne National Laboratory)

12E2: Oxidation in Air/Oxygenf

EFFECT OF OXIDATION ON TENSILE BEHAVIOR OF V-5Cr-5Ti ALLOY 119
by K. Natesan and W. K. Soppet (Argonne National Laboratory)

12F NEUTRON IRRADIATION EFFECTS ON PROPERTIES OF VANADIUM ALLOYS

12F1: Swelling

EFFECT OF NEUTRON IRRADIATION ON SWELLING OF VANADIUM-BASE ALLOYS 123
by H. M. Chung, B. A. Loomis, and D. L. Smith (Argonne National Laboratory)

12F2: Microstructures

MICROSTRUCTURAL EVOLUTION OF V-4Cr-4Ti DURING NEUTRON IRRADIATION. 131
by H. M. Chung, J. Gazda and B. A. Loomis
(Argonne National Laboratory)

12F3: Tensile Properties

EFFECTS OF NEUTRON IRRADIATION ON TENSILE PROPERTIES OF VANADIUM-BASE ALLOYS. 139
by B. A. Loomis, H. M. Chung, and D. L. Smith
(Argonne National Laboratory)

12F4: Fracture Properties

EFFECTS OF NEUTRON IRRADIATION ON THE IMPACT PROPERTIES AND FRACTURE BEHAVIOR OF VANADIUM-BASE ALLOYS. 147
by H. M. Chung, B. A. Loomis, and D. L. Smith
(Argonne National Laboratory)

12G HELIUM EFFECTS ON NEUTRON IRRADIATED V-ALLOYS

12G1:Swelling

EFFECTS OF DYNAMICALLY CHARGED HELIUM ON SWELLING AND MICROSTRUCTURE OF VANADIUM-BASE ALLOYS 157
by H. M. Chung, L. Nowicki, J. Gazda, and D. L. Smith
(Argonne National Laboratory)

12G2: Tensile Properties

EFFECTS OF DYNAMICALLY CHARGED HELIUM ON TENSILE PROPERTIES OF V-4Cr-4Ti. 167
by H. M. Chung, B. A. Loomis, L. Nowicki, and D. L. Smith
(Argonne National Laboratory)

12G3: Fracture Properties

FRACTURE PROPERTIES OF V-4Cr-4Ti IRRADIATED IN THE DYNAMIC HELIUM CHARGING EXPERIMENT 175
by H. M. Chung, L. J. Nowicki, D. E. Busch and D. L. Smith (Argonne National Laboratory)

12H IRRADIATION EXPERIMENTS

12H1: Status and Schedule

VANADIUM ALLOY IRRADIATION EXPERIMENT X530 IN EBR-II 183
by H. Tsai, R. V. Strain, A. G. Hins, H. M. Chung, L. J. Nowicki, and D. L. Smith (Argonne National Laboratory)

12H2: Disassembly and PIE Preparation

STATUS OF THE DYNAMIC HELIUM CHARGING EXPERIMENT 191
by H. Tsai, R. V. Strain, H. M. Chung, and D. L. Smith (Argonne National Laboratory)

Subtask 12A1: FABRICATION OF PRODUCTION–SCALE HEAT OF V–4Cr–4Ti, H. M. Chung, H.–C. Tsai, and D. L. Smith (Argonne National Laboratory)

OBJECTIVE

On the basis of excellent properties that were determined for a laboratory–scale heat, V–4Cr–4Ti has been identified previously as the most promising vanadium–based candidate alloy for application in fusion reactor structural components. The objective of this work is to produce a large–scale (500–kg) ingot of the alloy and fabricate various plates and sheets from the ingot, thereby demonstrating a reliable method of fabricating an industrial–scale heat of V–4Cr–4Ti that exhibits excellent properties.

SUMMARY

A 500-kg heat of V-4Cr-4Ti, an alloy identified previously as the most promising vanadium–based candidate alloy for application in fusion reactor structural components, has been produced. The ingot was produced by multiple vacuum–arc melting using screened high–quality raw materials of vanadium, chrome, and titanium. Several long bars ≈64 mm in thickness and ≈200 mm in width were extruded from the ingot, and plates and sheets of various thicknesses ranging from 1.0 to 29.2 mm were fabricated successfully from the extruded bars. The chemical composition of the ingot and the secondary fabrication procedures, specified on the basis of the experience and knowledge gained from fabrication, testing, and microstructural characterization of a laboratory–scale heat, were found to be satisfactory. Charpy–impact tests showed that mechanical properties of the production–scale heat are as good as those of the laboratory–scale heat. This demonstrates a method of reliable fabrication of industrial–scale heats of V–4Cr–4Ti that exhibit excellent properties.

INTRODUCTION

Vanadium-base alloys have significant advantages over other candidate alloys (such as austenitic and ferritic steels) for use as structural materials in fusion devices. In the past, extensive investigations have been conducted on the swelling behavior, tensile properties, impact toughness, and microstructural evolution of V, V-Ti, V-Cr, V-Cr-Ti, and V-Ti-Si alloys after irradiation by fast neutrons at 420°C–600°C. These investigations revealed that V-Cr-Ti alloys containing ≈4 wt.% Cr, ≈4 wt.% Ti, 400-1000 wt. ppm Si, and <1000 wt. ppm O+N+C were most desirable because they exhibit superior physical and mechanical properties.[1–6] These results were obtained, however, on small (<30 kg) laboratory–scale heats, including a small heat (ANL ID BL–47) of V-4Cr-4Ti that exhibited excellent resistance to irradiation–induced embrittlement, swelling, and helium embrittlement.[7–9] In the meantime, a relatively larger (≈100 kg) heat of V–5Cr–5Ti (ANL ID BL–63) and a small (≈15 kg) heat of V–5Cr–3Ti (ANL ID BL–54), fabricated subsequently under procedures significantly different from those of the small laboratory heat of V–4Cr–4Ti, were found to exhibit less–desirable mechanical properties despite the small differences in alloying element contents.[10] Based on these backgrounds, a joint campaign was initiated between Argonne National Laboratory and Teledyne Wah Chang (Albany, Oregon) to identify an optimal fabrication procedure of the V–(4–5)Cr–(3–5)Ti alloys and to demonstrate a reliable method of producing an industrial–scale heat of V–4Cr–4Ti that exhibits the excellent properties reported for the laboratopry heat (ANL ID BL–47) in previous investigations.

SPECIFICATIONS AND PROCEDURES

The production campaign consisted of a large–scale (500–kg) melting of a V–4Cr–

4Ti ingot; extruding the ingot into rectangular bars; and subsequent rolling and heat–treatments to manufacture final products in the form of plates and sheets of various thickness; analyses of chemical composition and phase structure; and Charpy–impact testing to determine the ductile–brittle transition temperatutre (DBTT) of the final products. The latter information is described in a separate article in this report.[11]

1. Specification of Chemical Composition

The specification of chemical composition was carefully evaluated to reflect the valuable experience and knowledge gained from fabrication, testing, and microstructural examination of the laboratory–scale heats of V–Ti and V–Cr–Ti alloys, in particular, V–4Cr–4Ti (BL–47), V–5Cr–3Ti (BL–54), and the relatively larger heat of V–5Cr–5Ti (BL–63).[10] Particular attention was given to control of the following impurities: Nb and Mo (minimize to ensure low neutron activation); Cu (minimize to suppress Cu–rich vanadium oxycarbochlorides precipitation);[10] Si (optimize to 400–1000 wppm to suppress swelling);[5] O, N, and C (limit the combined concentration to <1000 wppm); S, P (minimize to avoid segregation to grain boundary and precipitation);[10] and Cl, Ca, K, Mg, Na, and B (minimize to avoid formation of vanadium–based precipitates oxycarbochlorides, vanadates, and borides).[10] The final specification of ingot chemistry is listed in the following:

1.1 Ingot Chemical Specifications

NOTE: Use only low–chlorine (< 5 wppm) double– or triple–melted titanium feedstock in making the ingot.

Cr	4±0.5 wt.%	Ti	4±0.5 wt.%
Si	400 - 1000 wppm	O	< 400 wppm
N	< 200 wppm	C	< 200 wppm
Al	< 200 wppm	Fe	< 300 wppm
Cu	< 50 wppm	Mo	< 500 wppm
Nb	< 50 wppm	Cl	< 2 wppm
P	< 30 wppm	S	< 30 wppm

1.2 Alloying Component Inhomogeneity

Local inhomogeneity of Cr and Ti shall not exceed ±0.3 wt.%.

2. Screening of Raw Materials

The source of the last group of impurities, except for Ca and B (i.e., Cl, K, Mg, and Na), is known to be primarily low–quality Ti. Ti is normally produced by the Kroll process, in which $TiCl_2$ vapor is reduced by molten Na or Mg. Therefore, only double– or triple–melted Ti was used in ingot melting. This is in contrast to the use of sponge titanium which was used to melt the ingots of the V–5Cr–5Ti (BL–63) and V–5Cr–3Ti (BL–54), the two heats reported to exhibit inferior mechanical properties.[10]

Chemical composition of the raw vanadium (ingot prepared by electron–beam melting) designated for melting of the alloy ingot was also checked (Table 1). At the same time, a piece of the raw vanadium was set aside and machined into 1/3–size Charpy–impact specimens. Normally, unalloyed vanadium of good quality (e.g., iodide[12] or electrorefined[13] vanadium containing low O, N, C, Ca, and B) should exhibit a DBTT lower than –200°C. However, unusually higher DBTTs have been observed for unalloyed vanadium occasionally in the past, in particular for some of the vanadium produced by the

calcium–reduction process.[13,14] For example, specimens from one of the unalloyed vanadium (ANL ID BL–51) that were impact–tested in a previous investigation exhibited a DBTT as high as –150°C.[2] From a subsequent microstructural characterization by analytical electron microscopy, the unusually high DBTT of Heat BL–51 has been attributed to dense coherent precipitation of very fine (<60 nm diameter) calcium vanadates.[10] In view of these observations, impact tests were conducted on the 1/3–size Charpy specimens of the raw vanadium, and it was verified that the DBTT of the raw material is indeed lower than –196°C.

3. Specification of Secondary Fabrication and Conversion

The procedures for extrusion, secondary fabrication, and conversion to plates and sheets were specified as follows to closely reproduce the procedures used in the fabrication of the excellent laboratory heat of V–4Cr–4Ti (i.e., ANL ID BL–47):

1. Extrude ingot in stainless steel jacket at 1150°C into ≈65–mm–thick slab.
2. Subsequent warm rolling at 400°C to desired intermediate dimensions.
3. No more than 15% thickness reduction per each rolling step.
4. No more than 50% thickness reduction accumulated between annealing.
5. Anneal at 1050°C–1070°C for 2 h in high–vacuum furnace between rolling.
6. Anneal at 1050°C for 2 h in high–vacuum furnace only for selected final products thicker than ≈3.8 mm. Other products deliver in as–rolled condition.

FINAL PRODUCTS

The ≈500-kg ingot was produced by multiple vacuum–arc melting for constituent homogeneity. Ingots of the smaller laboratory heats (including Heat BL–47 and a new 15–kg heat of V–5Cr–5Ti, #T87) were also produced by vacuum–arc melting. The results of chemical analyses, averaged over three measurements on 63–mm–thick extruded bars, are given in Table 1. For comparison, the chemical composition of the excellent laboratory heat of V–4Cr–4Ti (ANL ID BL–47) is also given in the table. The machined ingot was encased in a vacuum–pumped stainless jacket, and extruded at 1150°C into bar with a nominal thickness of 63.5 mm (2.5 inch). Three pieces of the ≈63.5–mm–thick extruded bars are shown in Fig. 1.

Table 1. Chemical composition (impurities in wppm) of the industrial–scale (500 kg) heat of V–4Cr–4Ti[a] and the V raw stock used to melt the ingot.

Heat ID	Material	Spot	Cr, wt.%	Ti, wt.%	Al	Fe	Mo	Nb	Cu	Si	O	N	C	S	P	Ca	Cl	B
820630	Raw V	–	<100	<50	100	230	410	<50	<50	800	200	62	75	10	<30	–	<2	<5
832665	V–4Cr–4Ti	1	3.75	4.16	180	180	330	<50	<50	790	280	82	64	<10	<30	<10	<2	7
		2	3.72	3.79	190	220	350	50	<50	840	360	80	80	<10	<30	<10	<2	<5
		3	3.83	3.80	105	270	260	<50	<50	720	290	93	94	<10	<30	<10	<2	<5

[a]Determined from 3 different positions in the 64–mm–thick and 200–mm–wide extruded bar.

Following extrusion, ≈72 kg (or 17%) of the extruded bar (≈430 kg recovered) has been used to produce plates and sheets of nominal thicknesses of 29.2, 12.7, 6.35, 3.81, and 1.02 mm. Plates with a thickness of 3.81 mm and greater were produced by multiple-pass cross–rolling at ≈400°C; the thinner, 1.02-mm-thick sheets were produced by further rolling at room temperature. The thickness reduction was limited to <15% per pass. Annealing treatments of the plates were conducted between rolling at 1050°C-1070°C for 2 h in a vacuum better than ≈1.33 x 10^{-3} Pa.

Most of the plates and sheets were received in as–rolled condition, except for a limited amount of the 3.81–mm–thick plate which was final–annealed at a nominal temperature of 1050°C for 2 h. This annealed plate was fully recrystallized.

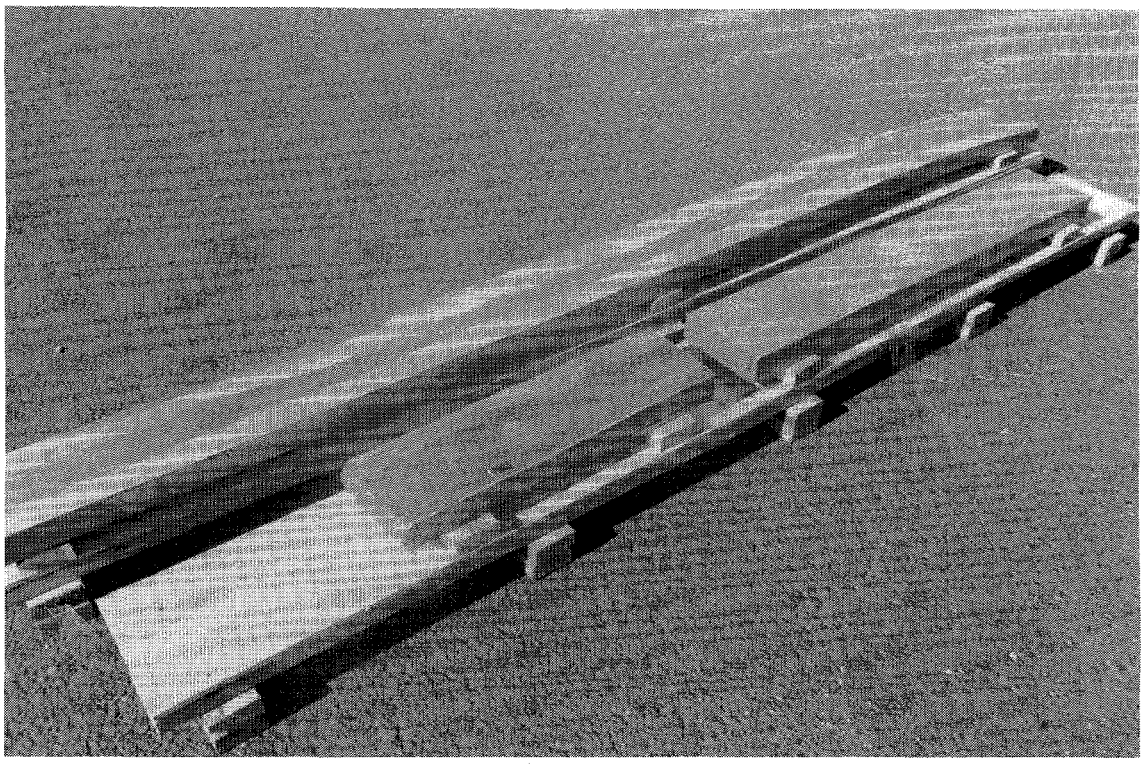

Fig. 1. Three pieces of ≈63–mm–thick bars extruded from 500–kg industrial–scale heats (ID 832665) of V–4Cr–4Ti.

The chemical composition of the heat, similar to that of the excellent laboratory heat (BL–47), conforms with the specification. As expected, results of impact tests of 1/3–sizes Charpy specimens machined from the 3.81–mm plate showed that mechanical properties of the large–scale heat are as good as those of the laboratory–scale heat.[11]

CONCLUSION

A production–scale (500-kg) heat of V-4Cr-4Ti, an alloy identified previously as the reference vanadium–based candidate alloy for application in fusion reactor structural components, has been produced successfully by multiple vacuum–arc melting of screened high–quality raw materials of vanadium and titanium. Several ≈63.5–mm–thick bars were extruded from the ingot, and plates and sheets of various thicknesses ranging from 1.0 to 12.7 mm were fabricated successfully from the extruded bar. The chemical composition of the ingot and the secondary fabrication procedures, specified on the basis of the experience and knowledge gained from fabrication, testing, and microstructural examination of a laboratory–scale heat, were found to be satisfactory. Results of Charpy–impact tests showed that mechanical properties of the large–scale heat are as good as those of the laboratory–scale heat. This demonstrates a method of reliable fabrication of industrial–scale heats of V–4Cr–4Ti of excellent properties.

REFERENCES

[1] B. A. Loomis, L. Nowicki, and D. L. Smith, "Effect of Neutron Irradiation on Tensile Properties of V–Cr–Ti Alloys," in Fusion Reactor Materials, Semiannual. Prog. Report, DOE/ER-0313/15, Oak Ridge National Laboratory, Oak Ridge, TN (1994), pp. 219–222.

[2] B. A. Loomis, H. M. Chung, L. Nowicki, and D. L. Smith, "Effects of Neutron Irradiation and Hydrogen on Ductile-Brittle Transition Temperatures of V–Cr–Ti Alloys," ibid., pp. 253–257.

[3] H. M. Chung, B. A. Loomis, L. Nowicki, J. Gazda, and D. L. Smith, "Irradiation-Induced Density Change and Microstructural Evolution of Vanadium-Base Alloys," ibid., pp. 223–231.

[4] H. M. Chung, B. A. Loomis, and D. L. Smith, "Thermal Creep Behavior of V–5Cr–5Ti and V–10Cr–5Ti Alloys," in Fusion Reactor Materials, Semiannual. Prog. Report, DOE/ER-0313/14, Oak Ridge National Laboratory, Oak Ridge, TN (1993), pp. 309-317.

[5] H. M. Chung, B. A. Loomis, and D. L. Smith, in Effects of Radiation on Materials, ASTM-STP 1175, A. S. Kumar, D. S. Gelles, R. K. Nanstad, and T. A. Little, eds., American Society for Testing and Materials, Philadelphia, 1993, pp. 1185–1200.

[6] H. M. Chung, B. A. Loomis, and D. L. Smith, "Properties of V-4Cr-4Ti for Application as Fusion Reactor Structural Components," Proc. 3rd Intl. Symp. on Fusion Nuclear Technology, June 27-July 1, 1994, Los Angeles, CA, in press.

[7] H. M. Chung, B. A. Loomis, L. Nowicki, and D. L. Smith, "Effect of Dynamically Charged Helium on Tensile Properties of V–4Cr–4Ti," in this report.

[8] H. M. Chung, L. J. Nowicki, D. E. Busch, and D. L. Smith, "Fracture Properties of V–4Cr–4Ti Irradiated in the Dynamic Helium Charging Experiment," in this report.

[9] H. M. Chung, L. Nowicki, J. Gazda, and D. L. Smith, "Effects of Dynamically Charged Helium on Swelling and Microstructure of Vanadium-Base Alloys Irradiated in the," in this report.

[10] H. M. Chung, J. Gazda, L. Nowicki, J. E. Sanecki, and D. L. Smith, "Effects of Fabrication Variables on Impact Properties and Microstructure of V–Cr–Ti Alloys," in Fusion Reactor Materials, Semiannual. Prog. Report, DOE/ER-0313/15, Oak Ridge National Laboratory, Oak Ridge, TN (1994), pp. 207–218.

[11] H. M. Chung, L. Nowicki, J. Gazda, and D. L. Smith, "Impact Properties of Production Heat of V–4Cr–4Ti," in this report.

[12] R. W. Thompson and O. N. Carlson, J. Less–Common Met., 9 (1965), 354.

[13] D. R. Mathews, G. H. Keith, and E. A. Loria, Bureau of Mines Report 6637 (1965), U.S. Dept. of Interior, Washington, DC.

[14] W. R. Clough and A. S. Pavlovic, Trans. ASM 52 (1960) 948.

Subtask 12A2: FABRICATION AND PROPERTIES OF LABORATORY-SCALE HEAT OF V-5Cr-5Ti, H. M. Chung, L. Nowicki, and D. L. Smith (Argonne National Laboratory)

OBJECTIVE

The immediate objective of this work is to fabricate a new laboratory–scale heat of V–5Cr–5Ti and identify optimal annealing procedure that produces the highest impact toughness in the alloy. By comparing the result with the optimal annealing procedure identified for the production– and laboratory–scale heats of V–4Cr–4Ti, the eventual objective of the study is to demonstrate that excellent and reliable mechanical properties of V–(4–5)Cr–(4–5)Ti alloy class can be produced through a common annealing procedure.

SUMMARY

Impact properties were determined on a new 15-kg laboratory heat of V-5Cr-5Ti, fabricated by the same procedures as those used to produce the 500–kg production–scale heat of V–4Cr–4Ti, to identify optimal annealing procedure of the alloy. Charpy–impact tests were conducted on one–third–size specimens because low–temperature (<0°C) impact properties have been known to be most sensitive to the structure and quality of V–(4–5)Cr–(4–5)Ti alloy class. After final annealing at ≈1000°C for 1 h in high–quality vacuum, the laboratory heat V–5Cr–5Ti exhibited impact properties as excellent as those of the production–scale heat V–4Cr–4Ti; i.e., DBTT < –200°C and absorbed energies of 10–16 J. This demonstrates that when annealed at common optimal condition of 1000°C for 1 h, the V–(4–5)Cr–(4–5)Ti alloy class exhibit excellent impact toughness and a sufficient tolerance to minor variations in alloying element composition.

INTRODUCTION

V–(4–5)Cr–(4–5)Ti has been identified previously as the most promising vanadium–base candidate alloys for application in fusion reactor structural components.[1,2] Subsequently, some laboratory heats of V–5Cr–3Ti (ANL ID Heat BL–54) and V–5Cr–5Ti (BL–63), fabricated by procedures different from that of the excellent laboratory heat of V–4Cr–4Ti (Heat BL–47), were found to exhibit impact properties significantly inferior to those of the V–4Cr–4Ti heat in spite of the small differences in alloying element composition.[3] Because of this, two opposing but related concerns were raised: One was on tolerance of the most promising V–(4–5)Cr–(4–5)Ti alloy class to inevitable minor variations in Cr and Ti contents. The other was on proper fabrication procedures, i.e., the effects of minor impurities, use of low–quality raw materials, and incorrect rolling and annealing procedures that may upset reliable fabrication of the alloy class.[3] Subsequently, a new heat of 500–kg V–4Cr–4Ti was produced successfully by a procedure essentially same as that used to produce the excellent laboratory heat of V–4Cr–4Ti (Heat BL–47).[4] Charpy–impact testing showed that the new production–scale heat of V–4Cr–4Ti (Heat #832665) exhibited properties as excellent as those of the laboratory heat BL–47.[5] Parallel to this effort, it was decided to demonstrate fabrication of a new laboratory–scale heat of V–5Cr–5Ti that exhibits mechanical properties as good as those of V–4Cr–4Ti. This paper describes a brief outline of the fabrication procedure of a new 15–kg heat of V–5Cr–5Ti and presents a comprehensive result of impact tests of the

heat. By comparing the result with the optimal annealing procedure identified for V–4Cr–4Ti in a separate investigation,[5] the real objective of the study was to demonstrate that excellent and reliable mechanical properties of V–(4–5)Cr–(4–5)Ti alloy class can be produced through a common annealing procedure.

EXPERIMENTAL PROCEDURES

The fabrication procedure of the 15–kg heat of V–5Cr–5Ti was essentially the same as that of the 500–kg production–scale heat V–4Cr–4Ti,[4] except that the former was produced in laboratory in a small scale and the latter was produced in the production facility in Teledyne Wah Chang, Albany, Oregon. Therefore, details of specification and fabrication procedure are referred to Ref. 4. Same raw materials were used to melt the ingots of both heats by multiple vacuum–arc melting. Extruding the ingot at 1150°C and subsequent rolling (at 400°C) and heat–treating between rolling (at 1050°C–1070°C), to manufacture final products in the form of plates and sheets of various thickness, were also similar.

Chemical compositions of the alloy ingot as well as raw vanadium are given in Table 1. The raw vanadium feedstock was produced by electron–beam melting. Out of the 3.8–mm–thick alloy plates, Charpy–impact specimens were machined, cleaned, and annealed at high temperatures before testing. Typical test specimens were annealed at 1000°C, 1050°C, or 1100°C for 1 h in high–quality vacuum (in ion–pumped system). Orientation of Charpy–impact specimens was such that crack propagation was perpendicular to rolling direction and parallel to thickness direction of the 3.8–mm–thick plates. The one–third–size (3.33 x 3.33 x 25.4 mm) specimens were 30°– or 45°–notched, with root radius of 0.08 mm and 0.25 mm, respectively. Notch depth was kept constant at 0.61 mm.

Table 1. Chemical composition (impurities in wppm)[a] of the laboratory (15 kg) heat of V–5Cr–5Ti and the V raw stock used to melt the ingot.

Heat	Material	Spot	Cr	Ti	Al	Fe	Mo	Nb	Cu	Si	O	N	C	H	S	P	Ca	Cl	B
820630	raw V	–	<100	<50	100	230	410	<50	<50	780	200	62	75	3	10	<30	–	<2	<5
T87	V–5Cr–5Ti	top	4.96 wt.%	5.10 wt.%	160	150	520	<100	71	570	380	86	111	7	<20	<30	<17	<5	<5
		bottom	4.92 wt.%	5.03 wt.%	160	170	510	<100	63	520	380	93	107	27	<20	<30	<55	<5	<5

[a]Determined from ingot

RESULTS AND DISCUSSION

Charpy impact energies were measured between –196°C and 200°C by instrumented drop–weight machine. Effects of annealing temperature on impact properties of the 45°– and 30°–notched specimens are shown in Figs. 1 and 2, respectively. Some specimens in Fig. 1 were tested in as–rolled condition, i.e., without any annealing (at 1000°C–1100°C) or the customary degassing treatment (400°C for 1 h). For impact temperatures <25°C, these unannealed specimens were characterized by a tendency to exhibit laminated cracking parallel to rolling direction and perpendicular to thickness direction of the 3.8–mm–thick plate (from which the Charpy specimens were machined). That is, the direction of the laminated cracking was perpendicular to the normal crack propagation of annealed specimens. As a result, relatively low absorbed energy was registered. However, the fracture surface of the laminated cracking was found to be ductile when examined in SEM. Similar mode of laminated cracking was observed also in unannealed specimens from the 500–kg heat V–4Cr–4Ti.[5] Although mechanism of the peculiar laminated cracking is not well understood at this time, these observations underscore the importance of proper annealing of the V–(4–5)Cr–(4–5)Ti alloy class.

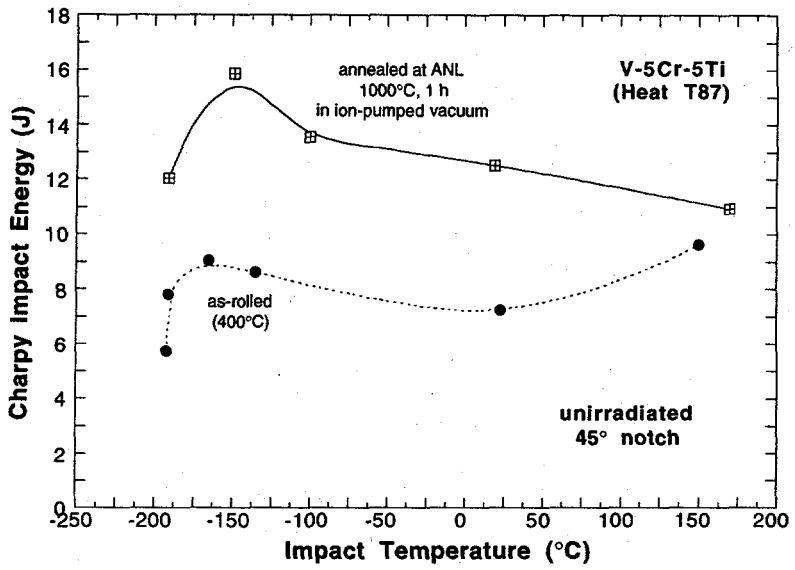

Fig. 1. Impact properties of 45°–notch Charpy specimens in as–rolled condition and after annealing at 1000°C for 1 h.

Effects of annealing at 1000°C, 1050°C, and 1100°C (for 1 h in ion–pumped vacuum) on impact properties of 30°–notched specimens are shown in Fig. 2. Also shown in the figure are data obtained on similar specimens annealed in factory in oil–diffusion–pumped vacuum at a nominal temperature of 1050°C for 2 h. Absorbed energy measured at –196°C and ductile–brittle–transition temperature (DBTT) of the heat were markedly sensitive to annealing temperature. This is shown in Figs. 3 and 4, respectively. Obviously, the results given in Figs. 1–4 show that the optimal annealing condition is to anneal at 1000°C for 1 h in high–quality (ion–pumped system) vacuum. Evidently, annealing at >1050°C is conducive to inferior impact properties.

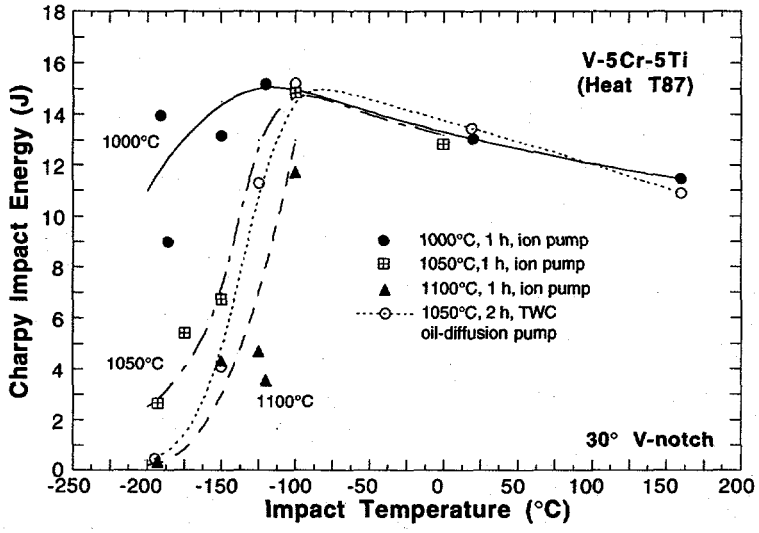

Fig. 2. Effect of annealing on impact properties of 30°–notch Charpy specimens.

In Figs. 3 and 4, similar effects of annealing temperature on the absorbed energy (measured at –196°C) and DBTT of the 500–kg heat of V–4Cr–4Ti are also shown for comparison. In the figures, it is important to note that sensitivity to annealing of impact properties of the two alloy heats is quite different. That is, the V–5Cr–5Ti laboratory heat is significantly more sensitive than the V–4Cr–4Ti production–scale heat. Although not shown in the figures, it was found that the laboratory Heat BL–47 (V–4Cr–4Ti) is least sensitive and that the laboratory Heat BL–63 (V–5Cr–5Ti) is most sensitive to annealing condition.[3] At present, the root cause of the heat–to–heat variation (in sensitivity to annealing condition) is not well understood. Minor impurities, Cr content, or both could be contributing factors.

In Fig. 5, effects of notch geometry on impact properties of the laboratory heat, annealed at the optimal condition of 1000°C for 1 h, are shown. The results in the figure demonstrate that, when annealed properly, impact properties of V–5Cr–5Ti is not sensitive to notch geometry.

When annealed at the optimal condition, impact properties of the 15–kg laboratory heat of V–5Cr–5Ti and the 500–kg production–scale heat of V–4Cr–4Ti were essentially the same (in unirradiated state).[5] This also means that, as long as a component is annealed properly, a sufficient tolerance of impact toughness to minor variations in alloying composition can be assured for V–(4–5)Cr–(4–5)Ti class.

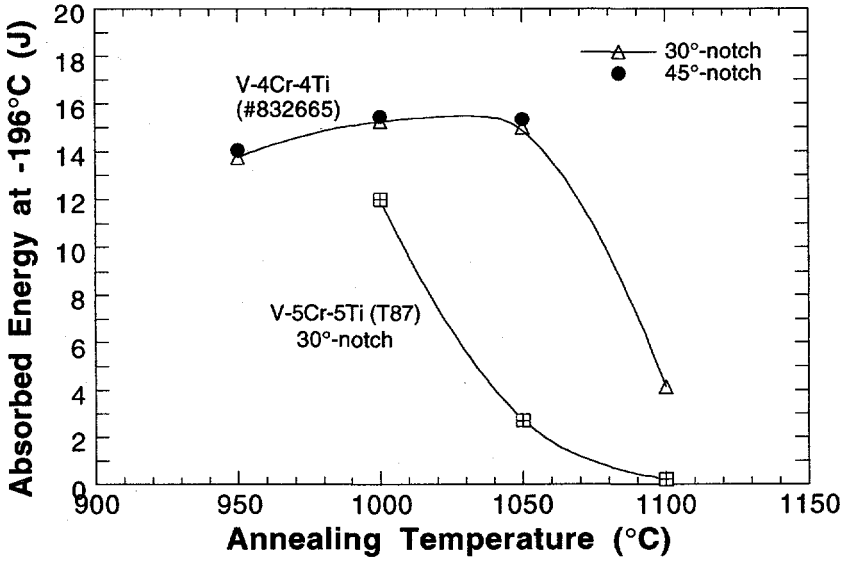

Fig. 3. Effect of annealing on Charpy absorbed energies of 15–kg V–5Cr–5Ti (#T87) and 500–kg V–4Cr–4Ti (#832665) measured at –196°C.

CONCLUSIONS

1. Impact properties were determined on a 15-kg laboratory heat of V-5Cr-5Ti, fabricated by the same procedure as that of the 500–kg production–scale heat of V–4Cr–4Ti. After final annealing at 1000°C for 1 h, the laboratory heat V–5Cr–5Ti exhibited impact properties as excellent as those of the production–scale heat V–4Cr–4Ti, i.e., DBTT <–200°C and absorbed energies of 10–16 J. When annealed at 1050°C or 1100°C, DBTT of the alloy increased to –175°C and –125°C, respectively.

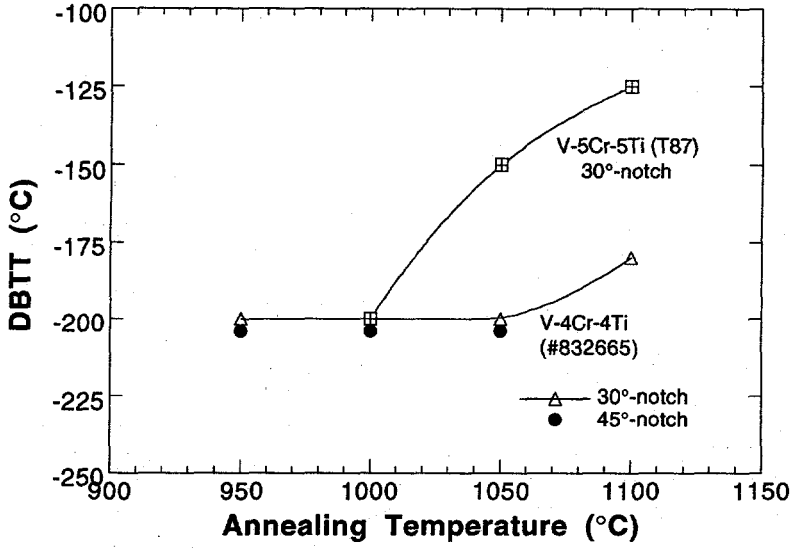

Fig. 4. Effect of annealing on DBTT of 15–kg V–5Cr–5Ti and 500–kg V–4Cr–4Tii.

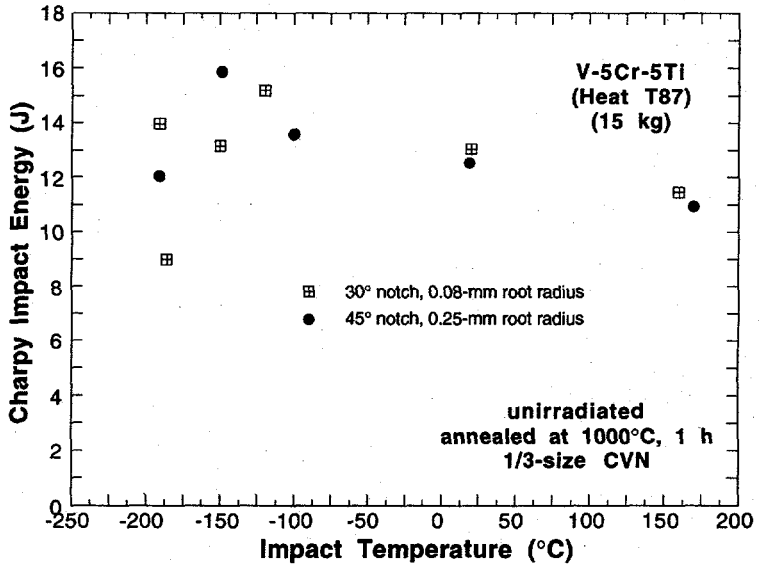

Fig. 5. Effect of notch geometry on Charpy impact properties of the V–5Cr–5Ti laboratory heat annealed at 1000°C for 1 h.

2. Unannealed as–rolled plates of V–(4–5)Cr–(4–5)Ti alloys are susceptible to laminated cracking parallel to rolling plane, a ductile fracture mode of relatively low resistance to fracture. Although the mechanism of the laminated cracking is not well understood at this time, the observations from this study underscore the importance of proper annealing of this class of alloys.

3. Impact properties of some heats of V–(4–5)Cr–(4–5)Ti alloys are more sensitive to annealing than others. Although this significant heat–to–heat variation is not well understood at present, minor impurities are believed to play an important role.

4. Final annealing at 1000°C for 1 h in high–quality vacuum is the optimal annealing condition for as–rolled or as–worked components fabricated from V–(4–5)Cr–(4–5)Ti alloys. When annealed at this condition, the alloy class in unirradiated state can be assured of excellent impact toughness regardless of minor variations in alloying element composition.

REFERENCES

[1] D. L. Smith, B. A. Loomis, and H. M. Chung, Plasma Devices and Operations, Vol. 3, 1994, pp. 167–179.

[2] H. M. Chung, B. A. Loomis, and D. L. Smith, "Properties of V-4Cr-4Ti for Application as Fusion Reactor Structural Components," Fusion Eng. Design, 1995, in press.

[3] H. M. Chung, J. Gazda, L. Nowicki, J. E. Sanecki, and D. L. Smith, "Effects of Fabrication Variables on Impact Properties and Microstructure of V–Cr–Ti Alloys," in Fusion Reactor Materials, Semiannual. Prog. Report, DOE/ER-0313/15, Oak Ridge National Laboratory, Oak Ridge, TN (1994), pp. 207–218.

[4] H. M. Chung, H.–C. Tsai, and D. L. Smith, "Fabrication of Production–Scale Heat of V–4Cr–4Ti," in this report.

[5] H. M. Chung, L. Nowicki, and D. L. Smith, "Impact Properties of Production Heat of V–4Cr–4Ti," in this report.

Subtask 12A3: FABRICATION AND PROPERTIES OF COMPOSITIONAL VARIANTS OF VANADIUM ALLOYS, by M. L. Grossbeck, D. J. Alexander, and A. N. Gubbi (Oak Ridge National Laboratory)

OBJECTIVE: Procurement of five 15 kg heats of V-Cr-Ti alloys with variations in Cr and Ti concentrations from the primary V-4Cr-4Ti composition. Fabrication into sheet product, determination of the tensile and Charpy impact properties, and preparation of specimens for reactor irradiation experiments. Data obtained from these alloys will be used to define the allowable ranges of Cr and Ti within which consistent properties may be obtained.

SUMMARY: Four 15 kg heats with variations in Cr and Ti concentration have been procured in various plate and sheet thicknesses. Measurements of recovery and recrystallization kinetics, precipitation behavior, and Charpy impact properties are in progress to compare properties with the behavior of the primary alloy composition V-4Cr-4Ti. In the fully recrystallized condition, the impact properties of the V-6Cr-3Ti alloy are inferior to those of the 500 kg heat of V-4Cr-4Ti. However, properties comparable to those of the V-4Cr-4Ti can be obtained of the V-6Cr-3Ti as tested in a partially-recrystallized condition.

INTRODUCTION: Extensive work on comparison of V-Cr-Ti alloys has been reported by Argonne National Laboratory (ANL). Most of the compositions were of 1 to 20% Cr or Ti with large steps in concentration between alloys. The composition V-4Cr-4Ti was reported to be superior to all other alloys tested primarily on the basis of Charpy impact tests. The only other alloy compositions in the low Cr and low Ti range were the alloys V-5Cr-5Ti and V-5Cr-3Ti, which demonstrated properties significantly different from V-4Cr-4Ti.

The present study selects a series of low Cr, low Ti alloys near the V-4Cr-4Ti composition in pilot plant heats. Well controlled fabrication and testing of the different alloys to optimize the composition of the primary vanadium alloy are in progress. Only four of the alloys, which will be reported on here, were obtained by ORNL. The remaining variant, V-5Cr-5Ti, was procured by ANL.

EXPERIMENTAL RESULTS: Procurement specifications were written to obtain a series of four alloys to match the fifth of the series, V-5Cr-5Ti, and the large heat of V-4Cr-4Ti procured by ANL. The nominal compositions of the four alloys and the product forms are provided in Tables 1 and 2.

Table 1. Nominal Compositions, wt %

Element	V-6Cr-3Ti	V-4Cr-4Ti	V-6Cr-6Ti	V-3Cr-3Ti
Heat No.	T92	T89	T90	T91
Cr	6	4	6	3
Ti	3	4	6	3
Si*	400-1000	800-1000	400-1000	400-1000
V	bal	bal	bal	bal

*wt ppm

Table 2. Product Form for 30 kg Heats

Form	Thickness (mm)	Size (mm)
Sheet	0.76	300 x 500
Sheet	1.02	300 x 500
Plate	3.81	300 x 500
Plate	6.35	300 x 190
Bar	12-20	>50

Glow discharge mass analysis has been initiated to check on major element composition as well as impurity elements. Certain impurity elements are best detected ;by nuclear activation analysis. Mo and As are two such elements present in the materials that are suited to this technique. Samples of the feed materials used to prepare the alloys were also supplied by the vendor. Analyses of these elements are included in Table 3, which shows preliminary results of activation analysis.

The results for Ti are not valid since there is a serious interference with a gamma ray from vanadium. The results for pure Cr contain large errors because of self-shielding of the incident neutrons. This problem will be corrected by dissolution and dilution followed by re-irradiation.

Two of the minor elements that appear in Table 3 were specified in the order. The Mo, which is shown to originate from the vanadium, was kept below the specification limit. The Fe appears to be above the specification in one case, but the error limits by this analysis technique were sufficiently large that the specification may have in fact been met. The Fe appears to originate from all three elements of the alloys, especially the Cr. It is interesting that the Ti stock contained 30 ppm As, and this led to about 1 ppm As in the alloys. This element and the Ga that arises from the Cr stock might affect grain boundary cohesion.

Interpass annealing was done at 1050-1075°C, which resulted in a grain size slightly larger than intended, but the higher temperatures were permitted in order to match the large heat of V-4Cr-4Ti. Excellent properties, reported earlier, were obtained in the V-5Cr-5Ti alloy with annealing at 950°C for 2 hrs, which resulted in a grain size of ASTM 8. The grain sizes in the present series of alloys appears in Table 4. The alloys were received in the as hot rolled condition with 40-50% deformation. Rolling was done at 400°C except for the 1.02 mm and 0.76 mm sheet materials, which were rolled to final size at room temperature.

One third size Charpy (MCVN) impact testing is being used in an initial characterization of the properties of these alloys. For comparison, a set of Charpy tests were also carried out on the large heat of V-4Cr-4Ti. All tests were carried out following annealing treatments for two hours at 950, 1000, or 1050°C. The large heat was received in a factory-annealed condition so that the subsequent annealing treatments had little or no effect on the microstructure and resulted in the same grain size (16 ± 4 μm) for each treatment. The impact data (Fig. 1) and hardness data (Fig. 2) showed reproducible behavior with a DBTT in the vicinity of -190°C, and an annealed hardness of ~142 VHN.

Table 3

	PRELIMINARY RESULTS CONCENTRATION IN PPM UNLESS OTHERWISE NOTED UNCERTAINTY ±5% UNLESS OTHERWISE NOTED							
Element	4Cr45ISI	V6Cr6Ti	V3Cr3Ti	V6C43Ti	V	Ti	Cr	Specification Limit
TI	1.5% ± 1.1%	3.0 ± 1.2%	7.8% ± 2.9%	1.8% ± 1.2%	ND	101%	ND	
V	90%	83%	95%	90%	100%	169	306 ± 33	
MN	1.7 ± 0.1	2.1 ± 0.1	1.2 ± 0.1	1.7 ± 0.1	0.6 ± 0.1	11.2	8.3	
AS	1.4 ± 0.1	2.5 ± 0.8	1.1 ± 0.1	1.1 ± 0.1	0.12 ± 0.5	31	1.0 ± 0.4	
GA	2.8 ± 0.3	ND	1.5 ± 0.1	3.0 ± 1.4	ND	ND	70 ± 16	
MO	346	329	342	330	354	6.8 ± 0.8	ND	500
SB	0.58	0.83	0.45	0.47	ND	15.8	ND	
W	54	48	52	50	86	4.8 ± 0.2	27.4 ± 0.5	
CO	3.8 ± 0.3	2.7 ± 0.2	1.2 ± 0.1	2.5 ± 0.2	1.8 ± 0.2	4.4 ± 0.4	6.7 ± 1.0	
CR	3.6%	5.9%	2.9%	6.3%	39	189	90%	
FE	497 ± 174	214 ± 77	182 ± 43	283 ± 78	324 ± 103	652 ± 168	1.72E3 ± 500	300
SC	0.04 ± 0.01	0.09 ± 0.01	0.04 ± 0.01	0.045 ± 0.01	ND	1.33	ND	
ZN	ND	ND	3.5 ± 1.6	ND	ND	ND	ND	

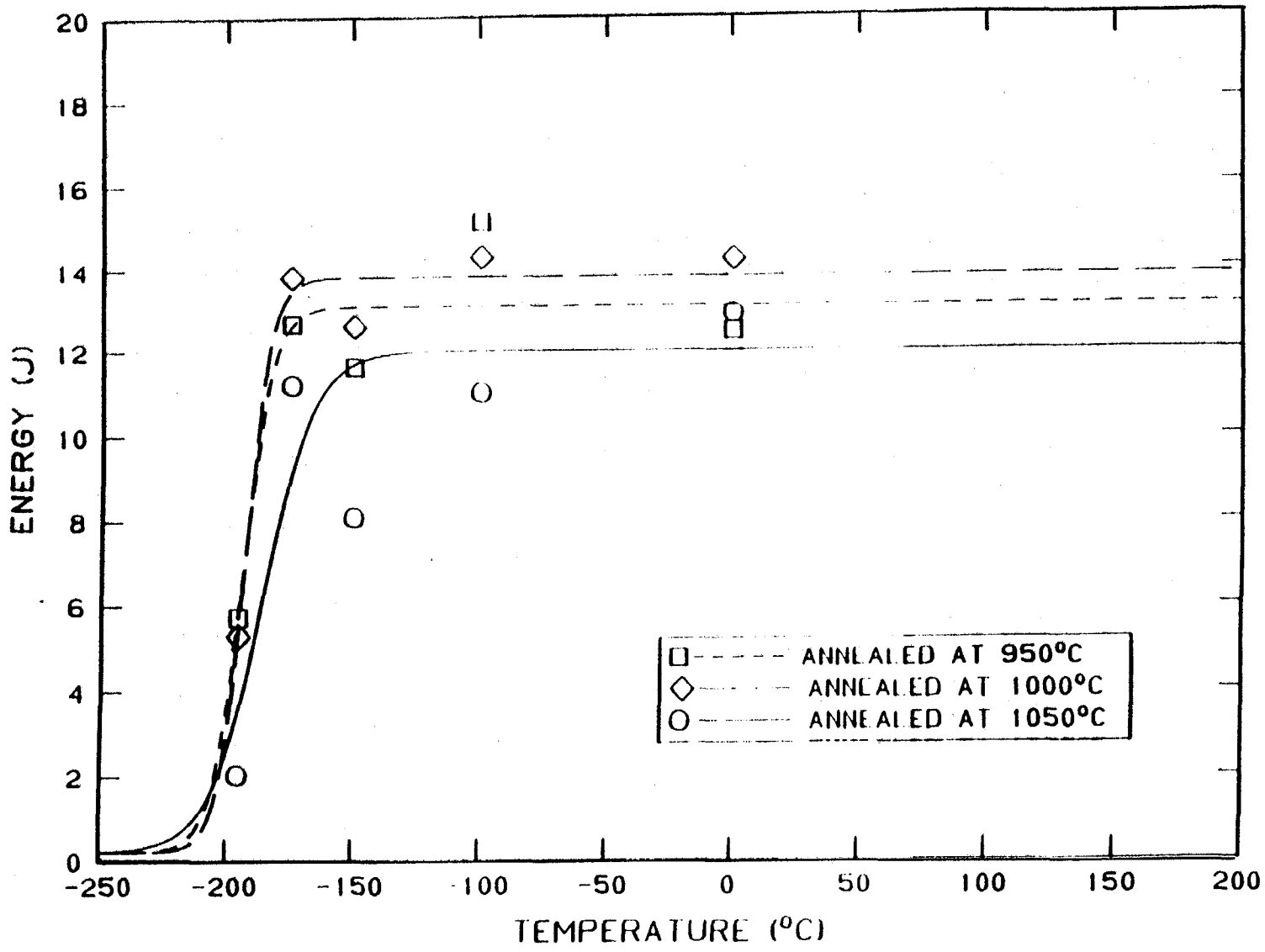

Fig. 1. Absorbed energy versus test temperature for third-size Charpy specimens of V-4Cr-4Ti (HT 832665) annealed at three different temperatures.

Table 4. Approximate Grain Sizes in As Received Plates

Alloy	ASTM Grain Size
V-3Cr-3Ti	7.0
V-4Cr-4Ti-Si	7.5
V6Cr-3Ti	7.5-8.0
V6Cr-6Ti	7.5

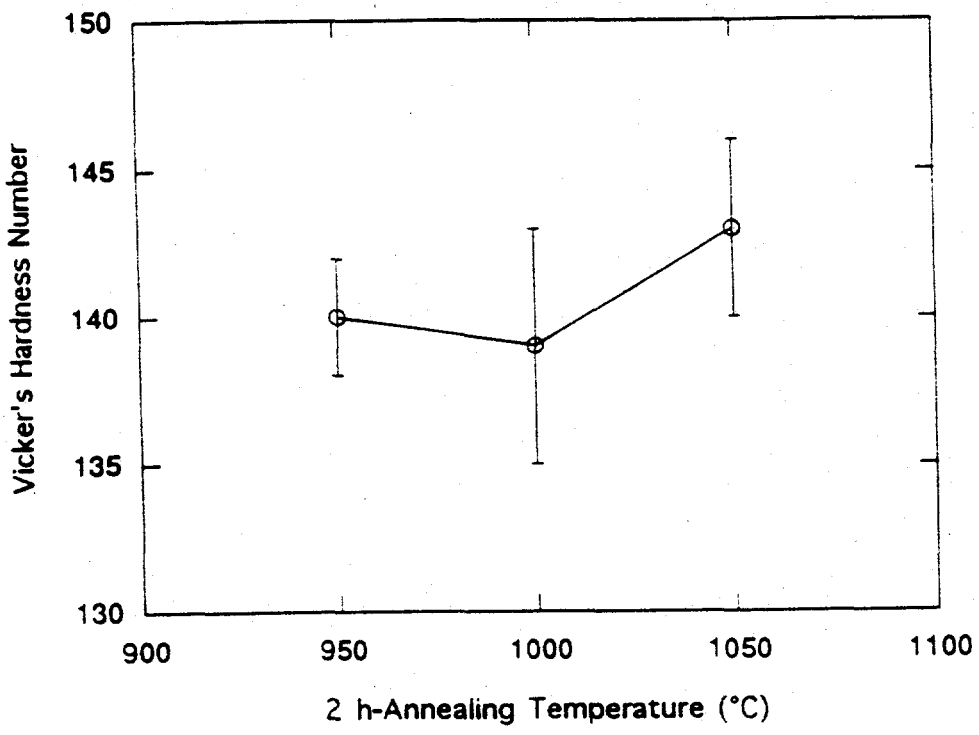

Fig. 2. Variation of microhardness with annealing temperature for V-4Cr-4Ti (HT 832665)

Impact data for the V-6Cr-3Ti alloy (Heat T92) are shown in Fig. 3. In the fully annealed condition (1050°C for 2 hours) the DBTT for this alloy was approximately 120°C higher than that of the V-4Cr-4Ti, although the upper shelf energy was similar.

However, the low temperature impact properties improved significantly when the final annealing temperature was reduced to 1000°C and 950°C, this material is less than 50% recrystallized and that recrystallization is not complete at 1000°C.

Recovery, recrystallization, and grain growth studies were initiated on the 1.02 mm thick sheet of the four 15 kg heats of compositional variants. Annealing was carried out for temperatures ranging from 900 to 1050°C in a vacuum better than $1x10^{-6}$ torr. Figures 4 and 5 show some initial microhardness data for 1 hour and 2 hour anneals.

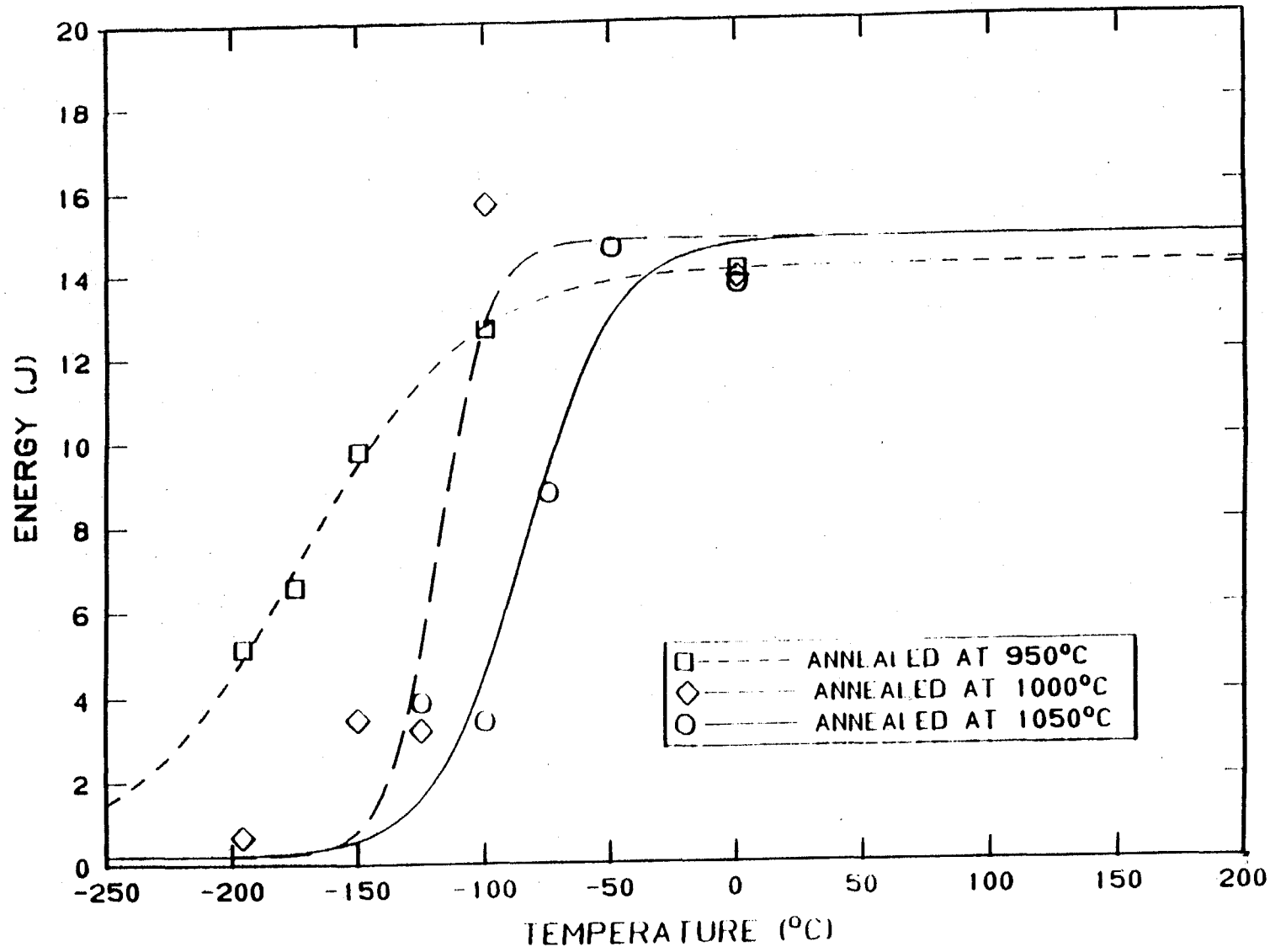

Fig. 3. Absorbed energy versus test temperature for third-size Charpy specimens of V-6Cr-3Ti (Heat T92) annealed at three different temperatures.

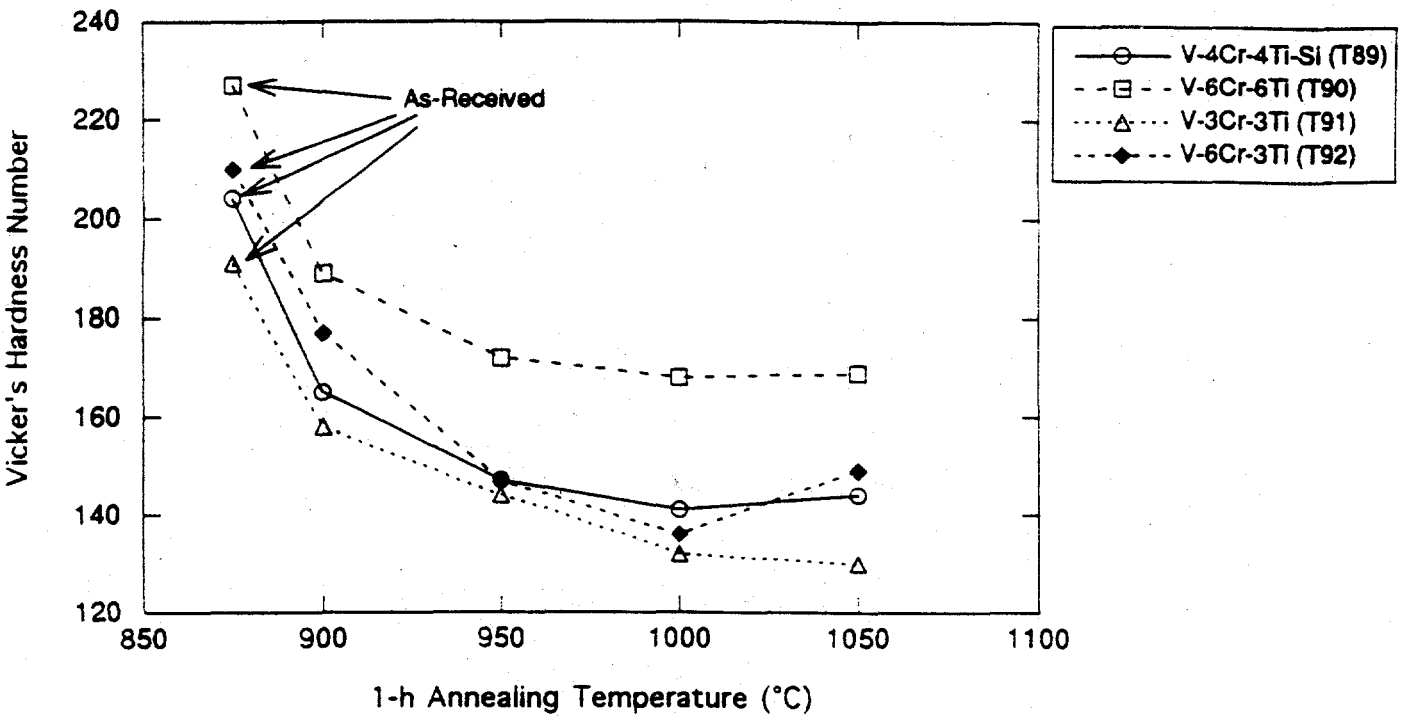

Fig. 4. Variation of Microhardness with 1-h Annealing Temperature

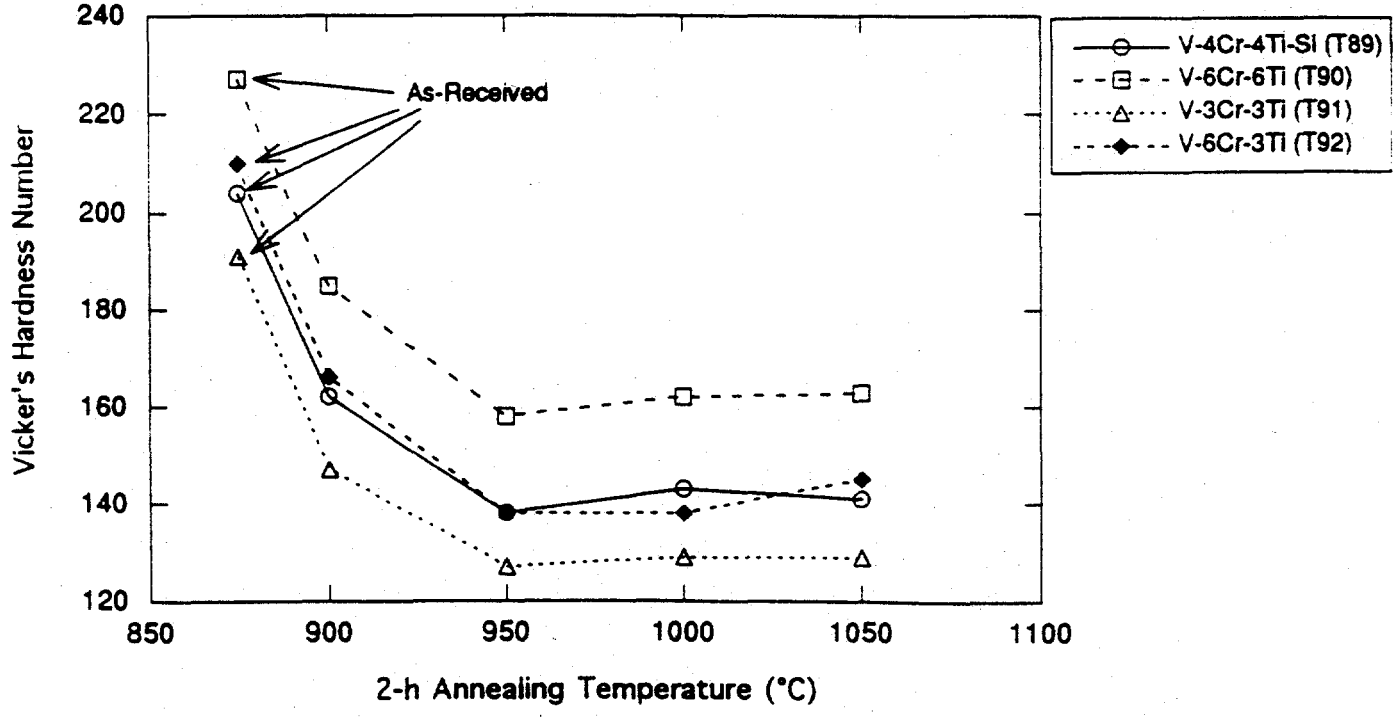

Fig. 5. Variation of Microhardness with 2-h Annealing Temperature

For all 4 alloys, recrystallization was complete at 950°C following a 2 hour anneal, but only partially complete after 1 hour. These observations were confirmed by optical microscopy. It therefore appears, from the preceding paragraph, that the recrystallization kinetics for the V-6Cr-3Ti alloy are different for the 3.81 mm and 1.02 mm thick plate. For all four alloys, recrystallization at 1000 and 1080°C was complete after 1 hour.

The hardness of the fully recrystallized V-6Cr-6Ti was significantly higher than that of the alloys, consistent with the highest solute concentration of the set of alloys.

Subtask 12B1: WELDING DEVELOPMENT FOR V-Cr-Ti ALLOYS, J. F. King, G. M. Goodwin, M. L. Grossbeck, and D. J. Alexander (Oak Ridge National Laboratory)

OBJECTIVE: Development of the metallurgical and technological basis for the welding of thick sections of V-Cr-Ti alloys.

SUMMARY: The weldability and weldment properties of the V-5Cr-5Ti alloy have been evaluated. Results for the Sigmajig test of the vanadium alloy were similar to the cracking resistance of stainless steels, and indicates hot-cracking is unlikely to be a problem. Subsize Charpy test results for GTA weld metal in the as-welded condition have shown a significant reduction in toughness compared to the base metal. The weld metal toughness properties were restored to approximately that of the base metal after exposure to a PWHT 950°C. The subsize Charpy toughness results for the EB weld metal from this same heat of vanadium alloy has shown significant improvement in properties compared to the GTA weld metal and the base metal. Further testing and analysis will be conducted to more fully characterize the properties of weld metal for each welding process and develop a basic understanding of the cause of the toughness decrease in the GTA welds.

INTRODUCTION: The reactive nature of vanadium alloys raises concerns with welding the potentially large components of the ITER system, and the selection of weld processes and procedures will have a strong economic impact on component fabrication. The gas tungsten arc (GTA) and electron beam (EB) welding processes are being evaluated, with the primary consideration being the effect of interstitial pickup on weld metal mechanical properties.

EXPERIMENTAL RESULTS: Weldability hot cracking tests were performed on 0.75 mm thick sheet material of vanadium alloy BL63 (Ht. 832394) which contains 4.6 wt% Cr, 5.1 wt% Ti, 440 wppm O, 28 wppm N, 73 wppm C, and 310 wppm Si. Sensitivity to hot cracking was measured using the Sigmajig test, which gave a threshold cracking stress of 138-172 MPa. This level of cracking resistance is similar to some stainless steels, and indicates that hot cracking is unlikely to be a problem, except possibly in thick sections under high restraint.

GTA welds were produced with various levels of oxygen contamination by welding with conventional argon gas shielding and by using an argon-filled glove box containing 2% and <10 ppm oxygen. Tensile specimens were prepared from the sheets with the weld bead located in the middle of the 12.7 mm gage length. Tests were performed on a Gleeble thermomechanical simulator at strain rates of 1.6×10^{-3}, 7.9×10^{-2}, and 1.6 per second. As summarized in Table 1, increasing strain rate typically increased yield and ultimate strength and decreased total elongation. Specimens made in the high purity atmosphere (<10 ppm oxygen) all failed in the base metal while the other two environments (2% oxygen and conventional torch shielding) resulted in all failures at the weld centerline with less than 5% total elongation. Microhardness measurements showed the high purity atmosphere welds were hardened to levels of 650 dph in the heat affected zone and 1000 dph in the fusion zone. Additional testing is planned to determine more specifically how much

Table 1. Summary of Tensile Properties (V-5Cr-5Ti Alloy Weldments)

		Strain rate, per second			Notes
		1.6×10^{-3}	7.9×10^{-2}	1.6	
Base metal	Yield (ksi)	37.7	40.2	42.7	
	Ultimate (ksi)	66.4	70.4	87.0	
	Total elongation (%)	19.3	17.1	13.7	
Glovebox weld <10 ppm O_2	Yield (ksi)	35.7	58.3	51.8	All base metal failures
	Ultimate (ksi)	46.3	77.4	92.5	
	Total elongation (%)	12.5	11.6	9.2	
Conventional gas shielded weld	Yield (ksi)	22.6	–	38.7	All weld centerline failures
	Ultimate (ksi)	61.9	72.9	68.9	
	Total elongation (%)	2.0	3.9	0.7	
Glove box weld in Argon + 2% O_2	Yield (ksi)	29.2	27.2	34.2	All weld centerline failures
	Ultimate (ksi)	47.8	39.2	34.2	
	Total elongation (%)	0.3	0.3	0.2	

oxygen can be tolerated and the types of weld shielding techniques that will be required.

Multipass GTA welds, designated GTA-I and GTA-II, were made in 7 mm thick plate with filler metal from the same heat of vanadium alloy (BL63). The welding chamber atmosphere was maintained at less than 50 ppm water vapor plus oxygen throughout the welding operation. Microhardness measurements across the weldment showed approximately 200 dph at all locations which indicates minimal interstitial embrittlement. Metallographic examination of a GTA weld cross section (Fig. 1) shows large columnar fusion zone grains, and a narrow, but coarse grained heat affected zone (HAZ).

The Charpy properties of the GTA welds were significantly worse than those of the base metal annealed at 1125°C (Fig. 2). Although the number of specimens used was insufficient to define a complete impact energy-temperature curve, the CVN transition temperature of the weldments is clearly 100-150°C higher than that of the base metal. A set of specimens from GTA II was vacuum annealed at 400°C to remove any hydrogen that may have been picked up during welding or subsequent handling. As shown in Fig. 2, the 400 °C anneal did not significantly affect CVN properties and it is concluded that hydrogen is not responsible for the poor fracture resistance of the GTA weld. On the other hand, annealing in vacuum at 950°C for 1 hour produced a dramatic improvement in impact properties (Fig. 2). Following the 950°C anneal, the impact properties were similar to those of the base metal.

Autogenous full penetration EB welds were produced in 7 mm thick plate using welding parameters of 15 mA beam current at 150 kV accelerating voltage and a welding speed of 8.5 mm/s for weldment EB-I and 20.6 mA at 150 kV with a welding speed of 12.7 mm/s for weldment EB-II. A section of the completed weld was removed for metallographic examination. Examination of the weld cross section (Fig. 3) revealed no indication of weld discontinuities and little evidence of grain coarsening (Fig. 4) in the HAZ. Hardness measurements were made across the weldment at approximately the middle of the plate thickness. The base metal had an average hardness of 177 DPH. The HAZ exhibited a higher average hardness of 198 DPH with measurements ranging from 180 to 229 DPH. The weld metal was very uniform with an average of 194 DPH. The variation in hardness values is relatively small across the weldment which would indicate mechanical properties should be uniform across this region.

Subsize Charpy V-notch specimens were machined from the weldment and notched in the center of the weld fusion zone such that the fracture occurs in the direction of welding. Four of these specimens were tested in the as-welded condition at temperatures ranging from ~100°C down to ~-200°C. At each temperature, specimens failed in a predominantly ductile mode with high values of absorbed energy (Fig. 4). This is a rather surprising result in view of the coarse-grained (~500 μm) microstructure of the fusion zone; and implies that a post weld heat treatment may not be required.

DISCUSSION AND CONCLUSIONS: The reactive nature of vanadium alloys at elevated temperature causes concerns with welding the potentially large components of the ITER system. Vanadium alloys have high solubilities for carbon, oxygen, nitrogen, and hydrogen, which dissolve interstitially. These elements can significantly affect the mechanical properties of these alloys. The welding experience to date indicates GTA welds in these alloys will require high purity welding atmospheres to minimize the pickup of these elements during welding. The subscale Charpy test results have shown relatively poor toughness properties for as-welded GTA vanadium alloy weldments produced in welding environmental chambers with high purity atmospheres. PWHT of these weldments in vacuum at 950°C restores the toughness of these welds to near the base metal values. The arc welding fabrication of large components will possibly require large environmental chambers for welding and vacuum furnaces for PWHT.

The electron beam welding process is also being evaluated for welding the vanadium alloys. The electron beam welds are produced in a high vacuum environment and are not exposed to the interstitial elements which are potentially present in the shielding gases of the arc processes. The preliminary subsize Charpy test results for as-welded electron beam weld metal from the V-5Cr-5Ti alloy has shown significant improvement in toughness compared to both GTA weld metal and base metal itself. This implies that EB weldments may not require postweld heat treatment before service. The problem with large component welding is the necessity for large chamber electron beam welders and the difficulty of accessing all conceivable weld joints.

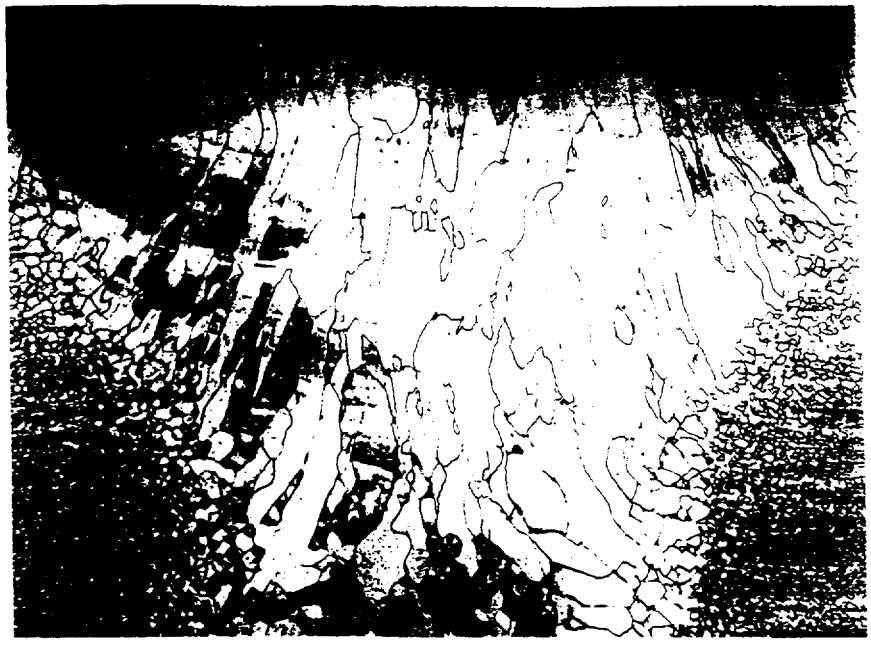

Fig.1. Fusion zone and heat affected zone of a multipass GTA weld in V-5Cr-5Ti.

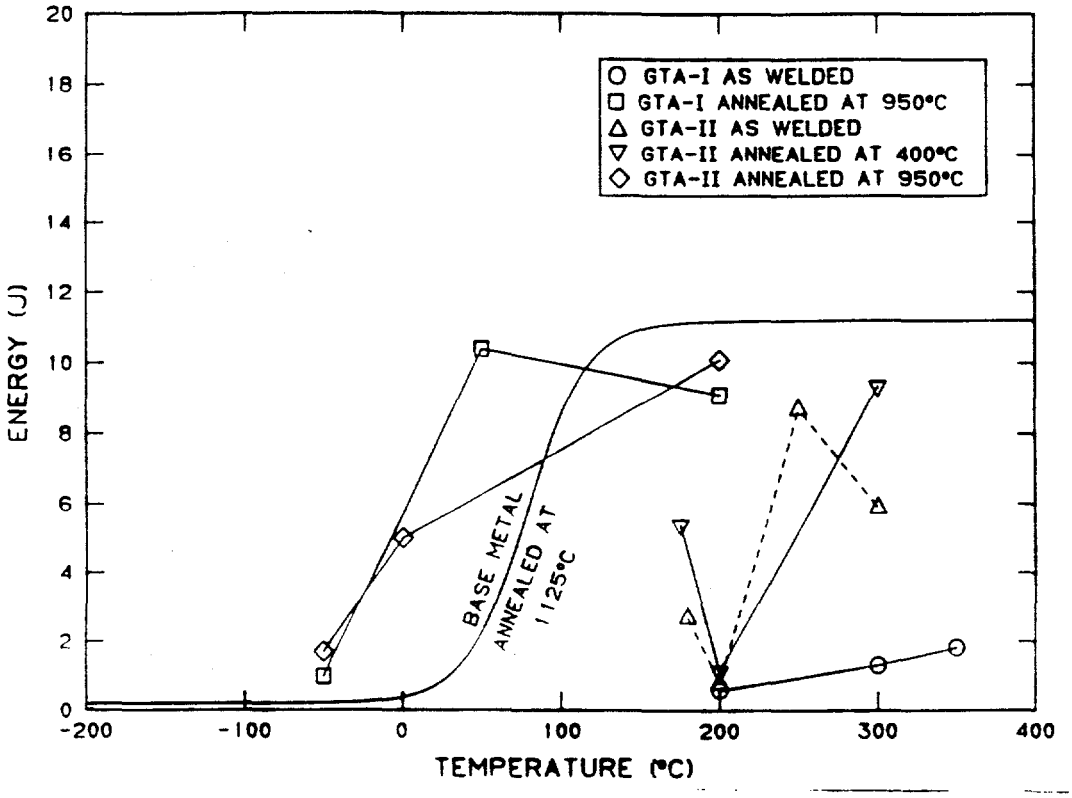

Fig. 2. Charpy impact properties of GTA welds and the effects of post-weld heat treatments.

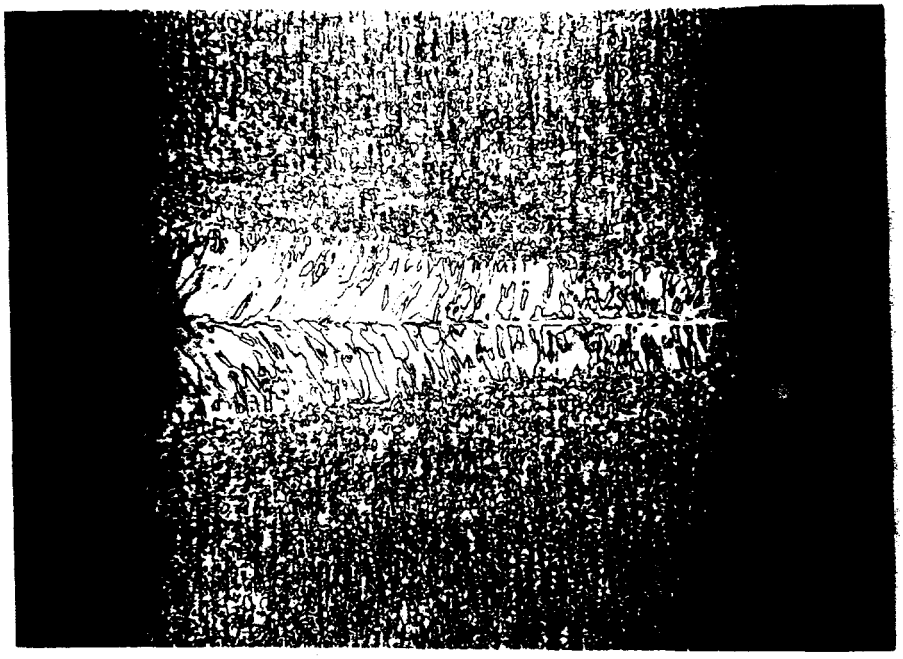

Fig. 3 Transverse cross-section of full penetration electron beam weld in 7 mm thick V-5Cr-5Ti alloy.

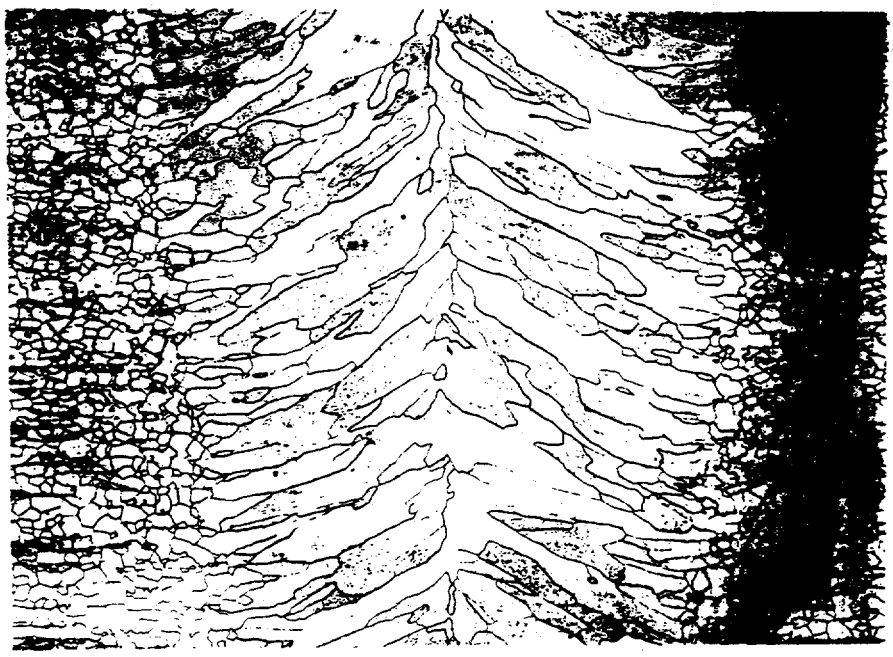

Fig. 4. Transverse cross-section of the HAZ of the electron beam weld in the V-5Cr-5Ti alloy shows little evidence of grain coarsening.

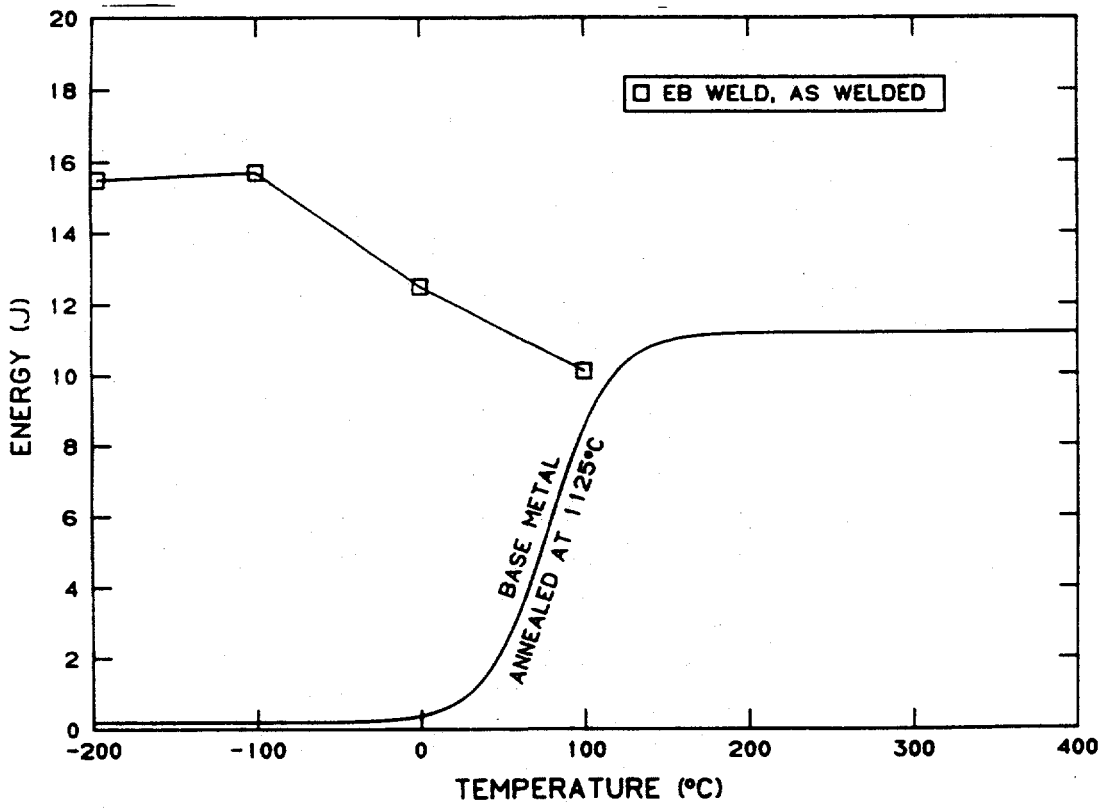

Fig. 5. Charpy impact properties of EB weld and base metal V-5Cr-5Ti.

Subtask 12B2: DEVELOPMENT OF LASER WELDING TECHNIQUES FOR VANADIUM ALLOYS, R. V. Strain, K. H. Leong, E. E. Keppler, and D. L. Smith (Argonne National Laboratory)

OBJECTIVE

The development of techniques for joining vanadium alloys will be required for the construction of fusion devices utilizing the desirable properties of these alloys. The primary objective of this program is to develop of laser welding techniques for vanadium alloys, particularly for the manufacture of welded materials testing specimens.

SUMMARY

Laser welding is potentially advantageous because of its flexibility and the reduced amount of material effected by the weld. Lasers do not require a vacuum (as does electron beam welders) and the welds they produce have large depth-to-width ratios. Results of scoping tests using a small, pulsed laser (50 joule, YAG laser) indicated that lasers could produce successful welds in vanadium alloy (V-5%Cr-5%Ti) sheet (1-mm thick) when the fusion zone was isolated from air. The pulsed laser required an isolating chamber filled with inert gas to produce welds that did not contain cracks and showed only minor hardness increases. Successful bead-on-plate welds have been made to depths of about 4-mm using a 6 kW continuous CO_2 laser with argon purging.

EXPERIMENTAL PROGRAM

Because of the potential advantages of laser welding, it is important to include laser welded samples in the materials testing program for vanadium alloys. As a result laser welding tests on vanadium alloy were begun in the fall of 1994. Initial scoping tests using a small, pulsed laser were performed to determine the environment required to make successful welds and determine the depth of penetration capability of this welder. Results from these tests indicated that successful welding of these alloys would require protection of the molten metal from contamination by interstitial elements (primarily oxygen). Some initial test have been performed using a 6000 W continuous CO_2 laser using purging with argon to protect the weld. Successful bead-on-plate welds have been made on 1-mm thick sheet and 4-mm thick plates. Modification of the configuration of the purge streams and adjustment of the welding parameters will be pursued as methods of optimizing these welds.

RESULTS

Weld beads were generated during scoping tests using a pulsed laser by overlapping individual spot welds. Welds made in air using argon purging to protect the welds resulted in welds that contained cracks. A successful weld was made by placing the sample in a glass chamber filled with argon. In this case, metal vaporized during the individual shots coated the glass and significantly reduced the penetration depth near the end of the bead. These results showed that laser welding was feasible, but protection of the weld from interstitial impurities would be required.

Previous experience of the operators of the 6 kW continuous laser indicated that successful welds could probably be made on the vanadium alloys using inert gas purges,

which would avoid the complications involved in enclosing the work piece. Initial weld trials have shown that bead-on plate welds could be obtained to depths of about 4-mm using a power of 5.5 kW and a speed of 45 cm/s. Argon at a flow rate of 100 cfh was distributed through a diffuser nozzle aimed just behind the laser beam on the upper surface of the work-piece. The rapid solidification rate in these weld resulted in a fine, highly elongated grain structure as shown in Fig. 1. Results of micro-hardness measurements (Fig. 2) show an increase from about 180 dph in the bulk material to about 220 dph in the fusion zone.

FUTURE ACTIVITIES

The next step in the development of the laser welding techniques is to improve the purging system so that both the top and the bottom of the work piece can be shielded. Efforts will be made to optimize the power and speeds used to weld 1 mm and 4 mm thick material. This information will then be used to generate welded material that can be used to manufacture materials testing specimens that will be included in future irradiation tests.

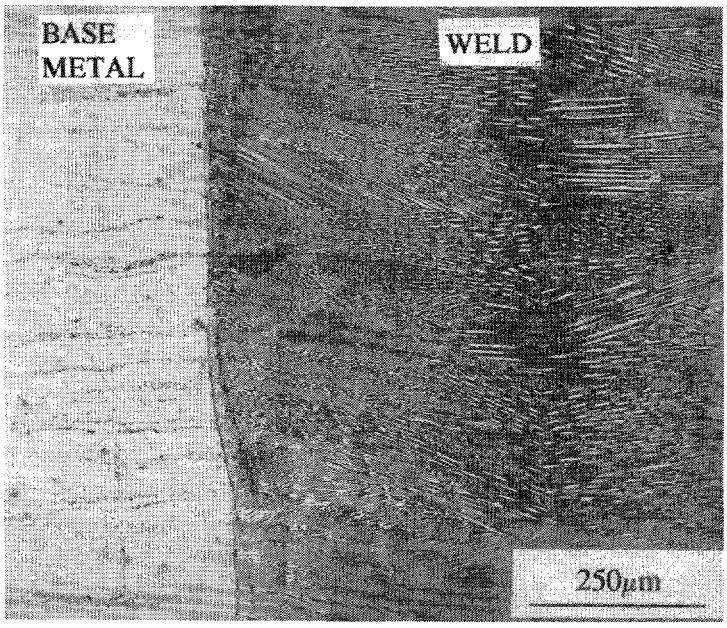

Fig. 1. Microstructure of Laser Weld of V-4%Cr-4Ti (500 kg Heat).

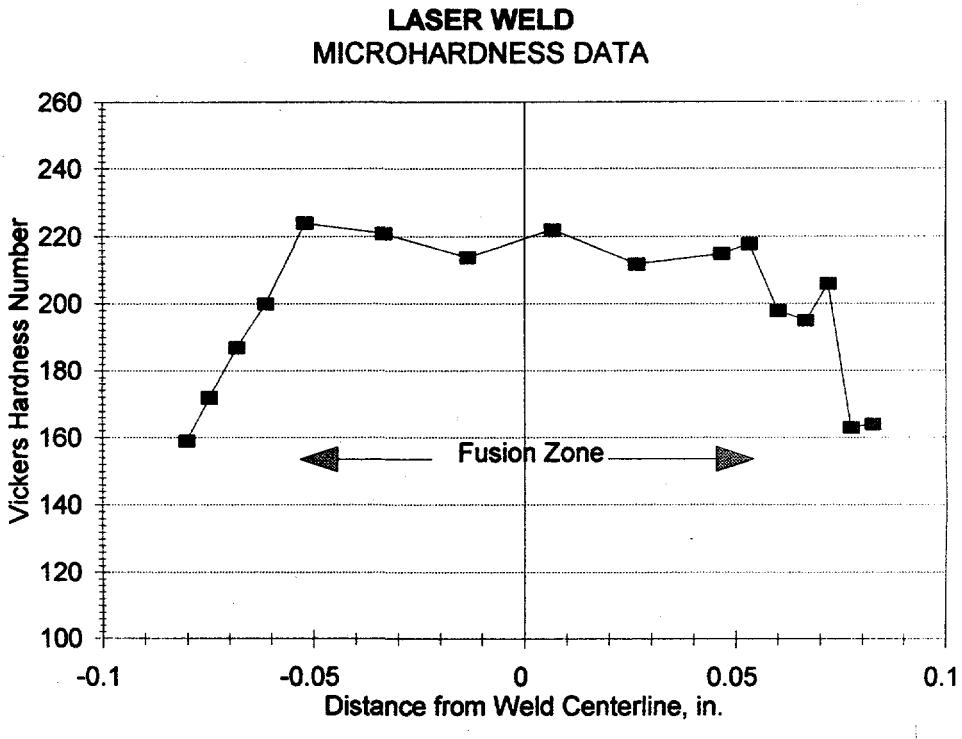

Fig. 2. Microhardness Data for Laser Weld of V-4%Cr-4%Ti (500 kg Heat).

Subtask 12C1: DETERMINATION OF THERMOPHYSICAL PROPERTIES OF V-5Cr-5Ti, W.D. Porter, R.B. Dinwiddie, W.A. Simpson, and M.L. Grossbeck (Oak Ridge National Laboratory)

OBJECTIVE: Measurement of thermal expansion, thermal conductivity, specific heat, elastic constants to provide a single source of data on V-5Cr-5Ti to support design efforts on the V-Li blanket.

SUMMARY: The available tentative data on the physical properties required for thermal stress analyses are largely confined to pure vanadium. Using a V-5Cr-5Ti alloy, in a fully-annealed condition, a series of property measurements have been completed including linear thermal expansion, specific heat, thermal conductivity and the primary elastic constraints. These data have been submitted to the ITER Materials Property Data Handbook.

INTRODUCTION: Considerations such as thermal stress and thermal fatigue life require accurate values for physical properties such as thermal expansion, thermal conductivity, and Young's modulus. Thermal stress and thermal fatigue are necessary to determine the design lifetime for first wall and blanket structures. At least some measurements on the actual candidate V-Cr-Ti alloys are required rather than relying entirely on data on pure vanadium.

EXPERIMENTAL RESULTS

Linear Thermal Expansion

Experimental Methods

The alloy V-5Cr-5Ti from Teledyne Wah Chang heat 832394, designated BL-63 by Argonne National Laboratory, was used for the measurements. The specimen was a rectangular solid 25.0 x 5.84 x 5.84 mm. It was used in the condition as received from Teledyne Wah Chang, annealed at 1100°C.

Measurements are made using a differential push-rod dilatometer to measure the thermal expansion of a test specimen determined relative to that of a standard reference specimen. The two samples are placed side by side in a furnace, and two alumina push rods, that extend from the furnace to a thermally isolated linearly variable displacement transducer (LVDT), bear on the samples. The difference in expansion between the two specimens results in the differential movement of the push rods, thus allowing the linear thermal expansion of the unknown sample to be determined. The advantage of such a device is that instrument expansion is canceled out. The dilatometer is of the horizontal configuration with push rods and sample holder constructed of high density alumina. A sapphire rod with a length of 25 mm is used as the reference material. Differential changes in length between the sample and the reference are transmitted to the LVDT mounted on an Invar rod using separate pairs of leaf springs for the coil and core. The leaf springs provide frictionless

movement of the LVDT and also maintain a push rod load of 25-30 g on the sample and reference. The LVDT is housed in an enclosure that is maintained at 40°C by means of water circulated from a constant temperature bath. A platinum/platinum-10% rhodium type S thermocouple is used to monitor the sample temperature. The accuracy of the expansion measurements is determined to be better than ±2% over the range of 20 to 1450°C by means of verification tests using sapphire and tungsten reference materials in the sample and reference positions.

Oxidation of the sample during the dilatometer runs was minimized by evacuating the system using a mechanical vacuum pump followed by back filling with titanium-gettered helium. This process was repeated three times prior to the dilatometer run. During the test a helium flow rate of 5 ml/min was maintained at a slight over pressure of 20.7 kPa.

Expansion measurements were made using a computerized data acquisition system while the sample was heated and cooled at a rate of 3°C/min. The sample was heated to a maximum temperature of 600°C. Data sets were stored at 30 sec intervals. After the initial heating and cooling cycle, the sample was heated a second time and data were collected during heating only.

Results and Discussion

Results for the linear thermal expansion measurements appear in Table 1. The data are plotted as a function of temperature in Fig. 1 where a least squares fit curve is also shown. The polynomial expression describing the expansion is as follows:

$$DL/L_o = -179.97570689 + 9.0363848739\ T + 0.0015407532037\ T^2$$

where DL/L_o is the incremental thermal expansion in parts per million relative to the value at 20°C and T is the temperature in degrees Celsius. The instantaneous coefficient of expansion, expansivity, is shown in Fig. 2.

Figure 3 shows the curve for thermal expansion of V-5Cr-5Ti plotted with similar curves for pure vanadium and for the alloys V-15Cr-5Ti and V-7.5Cr-15 Ti. The curves for V-5Cr-5Ti and V-7.5Cr-15Ti are nearly coincident, and the curve for pure vanadium is nearly coincident with the curves for the two previously mentioned alloys. This indicates that minor variations in alloy composition in the class of low alloy V-Cr-Ti alloys need not have thermal expansion evaluated for each composition. For many scoping studies, values for pure vanadium are sufficient.

Specific Heat

Experimental Method

Specific heat was measured with a Stanton-Redcroft differential scanning calorimeter. The operation of this instrument is based on measurement of the thermal response of an unknown specimen as compared with a standard when the two are heated

Table 1. Linear Thermal Expansion of V-5Cr-5Ti Alloy Referenced to 20°C*

Temperature (°C)	Specimen Exp. (ppm)	Average CTE (ppm/°C)	Instantaneous CTE (ppm/°C)
20	0	9.1	9.1
40	184	9.2	9.2
60	368	9.2	9.2
80	553	9.2	9.3
100	739	9.2	9.3
120	927	9.3	9.4
140	1116	9.3	9.5
160	1306	9.3	9.5
180	1497	9.4	9.6
200	1690	9.4	9.7
220	1884	9.4	9.7
240	2079	9.4	9.8
260	2275	9.5	9.9
280	2473	9.5	9.9
300	2672	9.5	10.0
320	2773	9.6	10.1
340	3074	9.6	10.1
360	3277	9.6	10.2
380	3487	9.6	10.3
400	3687	9.7	10.3
420	3894	9.7	10.4
440	4103	9.7	10.5
460	4312	9.8	10.5
480	4523	9.8	10.6
500	4736	9.8	10.7
520	4949	9.9	10.7
540	5164	9.9	10.8
560	5381	10.0	10.9
580	5598	10.0	11.0
600	5818	10.0	11.0

*Calculated values using fitted equations.

uniformly at a constant rate. The instrument consists of a furnace containing two identical crucibles, each of which rests on a thin plate located inside the measurement head. Directly beneath the center of the crucible is the junction of a Pt vs Pt-10Rh differential thermocouple. Any difference in temperature between the two specimens is caused by differences in mass, specific heat, heats of reaction, or phase transitions.

To determine specific heat, a baseline is established by measuring the temperature differential of the empty crucibles as the temperature is changed at a constant rate over the temperature range of interest. Thermal response records are then acquired for a standard material, in this case sapphire, and an unknown under identical

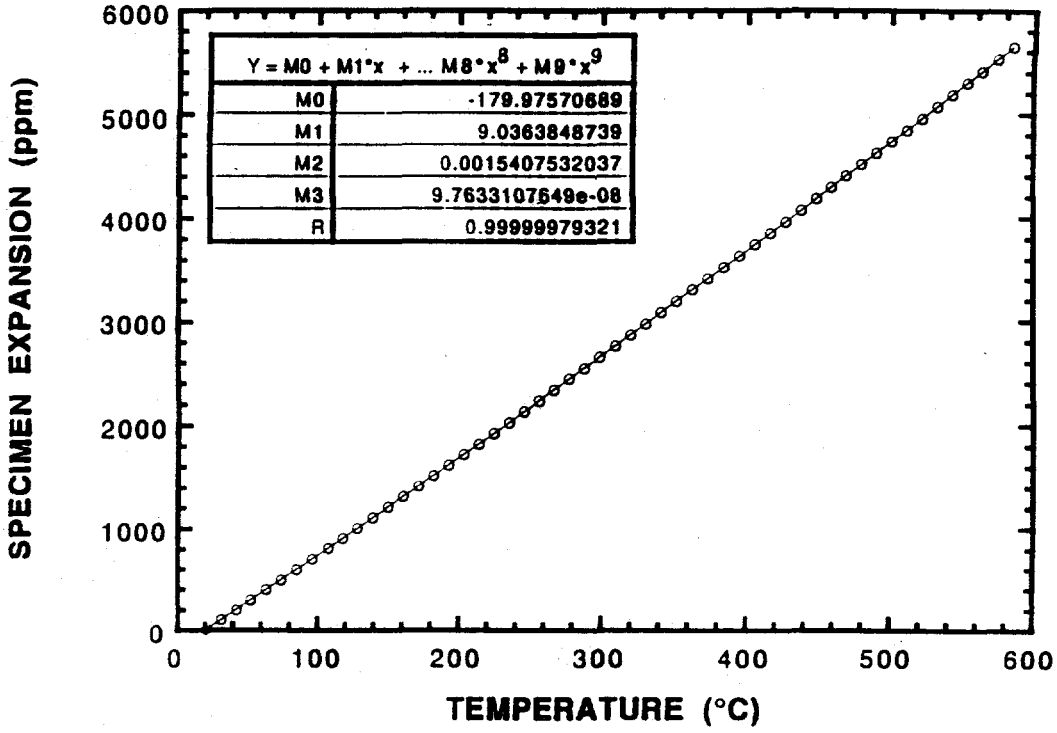

Fig. 1. Linear Thermal Expansion of V-5Cr-5Ti (wt%).

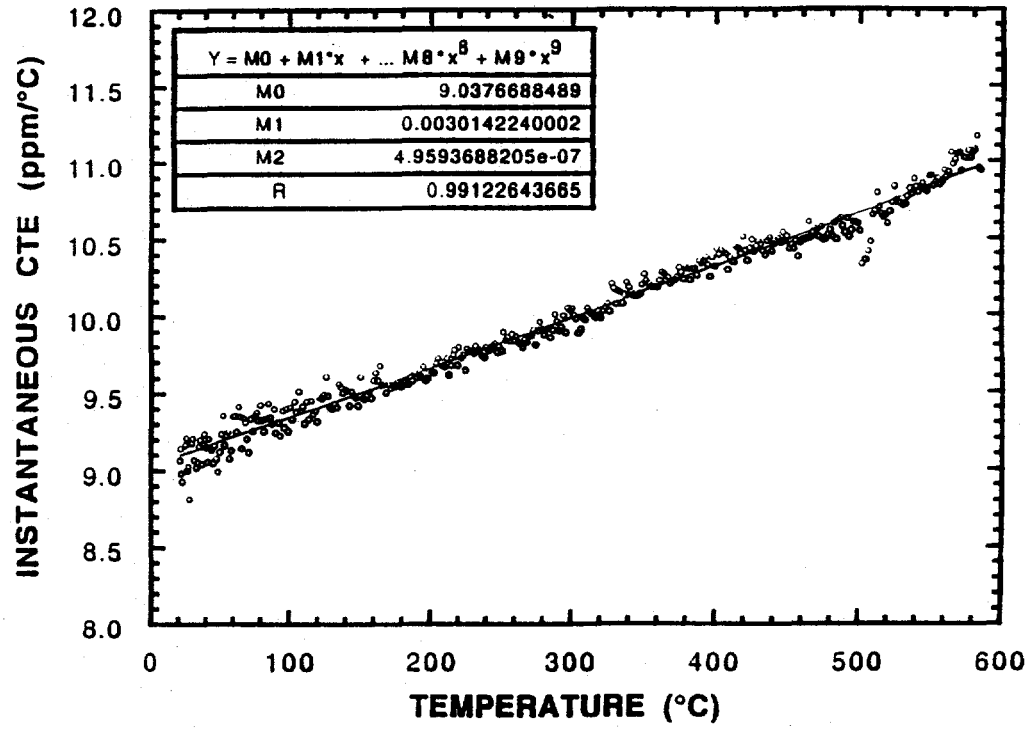

Fig. 2. Instantaneous Coefficient of Expansion of V-5Cr-5Ti (wt%).

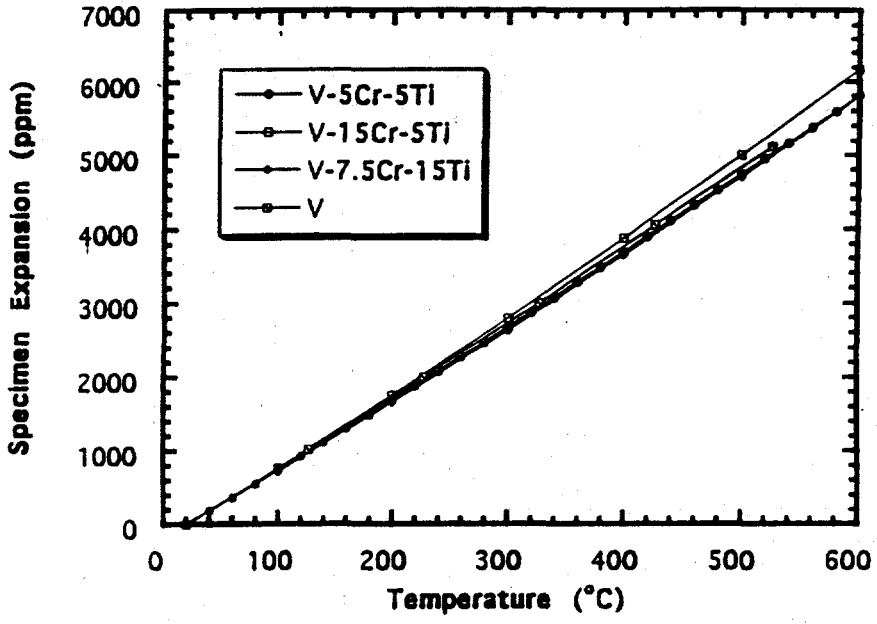

Fig. 3. Linear thermal expansion as a function of temperature for V-5Cr-5Ti as shown in Fig. 2 accompanied by similar values for pure vanadium (from Y.S. Touloukian, R.K. Kirby, R.E. Taylor, and P.D. Desai, Thermophysical properties of Matter Vol. 12, Plenum Press, New York (1975)) and for two V-Cr-Ti alloys (F.L. Yaggee, E.R. Gilbert, and J.W. Styles, "Thermal Expansivities, Thermal Conductivities, and Densities of Vanadium, Titanium, Chromium and some Vanadium-Base Alloys," J. Less Com. Metals 19 (1969) 39.)

conditions. The ratio the departure of the standard and unknown from the baseline is then used to calculate the specific heat of the unknown.

Results and Discussion

The results of the measurement appear in Fig. 4. A least squares fit to these data result in the following relation:

$$C_p = 0.57551 - 21.094/T \text{ J/g-K}$$

where C_p is the specific heat at constant pressure, and T is the temperature in Kelvin. This empirical expression is only valid over the range of the measurements.

Values of specific heat for pure vanadium are also plotted in Fig 4. At first it appears that the curves for the alloy and pure vanadium are very different in functional form. However, the ordinate is greatly expanded so that very small differences are magnified. Over a larger temperature range, the expected T^3 dependence at low temperature and the slow increase with increasing temperature at higher temperatures is apparent as shown in Fig. 5 for pure vanadium.

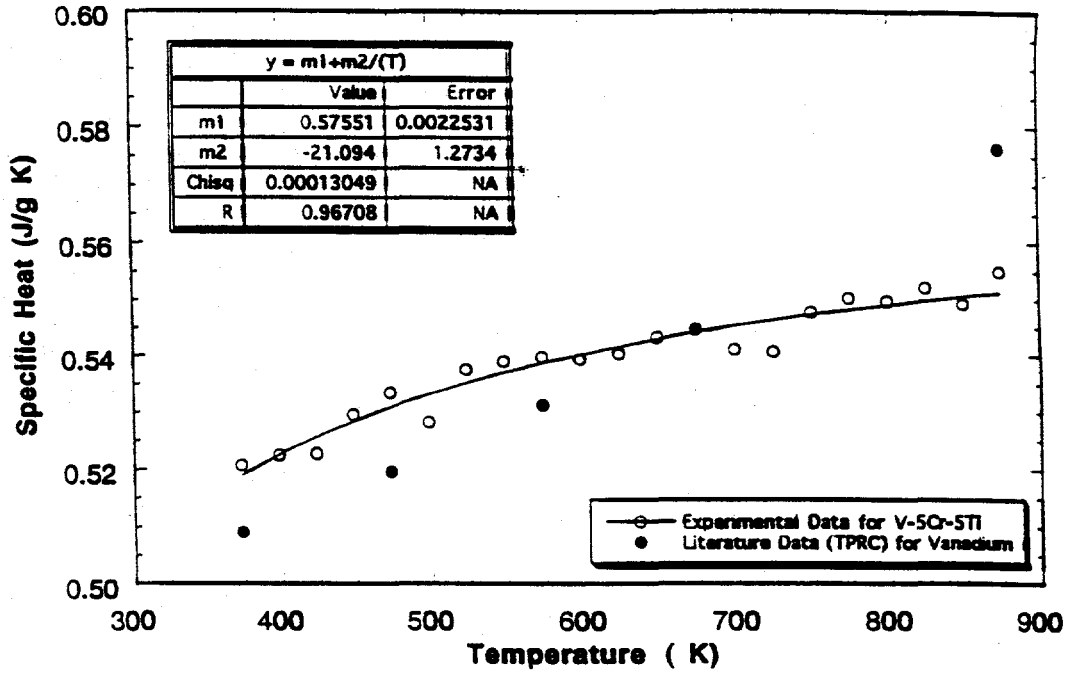

Fig. 4. Specific heat for V-5Cr-5Ti as a function of temperature. Data for pure vanadium are also shown for comparison (Y.S. Touloukian and E.H. Buyco, Thermophysical Properties of Matter, Vol. 4, Plenum Press, New York (1970)).

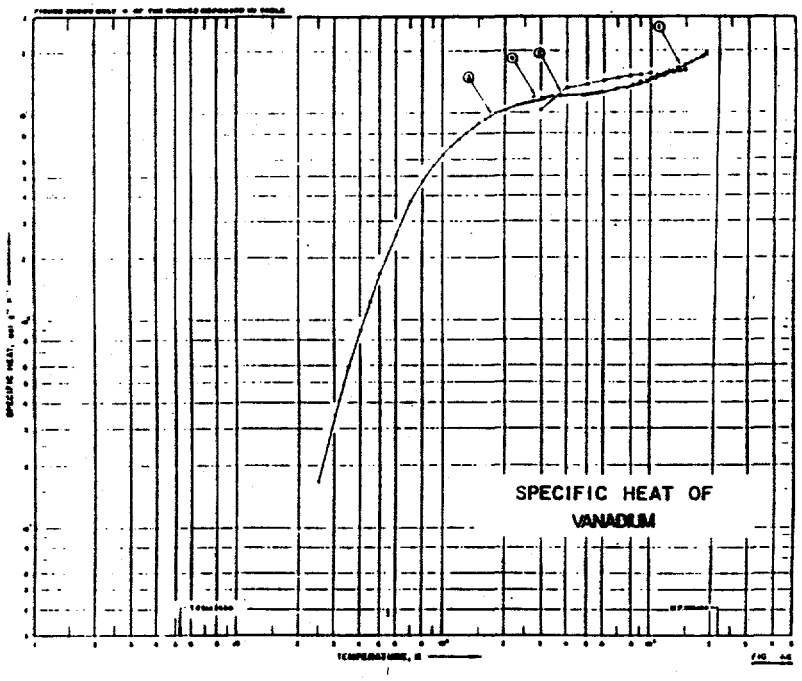

Fig. 5. Specific heat of pure vanadium over a wide temperature range (Y.S. Touloukian and E.H. Buyco, Thermophysical Properties of Matter, Vol. 4 Plenum Press, New York (1970)).

Thermal Conductivity

Experimental Method

Direct thermal conductivity measurements, especially at high temperatures, are difficult, time consuming, and they require relatively large specimens. Thermal conductivity, k, may be calculated from measurements of thermal diffusivity, α, specific heat, C_p, and bulk density, ρ, by using the relationship $k=\alpha\rho C_p$. This method for obtaining thermal conductivity is relatively fast and requires only a small amount of material. The laser flash thermal diffusivity (LFTD) technique, used for elevated temperatures in this study, and the xenon flash technique, used for the room temperature measurements, have been used extensively to study a wide range of materials including glasses, plastics, metals, ceramics, composites, crystals, and foams.

Two different systems were employed in obtaining thermal diffusivity at room temperature and at elevated temperatures. The elevated temperature system employs the LFTD technique. A small disk shaped specimen 12.45 x 1.9 mm thick was placed in an evacuated tube furnace, as shown in Fig. 6, and oriented with its flat surfaces perpendicular to the furnace axis. A neodymium glass laser was used to supply a high intensity, short-duration, pulse of thermal energy to one face of the test specimen. The intensity of the beam was controlled by varying the laser power supply and by use of attenuating filters. The resulting temperature rise of the other face of the test specimen was monitored as a function of time by an indium antimonide infrared (IR) detector and stored in computer memory. The thermal diffusivity was then determined from a numerical analysis of the IR detector output.

The xenon flash system used for room temperature measurements was very similar in principle to the elevated temperature system. A short pulse (<1 ms) of heat was applied to the front face of the specimen, and the temperature change of the rear face was measured with an infared detector. The system was, of course, optimized for room temperature measurements. The system is illustrated by the sketch in Fig. 7.

Results

The results of the measurements are shown in Fig. 8 where thermal conductivity has been calculated from the relation given above, $k=\alpha\rho C_p$. Also plotted in Fig. 8 are data for pure vanadium which fall within the limits of error for the V-5Cr-5Ti alloy. Thermal conductivity increases slightly with temperature following the Wiedemann-Franz law relating thermal conductivity with electrical conductivity. Thermal conductivity of V-5Cr-5Ti may be expressed by:

$$k = 0.0086029\ T + 27.827\ \text{W/m-K}$$

where T is the temperature in Kelvin.

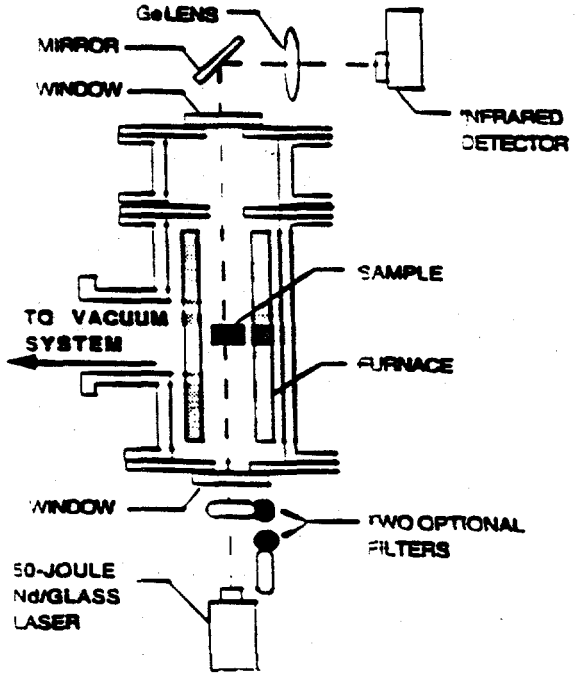

Fig. 6. Laser flash thermal diffusivity apparatus used for elevated temperature measurements.

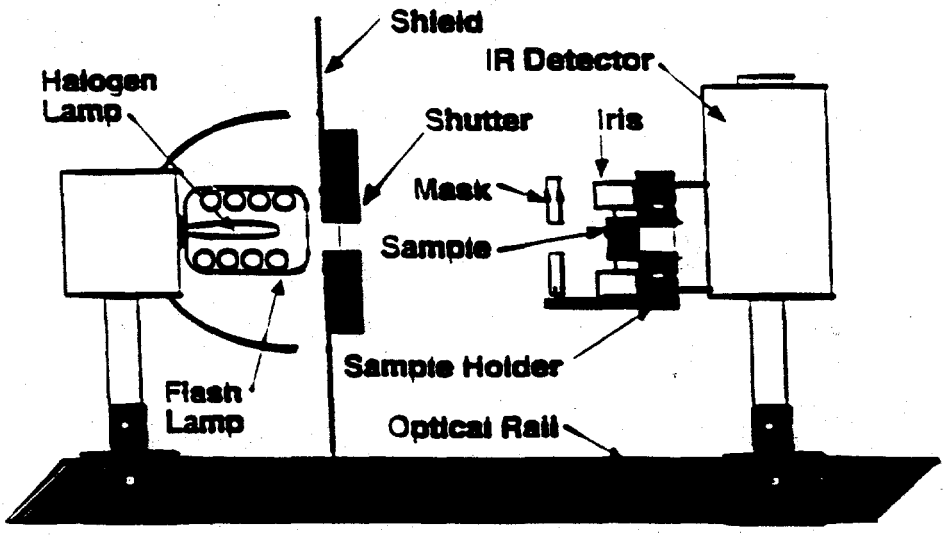

Fig. 7. Xenon flash thermal diffusivity system used for room temperature measurements.

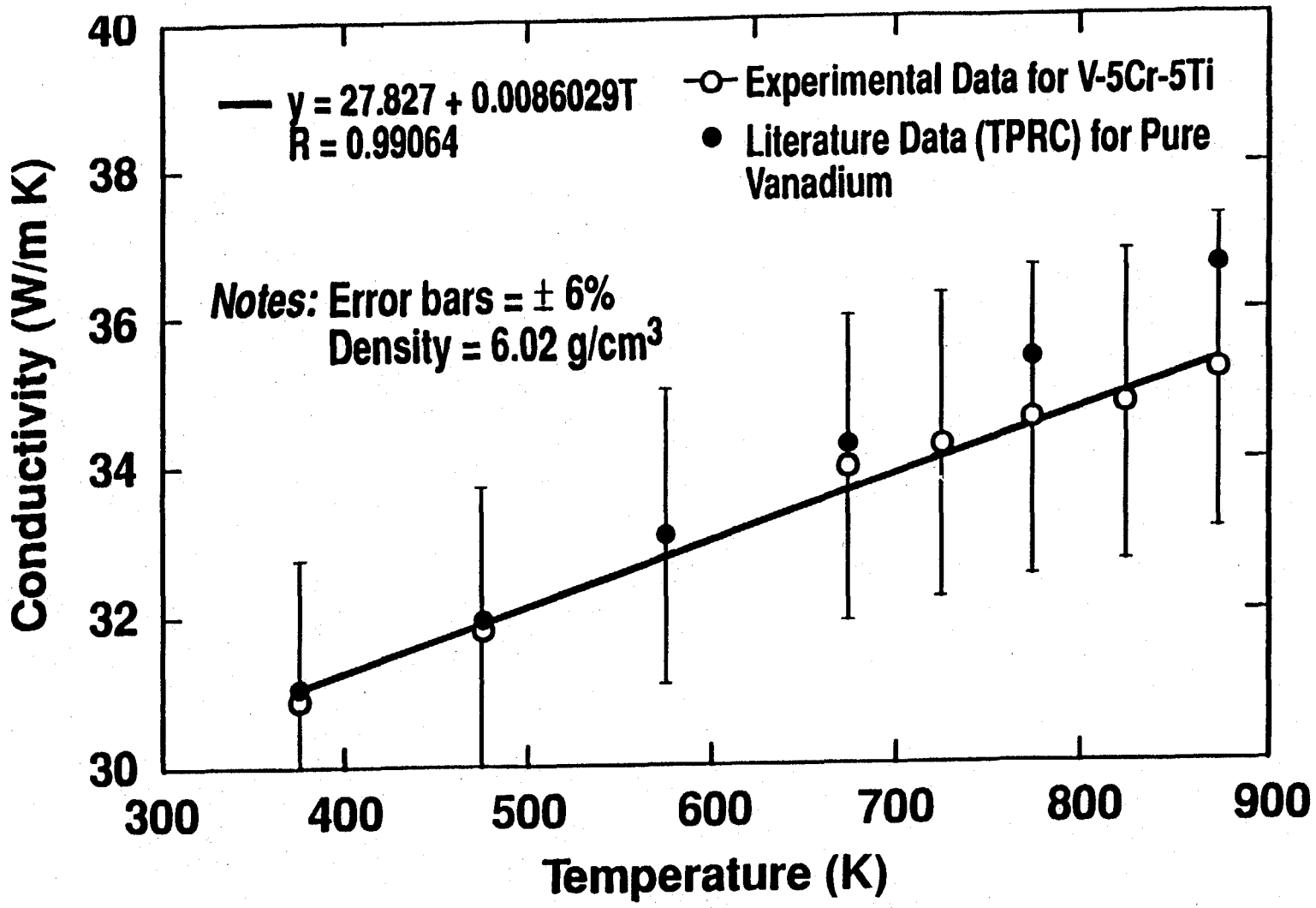

Fig. 8. Thermal conductivity of V-5Cr-5Ti as a function of temperature. Values for pure vanadium are also plotted for comparison (Y. S. Touloukian, R. W. Powell, C. Y. Ho, and P. G. Klemens, Thermophysical Properties of Matter, Vol. 1, Plenum Press, New York (1970).

Elastic Constants

Experimental Methods

A small coupon of V-5Cr-5Ti 6.35 mm in thickness was obtained for ultrasonic nondestructive determination of the elastic moduli. Because of the relatively low attenuation of this alloy for elastic waves in the frequency range 5 to 10 MHz, simple digital pulse-echo techniques were applied. The compressional wave velocity at 10 MHz and the transverse wave velocity at 5 MHz were measured using a digital oscilloscope for data acquisition and impulse excitation to the appropriate ultrasonic transducer. The density of the coupon was determined to be 6028 kg/m^3.

Results

The measured values for this sample were 6.023 ± 0.013 km/s and 2.760 ± 0.006 km/s for the compressional and transverse wave velocities, respectively. Employing the usual linear equations relating elastic wave velocities and elastic moduli, the mechanical properties were calculated to be Young's modulus 125.6 ± 0.4 GPa, Shear modulus 45.9 ± 0.2 GPa, and Poisson's ratio 0.367 ± 0.001.

Discussion

Young's modulus for pure vanadium from room temperature to 1900 K and shear modulus from room temperature to about 950 K have been determined by Farraro and McLellan. They give the following relations for the modulus values as a function of temperature:

$$E_y = ((1.28 - 9.61 \times 10^{-5} \times T) \pm 0.040) \times 10^{11} \text{ N/m}^2$$

$$G = ((0.488 - 8.43 \times 10^{-5} \times T) \pm 0.011) \times 10^{11} \text{ N/m}^2$$

E_y is Young's modulus, G is the shear modulus, and T is the temperature in Kelvin. At 300 K the value for E_y is 125 GPa and the value for G is 46.3 GPa. Both of these values agree with the measured values for V-5Cr-5Ti within the limits of error given by Farraro and McLellan [1, 2]. It is also apparent from the data of Farraro and McLellan that the moduli have a weak temperature dependence. Although a few high temperature measurements may be necessary, room temperature values are probably sufficient for most comparison studies and even most design studies. It is also apparent that the values are pure vanadium are very close to those of the alloy.

Conclusions

1. Linear thermal expansion

$$= DL/L_o = -179.97570689 + 9.0363848739\ T + 0.0015407532037\ T^2$$

where DL/L_o is the incremental thermal expansion in parts per million relative to the value at 20°C and T is the temperature in degrees Celsius.

2. Specific heat

$$= C_p = 0.57551 - 21.094/T \text{ J/g-K}$$

where C_p is the specific heat at constant pressure and T is the temperature in Kelvin.

3. Thermal conductivity

$$= k = 0.0086029\ T + 27.827 \text{ W/m-K}$$

where T is the temperature in Kelvin.

4. Elastic Constants

Young's Modulus
$=125.6 \pm 0.4$ GPa

Shear Modulus
$= 45.9 \pm 0.2$ GPa

Poisson's Ratio
$=0.367 \pm 0.001$

REFERENCES

1. R. J. Farraro and Rex B. McLellan, "High Temperature Elastic Properties of Polycrystalline Niobium, Tantalum, and Vanadium," Met Tran 10A (1979) 1699.

2 R. J. Farraro and Rex B. McLellan, "High Temperature Elastic Properties of Polycrystalline Niobium, Tantalum, and Vanadium," Met Trans 10A (1979) 1699.

Subtask 12D1: IMPACT PROPERTIES OF PRODUCTION HEAT OF V–4Cr–4Ti,

H. M. Chung, L. Nowicki, and D. L. Smith (Argonne National Laboratory)

OBJECTIVE

Following previous reports of excellent properties of a laboratory heat of V–4Cr–4Ti, the alloy identified as the primary vanadium–based candidate for application as fusion reactor structural components, a large production–scale (500–kg) heat of the alloy was fabricated successfully. Since impact toughness has been known to be most sensitive to alloy composition and microstructure, impact testing of the production–scale heat was conducted in this work between –200°C and +200°C.

SUMMARY

A 500-kg heat of V-4Cr-4Ti, an alloy identified previously as the primary vanadium–based candidate alloy for application as fusion reactor structural components, has been produced successfully. Impact tests were conducted at –196°C to 150°C on 1/3–size Charpy specimens of the scale–up heat in as–rolled condition and after annealing for 1 h at 950, 1000, and 1050°C in high–quality vacuum. The annealed material remained ductile at all test temperatures; the ductile–brittle transition temperature (DBTT) was lower than –200°C. The upper–shelf energy of the production–scale heat was similar to that of the laboratory–scale (≈30–kg) heat of V–4Cr–4Ti investigated previously. Effect of annealing temperature was not significant; however, annealing at 1000°C for 1 h not only produces best impact properties but also ensures a sufficient tolerance to effect of temperature inhomogeneity expected when annealing large components. Effect of notch geometry was also investigated on the production heat. When annealed properly (e.g., at 1000°C for 1 h), impact properties were not sensitive to notch geometry (45°–notch, root radius 0.25 mm; and 30°–notch, root radius 0.08 mm).

INTRODUCTION

To develop and identify an optimal vanadium–base alloy for application in fusion reactor first wall/blanket structures, extensive investigations were conducted earlier on the swelling behavior, tensile properties, creep strength, impact toughness, and microstructural stability of V-Ti, V-Cr-Ti, and V-Ti-Si alloys before and after irradiation by fast neutrons at 420°C–600°C. These investigations revealed that V-Cr-Ti alloys containing ≈4 wt.% Cr, ≈4 wt.% Ti, 400-1000 wt. ppm Si, and <1000 wt. ppm O+N+C were most desirable because they exhibit superior physical and mechanical properties.[1–5] These results were obtained, however, on laboratory–scale (<30–kg) heats, including a small heat (ANL ID BL–47) of V-4Cr-4Ti that exhibited excellent resistance to thermal creep,[4] irradiation–induced embrittlement,[1,2] swelling,[3,5] and helium embrittlement.[6–9] In this reporting period, a large (≈500–kg) industrial–scale heat of V–4Cr–4Ti (Heat ID #832665) was fabricated successfully in a joint effort between Argonne National Laboratory and Teledyne Wah Chang (Albany, Oregon) with the objective of demonstrating reliable industrial production of good–quality V–4Cr–4Ti.[10] This report describes results of metallographic examination and Charpy–impact testing of the 500–kg heat. The Charpy–impact test (at –196°C to 150°C) was chosen because it has been shown to be most sensitive to the quality of vanadium–base alloys.

EXPERIMENTAL PROCEDURE

Chemical composition of the 500–kg heat is given in Table 1. Also in the table is the chemical composition of the laboratory–scale heat of V–4Cr–4Ti (ANL ID BL–47) that was shown earlier to exhibit excellent properties.[1–9]

One–third–size Charpy specimens (3.33 x 3.33 x 25.4 mm) were machined from 3.81–mm–thick plates of the material, some of which had been annealed in factory for 2 h at a nominal temperature of ≈1050°C and some of which had been received in as–rolled (≈50% work at 400°C) condition. The Charpy specimens were machined so that the plane of crack

Table 1. Chemical composition (impurities in wppm) of industrial– (500 kg) and l laboratory–scale heats of V–4Cr–4Ti.

Heat ID	ANL ID	Heat Type	Cr	Ti	Cu	Si	O	N	C	S	P	Ca	Cl	Na	K	B
–	BL–47	laboratory 30 kg	4.1 wt.%	4.3 wt.%	6	870	350	220	200	20	<40	1	1	0.1	0.1	15
832665	BL–71	production 500 kg	3.8 wt.%	3.9 wt.%	<50	783	310	85	80	<10	<30	<10	<2	–	–	<5

propagation was perpendicular to rolling direction (i.e., the L–S direction in Fig. 1). To investigate the effect of notch geometry, two types of V–notch geometry were investigated; one with a 45° notch angle and 0.25–mm root radius and the other with a 30° angle and 0.08–mm root radius. Notch depth in both types of specimens was kept constant at 0.61 mm. The impact specimens machined from the factory–annealed plates were tested following a degassing heat treatment at 400°C for 1 h in vacuum,, a customary procedure used to expel hydrogen that could be picked up during specimen machining and preparation. To identify the optimal annealing condition, specimens machined from as–rolled (cross–rolled at 400°C)[10] plates were annealed at 950°C, 1000°C, and 1050°C for 1 h in a vacuum of ≈6 x 10^{-6} Pa prior to testing. Details of the drop–weight–type impact test have been described elsewhere.[2]

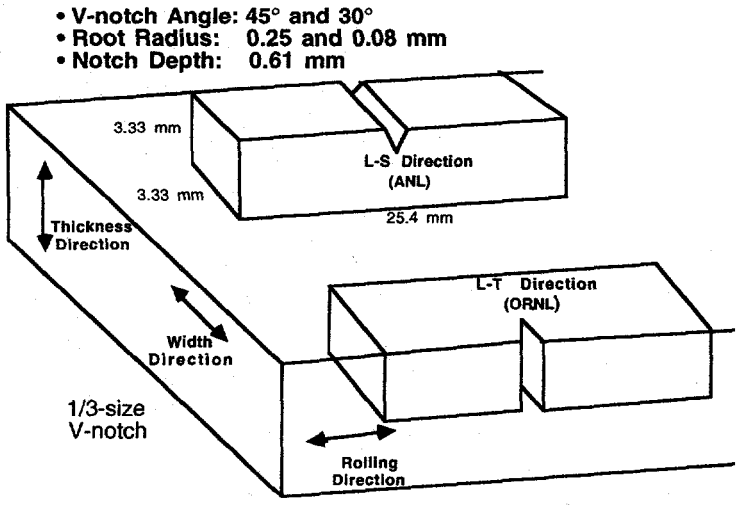

Fig. 1.

Orientation of Charpy impact specimens with respect to the plate rolling direction of production–scale heat of V–4Cr–4Ti

RESULTS AND DISCUSSION

Impact energies, measured on the 45°–notch (root radius 0.25 mm) Charpy specimens from the production–scale heat of V–4Cr–4Ti in as–rolled condition and after annealing for 1 h at 950, 1000 and 1050°C, are shown in Fig. 2 as a function of impact temperature. All specimens in the figure had the same geometry used in previous investigations, including the laboratory–scale (30–kg) heat of V–4Cr–4Ti (BL–47, Table 1).[2] From the results in the figure, the optimal annealing temperature appears to be ≈1000°C, the same as that found to produce minimum hardness in ≈85% cold–worked V–4Cr–4Ti (i.e., the 30–kg laboratory heat, BL–47, Table 1).[11] Results in Fig. 2 show that the impact properties of the production–scale heat are as good as those of the smaller laboratory heat, which was also vacuum–arc melted. The DBTT of the production heat is no higher than ≈–200°C, similar to that of the laboratory heat. To show a direct comparison, Charpy energies of the two heats are plotted in Fig. 3.

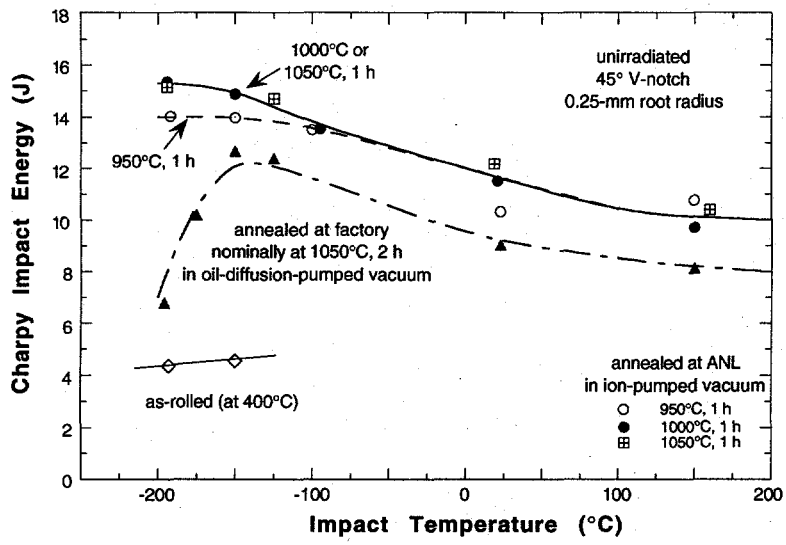

Fig. 2.

Charpy energy as function of impact temperature of production–scale heat of V–4Cr–4Ti after annealing for 1 h at 950, 1000, and 1050°C. Optimal annealing temperature is ≈1000°C.

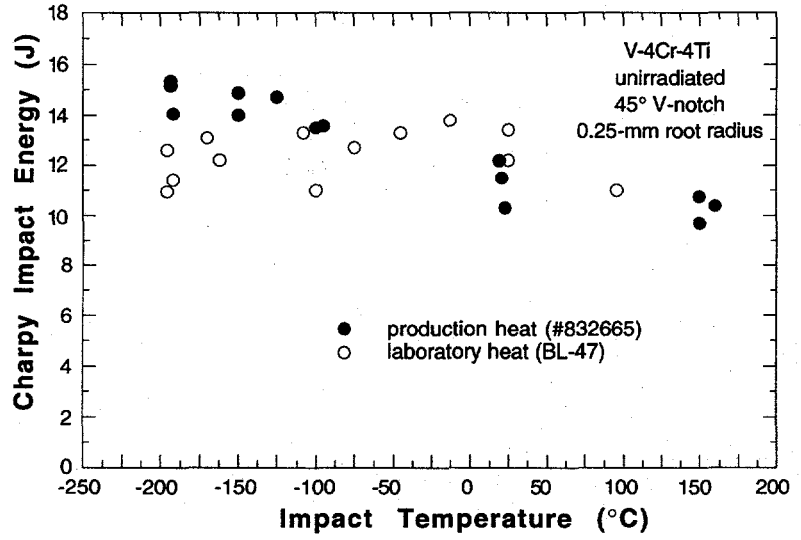

Fig. 3.

Comparison of impact properties of the production– and laboratory–scale heats of V–4Cr–4Ti.

Impact properties similar to those in Fig. 2 were determined also for 30°–notched specimens (root radius 0.08 mm). The results are shown in Fig. 4. Slight effects of notch geometry were observed only for specimens (average grain size ≈28 mm) annealed at a nominal temperature of 1050°C for 2 h in a vacuum of inferior quality (oil–diffusion pump) at factory (Teledyne Wah Chang). However, the 30°–notched specimens exhibited impact properties as excellent as those of the 45°–notched specimens (DBTT <–200°C) when annealed at 1000°C or 1050°C for 1 h in ion–pumped vacuum. In the direct comparisons shown in Fig. 5, the negligible effect of notch geometry of the properly annealed (1000°C or 1050°C for 1 h in high–quality vacuum) specimens is obvious.

Grain structures of the specimens annealed at 950, 1000, and 1050°C are shown in Fig. 6. The material annealed at factory at the nominal temperature of ≈1050°C (probably less accurate than the temperature of laboratory annealing) for 2 h was fully recrystallized, exhibiting an average grain size of ≈28 mm (Fig. 6A). The material annealed at 1050°C for 1 h in laboratory exhibited fully recrystallized grains of very fine size (Fig. 6B). In comparison, the material was recrystallized only ≈50% after annealing at 1000°C for 1 h (Fig. 6C). When annealed at 950°C for 1 h, only recovered structure was observed (Fig. 6D). When examined under polarized light, etched specimens of the alloy annealed at 950°C revealed what appears to be a lath–shaped, gold–colored secondary phase (the light–contrasted feature denoted by arrows in Fig. 6D). Volume fraction of the phase was negligible, however, when annealed at 1000°C (Fig. 6C). Although the nature of the phase could not be identified at this time, precipitation of the secondary phase does not appear to influence the impact properties significantly.

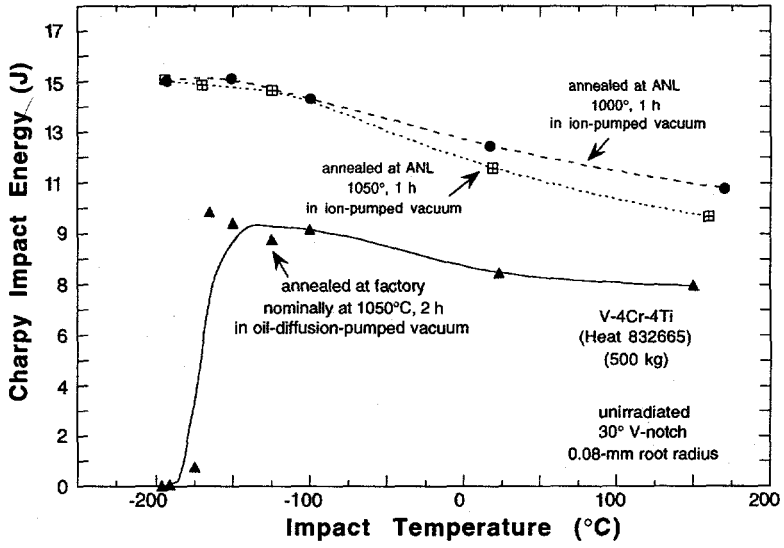

Fig. 4.

Effect of annealing on Charpy impact energy of 30°–notch specimen as function of temperature for the production–scale heat of V–4Cr–4Ti.

CONCLUSIONS

(1) Impact tests were conducted on production–scale (≈500-kg) heat of V-4Cr-4Ti at –196°C to 200°C. Results showed that the material remained ductile at –196°C and that the ductile–brittle transition temperature (DBTT) was no higher than –200°C. Upper–shelf energies of the production–scale heat were similar to those of the laboratory–scale heat.

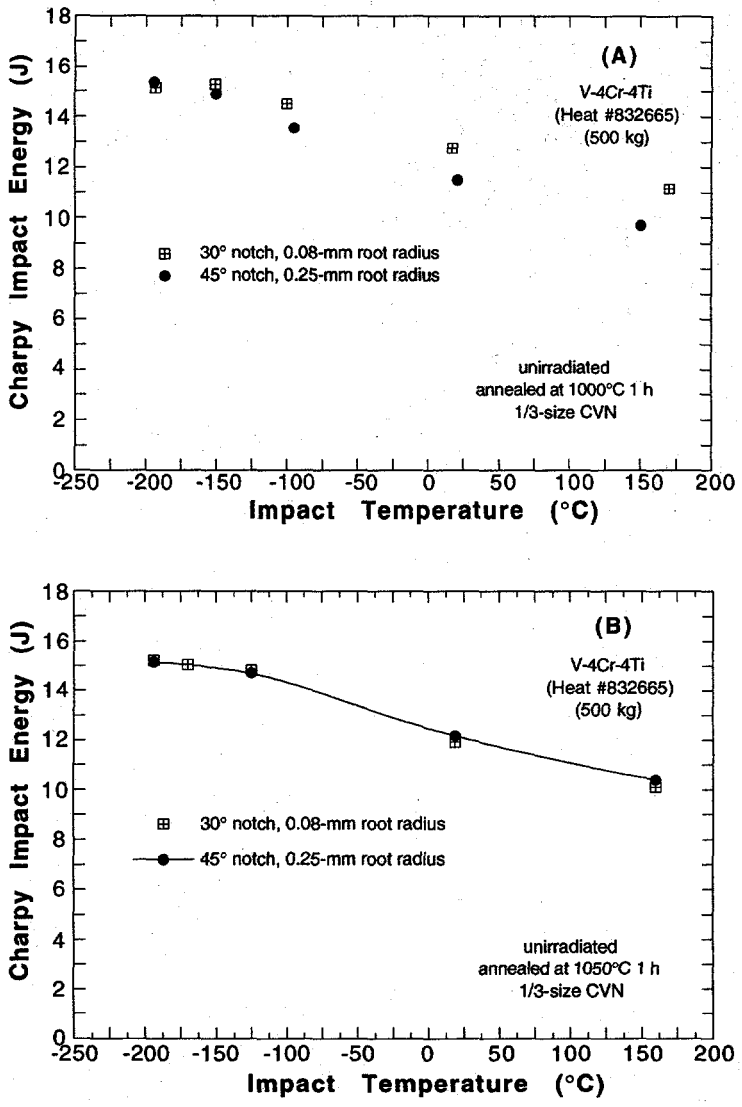

Fig. 5. Effects of notch geometry on impact properties of 500–kg V–4Cr–4Ti annealed at 1000°C (A) and 1050°C (B) for 1 h.

(2) Effect of annealing temperature (950°C–1050°C) on impact properties of the production–scale heat was not significant, a finding similar to that of the laboratory–scale heat. This is in contrast to the very significant effect of annealing temperature on the impact properties of one heat of V–5Cr–5Ti (Heat BL–63) produced by an incorrect process and found to exhibit inferior mechanical properties. Annealing at 1000°C for 1 h not only produces optimal impact properties in the production–scale heat but also provides sufficient tolerance to temperature inhomogeneity.

(3) When annealed properly (e.g., at 1000°C or 1050°C for 1 h), impact properties of the production–scale heat was not sensitive to notch geometry and excellent toughness was observed at >–200°C.

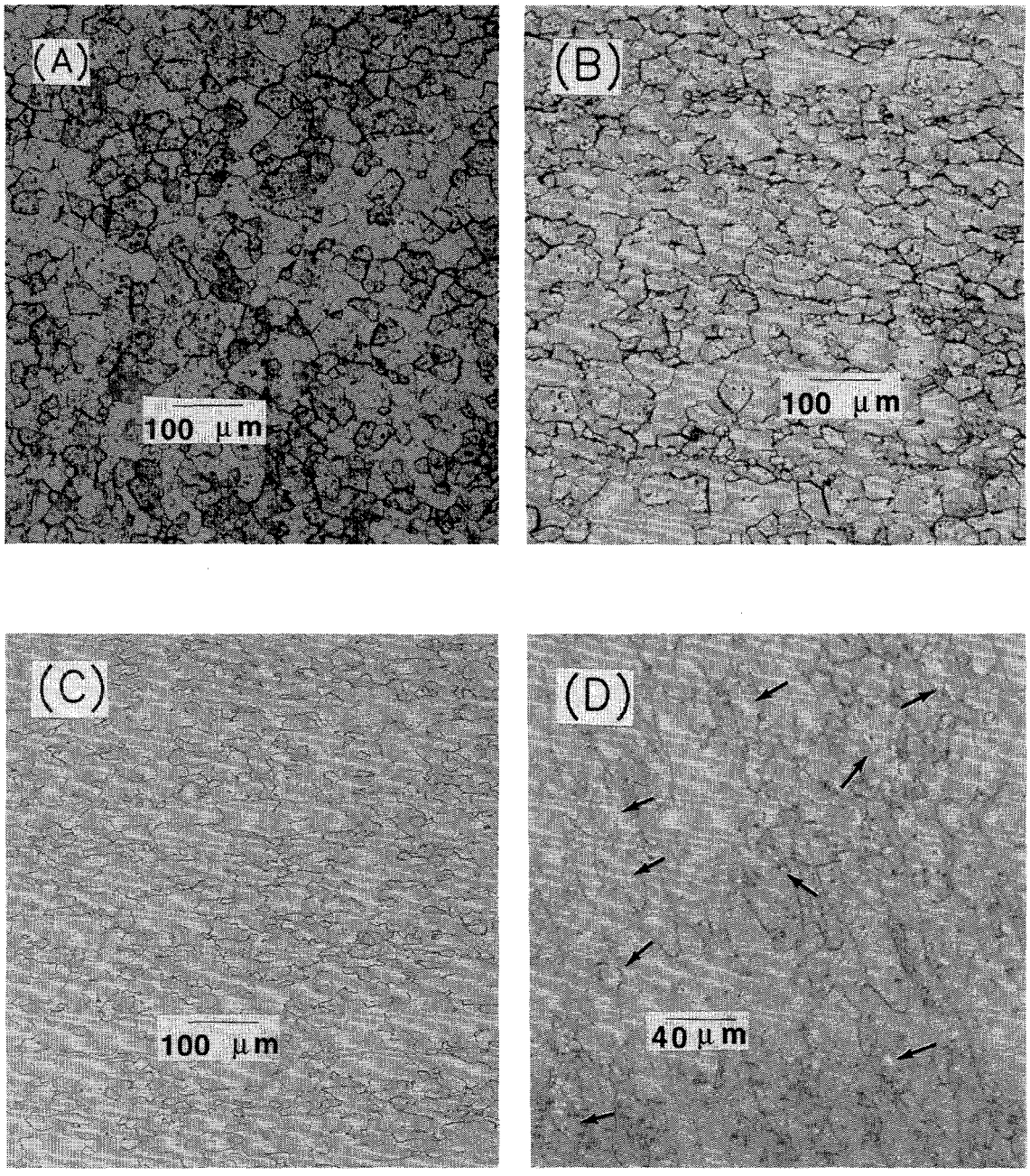

Fig. 6. Optical micrographs of production–scale heat of V–4Cr–4Ti annealed at (A) a nominal temperature of 1050°C for 2 h in factory; (B) 1050°C for 1 h in laboratory; (C) 1000°C for 1 h; and (D) 950°C for 1 h. Presence of second–phase precipitates is indicated by lath–like light–contrasted features denoted by arrows in (D).

REFERENCES

1. B. A. Loomis, L. Nowicki, and D. L. Smith, "Effect of Neutron Irradiation on Tensile Properties of V–Cr–Ti Alloys," in Fusion Reactor Materials, Semiannual. Prog. Report, DOE/ER-0313/15, Oak Ridge National Laboratory, Oak Ridge, TN (1994), pp. 219–222.
2. B. A. Loomis, H. M. Chung, L. Nowicki, and D. L. Smith, "Effects of Neutron Irradiation and Hydrogen on Ductile-Brittle Transition Temperatures of V–Cr–Ti Alloys," ibid., pp. 253–257.
3. H. M. Chung, B. A. Loomis, L. Nowicki, J. Gazda, and D. L. Smith, "Irradiation-Induced Density Change and Microstructural Evolution of Vanadium-Base Alloys," ibid., pp. 223–231.
4. H. M. Chung, B. A. Loomis, and D. L. Smith, "Thermal Creep Behavior of V–5Cr–5Ti and V–10Cr–5Ti Alloys," in Fusion Reactor Materials, Semiannual. Prog. Report, DOE/ER-0313/14, Oak Ridge National Laboratory, Oak Ridge, TN (1993), pp. 309-317.
5. H. M. Chung, B. A. Loomis, and D. L. Smith, in Effects of Radiation on Materials, ASTM-STP 1175, A. S. Kumar, D. S. Gelles, R. K. Nanstad, and T. A. Little, Eds., American Society for Testing and Materials, Philadelphia, 1993, pp. 1185–1200.
6. H. M. Chung, B. A. Loomis, and D. L. Smith, "Properties of V-4Cr-4Ti for Application as Fusion Reactor Structural Components," Proc. 3rd International Symposium on Fusion Nuclear Technology, June 27-July 1, 1994, Los Angeles, CA, in press.
7. H. M. Chung, B. A. Loomis, L. Nowicki, and D. L. Smith, "Effect of Dynamically Charged Helium on Tensile Properties of V–4Cr–4Ti," in this report.
8. H. M. Chung, L. J. Nowicki, D. E. Busch, and D. L. Smith, "Fracture Properties of V–4Cr–4Ti Irradiated in the Dynamic Helium Charging Experiment," in this report.
9. H. M. Chung, L. Nowicki, J. Gazda, and D. L. Smith, "Effects of Dynamically Charged Helium on Swelling and Microstructure of Vanadium-Base Alloys," in this report.
10. H. M. Chung, H.–C. Tsai, D. L. Smith, R. Peterson, C. Curtis, C . Wojcik, and R. Kinney, "Fabrication of Production–Scale Heat of V–4Cr–4Ti," in this report.
11. B. A. Loomis, "Recovery of Hardness of 85% Cold–Worked V–Ti and V–Cr–Ti Alloys on Annealing at 180°C to 1200°C," in Fusion Reactor Materials, Semiannual. Prog. Report for Period Ending September 30, 1994, DOE/ER-0313/17, Oak Ridge National Laboratory, Oak Ridge, in press.

Subtask 12D2: BASELINE IMPACT PROPERTIES OF VANADIUM ALLOYS, H. M. Chung, B. A. Loomis, and D. L. Smith (Argonne National Laboratory)

OBJECTIVE

The objective of this work is to determine the baseline impact properties of vanadium-base alloys as a function of compositional variables.

SUMMARY

Up–to–date results on impact properties of unirradiated V, V–Ti, V-Cr-Ti and V–Ti–Si alloys are presented and reviewed in this paper, with an emphasis on the most promising class of alloys, i.e., V–(4–5)Cr–(3–5)Ti containing 400–1000 wppm Si. Database on impact energy and ductile–brittle transition temperature (DBTT) has been established from Charpy impact tests on small laboratory as well as production–scale heats. DBTT is influenced most significantly by Cr contents and, to a lesser extent, by Ti contents of the alloys. When combined contents of Cr and Ti were ≤10 wt.%, V–Cr–Ti alloys exhibit excellent impact properties, i.e., DBTT<–200°C and upper shelf energies of ≈120–140 J/cm^2. Impact properties of the production–scale heat of the U.S. reference alloy V–4Cr–4Ti were as good as those of the laboratory–scale heats. Optimal impact properties of the reference alloy were obtained after annealing the as–rolled products at 1000°C–1050°C for 1–2 h in high–quality vacuum.

INTRODUCTION

Vanadium-base alloys have significant advantages over other candidate alloys (such as austenitic and ferritic steels) for use as first wall and blanket structural materials in fusion devices, e.g., the International Thermonuclear Experimental Reactor (ITER) and magnetic fusion reactors.[1–5] As part of a program to screen candidate alloys and develop an optimal alloy, extensive investigations have been conducted on the swelling behavior, tensile properties, impact toughness, and microstructural evolution of V, V-Ti, V-Cr, V-Cr-Ti, and V-Ti-Si alloys after irradiation to ≈120 dpa by fast neutrons at 420°C to 600°C.[6–15]

These investigations indicated that V-Cr-Ti alloys containing 4–5 wt.% Cr, 3-5 at.% Ti, 400-1000 wt. ppm Si, and <1000 wt. ppm O+N+C were most desirable because they exhibit superior resistance to swelling, neutron displacement damage, helium embrittlement, and hydrogen-induced effects during fast-neutron irradiation in lithium.[15] V–(4–5)Cr–(4–5)Ti alloys exhibited in particular excellent baseline impact behavior and superior resistance to irradiation embrittlement, which cannot be matched by other candidate materials such as ferritic/martensitic alloys. This paper presents an overview of baseline impact properties of unirradiated V, V–Ti, V-Cr-Ti and V–Ti–Si alloys, with an emphasis on up–to–dated database on impact energy and ductile–brittle transition temperature (DBTT) obtained on several laboratory– and production–scale heats of the most promising class of alloys V–(4–5)Cr–(3–5)Ti.

MATERIALS AND TEST PROCEDURES

The elemental composition of the alloys is given in Table 1. Typically, the alloy ingots were melted from low–chlorine titanium and low–impurity vanadium raw materials. Then the stainless–steel–clad ingot was extruded at 1150°C and annealed at 1050°C several times after 8–10 passes of warm rolling (at 400°C) between the anneals. Final forms of

the product were as–rolled plates and sheets 28.6–, 12.7–, 6.3–, 3.8–, 1.0–, and 0.5–mm in thickness.

Out of the 3.8–mm–thick alloy plates, Charpy–impact specimens were machined, cleaned, and annealed at high temperatures before testing. Typical test specimens were annealed at 1000–1125°C for 1 h in high–quality vacuum (in an ion–pumped system). Orientation of Charpy–impact specimens, relative to rolling direction of the 3.8–mm–thick plates, is illustrated in Fig. 1. Dimensions of the 45°– or 30°–V–notched specimens are summarized in Table 2. Most of the specimens were 45°–notched specimens, with a notch depth of 0.61 mm and a root radius of 0.25 mm.

RESULTS AND DISCUSSION

Examples of baseline impact data are shown in Figs. 2–5 for four types of alloy classes, i.e., unalloyed V and V–3Ti–1Si, V–Ti binary alloys, high–Cr ternary alloys V–(9–15)Cr–5Ti, and low–Cr ternary alloys V–(4–5)Cr–(4–5)Ti, respectively. Charpy impact energies were measured for these alloys between –196°C and 250°C by instrumented drop–weight machine.

Except for one heat of unalloyed V (BL–51) and the high–Cr ternary alloys V–(9–15)Cr–5Ti, all the alloys given in Figs. 2–5 exhibit ductile behavior at temperature as low as –196°C. In a previous report, it has been shown that the unalloyed vanadium heat (BL–51) contained very fine coherent precipitates of calcium vanadates in high density, which was suspected to be associated with the unusually high DBTT (–150°C) of the raw vanadium.[16] In contrast to this heat, another heat of unalloyed vanadium (Heat #832630, Table 1) was found to exhibit DBTT <–196°C, similar to those of the binary V–Ti (Fig. 3) and low–Cr ternary alloys of V–(4–5)Cr–(4–5)Ti (Fig. 5).

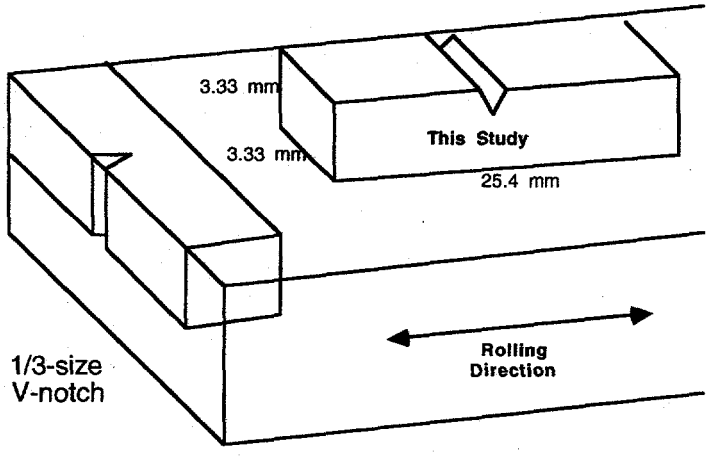

- **V-notch Angle: 45° and 30°**
- **Root Radius: 0.25 and 0.08 mm**
- **Notch Depth: 0.61 mm**

Fig. 1.

Orientation of Charpy–impact specimens tested in this study relative to rolling direction of the 3.8–mm–thick alloy plates.

Table 1. Chemical Composition of Vanadium–Base Alloys

ANL ID	Alloy Composition (wt.%)	Impurity Concentration (wt. ppm) O	N	C	Si
BL-19	V	1101	161	360	–
BL-20	V	570	110	120	325
BL-36	V	810	86	250	<50
BL-51	V	570	49	56	370
820630	V	200	62	75	780
BL-35	9.5Cr	340	45	120	<50
BL-4	10.0Cr	530	76	240	<50
BL-5	14.1Cr	330	69	200	<50
BL-50	1.0Ti	230	130	235	1050
BL-52	3.1Ti	210	310	300	500
BL-46	4.6Ti	305	53	85	160
BL-11	4.9Ti	1820	530	470	220
BL-34	8.6Ti	990	180	420	290
BL-12	9.8Ti	1670	390	450	245
BL-13	14.4Ti	1580	370	440	205
BL-15[a]	17.7Ti	830	160	380	480
BL-16	20.4Ti	390	530	210	480
BL-10	7.2Cr-14.5Ti	1110	250	400	400
BL-21	13.7Cr-4.8Ti	340	510	180	1150
BL-22	13.4Cr-5.1Ti	300	52	150	56
BL-23	12.9Cr-5.9Ti	400	490	280	1230
BL-24	13.5Cr–5.2Ti	1190	360	500	390
BL-25	14.4Cr-0.3Ti	390	64	120	<50
BL-26	14.1Cr-1.0Ti	560	86	140	<50
BL-40	10.9Cr-5.0Ti	470	80	90	270
BL-41	14.5Cr-5.0Ti	450	120	93	390
BL-43	9.2Cr-4.9Ti	230	31	100	340
BL-44	9.9Cr-9.2Ti	300	87	150	270
BL-49	7.9Cr-5.7Ti	400	150	127	360
BL-62	3.1Ti–0.1Si	320	86	109	660
BL-27	3.1Ti–0.25Si	210	310	310	2500
BL-42	3.1Ti–0.5Si	580	190	140	5400
BL-45	2.5Ti-1Si	345	125	90	9900
BL-47	4.1Cr-4.3Ti	350	220	200	870
832665	3.8Cr–3.9Ti	310	85	80	783
T87	4.9Cr–5.1Ti	380	89	109	545

Table 2. Summary of the Dimensions (in mm) of Subsize Charpy–Impact Specimens

Type	Length	Thickness	Width	Notch Depth	V–Notch Angle	Root Radius
Charpy–45	25.4	3.33	3.33	0.61	45°	0.25
Charpy –30	25.4	3.33	3.33	0.61	30°	0.08

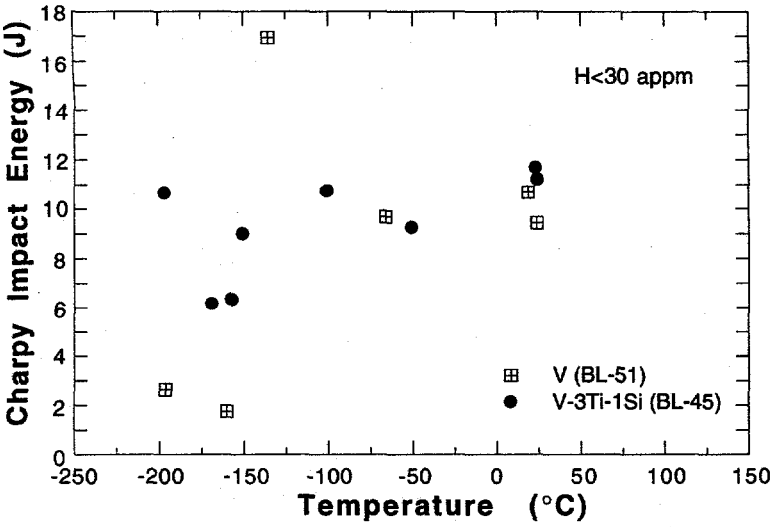

Fig. 2.

Impact properties of unalloyed V and V–3Ti–1Si.

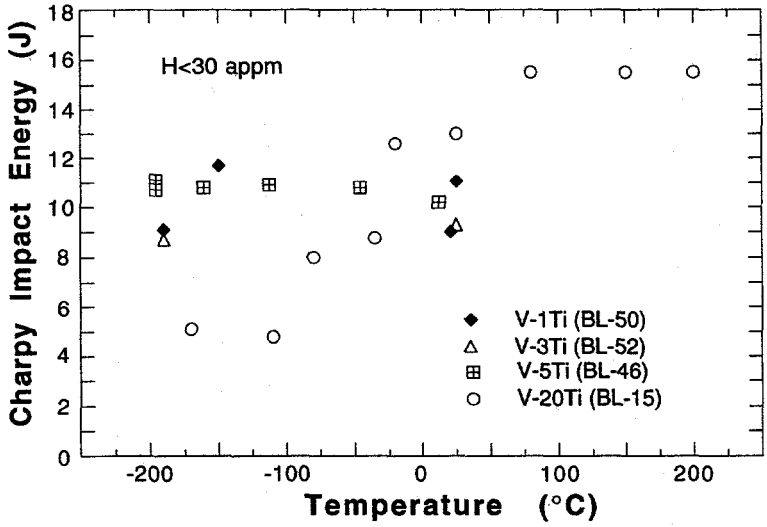

Fig. 3.

Impact properties of V–Ti Alloys

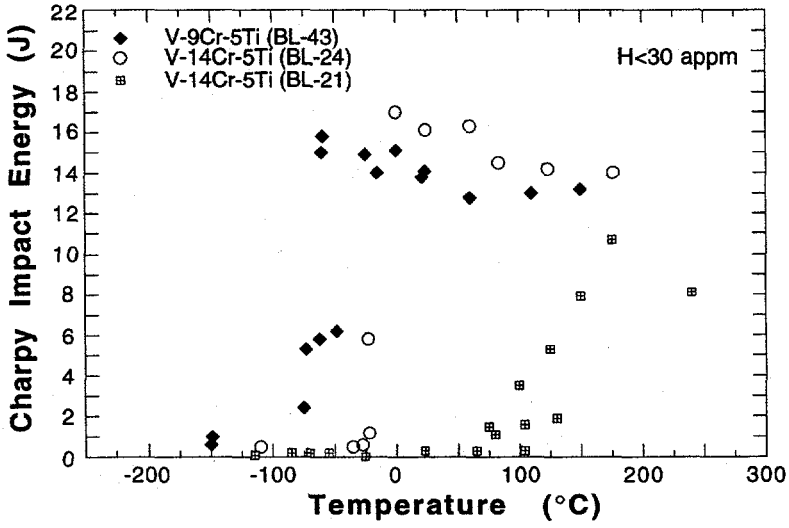

Fig. 4.

Impact properties of high–Cr ternary alloys V–(9–15)Cr–5Ti.

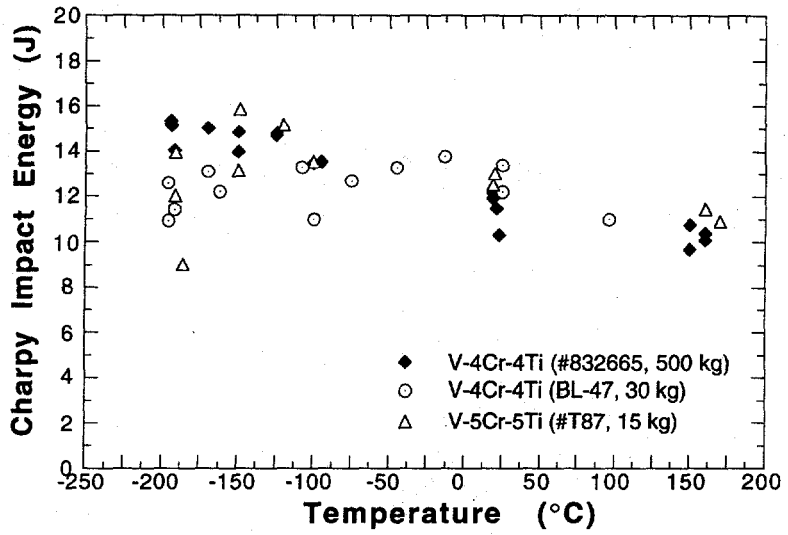

Fig. 5.

Impact properties of low–Cr ternary alloys V–(4–5)Cr–(4–5)Ti.

The 500–kg production–scale and 30–kg laboratory heats of the U.S. reference alloy V–4Cr–4Ti exhibited excellent impact properties; DBTT was no higher than –200°C and impact energies were greater than ≈10 J at all test temperatures (Fig. 5). The impact properties of the 15–kg laboratory heat (#T87, Table 1) of V–5Cr–5Ti were equally excellent. All of these heats were fabricated using high–purity raw materials of Ti and V according to proven procedures.[17] The excellent properties of these heats are drastically superior to those of some of the non prototypic heats of V–5Cr–3Ti and V–5Cr–5Ti that were melted using inferior raw materials, fabricated by incorrect procedures, and annealed at wrong temperatures.[16,17]

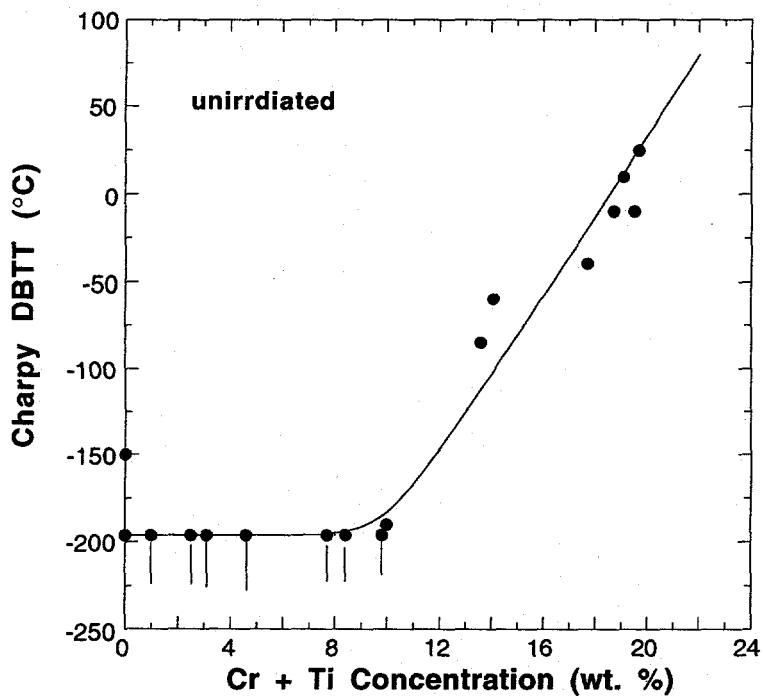

Fig. 6.

DBTT as a function of combined Cr and Ti contents measured on one–third–size Charpy specimens of V, V–Ti, V–Ti–Si, and V–Cr–Ti alloys.

In Fig. 6, DBTTs of all the tested V, V–Ti, V–Ti–Si, and V–Cr–Ti alloys are plotted as a function of combined concentrations of Cr and Ti. A good correlation is evident between DBTT and combined contents of Cr and Ti. The figure also demonstrates that excellent impact properties can be obtained by limiting combined contents of Cr and Ti to ≤10 wt.% (e.g., as in the U. S. reference alloy V–4Cr–4Ti).

CONCLUSIONS

(1) Impact tests were conducted on V, V–Ti, V–Ti–Si, and V-Cr-Ti alloys at –196°C to 250°C. Results showed that most of the low–Cr alloys remained ductile at temperatures as low as –196°C and that absorbed energies from one–third–size Charpy specimens were greater than ≈10 J for all the test temperatures. High–Cr alloys such as V–(9–15)Cr–5Ti exhibited unacceptably high DBTT.

(2) A good correlation is observed between DBTT and combined contents of Cr and Ti. To assure excellent impact properties in V–Cr–Ti alloys, combined contents of Cr and Ti must be limited to ≤10 wt.% (e.g., as in the U. S. reference alloy V–4Cr–4Ti).

(3) Impact properties of the production–scale and laboratory heats of V–4Cr–4Ti and V–5Cr–5Ti alloys were equally excellent, that is, DBTT <–200°C, upper–shelf energies ≈120–140 J/cm^{-2}, and good tolerance to notch geometry.

REFERENCES

1. T. Noda, F. Abe, H. Araki, and M. Okada, J. Nucl. Mater. 155-157 (1988) 581.
2. R. Santos, J. Nucl. Mater. 155-157 (1988) 589.
3. S. J. Piet, et al., J. Nucl. Mater. 141-143 (1986) 24.
4. F. L. Yaggee, E. R. Gilbert, and J. W. Styles, J. Less-Comm. Met. 19 (1969) 39.
5. D. L. Smith, B. A. Loomis, and D. R. Diercks, J. Nucl. Mater. 135 (1985) 125.
6. H. M. Chung and D. L. Smith, J. Nucl. Mater. 191–194 (1992) 942–947.
7. H. M. Chung, B. A. Loomis, and D. L. Smith, ASTM STP 1175, American Society for Testing and Materials, Philadelphia, 1993, pp. 1185–1200.
8. D. L. Smith, B. A. Loomis, and H. M. Chung, Plasma Devices and Operations, Vol. 3, 1994, pp. 167–179.
9. B. A. Loomis, L. Nowicki, and D. L. Smith, J. Nucl. Mater. 212–215 (1994) 790.
10. B. A. Loomis, H. M. Chung, L. Nowicki, and D. L. Smith, J. Nucl. Mater. 212–215 (1994) 799.
11. H. M. Chung, B. A. Loomis, and D. L. Smith, J. Nucl. Mater. 212–215 (1994) 772.
12. H. M. Chung, B. A. Loomis, and D. L. Smith, J. Nucl. Mater. 212–215 (1994) 804.
13. H. M. Chung, B. A. Loomis, and D. L. Smith, "Effect of Dynamically Charged Helium on Mechanical Properties of Vanadium-Base Alloys," Proc. 17th Symposium on Effects of Radiation on Materials, June 20-23, 1994, Sun Valley, Idaho, in press.
14. H. M. Chung, B. A. Loomis, and D. L. Smith, "Swelling and Structure of Vanadium-Base Alloys Irradiated in The Dynamic Helium Charging Experiment," Proc. 17th Symposium on Effects of Radiation on Materials, June 20-23, 1994, Sun Valley, Idaho, in press.

15. H. M. Chung, B. A. Loomis, and D. L. Smith, "Properties of V-4Cr-4Ti: A Promising Alloy for Fusion Reactor Structural Components," Proc. Third International Symposium on Fusion Nuclear Technology, June 27-July 1, 1994, Los Angeles, in press.

16. H. M. Chung, J. Gazda, L. Nowicki, J. E. Sanecki, and D. L. Smith, "Effects of Fabrication Variables on Impact Properties and Microstructure of V–Cr–Ti Alloys," in Fusion Reactor Materials, Semiannual. Prog. Report, DOE/ER-0313/15, Oak Ridge National Laboratory, Oak Ridge, TN (1994), pp. 207–218.

17. H. M. Chung, H.–C. Tsai, and D. L. Smith, "Fabrication of Production–Scale Heat of V-4Cr-4Ti," in this report.

Subtask 12D3: FRACTURE PROPERTIES OF V-5Cr-5Ti ALLOY, H. Li, M. L. Hamilton, and R. H. Jones (Pacific Northwest Laboratory)

OBJECTIVE

The purpose of this research is to investigate the effect of heat treatment on microstructure and fracture toughness of a V-5Cr-5Ti alloy in the range -50-100°C.

SUMMARY

Fracture toughness and impact tests were performed on a V-5Cr-5Ti alloy. Specimens annealed at 1125°C for 1 h and furnace cooled in a vacuum of 1.33×10^{-5} Pa were brittle at room temperature (RT) and experienced a mixture of intergranular and cleavage fracture. Fracture toughness (J_{1Q}) at RT was 52 kJ/m^2 and the impact fracture energy (IFE) was 6 J. The IFE at -100°C was only 1 J. While specimens exhibited high fracture toughness at 100°C (J_{IQ} is 485 kJ/m^2), fracture was a mixture of dimple and intergranular failure, with intergranular fracture making up 40% of the total fracture surface. The ductile to brittle transition temperature (DBTT) was estimated to be about 20°C. When some specimens were given an additional annealing at 890°C for 24 h, they became very ductile at RT and fractured by microvoid coalescence. The J_{IQ} value increased from 52 kJ/m^2 to ~1100 kJ/m^2. The impact test failed to fracture specimens at RT due to a large amount of plastic deformation.

Effect of Heat Treatment on Grain Boundary Microchemistry and Precipitate Density

A 6.35 mm thick plate of V-5Cr-5Ti (Heat No. BL-63) was utilized for characterizing the fracture toughness and Charpy impact properties. The chemical composition of the plate is given in Table 1.

Table 1. Composition of 6.35 mm V-5Cr-5Ti Alloy Plate (Heat No. BL-63).

Composition in ppm unless noted, balance Vanadium								
Al	B	C	Cr	Fe	H	Hf	Mo	Ni
200	<5	73	4.6%	<370	NA	NA	500	NA
Nb	O	P	S	Si	Ta	Ti	U	Zr
<50	<5	<30	NA	310	-	5.1%	<1	NA

In order to gain more information about the effect of heat treatment on grain size, grain boundary microchemistry, and number of precipitates the following heat treatments were performed.

(1) 1125°C / 1 h/ furnace cooled (FC) (HT1);
(2) HT1 plus 890°C / 24 h/ FC (HT2);
(3) 1050°C / 1 h/ FC (HT3);
(4) HT3 plus 890°C / 24 h/ FC (HT4);
(5) HT3 plus 730°C / 24 h/ FC (HT5).

All of the heat treatments were conducted in a vacuum of 1.33×10^{-5} Pa. Grain boundary microchemistry was determined by means of a scanning Auger electron spectrometer

(AES). Specimens were cooled with liquid nitrogen and fractured in the AES chamber in a vacuum of 1 X 10^{-7} Pa or better. All specimens, except for those heat treated using HT1, were hydrogen charged in order to obtain intergranular facets.

AES analysis of more than 40 intergranular facets in two specimens heat treated using HT1 showed significant enrichment of S (6 at%), as compared to 0.3 at% on cleavage facets. The specimens treated using HT3 displayed improved ductility and fractured in the AES by microvoid coalescence (MVC). AES analysis showed that the sulfur concentration on grain boundary facets (more than 20 facets) was 2 at%, three times less than that in the specimens treated by HT1. The effect of heat treatment on grain size, grain boundary chemistry, and number of precipitates is summarized in Table 2. The P, O, N, and C concentrations were also investigated with AES, but their concentrations did not vary significantly with heat treatment, so only S was listed in Table 2. From Table 2, it is evident that HT2 gives the second lowest grain boundary S concentration, HT1 gives the highest. The HT2 treatment also produced significantly more second phase precipitates than HT1, as determined by optical metallography. However, the grain sizes were almost same in the specimens treated using either HT1 or HT2. Therefore, HT1 and HT2 were chosen to investigate the effect of grain boundary S and number of precipitates on the fracture properties of V-5Cr-5Ti.

Table 2. Effect of Heat Treatment on Grain Size, Grain Boundary Sulfur Concentration and Number of Precipitates.

Heat Treatment	Grain Size, &m	Grain Boundary Sulfur Conc., at%	Number of Precipitates
As-received	37	-	some
HT1*	45	6.0	few
HT1	48	6.0	few
HT2	45	0.9	many
HT3	40	2.0	some
HT4	-	0.5	-
HT5	-	1.5	-

*Heat treated at Oak Ridge National Laboratory, the temperature may have been 1150%C as indicated by the plastic bag containing the specimens.

Effect of Temperature and Grain Boundary Microchemistry on Fracture Properties

The fracture toughness of V-5Cr-5Ti was determined at -50°C, room temperature (RT), and 100°C. Fracture toughness was determined by the J-test method for an HT1 specimen at 100%C and an HT2 specimen at RT. Fracture toughness was measured using the K-test method for an HT1 specimen at RT and for an HT2 specimen at -50°C. The K_{IQ} values were then converted to J_{IQ} values. The specimens used for fracture toughness and impact tests were machined in the T-L orientation. ASTM E813-89 was followed to determine critical J-integral (J_{IQ}) and ASTM E399-90 was used to determine the critical stress intensity factor (K_{IQ}). The subscript "Q" is used because our specimens did not always satisfy plane strain size requirements. Mechanical properties for another heat of V-5Cr-5Ti (BL-47) were used for determination of J_{IQ}. These data were provided by Loomis [1] and given in Table 3. The fracture surfaces of all specimens were examined in a scanning electron microscope.

Table 3 Room Temperature Mechanical Properties of V-5Cr-5Ti (Heat No. BL-47)

Test Temperature, °C	Yield Strength, MPa	Ultimate Tensile Strength, MPa	Elongation, %
25	387	454	34
100	325	420	33

Charpy V impact specimens of 23.6 x 3.33 x 3.33 mm (1/3 scaled) were tested in the range of -115°C to 90°C to estimate the ductile-to-brittle-transition-temperature (DBTT).

Specimens heat treated using HT1 were brittle at RT and below. They fractured with a mixture of intergranular and cleavage failure. Cleavage facets initiated at grain boundaries and passed through the entire grain. J_{IQ} at RT was 52 kJ/m^2. When tested at 100°C, specimens were ductile and exhibited stable crack growth. J_{IQ} was about 485 kJ/m^2 and the tearing modulus was 250 mJ/m^3. Despite the high J_{IQ} value at 100%C, the fracture surface consisted of intergranular and MVC features. The intergranular portion makes up about 40% of the total fracture surface. However, it was evident that the grains experienced a large amount of plastic deformation before fracturing along the grain boundaries, giving high fracture toughness. The Charpy impact fracture energy was 0.4 J at RT. The DBTT was estimated to be greater than 20°C.

Specimens heat treated using HT2 were very ductile at RT and fractured by MVC during J-integral testing. The specimens were so ductile that a complete J-R curve could not be constructed with the specimen geometry used. The J_{IQ} estimated from the partial J-R curve was about 1100 kJ/m^2. The fracture toughness was also very sensitive to temperature. J_{IQ} at -50°C was only 45 kJ/m^2. The fracture mode also changed to cleavage fracture. Charpy testing at RT failed to cause fracture (two specimens) due to a high level of plastic deformation. Therefore, the Charpy energy could not be determined. The Charpy energy was about 4 J at -115°C, and 0.5 J at -195°C. The DBTT was estimated to be less than -100°C. The effects of heat treatment and temperature on the fracture properties of V-5Cr-5Ti are summarized in Table 4.

The brittleness of HT1 specimens seems to be due to low grain boundary fracture strength. The relatively large proportion of intergranular fracture at both RT and 100%C indicates the grain boundary cohesive strength of HT1 specimens is low. The most plausible explanation for this observation is segregation of impurities (such as sulfur, phosphorous etc.) and/or precipitation of second phase particles to the grain boundaries. TEM analysis [2] revealed precipitation of Ti(O,C,N) on grain boundaries, and Auger electron spectroscopy analysis showed a significant enrichment of sulfur on grain boundaries in an HT1 specimen. Jones [3] showed that sulfur segregation to grain boundaries can reduce the grain boundary cohesive strength in steels and nickel.

Table 4 *Effect of Heat Treatment and Test Temperature on FractureToughness*

	Test Temperature		
Heat Treatment	-50°C	RT	100°C
HT1	-	52*	485
HT2	45	~1100	-

*All values in kJ/m^2.

Effect of Loading Mode on V-5Cr-5Ti Fracture Toughness

Traditionally, mode I loading conditions have been used to study the linear-elastic and elastic-plastic fracture behavior of materials. However, in recent years, mixed-mode fracture has become the focus of many studies because many observed failures included shear components. The fracture behavior of many materials may be a function of loading mode, depending on the microstructure, strength, and toughness level of the material.

Modified compact tension (MCT) specimens were machined from the 6.35 mm thick plate of V-5Cr-5Ti (Heat No. BL-63). All specimens were T-L orientation and given an HT1 heat treatment. The geometry of the MCT specimens is similar to a conventional compact tension specimen except that the crack-plane is slanted at an angle relative to the load-line. The magnitude of mode III components can be varied by changing the crack-plane slant angle. A 0° angle represents pure mode I loading and the specimen geometry is equivalent to the standard compact-tension specimen. As slant angle increases, the mode III loading component increases. The slant angles used in this study were 0°, 15°, and 45°. Specimens were side-grooved 20% to increase crack tip stress triaxiality at the specimen surfaces. Side-grooving helped to constrain the advancing crack to the original crack plane. An electric discharge machine (EDM) was used to make thin cuts with a radius of about 0.051 mm and a length of approximately 1.3 mm. The cuts were used as a substitute for fatigue precracking (PFC) because a PFC tends to grow out of the original crack plane in mixed-mode specimens. The EDM cuts were made before final heat-treatment.

The critical mode I and mode III J components (J_{iQ} and J_{iiiQ}) in mixed-mode specimens were calculated in terms of the corresponding resolved loads and displacements. The calculations of resolved mode I and mode III load and displacement and the determinations of J_{iQ} and J_{iiiQ} have been reported in detail in References 4-6.

Due to the brittleness and unstable crack growth of the V-5Cr-5Ti alloy at RT, J_{MQ} could not be determined by ASTM E813-89. Therefore, J_{MQ} values at RT were calculated from K-test results. K-tests were performed at RT by following the procedure specified in ASTM E399-90. Due to the shortage of material, the unbroken J specimens tested at 100°C were used for K testing. After finishing a J test at 100°C and cooling the specimens down to RT, the specimens were fatigue precracked at RT for a length of 0.5 to 1 mm. The J_{MQ} data at RT reported here might differ from those measured with a standard specimen because the specimens were previously deformed during J testing at 100°C and the ratios of crack length to specimen width were greater than 0.7.

The dependence of J_{MQ} on slant angle and test temperature is shown in Figure 1. In the limit of 0° slant angle, J_{MQ} is equal to J_{IQ}, while for other slant angles, J_{MQ} represents the total critical J values under mixed-mode I/III loading. Each of the data points in Figure 1 was obtained from a single specimen. Room temperature fracture toughness data from F-82H steel are included in Figure 1 for comparison. From Figure 1 it can be seen that the J_{MQ} of V-5Cr-5Ti at 100%C are comparable to F-82H steel at RT. The effect of mixed mode I/III loading on J_{MQ} is similar to that of F-82H steel. Introduction of a shear loading component decreased the fracture toughness of V-5Cr-5Ti considerably from pure mode I loading. For example, J_{IQ} at 100°C is about 470 kJ/m^2, but the J_{MQ} at a slant angle of 45° decreased to 180 kJ/m^2. At RT the fracture toughness of V-5Cr-5Ti was low and only weakly dependent on slant angle. The J_{MQ} varied from 61 to 43 kJ/m^2 when slant angle ranged from 0% (mode I) to 45°.

Fractographic examination revealed that the crack fronts of all specimens remained in their initial orientation during J testing at 100°C and K testing at RT. At 100°C all specimens (regardless of slant angle) fractured with a mixture of MVC and intergranular failure. However, the morphology of the fracture surface varied with crack extension during J testing. The fracture surface near the initial crack tip (the EDM cut tip) exhibited more MVC fracture than that close to the final crack tip. The fracture surface near the EDM cut tip is dominated with MVC fracture plus small amount of intergranular facets. As the crack propagated, intergranular fracture increased and MVC fracture decreased. Examination of the fracture surface near the final crack tip revealed that while a large portion of the fracture surface was intergranular, the grains were heavily deformed and there were a lot of slip bands on the intergranular facets. Therefore, although the V-5Cr-5Ti exhibited partially intergranular fracture at 100°C during J testing, its fracture toughness was still high. At RT the V-5Cr-5Ti fractured primarily with a mixture of intergranular, cleavage and some MVC. Some cleavage facets apparently initiated at grain boundaries and propagated through adjacent grains. The tendency of V-5Cr-5Ti for intergranular fracture at both RT and 100°C indicates that the grain boundary cohesive strength is low. The fracture data and fracture morphology at RT and 100°C indicate the DBTT of HT1 specimens is above RT, which is consistent with the present Charpy impact results and also those obtained by Hamilton, et. al. [7], and by Grossbeck, et. al. [2].

Dislocation Development in Pure Vanadium and V-5Cr-5Ti

Efforts to determine the fracture behavior of V-5Cr-5Ti suggest this material may be notch sensitive. Charpy impact specimens tested with a range of notch root radii showed that V-5Cr-5Ti may have higher notch sensitivity than ferritic steels. Microstructural examinations were completed on deformed tensile specimens of pure vanadium and V-5Cr-5Ti to determine if differences in microscopic plastic deformation characteristics can account for the notch sensitivity observed in V-5Cr-5Ti.

Pure vanadium sheet 1.44 mm in thickness was provided by Teledyne Wah Chang, Albany, Oregon. Composition information for the pure vanadium is given in Table 5. One millimeter thick V-5Cr-5Ti sheet from heat BL-63 (see Table 1 for composition) was also produced by Teledyne Wah Chang. Specimens to SS-3 specifications with a gauge section 1.52 x 0.76 x 7.62 mm in length were machined from the sheet, etched in 10% hydrofluoric acid and 30% nitric acid in water, and annealed for one hour at 1125°C. During heat treatment, they were wrapped in tantalum foil in a vacuum below 10^{-5} Pa.

Table 5. Composition of pure vanadium as supplied by Teledyne Wah Chang.

Composition in ppm unless noted, balance Vanadium								
Al	B	C	Cr	Fe	H	Hf	Mo	Ni
<300	<10	<100	<20	<200	<5	<100	<200	<20
Nb	O	P	S	Si	Ta	Ti	U	Zr
<250	<400	<100	<20	<400	<300	<50	<2	<100

Tensile specimens were deformed to 5% strain at a strain rate of 1.1×10^{-3} s^{-1} at room temperature. The gauge section was cut into 3 mm sections. Specimens were prepared for transmission electron microscopy using a Tenupol twin jet electropolishing device with a solution of 5% sulfuric acid in methanol at 40 V and moderate pump speed.

Microstructural examinations used a JEM 1200EX transmission electron microscope equipped with a double tilting goniometer stage. Procedures involved a series of dislocation imaging conditions using $P_g = 200$ as a stereo pair, $01\bar{1}$, $21\bar{1}$, $2\bar{1}1$, $1\bar{2}1$, $12\bar{1}$, and $\bar{1}10$, (or the equivalent) for a foil near an [011] orientation.

The load-elongation response for pure vanadium strained to 5% exhibited yield drop behavior. The upper yield strength was 410 MPa, and the tensile strength at 5% strain was 436 MPa. A similar response was observed for V-5Cr-5Ti with a slightly higher yield strength, but no yield drop and a lower work hardening rate. The yield strength was 421 MPa and the tensile strength at 5% strain was 507 MPa.

Dislocation development as a result of 5% deformation at room temperature was found to differ as a function of alloying. Pure vanadium developed a complex dislocation structure typical of Stage III deformation (forest dislocation development) with large spaces between tangles, whereas V-5Cr-5Ti dislocation structures were less complicated but more uniformly distributed, often containing long straight dislocations typical of Stage II. Both materials also showed dislocation loop formation with loop sizes on the order of 10 nm in diameter. Slip band orientations could not be identified based on stereoscopic examination of the dislocation structures.

The dislocation and loop structures were quantified, and the results are given in Table 6. From Table 6, it can be shown that the dislocations structures of the two conditions examined are similar in many ways, the major difference being a somewhat higher dislocation density, and a factor of three times higher loop density for V-5Cr-5Ti. It can be noted for example, the most prevalent Burgers vector present is the same in both cases and by a factor of two, that being $\frac{a}{2}[11\bar{1}]$.

Table 6. Results of quantitative dislocation analyses.

Alloy	Dislocations (cm^{-2})					Loops	
	$\frac{a}{2}[111]$	$\frac{a}{2}[\bar{1}11]$	$\frac{a}{2}[1\bar{1}1]$	$\frac{a}{2}[11\bar{1}]$	Total	# Density (cm^{-3})	Mean Diameter (nm)
Pure Vanadium	$1.2x10^8$	$1.4x10^9$	$1.2x10^8$	$2.7x10^9$	$4.3x10^9$	$6.2x10^{14}$	11.9
V-5Cr-5Ti	NM	$2.3x10^9$	NM	$4.2x10^9$	$6.5x10^9$	$1.8x10^{15}$	8.1

NM = not measured, too small to measure given the limited statistics.

The present effort has provided several results that may be relevant to the question of increased notch sensitivity in V-5Cr-5Ti. Those results will be summarized, and then the results will be considered in light of their effect on notch sensitivity.

Tensile tests to 5% deformation show that in comparison to pure vanadium, V-5Cr-5Ti has a higher yield strength and a lower work hardening rate, but no yield drop. A higher yield strength should correspond to a smaller crack tip plastic zone size, and the lower work hardening rate can be expected to provide higher toughness. The lack of a yield drop can also be expected to enhance toughness.

Microstructural examinations demonstrate that Stage II deformation is maintained to 5% strain in V-5Cr-5Ti, whereas in pure vanadium, Stage III behavior is found at 5% strain. Also, the density of loops is found to be higher in V-5Cr-5Ti. The observation of Stage II response in V-5Cr-5Ti is likely a consequence of a lower work hardening rate and may be a measure of a tendency to avoid cross slip, but the increased loop density is expected to be a measure of strain centers arising from the presence of increased titanium levels and the resultant tendency for formation of Ti(C,N,O) complexes.

Increases in notch sensitivity are likely to arise from three effects: interstitial impurity hardening, grain boundary segregation, and large precipitate particles ahead of the crack tip. The present work only points to an effect due to the interaction of a higher stress field (associated with a sharper crack) with crack nucleation sites ahead of the propagating crack. If sufficient potential nucleation sites for cavity formation exist, then a higher stress state will be more likely to activate cavitation ahead of the propagating crack. Conversely, notch insensitivity can be expected when the crack tip plastic zone size is small compared to the spacing of potential crack nucleation sites. Therefore, key factors affecting notch sensitivity can be expected to be plastic zone size and spacing between potential cavity nucleation sites.

The present work does not provide clear guidance on the effect of alloying on plastic zone size. Strength is increased due to alloying, but Stage II is prolonged to higher strains, and work hardening rates are reduced. The relative increase in strength is small due to the avoidance of yield drop behavior. Therefore, it is likely that the plastic zone sizes for pure vanadium and V-5Cr-5Ti are similar.

The most likely reason for increased notch sensitivity in V-5Cr-5Ti can be traced to potential cavity nucleation site density. Alloying is expected to promote the formation of Ti(C,N,O) complexes, and microstructural observation of enhanced loop density following deformation is interpreted as evidence supporting this assertion. However, the sites promoting loop formation are probably too small to be potential cavity nucleation sites. A

more reasonable feature for a cavity nucleation site is larger Ti(C,N,O) precipitate particles, approximately 100 nm or larger in diameter, that can easily be found in V-5Cr-5Ti. The distribution of these larger precipitate particles can be expected to be altered by heat treatment in the temperature range 900°C and above. Therefore, it can be tentatively concluded that enhanced notch sensitivity in V-5Cr-5Ti is a consequence of the scavenging effect of titanium additions and the resultant increase in the density of potential cavity nucleation sites. This density of sites can be altered, at least to some degree, by suitable heat treatment.

REFERENCES

1. B. A. Loomis, private communication, April 9, 1994.

2. M. L. Grossbeck et al., "Vanadium Alloy Research for Fusion Reactors", Oak Ridge National Laboratories, March 17, 1994.

3. R. H. Jones, in Mechanical Properties and Phase Transformations in Engineering Materials, S. D. Antolovich, R. O. Ritchie and W. W. Gerberich, Eds. The Metallurgical Society of AIME, 1986, pp. 227-249.

4. M. Manoharan, J. P. Hirth, and A. R. Rosenfield, J. of Test. and Eval., 18 (1990), No.2, pp. 106- 114.

5. S. Raghavachary, A. R. Rosenfield, and J. P. Hirth, Met. Trans. A, 21A (1990), pp. 2539-45.

6. M. Manoharan, Scripta Metall. Mater., 26 (1992), pp. 1187-1192.

7. M. L. Hamilton and R. H. Jones, Pacific Northwest Laboratories, 1994.

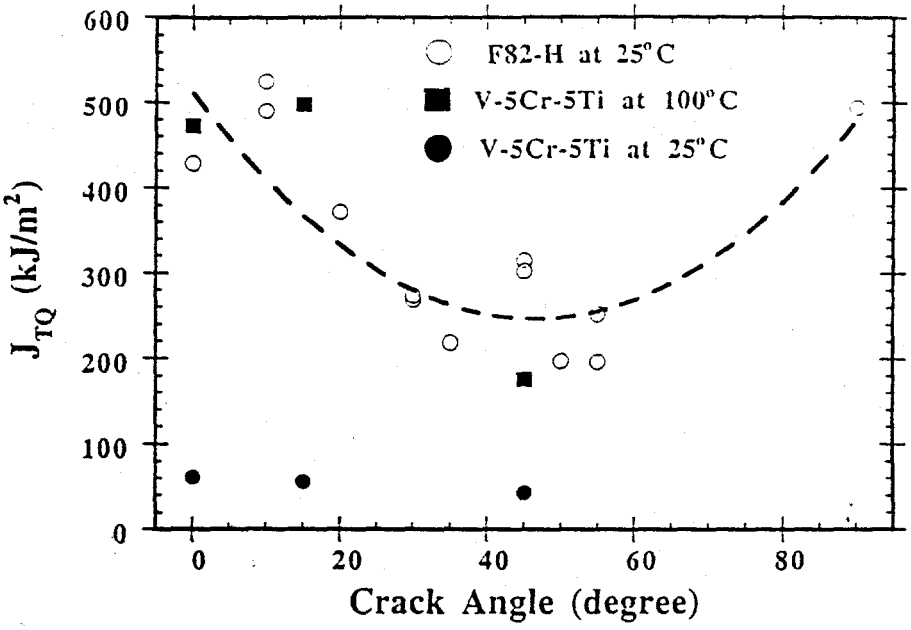

Fig. 1. The dependence of critical total J-integral of V-5Cr-5Ti on crack inclination angles and temperatures. A reduced activation ferritic/martensitic steel (F-82H) is included for comparison.

Subtask 12D4: BASELINE TENSILE PROPERTIES OF V–Cr–Ti ALLOYS, B. A. Loomis, H. M. Chung, and D. L. Smith (Argonne National Laboratory)

OBJECTIVE

The objective of this work is to provide a database on the baseline tensile properties of candidate V-Cr-Ti alloys.

SUMMARY

Vanadium-base alloys of the V-Cr-Ti system are attractive candidates for use as structural materials in fusion reactors. The current focus of the U.S. program of research on these alloys is on the V-(4-6)Cr-(3-6)Ti alloys containing 500–1000 wppm Si. In this paper, we present experimental results on baseline tensile properties of V–Cr–Ti alloys measured at 23°–700°C, with an emphasis on the tensile properties of the U.S. reference alloy V–4Cr–4Ti. The reference alloy was found to exhibit excellent tensile properties up to 700°C.

INTRODUCTION

Vanadium-base alloys have significant advantages over other candidate alloys (such as austenitic and ferritic steels) for use as structural materials in fusion devices, e.g., in the international thermonuclear experimental reactor (ITER) and in magnetic fusion reactors (MFRs). These advantages include intrinsically lower levels of long-term activation, irradiation afterheat, neutron-induced helium- and hydrogen-transmutation rates, biological hazard potential, and thermal stress factor.[1–5] However, to make use of these favorable neutronic and physical properties of structural materials in fusion systems, the alloys must retain adequate tensile strength and ductility and must be resistant to neutron-induced swelling, creep, and embrittlement, and they must also be compatible with the coolant.

In this paper, we report a comprehensive database on tensile strength and ductility of several major alloys of V–Cr–5Ti system. Up to ≈15 wt.% Cr was added in the alloys to investigate the effects of Cr on tensile properties. Laboratory–scale (≈30–kg) heats of the alloys, fabricated at about the same time by a similar procedure, contained 4–5 wt.% Ti, 350–800 wppm of combined O, N, and C impurities, and 340–870 wppm Si. The Si contents are consistent with the previous finding that 400–1000 wppm Si is optimal to minimize irradiation–induced swelling.[6] Ti contents <3 wt.% is not desirable from the standpoint of more pronounced swelling,[6] whereas Ti ≥ 8 wt.% is also not desirable from the standpoint of higher creep rate.[7] Therefore, Ti level of 4–5 wt.% was considered most desirable. Results of investigations on impact properties and irradiation–induced embrittlement indicated that it is also desirable to limit Cr content in the ternary alloy to <7 wt.%.[8] These considerations prompted an investigation of the effect of Cr on tensile properties of V–Cr–(4–5)Ti alloy class. Emphasis of the study was to obtain database and understanding of the tensile behavior of the U.S. reference alloy V–4Cr–4Ti, an alloy that meets all of the compositional requirements described above.

MATERIALS AND PROCEDURES

The chemical compositions of as-fabricated V–Cr–Ti alloys are given in Table 1. In the table, compositions of other types of alloys are also given that were investigated in the past but were found to be less promising than the V–Cr–(4–5)Ti alloys. Final forms of the

extruded product of the V–Cr–(4–5)Ti alloys were plates and sheets 3.8–, 1.0–, and 0.3–mm in thickness. Tensile specimens were machined from 0.7–1.0–mm–thick sheets such that the rolling direction of the sheet was parallel to the uniaxial loading direction.

Table 1. Composition of Vanadium Alloys Irradiated in the Fast Flux Test Facility Materials Open Test Assembly

	Nominal Comp.	Impurity Concentration (wt. ppm)			
Heat ID	(wt.%)	O	N	C	Si
BL-19	V	1101	161	360	-
BL-20	V	570	110	120	325
BL-36	V	810	86	250	<50
BL-51	V	570	49	56	370
820626	V	260	75	28	260
820630	V	200	62	75	780
BL-35	9.5Cr	340	45	120	<50
BL-4	10.0Cr	530	76	240	<50
BL-5	14.1Cr	330	69	200	<50
BL-50	1.0Ti	230	130	235	1050
BL-52	3.1Ti	210	310	300	500
BL-46	4.6Ti	305	53	85	160
BL-11	4.9Ti	1820	530	470	220
BL-34	8.6Ti	990	180	420	290
BL-12	9.8Ti	1670	390	450	245
BL-13	14.4Ti	1580	370	440	205
BL-15	17.7Ti	830	160	380	480
BL-16	20.4Ti	390	530	210	480
BL-10	7.2Cr-14.5Ti	1110	250	400	400
BL-21	13.7Cr-4.8Ti	340	510	180	1150
BL-22	13.4Cr-5.1Ti	300	52	150	56
BL-23	12.9Cr-5.9Ti	400	490	280	1230
BL-24	13.5Cr–5.2Ti	1190	360	500	390
BL-25	14.4Cr-0.3Ti	390	64	120	<50
BL-26	14.1Cr-1.0Ti	560	86	140	<50
BL-40	10.9Cr-5.0Ti	470	80	90	270
BL-41	14.5Cr-5.0Ti	450	120	93	390
BL-43	9.2Cr-4.9Ti	230	31	100	340
BL-44	9.9Cr-9.2Ti	300	87	150	270
BL-49	7.9Cr-5.7Ti	400	150	127	360
BL-54	5.1Cr-3.0Ti	480	82	133	655
BL-63	4.6Cr-5.1Ti	440	28	73	310
BL-62	3.1Ti–0.1Si	320	86	109	660
BL-27	3.1Ti–0.25Si	210	310	310	2500
BL-42	3.1Ti–0.5Si	580	190	140	5400
BL-45	2.5Ti-1Si	345	125	90	9900
QN74[a]	4.0Cr–4.1Ti	480	79	54	350
BL-47	4.1Cr-4.3Ti	350	220	200	870
T87	4.9Cr–5.1Ti	380	89	109	545
932665	3.8Cr–3.9Ti	310	85	80	783

The machined and polished specimens were annealed typically at 1050°C-1125°C for 1 h in high–quality vacuum before testing. Typical grain size of the annealed and recrystallized specimens was 15–30 mm. The only secondary phase in the as–annealed specimen was Ti(O,N,C) precipitates ≈300–500 nm in size, which is normally observed in titanium–containing vanadium alloys with O+N+C > 400 wppm. Gauge cross section of each polished specimens was measured individually. Tensile tests were conducted at 23°C–700°C at a strain rate of 0.0011 s^{-1}. The high–temperature tests were conducted in a quartz cylinder evacuated and continuously flushed with flowing argon.

RESULTS AND DISCUSSION

Yield strength, ultimate tensile strength, uniform elongation, and total elongation of four unirradiated alloys V–5Ti (BL–46), V–4Cr–4Ti (BL–47), V–9Cr–5Ti (BL–43), and V–10Cr–5Ti (BL–41) are shown in Figs. 1–4, respectively. Note that yield strengths of the alloys are nearly constant between 300 and 600°C. Ultimate strengths appear to be slightly lower at ≈250°C–300°C than at <200°C or >300°C. For temperatures >700°C, yield and ultimate tensile strengths are expected to decrease significantly.

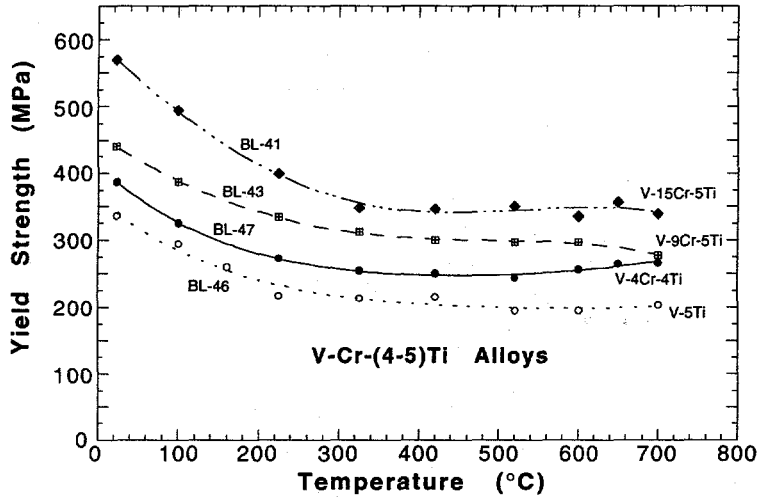

Fig. 1.

Yield strength of unirradiated V-Cr-(4–5)Ti alloys at 23°C–700°C.

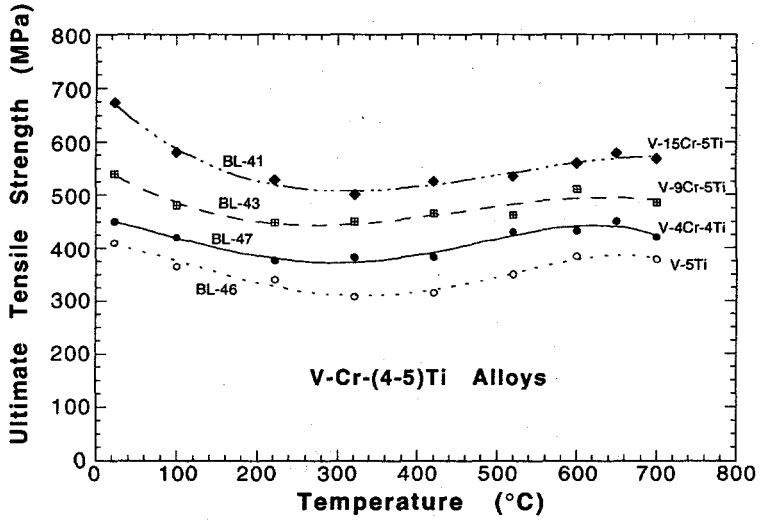

Fig. 2.

Ultimate tensile strength of unirradiated V-Cr-(4–5)Ti alloys at 23°C–700°C.

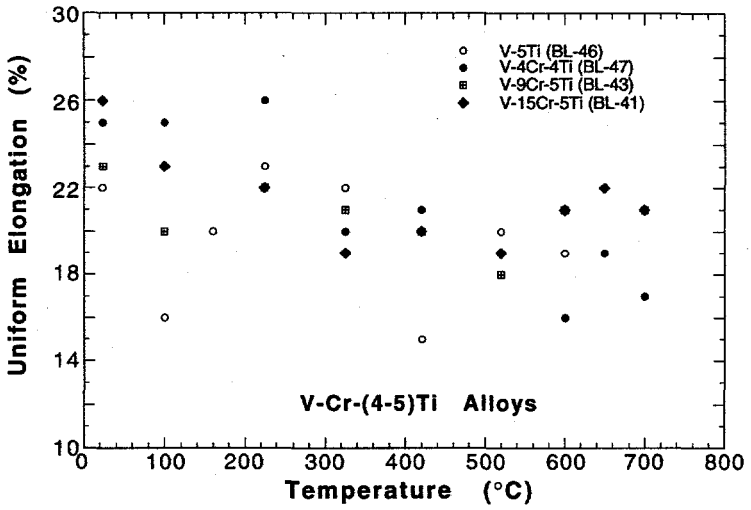

Fig. 3.

Uniform elongation of unirradiated V-Cr-(4–5)Ti alloys at 23°C–700°C.

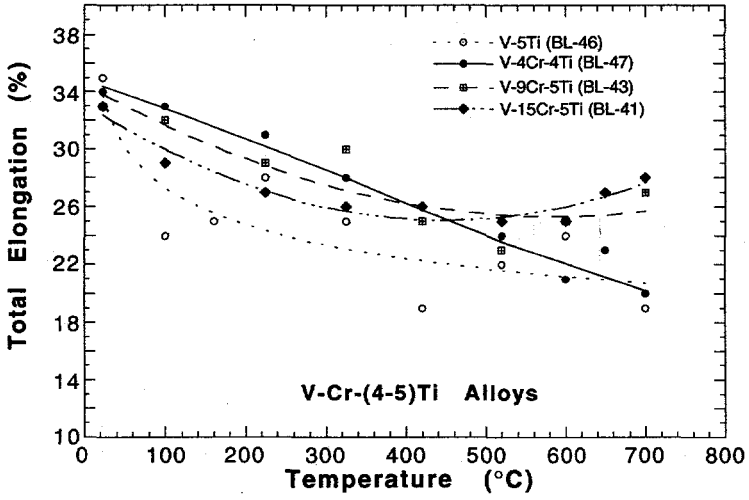

Fig. 4.

Total elongation of unirradiated V-Cr-(4–5)Ti alloys at 23°C–700°C.

For all test temperatures, the yield and ultimate strengths increased monotonically for increased Cr content, indicating the predominant role of Cr on tensile strength of the alloy system. Titanium and the combined contents of O, N, and C impurities in the four alloys were similar, i.e., 4–5 wt.% and 360–770 wppm, respectively.

The yield strength of all the alloys listed in Table 1 for room temperature and 420°C–600°C could be correlated well with combined content of Cr and Ti.[6] This is shown in Fig. 5. Excessive alloying addition of Cr (≥6 wt.%) is not desirable from the standpoint of irradiation–induced degradation of material toughness.[7] Likewise, excessive addition of Ti (≥9 wt.%) is not desirable from the standpoint of lower thermal creep resistance.[8]

Uniform elongations of V–15Cr–5Ti, V–9Cr–5Ti, V–4Cr–4Ti, and V–5Ti shown in Figs. 3 are similar for 300°C–700°C, i.e., 18–22 %, although room–temperature uniform elongations are somewhat higher, i.e., 22–26 %. Total elongations of the alloys at room temperature are in the range of 33–35 %, Fig. 4. In contrast to the total elongations of

low–Cr alloys (i.e., V–4Cr–4Ti and V–5Ti) which decrease monotonically for increasing temperature, the total elongations of the high–Cr alloys V–15Cr–5Ti and V–9Cr–5Ti seem to reach minima at ≈400°C and then increase on further increasing the test temperature.

Tensile strength and ductility of the U.S. reference alloy V–4Cr–4Ti are shown in Figs. 6 and 7, respectively. The alloy has been identified as the most promising candidate alloy on the basis of its excellent resistance to irradiation–induced embrittlement, swelling, creep, and microstructural instability.[9] As shown in Figs. 6 and 7, the laboratory (30–kg) heat of this alloy exhibited excellent baseline tensile properties for up to 700°C. Yield and ultimate strength of the alloy are 270–280 MPa and 400–440 MPa, respectively for the temperature range of 200°C to 700°C. Uniform and total elongation are 16–25 % and 20–31 %, respectively, for the same temperature range.

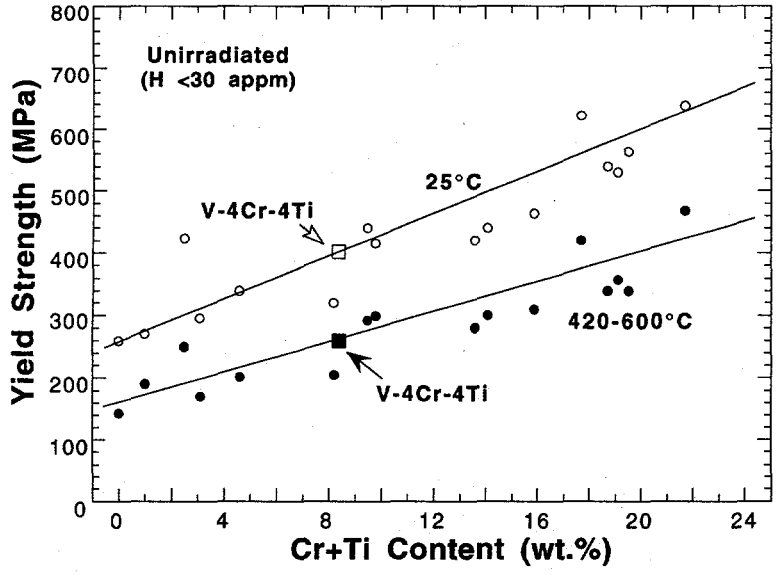

Fig. 5.

Yield strength of unirradiated V, V–Ti, V–Cr–Ti, and V–Ti–Si alloys at 25°C and 420°C–600°C as function of combined Cr and Ti content.

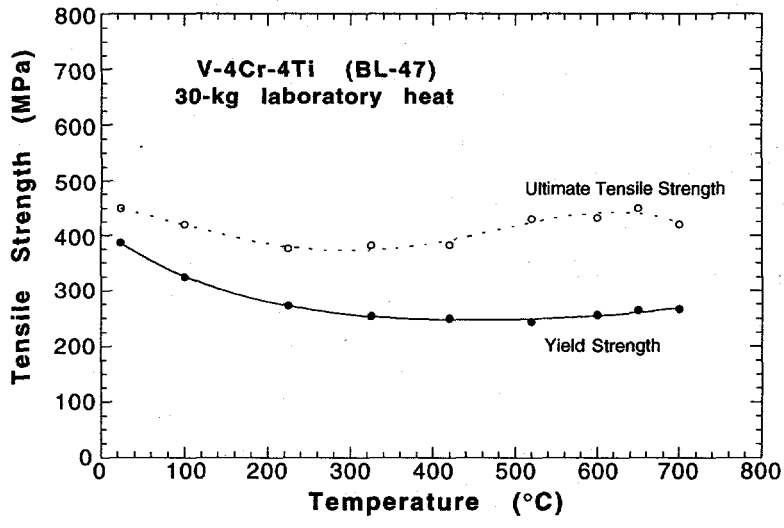

Fig. 6.

Yield and ultimate tensile strength of unirradiated reference alloy V-4Cr-4Ti at 23°C–700°C.

In Fig. 8, uniform–to–total–elongation and yield–to–ultimate–strength ratios of the U.S. reference alloy are plotted as function of temperature. The ratio of uniform to total elongation remains constant at ≈0.8 regardless of the test temperature. In contrast to this, however, the ratio of yield to ultimate tensile strength decreases monotonically from ≈0.9 at room temperature to ≈0.6 at 700°C, indicating more pronounced work–hardening of the alloy at higher temperatures.

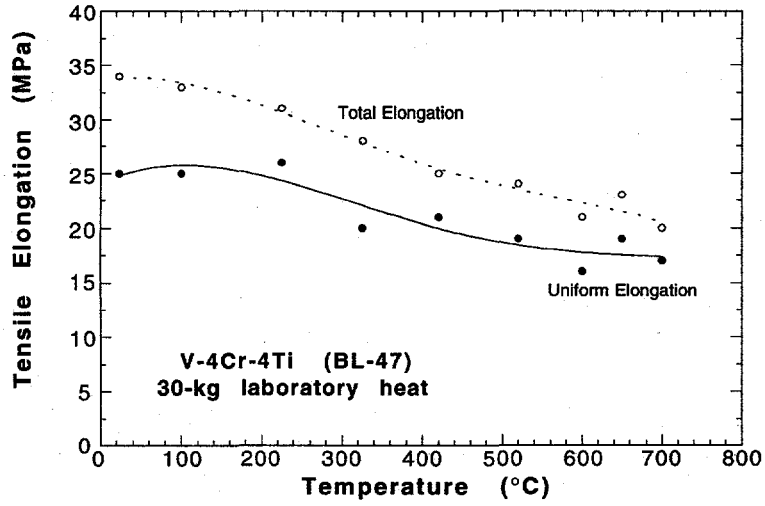

Fig. 7.

Uniform and total elongation of unirradiated reference alloy V-4Cr-4Ti at 23°C–700°C.

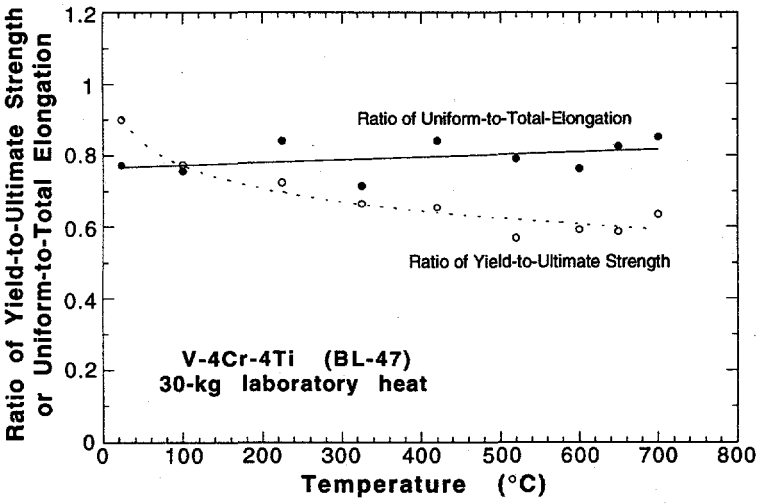

Fig. 8.

Ratio of yield strength to ultimate tensile strength (A) and uniform elongation to total elongation (B) of unirradiated reference alloy V-4Cr-4Ti at 23°C–700°C.

CONCLUSIONS

1. Baseline tensile properties of V–Cr–Ti alloys containing 0–15 wt.% Cr and 4–5 wt.% Ti have been determined at 23°C–700°C. Yield strengths of the alloys were nearly constant at 300°C–600°C, whereas ultimate strengths were slightly lower at ≈250°C–300°C than at <200°C or >300°C.

2. For all test temperatures, the yield and ultimate strengths of V–(0–15)Cr–(4–5)Ti

alloys increased monotonically with increased Cr content, indicating the predominant role of Cr on tensile strength of the alloy family. Room–temperature and 420°C–600°C yield strength of V–(0–15)Cr–(0–20)Ti alloys could be correlated well with combined contents of Cr and Ti.

3. The U.S. reference alloy V–4Cr–4Ti, identified as the most promising candidate alloy on the basis of its excellent resistance to irradiation–induced embrittlement, swelling, creep, and microstructural evolution, exhibited excellent baseline tensile properties for up to 700°C. The ratio of uniform to total elongation of the alloy remained constant at ≈0.8 regardless of the test temperature, whereas the ratio of yield to ultimate tensile strength decreased monotonically from ≈0.9 at room temperature to ≈0.6 at 700°C, indicating more pronounced work–hardening of the alloy at higher temperatures.

ACKNOWLEDGMENTS

The authors are grateful to L. J. Nowicki and J. Gazda for their contributions to experimental efforts.

REFERENCES

1. T. Noda, F. Abe, H. Araki, and M. Okada, J. Nucl. Mater. 155-157 (1988) 581.
2. R. Santos, J. Nucl. Mater. 155-157 (1988) 589.
3. S. J. Piet, H. G. Kraus, R. M. Neilson, Jr. and J. L. Jones, J. Nucl. Mater. 141-143 (1986) 24.
4. F. L. Yaggee, E. R. Gilbert and J. W. Styles, J. Less-Comm. Met. 19 (1969) 39.
5. D. L. Smith, B. A. Loomis, and D. R. Diercks, J. Nucl. Mater. 135 (1985) 125.
6. B. A. Loomis, L. J. Nowicki, and D. L. Smith, in: Fusion Reactor Materials, Semiannual Progress Report for Period Ending March 31, 1991, DOE/ER-0313/10, U.S. Department of Energy, Office of Fusion Energy, July 1991, pp. 145-155.
7. H. M. Chung, B. A. Loomis, and D. L. Smith, "Fracture Behavior of Neutron–Irradiated Vanadium–Base Alloys," in this report.
8. H. M. Chung, B. A. Loomis, and D. L. Smith, J. Nucl. Mater. 212–215 (1994) 772–777.
9. H. M. Chung, B. A. Loomis, and D. L. Smith, "Properties of V–4Cr–4Ti for Application as Fusion Reactor Structural Components," Fusion Eng. Design, 1995, in press.

Subtask 12D5: THERMAL CREEP PROPERTIES OF VANADIUM-BASE ALLOYS, H. M. Chung, B. A. Loomis, and D. L. Smith (Argonne National Laboratory)

OBJECTIVE

The objective of this work is to provide baseline data on the thermal creep properties of candidate vanadium base alloys.

SUMMARY

Vanadium-base alloys are promising candidate materials for application in fusion reactor structural components because of several important advantages. V-4Cr-4Ti has been identified as one of the most promising candidate alloys and was selected for comprehensive tests and examination. In the present investigation, thermal creep rates and stress-rupture life of V-4Cr-4Ti and V-10Cr-5Ti alloys were determined at 600°C. The impurity composition and microstructural characteristics of creep-tested specimens were analyzed and correlated with the measured creep properties. The results of these tests show that V-4Cr-4Ti, which contains impurity compositions typical of a commercially fabricated vanadium-based alloy, exhibits creep strength substantially superior to that of V-20Ti, HT-9, or Type 316 stainless steel. The V-10Cr-5Ti alloy exhibits creep strength somewhat higher than that of V-4Cr-4Ti.

INTRODUCTION

Vanadium-base alloys are considered promising candidate structural materials for a fusion reactor first wall because they offer the important advantages of inherently low irradiation-induced activity, good mechanical properties, good compatibility with lithium, high thermal conductivity, and good resistance to irradiation damage. As part of a program to screen candidate alloys and develop an optimal alloy, extensive investigations have been conducted on the swelling behavior, tensile properties, impact toughness, and microstructural evolution of V, V-Ti, V-Cr, V-Cr-Ti, and V-Ti-Si alloys after irradiation by fast neutrons at 420, 520, and 600°C. From these investigations, V-Cr-Ti alloys containing 5-7 wt.% Cr, 3-5 at.% Ti, 400-1000 wt. ppm Si, and <1000 wt. ppm O+N+C were identified as desirable alloys that exhibit superior resistance to swelling, embrittlement, and hydrogen-induced effects during irradiation in lithium.[1–4] As a result, recent attention has focused primarily on the ternary alloys V-4Cr-4Ti, V-5Cr-3Ti, and V-5Cr-5Ti. For these alloys, however, no data base has been reported on thermal or irradiation creep, and a favorable creep behavior commensurate with the superior resistance of the alloys to swelling and embrittlement has not been demonstrated. In the work reported here, the thermal creep behavior of a V-4Cr-4Ti alloy was investigated at 600°C. The creep of V-10Cr-5Ti was also investigated to provide information on the effect of increased Cr content. Preliminary results of the creep tests have been described in a previous report.[5]

MATERIALS AND PROCEDURES

The chemical composition of the two alloys tested in the present investigation is given in Table 1. The 0.635-mm-thick tensile specimens were recrystallized prior to the creep test by annealing at 1125°C for 1 h in a vacuum of 2×10^{-5} Pa. The creep tests were conducted in an ion-pumped system in which vacuum was typically maintained at 2×10^{-6}

Pa during testing at 600°C. Details of experimental procedures have been reported elsewhere.[5] The specimen was wrapped with a Ti or Ta foil to reduce contamination with impurities during testing. The elongation of a specimen was determined with a linear variable differential transformer (LVDT) with digitized output. The concentration of interstitial impurities (i.e., O, N, and C) and Vickers hardness (VHN) of specimens were measured after testing. The phase and dislocation structures of the specimens were examined by transmission electron microscopy (TEM) before and after the creep test. In addition to the normal constant-load stress-to-rupture tests, applied stress was increased stepwise in some tests to measure a set of steady-state (minimum) creep rates corresponding to each stress level. An example of this kind of testing is shown in Fig. 1.

RESULTS AND DISCUSSION

Stress-Rupture Life and Creep Rate

The stress-to-rupture time of V-4Cr-4Ti and V-10Cr-5Ti is given in Fig. 2. The figure shows that the creep strength of the V-10Cr-5Ti alloy is significantly higher than that of V-4Cr-4Ti. This finding is consistent with the higher ultimate tensile strength (UTS) of V-10Cr-5Ti, i.e., ≈512 vs. ≈434 MPa.[6] At 600°C, the stress-to-rupture time of the two alloys is extremely sensitive to applied stress. For example, an increase in rupture time of more than two orders of magnitude was observed for V-4Cr-4Ti when applied stress was decreased only ≈5%. In previous investigations of creep properties of V-13Cr-3Ti, V-15Cr-3Ti, V-15Cr-5Ti, and Vanstar alloys at ≥650°C, a similar trend was observed.[7–9] Because of the high creep strength, determination of stress-rupture life of V-5Cr-5Ti at 600°C for stress ≤350 MPa is estimated to require impractically long test times (≥3 years).

Table 1. Chemical Composition of V-4Cr-4Ti and V-10Cr-5Ti Alloys

		Composition (wt.% or wt ppm)					
Material	ANL ID	Cr	Ti	Si	O	C	N
V-4Cr-4Ti	BL-47	4.1%	4.3%	870	350	200	220
V-10Cr-5Ti	BL-43	9.2%	4.9%	340	230	100	31

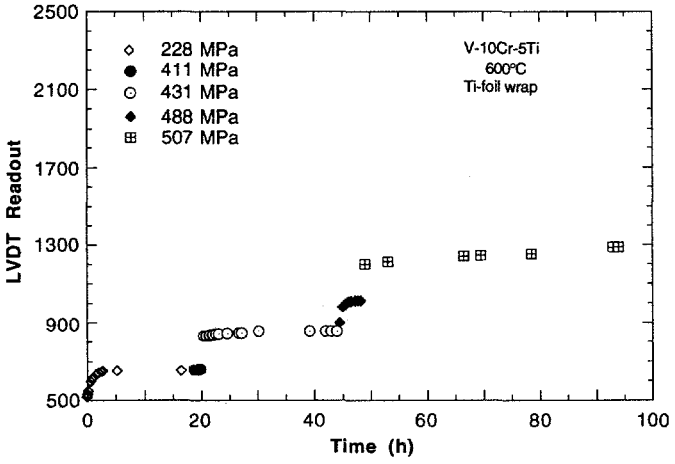

Fig. 1.

Elongation (LVDT readout) vs. time for V-10Cr-5Ti under stepwise increase in loading at 600°C, used to measure steady-state creep rates.

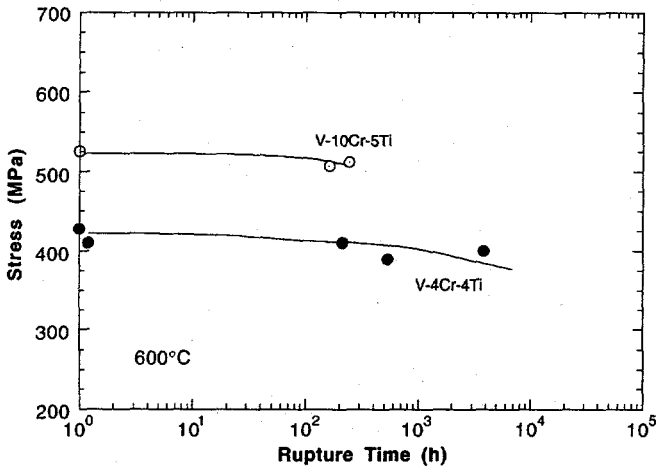

Fig. 2.

Relationship of stress to rupture time for V-10Cr-5Ti and V-4Cr-4Ti at 600°C.

In Fig. 3, steady-state (minimum) creep rates of V-4Cr-4Ti and V-10Cr-5Ti alloys are shown as a function of applied stress. In the stress range between ≈300 and ≈420 MPa, the steady-state creep rate of V-4Cr-4Ti at 600°C was between $\approx 10^{-3}$ and 5×10^{-2} %/h; for a comparable stress level, creep rate of V-10Cr-5Ti was ≈7-8 times lower.

In Fig. 4, the creep strengths of V-15Cr-5Ti, V-10Cr-5Ti, and V-5Cr-5Ti are given. Although data for V-15Cr-5Ti were obtained at temperatures higher than 600°C,[9] the creep strengths can be compared from a plot of the Larsen-Miller parameter, which is defined by the equation:

$$P = T(20 + \log t), \qquad (1)$$

where creep temperature T is in K and rupture time t is in hours. The V-15Cr-5Ti specimens tested by Bajaji and Gold[9] contained 200-1400 wppm O, 500 wppm N, and 170 wppm C. By comparison, the impurity content measured in the creep-tested specimens of V-10Cr-5Ti and V-4Cr-4Ti in the present investigation were significantly lower: i.e., O, 370-770 wppm; N, 99-200 wppm; and C, 252-270 wppm (see Table 2). Within the uncertainties associated with the variations in impurity content, the results indicate that the creep strengths of V-15Cr-5Ti and V-10Cr-5Ti are similar. The UTS of the present V-10Cr-5Ti (541 MPa) and that of a V-15Cr-5Ti alloy containing 400 wppm O, 490 wppm N, and 280 wppm C was found to be similar (555 MPa). Therefore, it is not surprising that the creep strengths of V-10Cr-5Ti and V-15Cr-5Ti, shown in Fig. 3, are similar.

Impurity Content and Microstructure

The creep of unalloyed V is known to be sensitive to impurities (in particular dissolved O), although the creep of V-15Cr-5Ti, V-20Ti, and Vanstar-7 (V-9Cr-3Fe-1.3Zr-0.05C) appears to be less sensitive to O contamination (see Fig. 4).[7–9] In view of this, it was considered necessary to characterize the specimen impurity content, hardness, phase distribution, and other undesirable microstructural changes associated with the creep test to qualify the data obtained in this study.

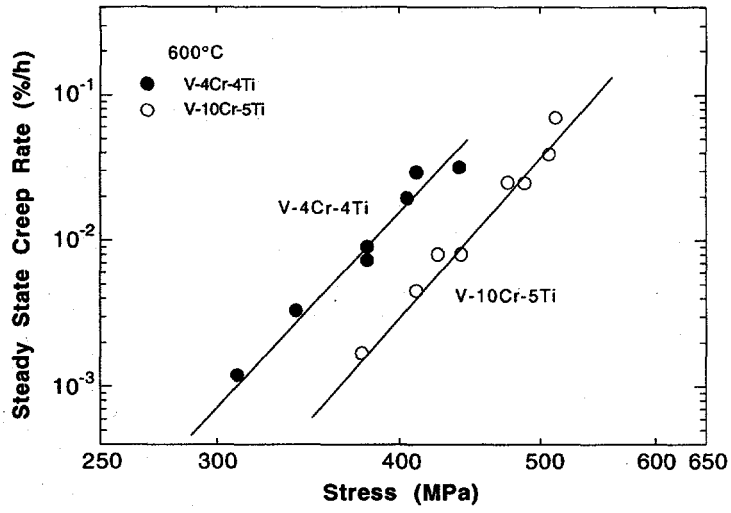

Fig. 3.

Steady-state creep rate vs. stress for V-10Cr-5Ti and V-4Cr-4Ti at 600°C.

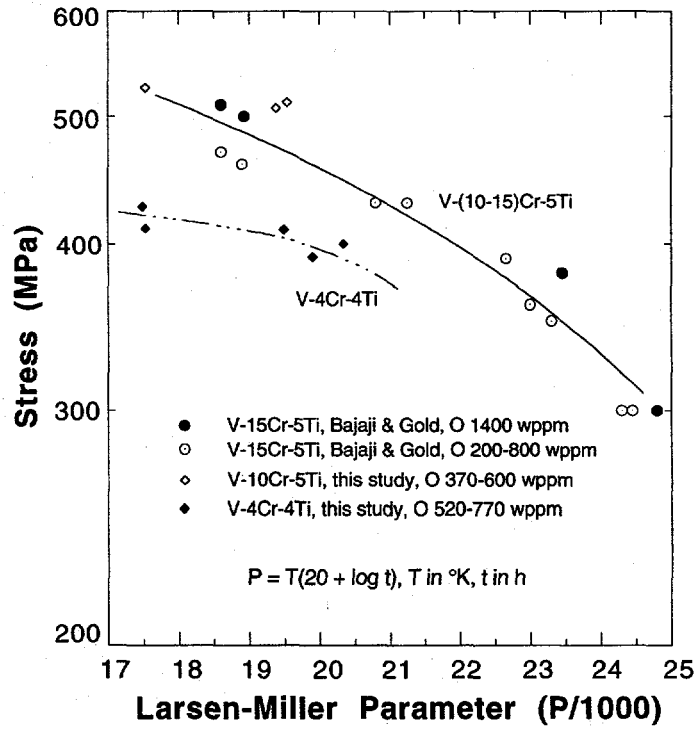

Fig. 4. Larsen-Miller plots for V-15Cr-5Ti, V-10Cr-5Ti, and V-4Cr-4Ti.

The results obtained from analysis for O, N, and C concentrations are summarized in Table 2. Compared with the impurity content of the as-annealed specimens before the test (Table 1), N content in V-4Cr-4Ti decreased to some extent (from 220 to 160-190 wppm) and C content increased modestly (from 200 to 250-270 wppm). Nitrogen content in V-10Cr-5Ti increased from 31 to ≈100 wppm. However, the O content of both alloys

increased significantly after testing (from 230-350 wppm to 370-770 wppm). The increase in O content was more pronounced in specimens tested without a wrap or with a Ta-foil wrap. For a specimen with a Ti wrap, the increase in O content was minimal (e.g., from 230 to 370 wppm). The more pronounced O contamination in the Ta-wrapped specimens is probably associated with the volatility of tantalum oxide. Because of the smaller contamination when Ti foil was used, all subsequent tests are being conducted with a Ti wrap. Despite the increase in O and C, the impurity content of the two alloys is still comparable to that typical of a commercial V-base alloy.

Table 2. Impurity Content of Creep Specimens from V-4Cr-4Ti[a] and V-10Cr-5Ti[b] after Testing at 600°C.

Material	Specimen ID	Stress (MPa)	Time to Rupture (h)	Wrap	Composition (wt ppm) O	C	N
V-4Cr-4Ti	BL-47A	420	1	none	560	252	160
V-4Cr-4Ti	BL-47C	408	1.1	Ta	520	261	200
V-4Cr-4Ti	BL-47E	387	541	Ta	770	–	200
V-4Cr-4Ti	BL-47F	410	213	Ta	520	270	190
V-10Cr-5Ti	BL-43A	512	243	none	600	–	120
V-10Cr-5Ti	BL-43B	507	162	Ti	370	–	99

[a]Ultimate tensile strength ≈434 MPa, hardness VHN ≈171.
[b]Ultimate tensile strength ≈512 MPa, hardness VHN ≈192.

To detect undesirable phase structure that might have been produced during testing, TEM specimens excised from near the gage section were examined. The results are shown in Fig. 5. A comparison of Figs. 5A and 5B shows that the phase structure of V-4Cr-4Ti did not change appreciably during testing at 600°C for 541 h. That is, the size and distribution of the Ti(O,N,C) precipitates, normally observed in these alloys after fabrication,[3] were similar before and after testing, and no new types of precipitates were produced.

However, dislocation loops were observed in high density in creep-tested specimens of both V-4Cr-4Ti and V-10Cr-5Ti (Figs. 5C and 5D, respectively). From bright-field imaging alone, the dislocation loops (≤100 nm in size) can be mistakenly confused with small precipitates. However, results of selected-area diffraction and dark-field imaging showed that they are indeed dislocation loops. Line dislocations were also observed frequently in conjunction with loops. A major difference in the microstructural aspect of creep-tested V-4Cr-4Ti and V-10Cr-5Ti specimens was the distribution of dislocation loops. In V-10Cr-5Ti, loop distribution was more or less uniform within a grain. In contrast, size and density of the loops were higher near a grain boundary in V-4Cr-4Ti. This can be seen by comparing the two images of Figs. 5C and 5D. The dark-field image shown in Fig. 5C reveals clearly a dense loop distribution of V-4Cr-4Ti in the vicinity of a grain boundary.

Hardness profiles were measured across the specimen thickness (nominal thickness 0.635 mm) after the creep test. An example of typical hardness profiles is given in Fig. 6, which was determined for a V-10Cr-5Ti specimen that ruptured after 162 h. Except for narrow regions ≤0.01 mm underneath the free surfaces, a more or less uniform hardness of ≈205 VHN was observed, a slight increase from the original hardness of ≈192 VHN.

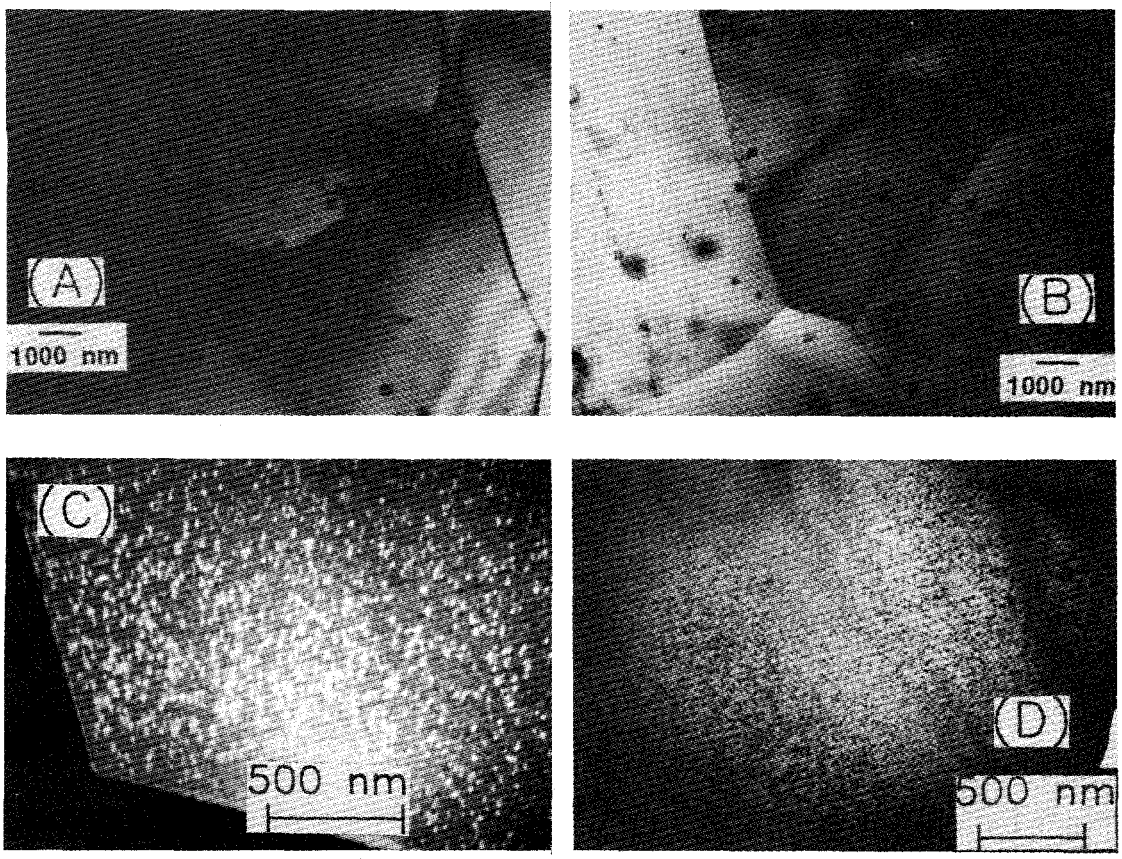

Fig. 5. Grain size and phase structure of V-4Cr-4Ti (A) before and (B) after creep test at 600°C for 541 h. Dislocation loops in creep-tested V-4Cr-4Ti and V-10Cr-5Ti are shown in (C) and (D), respectively, in dark- and bright-field image.

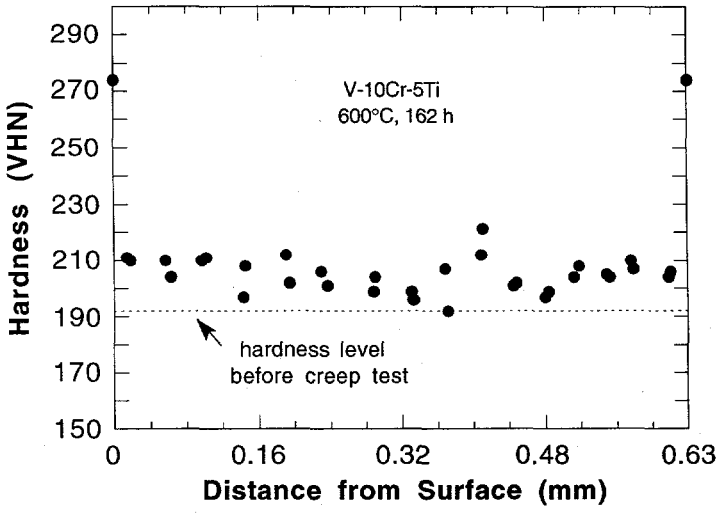

Fig. 6.

Vickers hardness profile across wall thickness of V-10Cr-5Ti after creep test at 600°C for 162 h.

The hardness increase is attributed not only to the effect of the increase in O content (i.e., from 230 to 370 wppm) but also to the effect of the high-density dislocation loops. In summary, no unusual features were observed that indicate an unacceptable effect of the

environment of the creep test at 600°C. Impurity content and phase structure of the test specimens were similar to those of typical commercial alloys.

Comparison with Other Materials

In Fig. 7, the creep property of V-4Cr-4Ti and ferritic and austenitic steels is shown in Larsen-Miller plots. From the figure, it is obvious that the creep strength of V-4Cr-4Ti is substantially superior to that of HT-9, Type 316 stainless steel (either annealed or cold–worked), and V-20Ti. In particular, this difference in creep strength is more pronounced when Larsen-Miller parameters are higher, i.e., at higher temperatures or longer times.

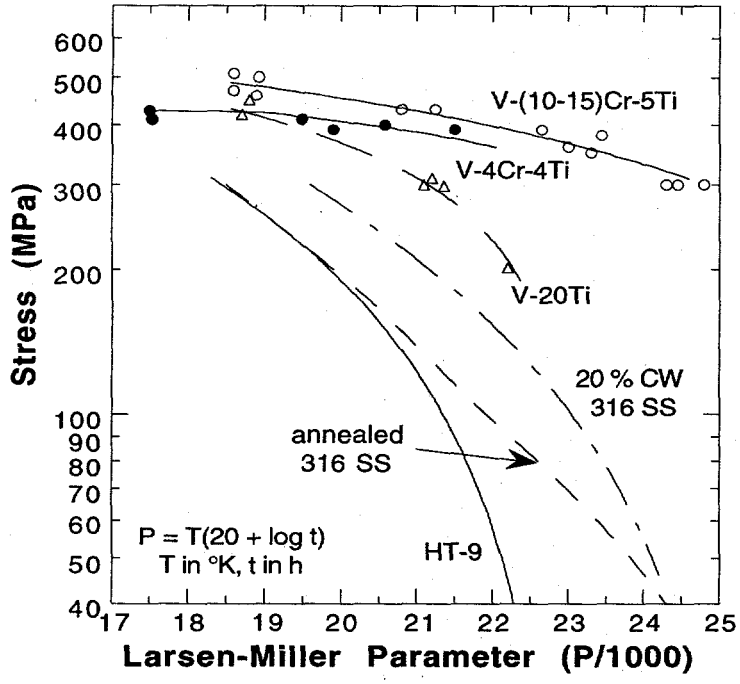

Fig. 7.

Larsen-Miller plots of creep strength of V-4Cr-4Ti and ferritic and austenitic steels.

It has been reported that creep strength of binary V-Ti and ternary V-15Cr-Ti and V-3Cr-Ti alloys is maximum for 3 wt.% Ti.[7,8] Titanium content greater or less than ≈3 wt.% resulted in significantly decreased creep strength. Based on these reports, the creep strength of V-5Cr-3Ti could be substantially higher than that of V-4Cr-4Ti. Increasing the Cr content to 6 wt.% is also expected to improve the creep strength of V-4Cr-4Ti. However, selection of optimal content of Cr (4-6 wt.%) and Ti (3-6 wt.%) must be tied closely to other important considerations, in particular, to the effects of neutron damage and helium generation on embrittlement and fracture toughness.

CONCLUSIONS

1. Stress-rupture life and steady-state creep rate of V-4Cr-4Ti and V-10Cr-5Ti have been determined at 600°C. Results of characterization of impurity contamination, hardness, phase structure, and dislocation and loop structures in the creep-tested specimens showed no unusual features that indicate an unacceptable effect of the test environment on the measured creep rates. Impurity content of the tested specimens

was comparable to that of a typical commercial vanadium-base alloy.

2. V-4Cr-4Ti exhibits a creep strength that is substantially superior to that of Type 316 stainless steel, HT-9, or V-20Ti, in particular, at higher Larsen-Miller parameters, i.e., at higher temperatures and/or longer service times.

3. Creep strength of V-10Cr-5Ti is similar to that of V-15Cr-5Ti and several times higher than that of V-4Cr-4Ti. However, if a creep strength higher than that of V-4Cr-4Ti is required, V-(4–6)Cr-(3–6)Ti appears to be a more attractive alternative than V-10Cr-5Ti from the standpoint of irradiation-induced embrittlement.

ACKNOWLEDGMENTS

The authors are grateful to L. J. Nowicki and J. Gazda for their contributions to experimental efforts.

REFERENCES

1. B. A. Loomis, A. B. Hull, and D. L. Smith, J. Nucl. Mater., 179-181 (1991) 148-154.
2. B. A. Loomis and D. L. Smith, J. Nucl. Mater., 191-194 (1992) 84-91.
3. H. M. Chung and D. L. Smith, J. Nucl. Mater. 191-194 (1992) 942-947.
4. H. M. Chung, B. A. Loomis, and D. L. Smith, "Irradiation-Induced Precipitation in Vanadium-Base Alloys Containing Titanium," in: Effects of Radiation on Materials: 16th International Symposium, ASTM STP 1175, A. S. Kumar, D. S. Gelles, R. K. Nanstad, and T. A. Little, eds., American Society for Testing and Materials, Philadelphia, 1993, 1185–1200.
5. B. A. Loomis, L. J. Nowicki, and D. L. Smith, in: Fusion Reactor Materials, Semiannual Progress Report for Period Ending September 30, 1992, DOE/ER-0313/13, U.S. Department of Energy, Office of Fusion Energy, pp. 309–317.
6. B. A. Loomis, L. J. Nowicki, and D. L. Smith, in: Fusion Reactor Materials, Semiannual Progress Report for Period Ending March 31, 1991, DOE/ER-0313/10, U.S. Department of Energy, Office of Fusion Energy, July 1991, pp. 145-155.
7. M. Schirra, "Das Zeitstandfestigkeits und Kriechverhalten von Vanad-Basis Legierungen," KfK-2440, April 1977, Karlsruhe Nuclear Research Center, Germany.
8. D. Harrod and R. Gold, "Mechanical Properties of Vanadium and Vanadium Base Alloys," Int. Met. Rev. 25 (1980) 163-221.
9. R. Bajaji and R. E. Gold, in: Alloy Development for Irradiation Performance Semiannual Progress Report, DOE/ER0045/10, Oak Ridge National Laboratory, Oak Ridge, TN, 1983, p. 74.

Subtask 12D6: FATIGUE BEHAVIOR OF UNIRRADIATED V-5Cr-5Ti

by B. G. Gieseke, C. O. Stevens and M. L. Grossbeck (Oak Ridge National Laboratory)

OBJECTIVE: The objective of this research is to eternination the low cycle fatigue behavior of V-5Cr-5Ti alloys for a range of temperatures and the extent of environmental effects at ambient temperatures.

SUMMARY: The results of in-vacuum low cycle fatigue tests are presented for unirradiated V-5Cr-5Ti tested at room temperature (25, 250, and 400°C). A comparison of the fatigue data generated in rough and high vacuums shows that a pronounced environmental degradation of the fatigue properties exists in this alloy at room temperature. Fatigue life was reduced by as much as 84%. Cyclic stress range data and SEM observations suggest that this reduction is due to a combination of increases in rates of crack initiation and subsequent growth. The relative contribution of each difference is dependent upon the strain range.

In high vacuum, the fatigue results also show a trend of increasing cyclic life with increasing temperature between 25 and 400°C. From the limited data available, life at 250°C averages 1.7 times that at 25°C, and at 400°C, life averages 3.2 times that at room temperature. Like the environmental effects at 25°C, the effect of temperature seems to be a function of strain range at each temperature.

The total strain range and cycles to failure were correlated using a power law relationship and compared to 20% cold-worked 316 stainless steel and several vanadium-base alloys. The results suggest that V-5Cr-5Ti has better resistance to fatigue than 316-SS in the temperature range of 25 to 400°C. At 400°C, the data also show that V-5Cr-5Ti out performs Vanstar alloys 7 and 8 over the entire range of strains investigated. Furthermore, the fatigue properties of the V-5Cr-5Ti alloy compare favorably to V-15Cr-5Ti (at 25°C) and Vanstar 9 (at 400°C) at strains greater than 1%. At lower strains, the lower fatigue resistance of V-5Cr-5Ti is attributed to the higher strengths of the V-15Cr-5Ti and Vanstar 9 alloys.

INTRODUCTION: Low cycle fatigue tests were conducted on samples of V-5Cr-5Ti from Teledyne Wah Chang Ht. 832394 (ANL designation BL63) at temperatures of 25, 250, and 400°C and pressures less than 7.3×10^{-6} Pa (5.5×10^{-8} torr). In addition to these data, the effect of environment on fatigue properties at ambient temperatures was examined by conducting additional tests in a rough vacuum of $\sim 2.6 \times 10^{3}$ Pa (20 torr). The results are compiled in the form of tables and plots. Where data permit, comparisons are made between this V-5Cr-5Ti alloy and other vanadium-base alloys and 316 stainless steel.

Materials and Procedures

Specimens were fabricated from a 6.35 mm (0.25 in) thick plate of V-5Cr-5Ti produced by Teledyne Wah Chang (Heat 832394). The chemical composition (wt.%) of the plate was 5.1 Ti, 4.5 Cr, 310 ppm Si, 35 ppm C, 364 ppm O, 52 ppm N, and 1.1 ppm H with the balance being vanadium. The mechanical properties of this heat have been studied extensively at the Argonne National Laboratory (ANL), where this heat of material is referred to as BL63. The plate was received in the annealed condition (1 *h* at 1125°C) and specimens were fabricated with the geometry shown in Fig. 1. Following machining, the specimens were etched using a solution of 60% H_2O - 30% HNO_3 - 10% HF for approximately two minutes, wrapped in Ta foil, and annealed at 1125°C for 1 *h* in a vacuum of less than 1×10^{-5} Pa (10^{-7} torr). The resulting microstructure is shown in Fig. 2. An equiaxed grain structure is present within an average ASTM grain size of 6.

Tests were conducted on a servo-hydraulic test frame using a strain computer to convert diametral strain to an equivalent axial strain. The tests were conducted in axial strain control at a constant strain rate of 4×10^{-3}/s. During the course of testing, it was observed that V-5Cr-5Ti exhibits serrated yielding under some combinations of strain and temperature such that the strain range often had to be gradually increased to the desired level during the first 10-25 cycles. The presence of this behavior prevented testing at total strain ranges greater than 1.75% at the elevated temperatures and became more prominent as temperature increased. Typically, serrated yielding occurred at the onset of cycling in tests with a strain range $\geq 0.75\%$ and would disappear within several hundred cycles, only to re-emerge near the end of the tests.

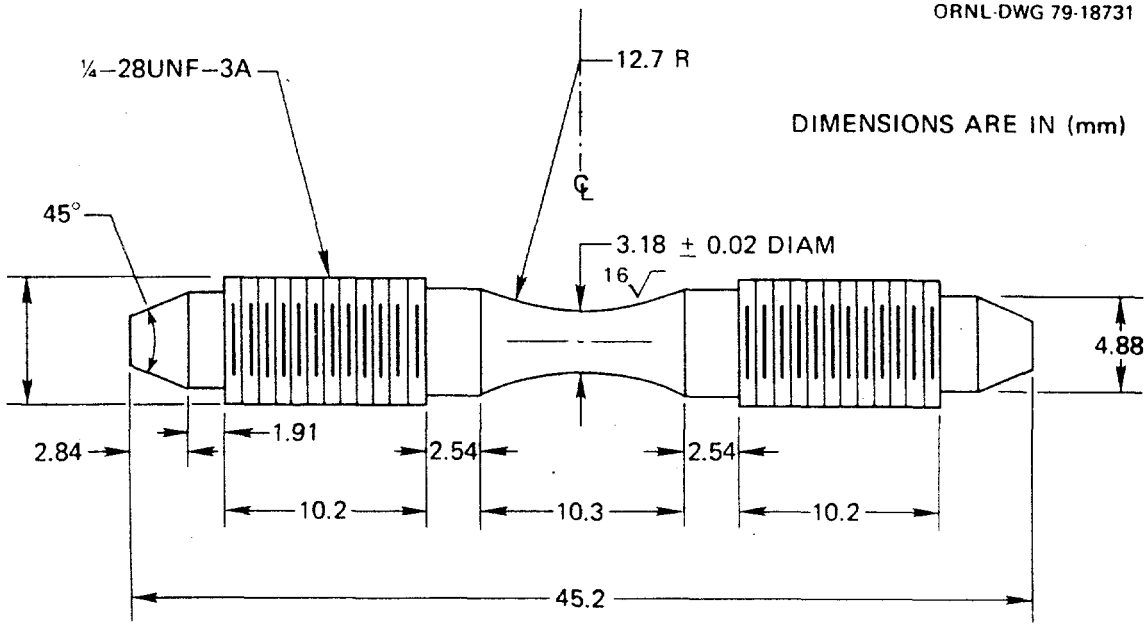

Fig. 1. Miniature hourglass fatigue specimen employed in fatigue testing. Dimensions are in millimeters.

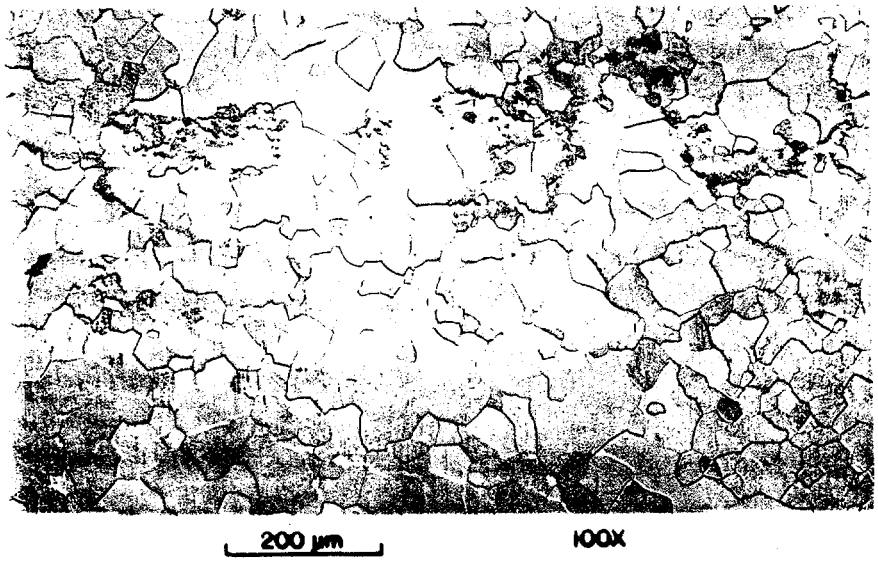

Fig. 2. Photomicrographs of V-5Cr-5Ti alloy (93-0991-1).

Heating was accomplished using RF induction, and temperatures were maintained within ±2°C of the desired setpoint. Initial tests at room temperature were conducted in a rough vacuum of ~ 2.6 x 10^3 Pa (20 torr) that was used to maintain the cleanliness of the test chamber. All other experiments were initiated after a pressure of less than 7.3 x 10^{-6} Pa (5.5 x10^{-8} torr) was obtained while at the desired test temperature. Pressures typically continued to drop to less than 2.0 x10^{-6} Pa during cycling.

Heating was accomplished using RF induction, and temperatures were maintained within ±2°C of the desired setpoint. Initial tests at room temperature were conducted in a rough vacuum of ~ 2.6 x 10^3 Pa (20 torr) that was used to maintain the cleanliness of the test chamber. All other experiments were initiated after a pressure of less than 7.3 x 10^{-6} Pa (5.5 x10^{-8} torr) was obtained while at the desired test temperature. Pressures typically continued to drop to less than 2.0 x10^{-6} Pa during cycling.

EXPERIMENTAL RESULTS: The results of the fatigue tests have been listed in Table 1 and plotted in Fig. 3. The data were fitted to a power law expression originally suggested by Manson [1] and given by:

$$\Delta\varepsilon_t = AN_f^{-\alpha} + BN_f^{-\beta}$$

where, $\Delta\varepsilon_t$ = total strain range in %, N_f = number of cycles to failure, and A, B, α and β are material constants. The values of these constants can be found in Table 2. The data for α have values on the same order of magnitude as reported by Liu [2] for V-15Cr-5Ti, but must be viewed with caution since the data used to generate them came from tests in which the cyclic lives are relatively short. The values for ß also compare well with those reported by Liu for V-15Cr-5Ti, but the values of β for both V-15Cr-5Ti and V-5Cr-5Ti differ from the 0.5 to 0.6 often reported in engineering alloys.

Table 1. Summary of Test Conditions and Results for LCF Experiments Conducted on V-5Cr-5Ti (TWC Ht. 832394)

Spec. No.	Δεt (%)	Temp. (°C)	Nf	Δεp (%)a	ΔεE (%)b	Δσ (MPa)a	Pressure (Pa)
VA 05	0.49	25	134,923	≈ 0	0.49	58.8	2.6 x103
VA 04	0.59	25	49,367	0.011	0.579	711.3	2.6 x103
VA 03	0.732	25	22,165	0.018	0.714	882.7	2.6 x103
VA 07	0.98	25	5906	0.121	0.859	1016.6	2.6 x103
VA 02	1.54	25	2240	0.62	0.92	1068.3	2.6 x103
VA 06	2.04	25	1088	1.12	0.92	1116.1	2.6 x103
VA 16	0.77	25	136,829	0.033	0.74	921.5	≤ 7.3 x10-6
VA 14	1.02	25	37,379	0.138	0.882	1007.2	≤ 7.3 x10-6
VA 15	1.52	25	11,613	0.60	0.92	1033	≤ 7.3 x10-6
VA 20	0.78	250	206,642	0.11	0.67	805.4	≤ 7.3 x10-6
VA 18	1.00	250	74,381	0.253	0.747	826.7	≤ 7.3 x10-6
VA 19	1.38	250	30,476c	0.74	0.64	843.7	≤ 7.3 x10-6
VA 21	1.54	250	18,550	0.80	0.74	851.4	≤ 7.3 x10-6
VA 17	0.76	400	336,030	0.07	0.69	811.3	≤ 7.3 x10-6
VA 09	1.00	400	164,277	0.286	0.714	869.9	≤ 7.3 x10-6
VA 11	1.23	400	75,052	0.482	0.748	905.0	≤ 7.3 x10-6
VA 13	1.53	400	33,476	0.743	0.787	940.0	≤ 7.3 x10-6
VA 12	1.77	400	25,272	0.98	0.79	921.1	≤ 7.3 x10-6

Notes: (a) Measured from a loop near midlife. $\Delta\varepsilon_p$ = width of hysteresis loop at zero load.
(b) The quantity $\Delta\varepsilon_E = \Delta\varepsilon_t - \Delta\varepsilon_p$.
(c) Strain range dropped during test, resulting in unusually long cycle life. Datum plotted but not considered in determination of material constants.

Table 2. Material Constants in Coffin-Manson Equation for V-5Cr-5Ti Alloy

Temperature (°C)	Press. (Pa)	A	α	B	β
25	2.6 x 103	2.85	0.1464	50,093	1.493
25	≤7.3 x 10-6	2.384	0.0983	35,143	1.176
250	≤7.3 x 10-6	1.47	0.0646	2611	0.823
400	≤7.3 x 10-6	1.39	0.0552	611	0.638

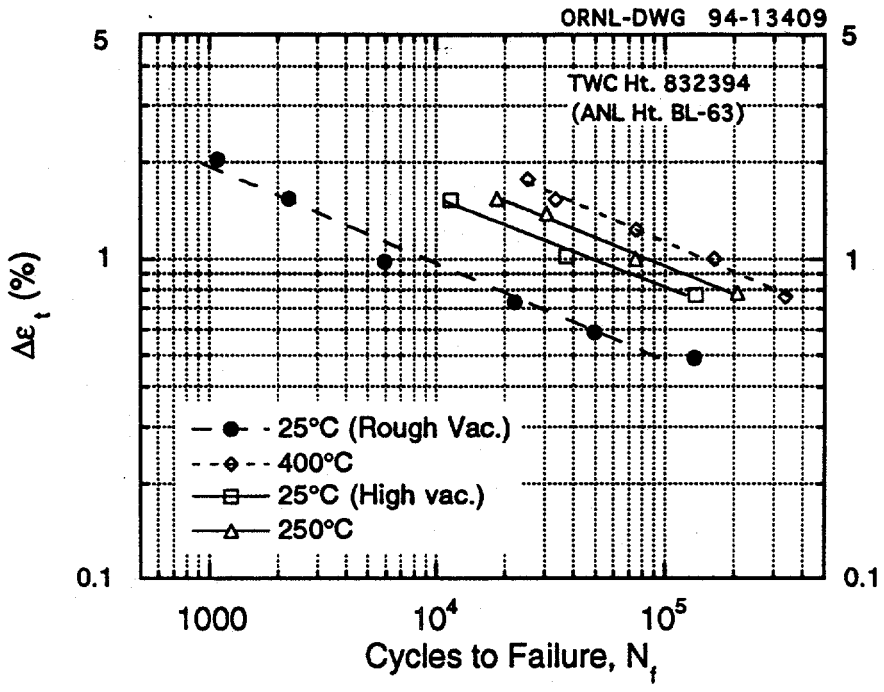

Fig. 3. Cyclic fatigue data for V-5Cr-5Ti tested at 25, 250, and 400°C in rough and high vacuums.

Two observations can be easily drawn from Fig. 3. First, the fatigue lives in high vacuum increase with increasing temperature over the range investigated. This increase in life varies from a factor of 1.5 to 4.4 times that observed at 25°C (refer to Table 3.). Swindeman [3] has reported similar results on niobium alloy D-43 where he observed increasing plastic strain resistance (*ie.*, life) at temperatures up to 871°C. Swindeman also noted that above 871°C, the magnitude of the increase began to decrease and it is likely that similar behavior would be observed in the V-5Cr-5Ti alloy. The second observation is that at room temperature there is a considerable effect of environment on the fatigue life. Between rough and high vacuum, there is an increase in life that ranges from a factor of about 5 to 6 (Refer to table 3.).

Table 3. Comparison of Cyclic Lives Under Various Conditions for Selected Strain Ranges

Nominal Δεt (%)	Nhv/Nrv at 25°C	N250/N25	N400/N25
0.75	6.17	1.51	2.46
1.00	6.33	1.99	4.39
1.53	5.18	1.60	2.88

Notes: (a) N_{hv}/N_{rv} is the ratio of observed life at 25°C in high vacuum to that observed in a rough vacuum.
(b) N_{250}/N_{25} is the ratio of fatigue life at 250°C to that at 25°C for tests conducted in a high vacuum.
(c) N_{400}/N_{25} is the ratio of fatigue life at 400°C to that at 25°C for tests conducted in a high vacuum.

In Figs. 4, 5 and 6, plots of the stress range as a function of cycle count ($\Delta\sigma$ vs. N) are shown for select fatigue tests at 25°C and all those conducted at 250 and 400°C. In all the tests, the V-5Cr-5Ti alloy cyclically hardens up to the point of crack initiation. At 25°C, in most tests conducted in high vacuum, initiation takes place early and a considerable fraction of life is spent propagating a crack. Conversely, plots of the stress range as a function of cycle count for tests (at 25°C) conducted in rough vacuum suggest that crack initiation dominated and crack propagation was rapid.

Fatigue fracture surfaces from six specimens were examined using scanning electron microscopy (SEM) to better understand the nature of crack propagation and the effect of environment. In all tests, crack propagation appears to have occurred in a predominantly transgranular fashion with small amounts of intergranular fracture. Intergranular fracture typically occurred when grain boundaries were oriented such as to trap an approaching crack.

In Fig. 7, SEM micrographs are shown for tests conducted in rough and high vacuums at a nominal total strain range of 0.75%. The fracture morphology for the test conducted in rough vacuum (Fig. 7a) shows a courser striation spacing in combination with secondary cracking and a more brittle appearance than that observed for the test conducted in high vacuum (Fig. 7b). When viewed at a higher magnification (refer to Fig. 8a), the area shown in Fig. 7b shows signs of ductility on a microscopic scale, which is not present for the test in rough vacuum (*cf.* Fig. 8b),. This microductility was also observed in tests conducted at elevated temperatures conducted in high vacuum. With increasing temperatures, the amount of ductility appears greater, as one might expect.

The fine dipples creating the appearance of microductility on some of these fracture surfaces are associated with very fine particles. Previous studies have shown that the primary precipitates identified in vanadium alloys are titanium oxycarbonitrides [4] and it is assumed that these are present here. In other areas, the average size of features associated with this phenomena suggest that crack face welding has occurred during the compressive portion of the strain cycle.

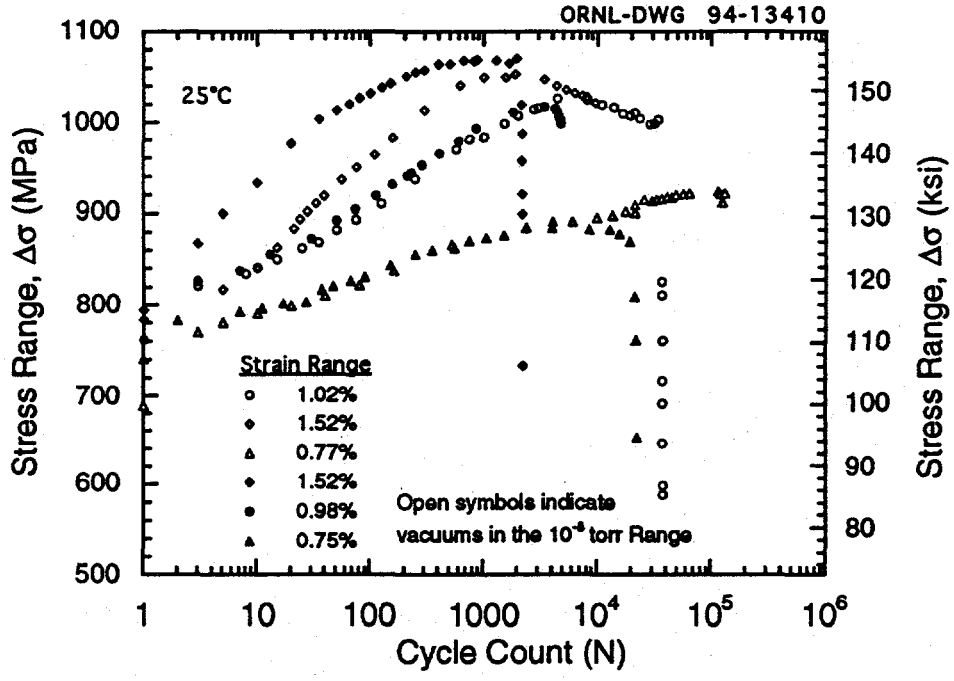

Fig. 4. Comparison of room temperature cyclic stress behavior of V-5Cr-5Ti alloy in rough and high vacuums.

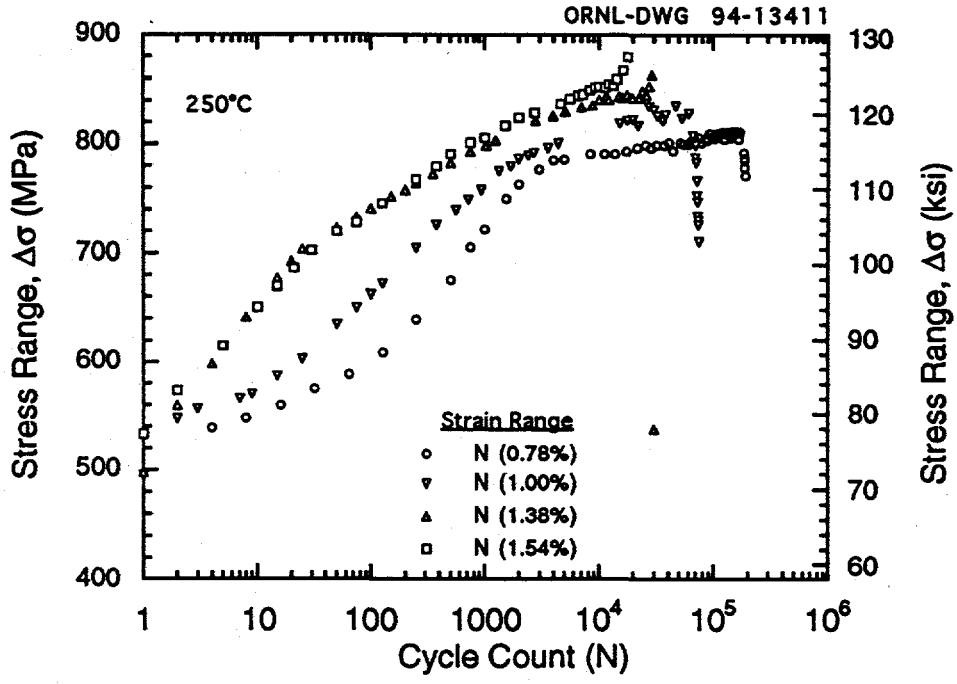

Fig. 5. Cyclic stress ranges vs cycle count for V-5Cr-5Ti alloy at 400°C.

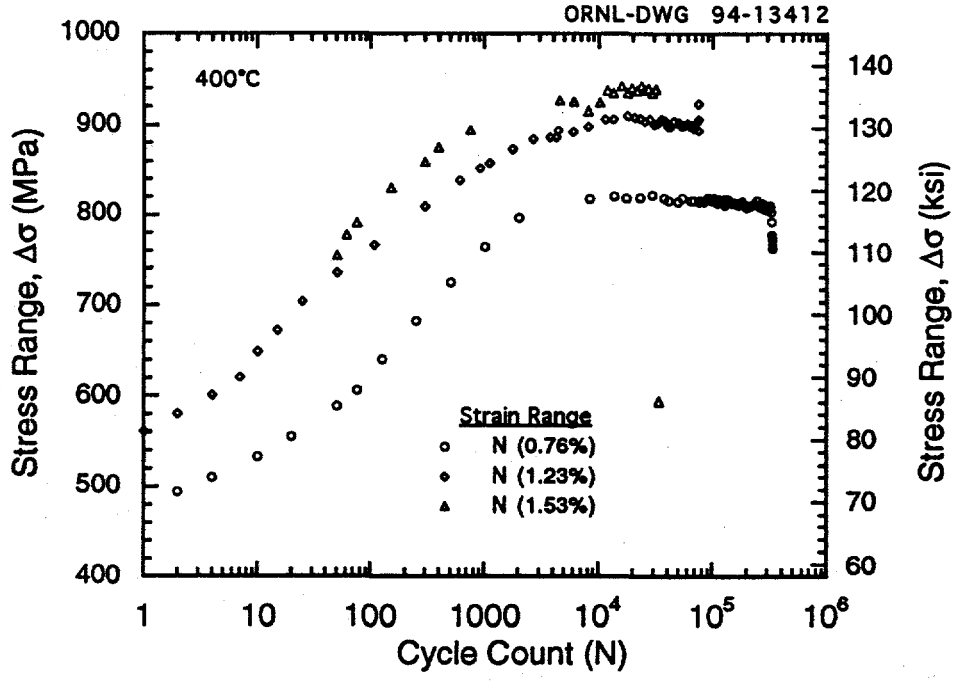

Fig. 6. Cyclic stress ranges vs cycle count for V-5Cr-5Ti alloy at 400°C.

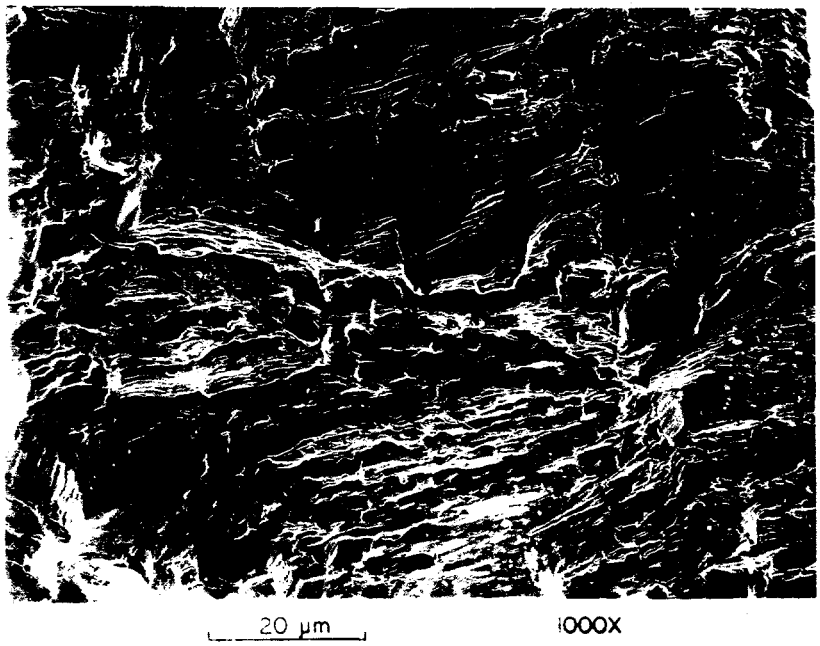

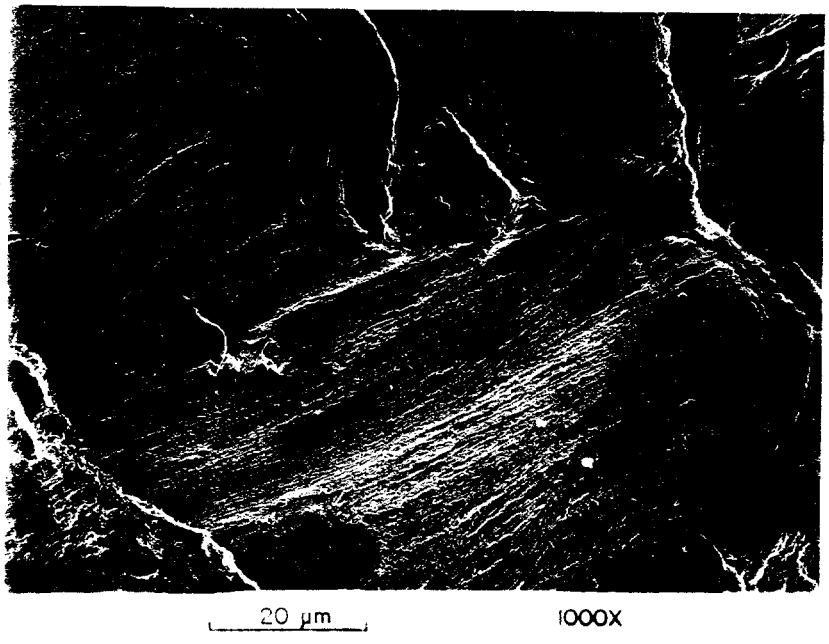

Fig. 7. Scanning electron microscopy of RT fatigue fracture surfaces indicates differences in the fatigue crack propagation process for a nominal 0.75% strain range. (a) Sample 03 - tested in rough vacuum (U 007477). (b) Sample 16 - tested under high vacuum (U 007479).

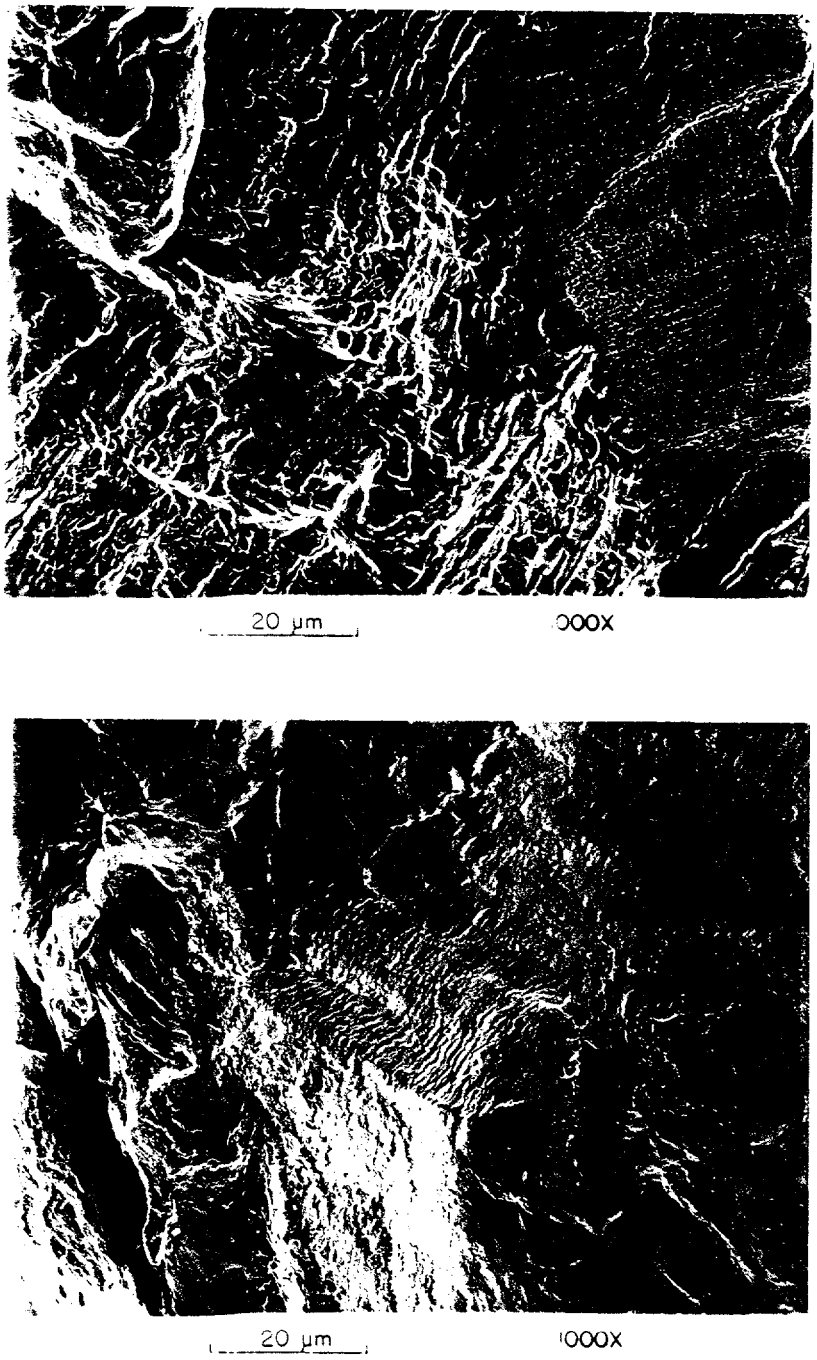

Fig. 8. Scanning electron microscopy of RT fatigue fracture surfaces from tests conducted at a nominal 0.75% strain range. (a) Sample 16 - tested under high vacuum showing ductility on a microscopic scale (U 007476). (b) Sample 03 - tested in rough vacuum (U 007480).

DISCUSSION OF RESULTS

Environmental Effects

Several possible mechanisms exist which may explain the reduction in life observed in experiments conducted in a rough vacuum, including; (1) pickup of O and N interstitials, (2) changes in the crack initiation and/or growth mechanisms, and (3) hydrogen embrittlement arising from the interaction of moisture with the alloy. Oxygen and nitrogen are potent hardeners, but it is unlikely that diffusion rates of these species are sufficiently high at 25°C to have penetrated into the alloy and embrittled the alloy to any notable extent. Korth and Schmunk [5] conducted tests in air on Vanstar alloys 7, 8, and 9 at 400°C and found no change in oxygen content in post-test analyses of their samples. Hence, negligible oxygen (and nitrogen) diffusion at 25°C can be assumed.
On the other hand, oxygen or moisture present in the vacuum chamber may have formed a brittle oxide layer on any freshly exposed surfaces, such as those created by the rupture of a surface oxide during plastic deformation in each cycle or at persistent slip bands. Oxidation at persistent slip bands would result in earlier initiation and the repeated process oxide formation and rupture at a crack tip would lead to increased rates of crack growth. Furthermore, the formation of an oxide layer on the crack faces may prevent rewelding of these surfaces during the compression portion of the strain cycle, again, leading to increased crack growth rates. From the results shown in Fig. 4, a combination of these mechanisms is likely.

As Fig. 4 indicates, at the two lower strain ranges (nominally 0.75 and 1.0%) the data show little difference between rough and high vacuum up to point of maximum $\Delta\sigma$. At a nominal strain range of 1.5%, there is a notable difference in the hardening behavior for the majority of life. The reason for this is not known. The curves suggest that initiation occurs at approximately the same cycle count in the 1.53% strain range tests and that the difference in life is the result of a difference in crack growth rates. At the 1% strain range, it appears that differences in both the rate of initiation and crack growth are present. At the lowest strain range (0.75%), the curves suggest that both crack initiation and crack growth proceed more slowly in high vacuum. Hence, these curves suggest that the failure processes are complex and dependent upon the strain range. Additional testing would be required to estimate the relative contributions of each mechanism at work.

Surface oxides function as a barrier to hydrogen, but if it is removed by polishing, scratching, or chemical etching, hydrogen may be introduced from an aqueous medium, moisture in air, or an acid [6]. Cycling prior to crack initiation and during crack growth may have created and maintained an avenue for airborne moisture to reach and oxidize the alloy with the release and absorption of free hydrogen.

Comparison to Competing Alloys

An attempt has been made to compare data generated on V-5Cr-5Ti to other alloys under consideration for use in fusion reactors, including Vanstar alloys at 400°C, V-15Cr-5Ti alloy at 25°C, and 316 stainless at 25°C [7] and 430°C [6]. In most cases, test conditions are not identical to those used in the current study and a very limited data base exists making any comparison difficult.

In Fig. 9, a comparison of the room temperature low cycle fatigue properties of the V-5Cr-5Ti alloy is made with both 316 stainless steel [7] and a V-15Cr-5Ti alloy [2]. From the limited data, both the vanadium alloys appear to have better plastic strain resistance than does 316 stainless. The data may suggest that the endurance strain in the 316 SS is 0.25%, whereas estimates for the V-5Cr-5Ti and V-15Cr-5Ti are 0.5% and 0.75%, respectively. At strains greater than 1%, the data for the V-base alloys appear to converge, as would be expected since the ductilities do not differ by more than two percent [8] and strain controls life in this regime. The difference found at longer lives (lower strains) is attributed to increased strength of the V-15Cr-5Ti alloy and the resulting reduction in plastic strain ranges. Loomis et al., [8] report that both the yield and tensile strengths of the 5Cr alloy are 71-72% of those for the 15% alloy (σ_{ys} = 387 vs. 545; σ_{uts} = 454 vs. 634 MPa).

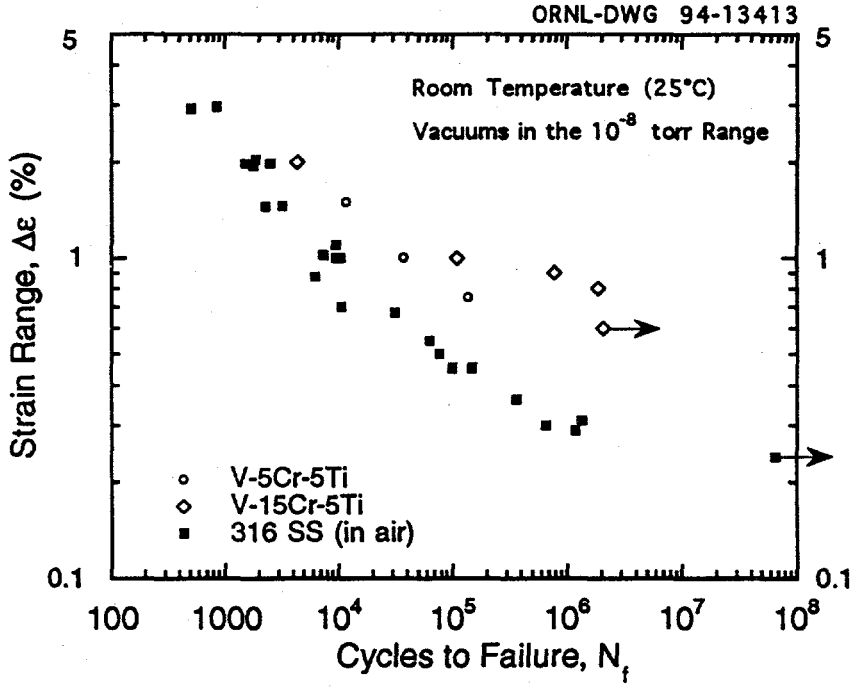

Fig. 9. Comparison of fatigue properties of V-5Cr-5Ti and V-15Cr-5Ti alloys to 316 SS at 25°C. Data for 316 stainless steel were obtained from Ref. 7 and those for V-15Cr-5Ti were obtained from Ref. 2.

Korth and Schmunk [5] tested Vanstar alloys 7, 8 and 9 in air at 400°C using a diametral extensometer and controlling the equivalent axial strain. Their data show little difference between the number of cycles, N_0, at initiation and the number of cycles to failure, N_f ,and they suggested that atmosphere had little effect on test results. In light of the results for V-5Cr-5Ti alloy, it is likely that N_f for tests conducted in vacuum would have been much greater. Notwithstanding this difficulty, the data are plotted in Fig. 10 and several observations can be drawn. First, at strain ranges of 1% or more, the V-5Cr-5Ti alloy shows better resistance to fatigue damage than Vanstar 9. At lower total strain ranges, the opposite is true. The better performance of Vanstar 9 at lower total strain ranges is, again, attributed to its higher yield strength (ie., 360 MPa [5] vs 250 MPa [8]) and the resulting reduction in plastic strains.

A second observation is that the V-5Cr-5Ti out performs alloys Vanstar 7 & 8 at all strain ranges shown. A comparison of the tensile data of Korth and Schmunk [5] on the Vanstar alloys to that of Loomis et al. [8] on V-5Cr-5Ti indicates that the V-5Cr-5Ti has greater strength than the Vanstar alloys 7 & 8 at 400°C. However, the authors believe that the testing of Vanstar alloys 7, 8, and 9 in vacuum would result in higher cyclic lives and probably eliminate much of the observed differences.

In Fig. 10, a comparison of the low cycle fatigue properties of the V-5Cr-5Ti alloy at 400°C is also made with 316 stainless steel [9] tested at 430°C. In this case, Grossbeck and Liu used the same specimen geometry and test method as was used in testing the V-5Cr-5Ti alloy such that the data should be very easily comparable with the exception of temperature. Again, the results suggest that the V-5Cr-5Ti alloy has better low cycle fatigue properties than does the 316 stainless around 400°C. While insufficient data exist to allow an endurance strain to be determined from the V-5Cr-5Ti alloy, it should be in the 0.5-0.6% range in comparison to the 0.3-0.4% value for the 316 stainless.

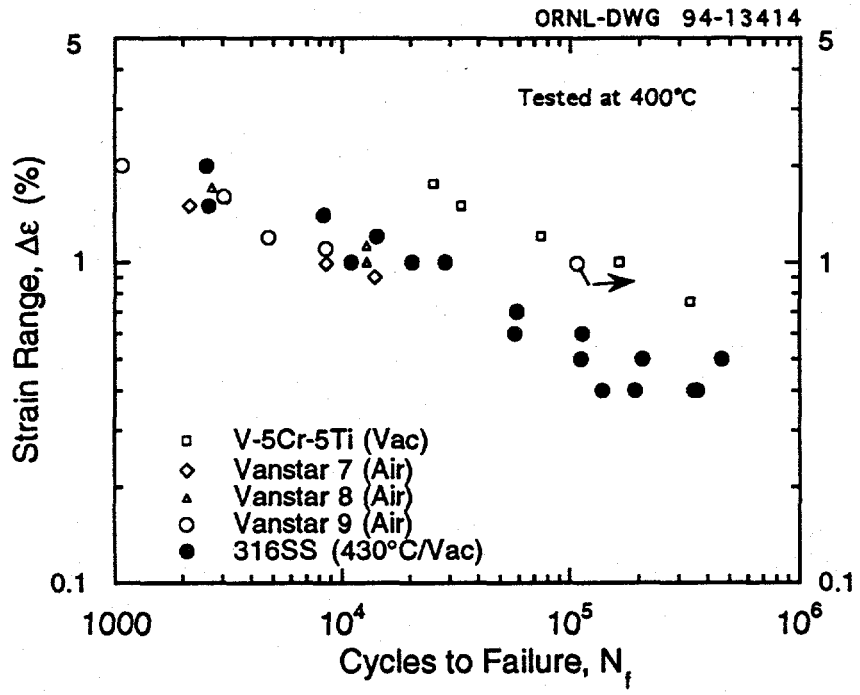

Fig. 10. Comparison of fatigue data for vanadium-base alloys and 316 stainless steel at temperatures 400 to 430°C. Data for 316 stainless were obtained from Ref. 9. Data for Vanstar alloys were obtined from Ref. 5.

CONCLUSIONS

In-vacuum low cycle fatigue tests have been conducted on unirradiated V-5Cr-5Ti tested at temperatures of 25, 250, and 400°C. A comparison of the fatigue data generated in rough and high vacuums shows that a pronounced environmental degradation of the fatigue properties exists in this alloy at room temperature. Fatigue life was reduced by as much as 84%. The cyclic stress range data and SEM observations suggest that this difference is due to a combination of differences in rates of crack initiation and subsequent crack growth. The relative contribution of each difference is dependent upon the strain range.

In high vacuum, the fatigue results also show a trend of increasing cyclic life with increasing temperature between 25 and 400°C. From the limited data available, life at 250°C averages 1.7 times that at 25°C, and at 400°C, life averages 3.2 times that at 25°C. Like the environmental effects at 25°C, the effect of temperature seems to be a function of strain range at each temperature.

The total strain range and cycles to failure were analyzed using a power law correlation and compared to 20% cold-worked 316 stainless steel and several vanadium-base alloys. The results suggest that V-5Cr-5Ti has better resistance to fatigue than 316-SS in the temperature range of 25 to 400°C. At 400°C, the data also show that V-5Cr-5Ti out performs Vanstar alloys 7, and 8 over the entire range of strains investigated. Furthermore, the fatigue properties of the V-5Cr-5Ti alloy compare favorably to V-15Cr-5Ti (at 25°C) and Vanstar 9 (at 400°C) at strains greater than 1%. Differences seen at higher lives (lower strains) are attributed to the higher strength of the V-15Cr-5Ti and Vanstar 9 alloys.

FUTURE WORK

Low cycle fatigue studies are complete on this heat of V-5Cr-5Ti. Additional LCF tests may be conducted on the new 500 kg heat of this alloy currently being melted by TWC for ANL. The emphasis of future testing will likely shift to fatigue crack propagation measurements on this new heat of material.

REFERENCES

1. S.S. Manson, discussion of ASME paper 61-WA-199 by Tavernelli and Coffin, **J. Basic Eng. (Trans. ASME), 84 (No. 4)**, Dec 1962, 537-541.

2. K.C. Liu, *High Temperature Fatigue Behavior of Unirradiated V-15Cr-5Ti Tested in Vacuum*, **Journal of Nuclear Materials, 103 & 104**, (1981) 913-918.

3. R.W. Swindeman, *Low-Cycle Fatigue Study of Columbium Alloy D-43*, in **Fatigue at High Temperature**, ASTM STP 459, American Society for Testing and Materials, 1969, 31-41.

4. T. Schober and D.N. Braski, *The Microstructure of Selected Annealed Vanadium-Base Alloys*, **Met. Trans., 20A**, (1989), 1927.

5. G.E. Korth and R.E. Schmunk, *Low-Cycle Fatigue of Three Irradiated and Unirradiated Vanstar Alloys*, in **Effects of Radiation on Structural Materials**, ASTM STP 683, J.A. Sprague and D. Krammer, Eds., American Society for Testing and Materials, 1979, 466-476.
6. M.L. Grossbeck, *et al.*, *Fabrication of Vanadium Alloy Product Forms for Specimen Preparation*, in **Fusion Reactor Materials Semiannual Progress Report for Period Ending March 31, 1994**, U.S. Department of Energy, DOE/ER-0313/16 (1994).

7. C.E. Jaske and N.D. Frey, *High Cycle Fatigue of Type 316 Stainless Steel at Temperatures Up to 593°C (1100°F)*, Rockwell International, Report No. ESG-DOE-13307.

8. B.A. Loomis, *et al.*, *Tensile Properties of Vanadium and Vanadium-Base Alloys*, in **Fusion Reactor Materials Semiannual Progress Report for Period Ending March 31, 1991**, U.S. Department of Energy, DOE/ER-0313/10 (1991) 145-155.

9. M.L. Grossbeck and K.C. Liu, *Fatigue Behavior of Type 316 Stainless Steel Irradiated in a Mixed Spectrum Fission Reactor Forming Helium*, **Nuclear Tech, 58**, Sep. 1982, 538-547.

Subtask 12E1: COMPATIBILITY OF STRUCTURAL MATERIALS IN LIQUID ALKALI METALS

K. Natesan, D. L. Rink, R. Haglund, and R. W. Clark (Argonne National Laboratory)

OBJECTIVE

The objectives of this task are to (a) evaluate the chemical compatibility of structural alloys such as V-5 wt.%Cr-5 wt.%Ti alloy and Type 316 stainless steel for application in liquid alkali metals such as lithium and sodium-78 wt.% potassium (NaK) at temperatures that are in the range of interest for the International Thermonuclear Experimental Reactor (ITER); (b) evaluate the transfer of nonmetallic elements such as oxygen, nitrogen, carbon, and hydrogen between structural materials and liquid metals; and (c) evaluate the effects of such transfers on the mechanical and microstructural characteristics of the materials for long-term service in liquid-metal environments.

SUMMARY

Candidate structural materials are being evaluated for their compatibility, interstitial-element transfer, and corrosion in liquid alkali-metal systems such as lithium and NaK. Type 316 stainless steel and V-5Cr-5Ti coupon specimens with and without prealuminizing treatment have been exposed to NaK and lithium environments of commercial purity for times up to 3768 h at temperatures between 300 and 400°C.

INTRODUCTION

Liquid metals are being considered for a coolant/tritium-breeding blanket in the ITER. These liquid metals include lithium, Pb-Li eutectic mixture, and sodium-78 wt.% potassium alloy (NaK). The structural materials considered for the first-wall application are Type 316 austenitic stainless steel and V- 4-5 wt.%Cr- 4-5 wt.%Ti alloy. In the fusion application, the structural material of the system must be compatible with the liquid metal and must also maintain structural integrity for long periods during exposure to moderately elevated temperatures, thermal cycling, and possible intense irradiation; it must also be amenable to low magetohydrodynamic (MHD) losses during flow in a magnetic field.

Some of the important key performance variables in the use of liquid metals in first-wall/blankets are:[1]

(a) Liquid Metal Compatibility
  Corrosion due to metallic element mass transfer
  Nonmetallic-element (oxygen, carbon, and nitrogen) mass transfer
  Influence of corrosion on mechanical properties
(b) Tritium Inventory and Transport
  Hydrogen/tritium solubility in liquid metal
  Hydrogen/tritium distribution between liquid metal and structural material
  Tritium recovery methods
  Effects on structural materials

BACKGROUND

For the ITER, the structural materials considered are Type 316 stainless steel and V-5Cr-5Ti alloy. The liquid metals of interest are NaK, lithium, and Pb-Li eutectic mixture. Physical properties of the three liquid metals are given in Table 1. In general, structural materials can undergo various interactions upon exposure to liquid metals. The extent of interaction depends on temperature, temperature gradient, liquid metal velocity and purity, alloy composition, and the materials of construction of the containment system. The peak temperature for the liquid metal in ITER is expected to be ≈400°C, with a maximum temperature gradient of ≈100°C around the loop. Under these conditions, metallic-element mass transfer between the structural materials and the liquid metal occurs predominantly by leaching of the alloy constituents of the materials. This leaching is dictated by the solubility of the alloy constituents in the liquid metal. Nonmetallic elements such as oxygen, carbon, nitrogen, and hydrogen are known to migrate in structural-material/liquid-metal systems as a result of differences in chemical activity. The transfer of these elements can affect the microstructural changes and long-term mechanical properties of the materials. In addition, distribution of hydrogen and hydrogen isotopes between the structural material and liquid metal, as well as permeation of these elements through the structural alloy, must be known so the desired inventory of tritium in the system can be controlled and maintained.

Table 2 lists the available data on the solubility of several substrate elements in NaK, lithium, and Pb-Li at 400°C. Also shown in Table 2 are the values for the constant B in the solubility expression that determines the temperature dependence of the solubility. The table shows that the solubility values are low for the primary constituents (iron, chromium, and nickel) of stainless steel in NaK. Further, the constituents of the V-5Cr-5Ti alloy will have a tendency to develop oxide scales in NaK that is purified by a cold-trapping technique. In lithium, the solubilities of iron and chromium are low but that of nickel is somewhat higher. As a result, the extent of corrosion of stainless steel in lithium involves loss of nickel from the steel and development of an Fe-Cr ferritic layer in the surface regions of the lithium-exposed steel. Elements such as vanadium and titanium tend to form respective nitrides in cold-trapped lithium. In Pb-Li, the solubility values for iron, chromium, and nickel are higher, with that of nickel substantially higher than that in lithium. The data also show that the dependence of solubility is less sensitive to temperature in Pb-Li than in lithium, indicating a potential for higher corrosion rates even at lower temperatures.

An assessment of corrosion loss rates for austenitic stainless steel and for the vanadium alloy in several liquid-metal environments is shown in Fig. 1 as a function of reciprocal temperature.[2-8] At a service temperature of 400°C, corrosion losses for stainless steel are ≈0.07, 2, and 20 μm/yr in NaK, lithium, and Pb-Li environments, respectively. At 400°C, the values for the vanadium alloy are 0.3 and 5 μm/yr in NaK and lithium environments, respectively. At present, data are not available for the vanadium alloy exposed to Pb-Li environments. It is imperative that a viable material resist not only dissolution of its constituents in liquid metal but also deposition of metallic/nonmetallic elements from the liquid-metal, especially in liquid metal loops constructed of dissimilar metals. Nonmetallic elements such as oxygen, carbon, and nitrogen are known to migrate in structural-material/liquid-metal systems as a result of differences in chemical activity. A detailed analysis was published earlier on the

thermodynamics of nonmetallic impurity elements in liquid metals, with emphasis on purification of the liquid metals and chemical compatibility of candidate structural materials.[9,10] Cold trapping, hot (getter) trapping, and molten-salt extraction are the three purification methods currently available to achieve the desired low concentrations of nonmetallic elements in liquid alkali metals and to maintain them at low levels for extended periods of time in dynamic loop systems. The effectiveness of each method in achieving the desired purification varies for different nonmetallic elements in the liquid and also differs for the same nonmetallic element in different liquid-alkali metals. In general, the complexity of the purification system and the relative cost of purification increases as one moves from cold trapping to molten-salt extraction.[1]

Figure 2 is a plot of solubility values excerpted from the literature for nonmetallic elements in liquid sodium, lithium, and Pb-Li as a function of temperature. The values for sodium can be used in the assessment of NaK. The primary impurity of concern in NaK is oxygen, whose level can be controlled by the cold-trapping method. Carbon and nitrogen concentrations in NaK are too low to be of concern, especially in the temperature range of interest for the ITER. The solubility curves for nonmetallic elements in liquid lithium indicate that concentrations of ≈30, 800, and 3800 ppm for oxygen, carbon, and nitrogen, respectively, can be achieved at a cold-trapping temperature of ≈200°C. The high concentrations of carbon, and nitrogen have been of concern in the compatibility of structural materials in liquid-lithium environments, especially at temperatures in excess of 450°C.

The major effects likely to occur in solid-metal/liquid-metal systems with large distribution coefficients are embrittlement of the solid metal as a result of increased interstitial-element concentration, and compound formation, i.e., oxide, nitride, or carbide formation, on the surface of the solid metal. Based on information developed on distribution coefficients, embrittlement and compound formation are expected with Group-IIIB, -IVB, and -VB metals with regard to oxygen and carbon in liquid sodium or NaK. The analysis suggests that structural metals such as vanadium, niobium, titanium, yttrium, and their alloys are prone to absorb oxygen and carbon upon exposure to liquid sodium or NaK. Because nonmetallic elements influence the ductile/brittle transition in many metals, the transfer of significant quantities of these interstitial elements to solid metals can substantially affect their mechanical integrity. The effect on ductility is particularly critical when thermal cycling and cyclic stresses are considered.

Unlike the distribution coefficients of oxygen in sodium and NaK, the distribution coefficients of oxygen in a lithium environment are much lower than unity for most metals, except yttrium. Two detrimental effects that can occur with low distribution coefficients are (a) reduction of mechanical strength of the metals as a result of loss of interstitial elements to the liquid metal and (b) grain-boundary penetration of solid metals that contain critical amounts of nonmetallic impurities. In liquid sodium and NaK environments, austenitic stainless steels will not develop iron or chromium oxides, especially at oxygen levels that correspond to cold-trapped liquid. Under such conditions, the corrosion rates of the materials are fairly low, and specific allowances (based on temperature, oxygen level in the liquid metal, and time) can be made to account for thickness loss. At temperatures of interest for the ITER, these rates will be essentially negligible. On the other hand, refractory metals such as vanadium, titanium, and yttrium will form their respective oxides upon exposure to liquid sodium and NaK at

oxygen levels corresponding to cold-trapped liquid. A nonadherent vanadium suboxide and titanium oxide can form on the surface of the vanadium alloy, together with diffusion of oxygen into the substrate. However, at temperatures of interest for the ITER, i.e., 200-400°C, the rate of formation of corrosion products, as well as diffusion rate for oxygen in the alloy, will be too small to be of any concern.

Unlike the behavior of refractory metals in sodium and NaK, the oxides of constituents of both stainless steel and V-Cr-Ti alloys are not stable in lithium at oxygen levels corresponding to a cold-trapped condition. The results also show that in general, the oxygen transfer will be from the structural metal to lithium, and the lack of oxide scale on the metal surface enables other interstitials (nitrogen and carbon) to play a larger role in the corrosion process. The high solubility of nitrogen in lithium, coupled with the absence of oxide barriers on metal surfaces exposed to a lithium environment, can result in significant nitridation of materials in lithium. However, at ITER temperatures, nitridation rates will be low and the hardened nitride layers will be confined to surface regions of the material.

Hydrogen gas dissolves in atomic form in metals, and, for dilute solutions of hydrogen in a metal, the relationship between the concentration and the partial pressure of hydrogen follows Sieverts' law, in which concentration is directly proportional to the square root of hydrogen partial pressure. The equations that relate the Sieverts' constant and temperature for various metal/hydrogen systems and the coefficients that describe the distribution of hydrogen among various structural metals and Li are presented elsewhere.[10,11] The hydrogen concentrations required for the formation of hydrides of selected metals are large, and calculations for hydride formation similar to those for other nonmetallic elements are generally not useful; however, calculations of hydrogen concentrations in various structural and liquid metals for specific hydrogen partial pressures are useful and are given elsewhere.[1] The calculations indicate that the hydrogen distribution ratio between lithium and vanadium is >1000 and that H concentrations in a vanadium-alloy exposed to lithium containing up to 100 wppm hydrogen are considerably lower than those corresponding to ductile/brittle transition in the alloy.[12,13]

EXPERIMENTAL PROCEDURE

Three static liquid-metal systems were designed and fabricated for studies on the compatibility of structural materials and insulator coatings in liquid metals. Figure 3 shows the experimental systems. Two of the systems were filled with ≈15 L of high-purity lithium, and the third system was filled with NaK; chemical compositions of the lithium and NaK environments are listed in Table 3. During the initial period of ≈3000 h, the two lithium systems were operated at 350 and 400°C and the NaK system was maintained at 300°C. Subsequently, the temperatures of all three systems were set at 300°C to examine the compatibility of insulator coatings, in support of the MHD test to be conducted at a maximum temperature of 300°C in an insulated test section . In one of the lithium systems, nitrogen gas was bubbled through a small tube immersed in lithium to increase the nitrogen concentration in the lithium.

Coupon specimens of V-5Cr-5Ti alloy and Type 316 stainless steel in bare and prealuminized conditions were exposed in the liquid-metal systems. Weight change

was measured to establish the corrosion rates for the structural alloys as a function of temperature, time, and liquid metal chemistry. After exposure, the specimens were examined with a scanning electron microscope (SEM) equipped with an energy-dispersive X-ray analyzer and by X-ray diffraction.

RESULTS

In the aluminizing pack-diffusion process, the substrate materials are encapsulated and heated for 4-12 h at ≈900°C with packing of powders. The composition of such powders (e.g., 65 wt.% Al_2O_3, 33 wt.% Al, 2 wt.% NH_4Cl) provides the packing with metallic aluminum, alumina as filler material, and NH_4Cl as activator. The aluminum deposited on the substrate surface diffuses into the subsurface regions of the material, where it forms intermetallic phases as aluminides of iron or nickel in stainless steel and of Al-V intermetallic in vanadium alloy. The aluminide layers reach thicknesses of 0.015–0.20 mm, depending on the composition of the substrate materials, length of exposure in the packing, and exposure temperature. Figure 4 shows the elemental concentration profiles of aluminum, vanadium, chromium, and titanium in a V-5Cr-5Ti alloy sample after an aluminizing treatment.

Figure 5 shows weight change data for both materials and bulk AlN specimens after exposure at 300°C to NaK of the purity given in Table 3. All of the specimens except prealuminized 316 stainless steel, showed very little weight change after 3768 h of exposure. The greater weight change of the prealuminized 316 stainless steel is primarily due to transfer of loose particles of Al_2O_3 powder that usually sticks to the surface of the samples during the pack-aluminizing process. This particle adherence is fairly random, and the particles can be removed from the surface (even though this is not done for the specimens tested at ANL) prior to exposure of the coupons in liquid-metal environments.

Figure 6 shows SEM photomicrographs of cross sections of coupon specimens of Type 316 stainless steel in bare and prealuminized condition after exposure to a lithium environment for 180 and 750 h at 350°C. Figure 7 shows similar photographs of the V-5Cr-5Ti alloy after exposure to a lithium environment. The figures show very little corrosion or surface recession in any of the specimens, and the rough surfaces on the prealuminized specimens are primarily due to separation of loose particles of powdered pack material, which generally sticks to the surface during the pack-diffusion process. Figure 8 shows weight change data for both structural materials in the bare and prealuminized condition and for bulk AlN material after ≈3000 h exposure to a lithium environment at 350°C. The base alloys exhibited very little weight change over a 3000-h exposure, indicating virtually no impurity-induced corrosion of the alloys in the lithium environment. The prealuminized specimens exhibit a somewhat greater weight change, especially during the initial 200 h of exposure. This change can be attributed to loss of loose powder particles embedded in the surfaces of the specimens from the aluminizing process. After ≈1500 h of exposure, weight losses were negligible for the balance of the exposure period. Because corrosion rates over long periods of time are determined by the slope of the weight change-versus-time curves in Fig. 8, it is evident that the rates are negligible for both substrate materials with or without aluminizing treatment and for AlN bulk samples at 350°C.

REFERENCES

1. K. Natesan, C. B. Reed, and R. F. Mattas, "Assessment of alkali metal coolants for the international thermonuclear experimental reactor blanket," Proc. 3rd Intl. Symp. on Fusion Nuclear Technology, Los Angeles, CA, June 27-July 1, 1994, to be published in Fusion Engineering and Design.

2. O. K. Chopra and D. L. Smith, "Influence of temperature and lithium purity on corrosion of ferrous alloys in a flowing lithium environment," J. Nucl. Mater. 141-143, 584-591 (1986).

3. H. U. Borgstedt, G. Frees, and G. Drechsler, "Corrosion of stainless steel in flowing PbLi eutectic," J. Nucl. Mater. 141-143, 561-565 (1986).

4. O. K. Chopra and D. L. Smith, "Compatibility of ferrous alloys in a forced circulation Pb-17Li system," J. Nucl. Mater. 141-143, 566-570 (1986).

5. H. Tas, J. Dekeyser, F. Casteels, J. Walnier, and F. De Schutter, "Mass transfer in pure lithium and lithium-lead dynamic environments: influence of system parameters," J. Nucl. Mater. 141-143, 571-578 (1986).

6. P. F. Tortorelli and J. H. DeVan, "Corrosion of ferrous alloys exposed to thermally convective Pb-17 at% Li," J. Nucl. Mater. 141-143, 592-598 (1986).

7. O. K. Chopra and D. L. Smith, "Corrosion behavior of vanadium alloys in flowing lithium," J. Nucl. Mater. 155-157, 683-689 (1988).

8. V. A. Evtikhin, I. E. Lyublinski, and V. Yu. Pankratov, "Vanadium alloys as structural materials for liquid lithium blanket of fusion reactors," J. Nucl. Mater. 191-194, 924-927 (1992).

9. D. L. Smith and K. Natesan, "Influence of nonmetallic impurity elements on the compatibility of liquid lithium with potential CTR containment materials," Nucl. Technol. 22, 392 (1974).
10. K. Natesan, "Influence of nonmetallic elements on the compatibility of structural materials with liquid alkali metals," J. Nucl. Mater. 115, 251-262 (1983).

11. K. Natesan and D. L. Smith, "Effectiveness of tritium removal from a CTR lithium blanket by cold trapping secondary liquid metals Na, K, and NaK," Nucl. Technol. 22, 138 (1974).

12. B. A. Loomis, A. B. Hull, and D. L. Smith, "Evaluation of low-activation vanadium alloys for use as structural material in fusion reactors," J. Nucl. Mater. 179-181, 148-154 (1991).

13. S. Yano, M. Tada, and H. Matsui, "Hydrogen embrittlement of MFR candidate vanadium alloys," J. Nucl. Mater. 179-181, 779-782 (1991).

Table 1. Selected physical properties of liquid metals of interest for ITER

Liquid Metal	Melting Point (°C)	Density at 400°C (kg/m^3)	Viscosity at 400°C (kg/m·s)	Volume Expansion at Melting (%)	Thermal Conductivity at 400°C (W/m·K)	Specific Heat at 400°C (kJ/kg K)	Electrical Resistivity (Ω·m)
NaK	-12.3	775	2.1×10^{-4}	2.5	24.1	0.76	6.0×10^{-7}
Li	181	518	6.7×10^{-5}	1.5	53.1	4.2	3.2×10^{-7}
Pb-Li	235	9600	1.5×10^{-3}	3.5	15.2	0.19	1.3×10^{-6}

Table 2. Solubility data for several elements of interest in various liquid metals

	NaK		Lithium		Lead–Lithium	
Element	Solubility at 400°C (wppm)	Constant B[a]	Solubility at 400°C (wppm)	Constant B[a]	Solubility at 400°C (wppm)	Constant B[a]
Fe	0.04	4116	0.94	3084	35	665
Cr	9×10^{-5}	9010	0.90	3219	5	500
Ni	0.55	1570	56.8	3304	2366	981
V	b	-	c	-	d	-
Ti	b	-	c	-	d	-
Al	24.2	440	4×10^{5}	-	2000	1680

[a]Solubility is expressed by log S(wppm) = A-B/T(K).

[b]Solubility is low V_9O or Ti_3O_2 are formed in cold-trapped NaK.

[c]Solubility is low and V_2N or TiN are formed in cold-trapped lithium.

[d]Data not available.

Table 3. Chemical compositions of lithium and NaK

Element	Lithium	NaK
Li	99.97%	<2 ppm
Na	50 ppm	20.4%
Ca	50 ppm	7.8 ppm
K	40 ppm	77.8 ppm
Fe	5 ppm	3.9 ppm
Si	10 ppm	-
Cl	10 ppm	-
N	80 ppm	-
Pb	-	<10 ppm
Sn	-	<20 ppm
Zn	-	6.2 ppm
Cu	-	2.4 ppm
Ni	-	<4 ppm

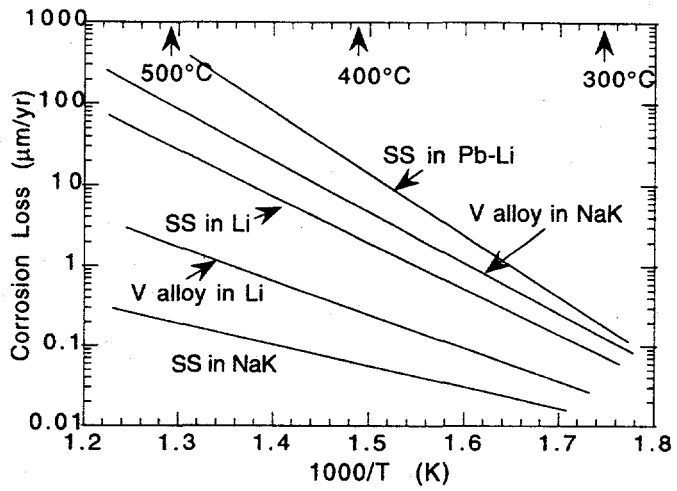

Fig.1. Corrosion loss versus reciprocal temperature for stainless steel and vanadium alloy in several liquid metals

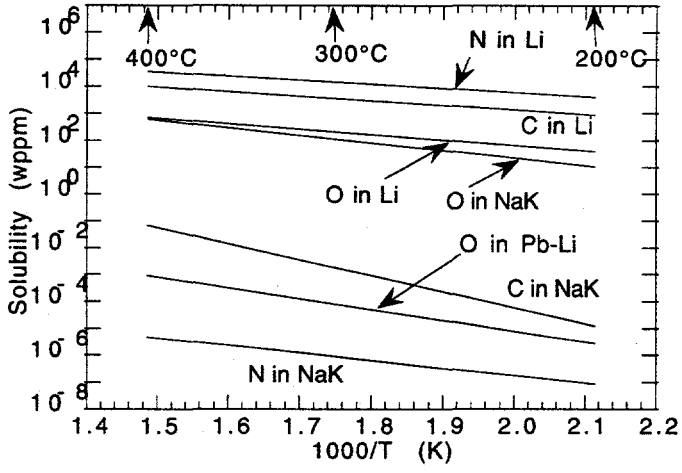

Fig. 2. Solubility as a function of reciprocal temperature for oxygen, carbon, and nitrogen in liquid metals

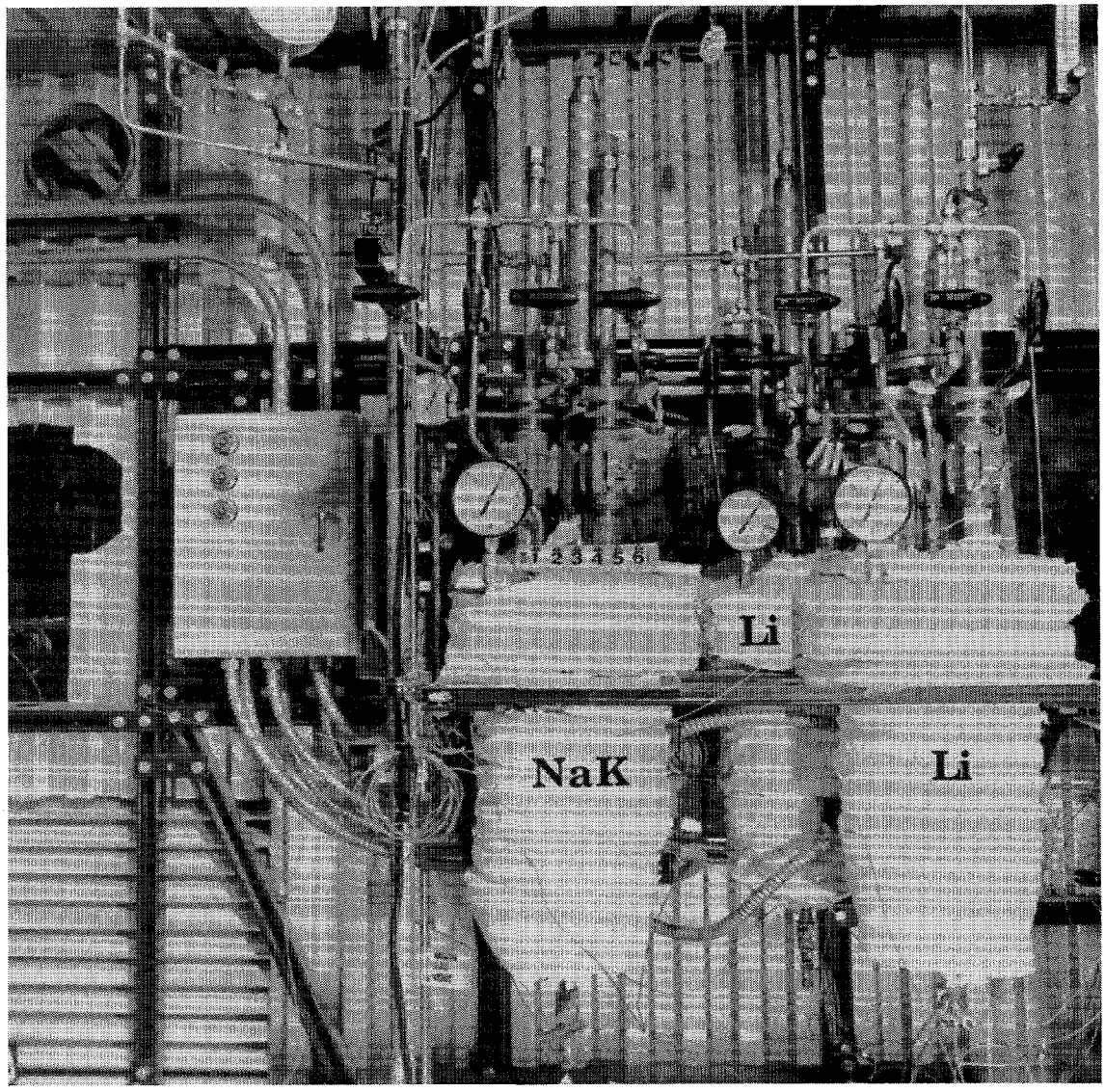

Fig. 3. Photograph of liquid-metal systems used in present study.

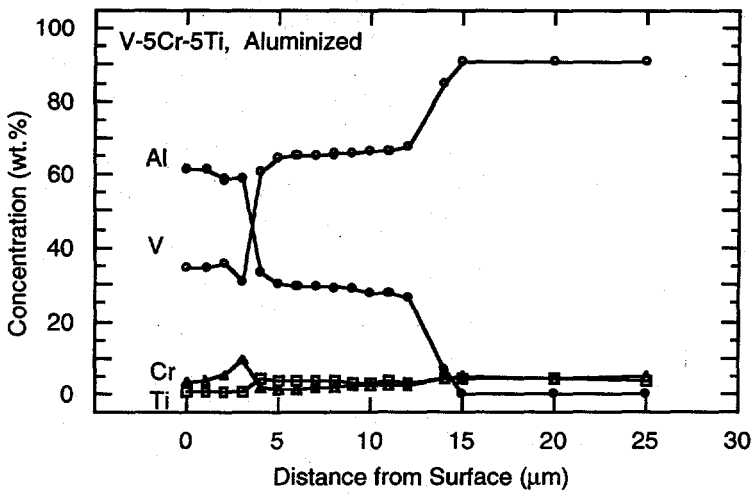

Fig. 4. Depth profiles for aluminum, vanadium, chromium, and titanium for aluminized specimen of V-5Cr-5Ti alloy

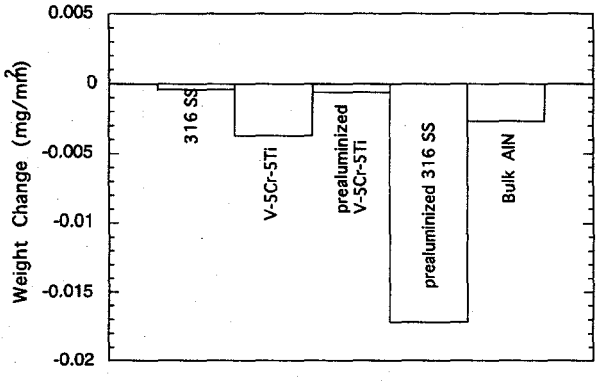

Fig. 5. Weight change data for V-5Cr-5Ti, Type 316 stainless steel, and bulk AlN specimens after exposure to NaK at 300°C

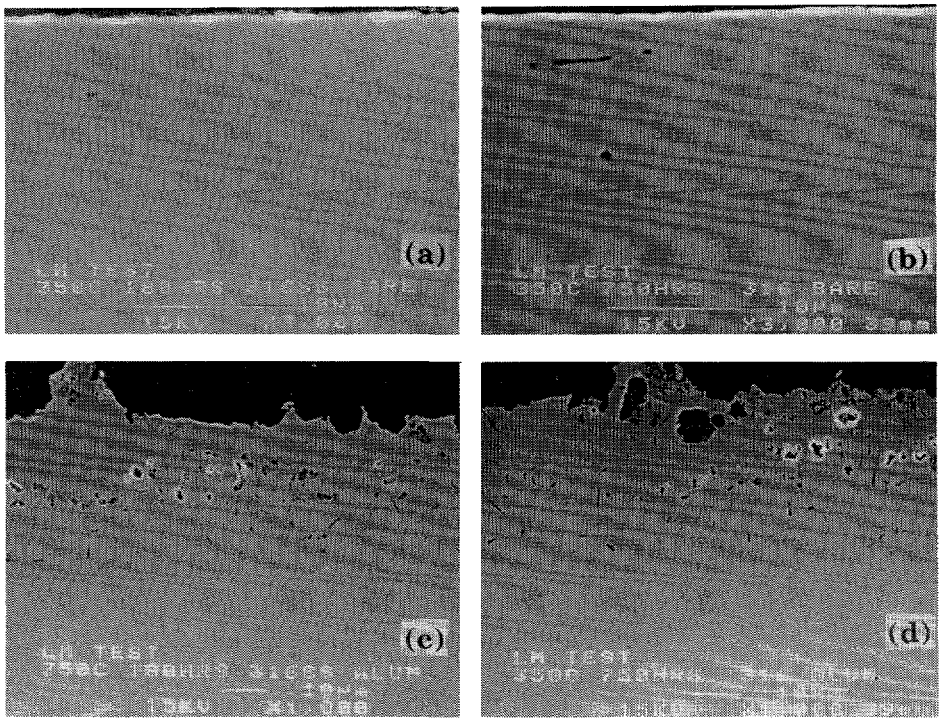

Fig. 6. SEM photomicrographs of cross sections of coupon specimens of Type 316 stainless steel in bare and prealuminized condition after exposure to lithium environment for 180 and 750 h at 350°C

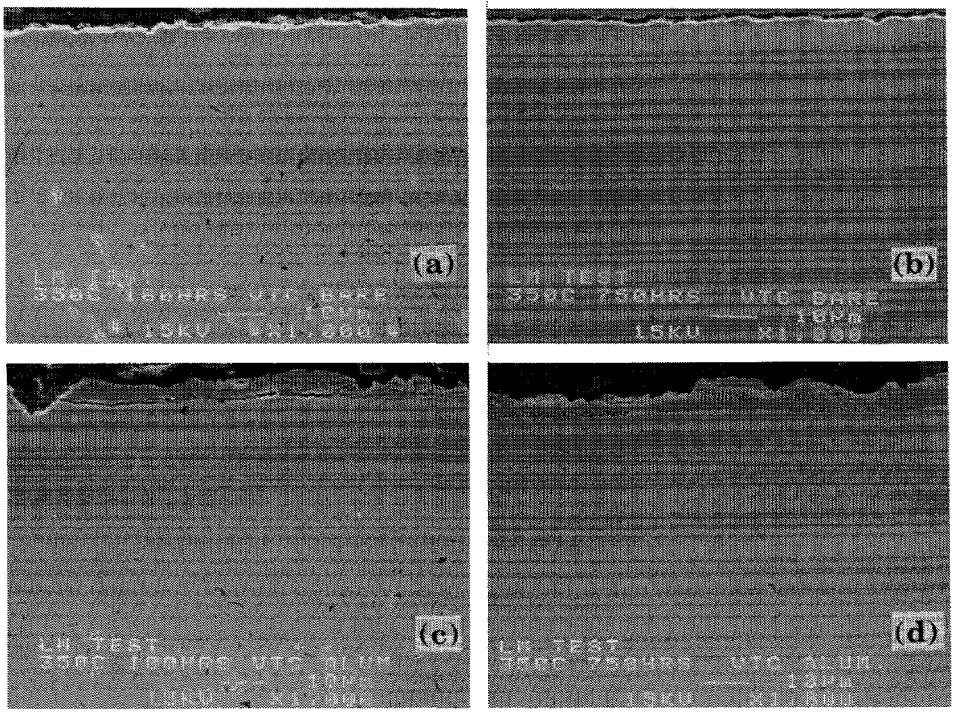

Fig. 7. SEM photomicrographs of cross sections of coupon specimens of V-5Cr-5Ti alloy in bare and prealuminized condition after exposure to lithium environment for 180 and 750 h at 350°C

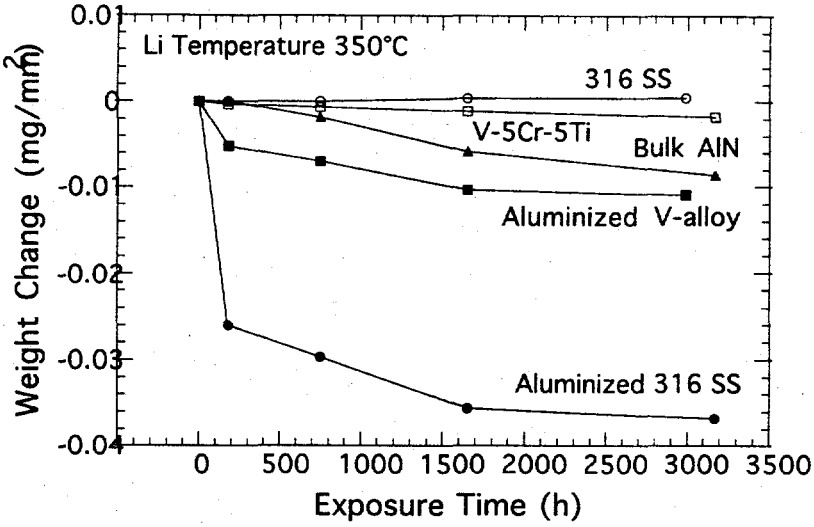

Fig.8. Weight change data for V-5Cr-5Ti, Type 316 stainless steel, and bulk AlN specimens after exposure to lithium at 350°C

Subtask 12E2: EFFECT OF OXIDATION ON TENSILE BEHAVIOR OF V-5Cr-5Ti ALLOY, K. Natesan and W. K. Soppet (Argonne National Laboratory)

OBJECTIVE

The objectives of this task are to (a) evaluate the oxygen uptake of V-5Cr-5Ti alloy as a function of temperature and oxygen partial pressure in the exposure environment, (b) examine the microstructural characteristics of oxide scales and oxygen entrapped at the grain boundaries in the substrate alloy, (c) evaluate the influence of oxygen uptake on the tensile properties of the alloy at room and elevated temperatures, (d) evaluate oxidation kinetics of the alloy with aluminum-enriched surface layers, and (e) determine the effect of oxygen uptake on the tensile behavior of the alloy.

SUMMARY

Oxidation studies were conducted on V-5Cr-5Ti alloy specimens at 500°C in an air environment. The oxidation rates calculated from measurements of thermogravimetric testing are 10, 17, and 25 μm/y at 400, 450 and 500°C, respectively. Uniaxial tensile specimens were oxidized for several time periods in air at 500°C and subsequently tensile-tested at 500°C in air. The hardened layer in each of these oxidized specimens was confined to 75 μm after 1000 h exposure at 500°C. The influence of the 1000-h oxidation is to increase the ultimate tensile strength of the alloy by ≈10% while decreasing the tensile rupture strain from 0.23 to 0.14.

INTRODUCTION

Refractory alloys in general and vanadium-alloys in particular are susceptible to pickup of interstitials such as oxygen, carbon, and nitrogen, which can affect the short- and long-term mechanical properties of the materials. The vanadium alloy with the composition V-5Cr-5Ti contains 5 wt.% titanium (a much more stable oxide-former than vanadium and chromium), which can have an even stronger effect on mechanical properties, especially tensile and creep ductility. The degree of influence of interstitials such as oxygen on the alloy's properties will be dictated by alloy grain size (the amount of grain-boundary areas), amount and distribution of oxygen in the alloy, amount and size of second-phase oxide precipitates (such as titanium oxide), and service temperature and time. The purpose of this study is to examine the role of oxygen and oxidation on the tensile properties of the material.

EXPERIMENTAL PROGRAM

The composition of the heat of vanadium alloy selected for the study (designated as BL-63) was V-5 wt.%Cr -5wt.% Ti. Sheet material of the alloy was annealed for 1 h at 1050°C prior to its use in oxidation and tensile testing. Coupon specimens measuring ≈15 x 7.5 x 1 mm were used for the oxidation studies. Oxidation experiments were conducted in air in a thermogravimetric test apparatus. The test temperatures ranged between 300 and 750°C.

Uniaxial tensile tests were conducted at 500°C in air with an Instron machine. The tensile specimens were fabricated according to ASTM specifications and had a

gauge length of ≈19 mm and a gauge width of ≈4.5 mm. The specimens were preoxidized in air at 500°C for 24, 250, 600, and 1000 h prior to tensile testing in air at 500°C. The Vickers hardness of the tested specimens was measured.

RESULTS AND DISCUSSION

Figure 1 shows weight change data for the alloy oxidized in air at several temperatures. The oxidation kinetics followed a parabolic relationship with time. Detailed scanning electron microscopy analysis of the oxidized samples showed the outer layer to be predominantly vanadium-rich oxide and the inner layer to be (V,Ti) oxide. Parabolic rate equations were used to calculate oxide scale thicknesses in the specimens; these were in agreement with the values determined by metallography. Figure 2 shows the oxidation rate (based on parabolic kinetics) as a function of temperature in the range 300-575°C. The results show that the oxide will grow at rates of 10, 17, and 25 μm/y at 400, 450, and 500°C, respectively. Even though the oxide thickness values are low at these temperatures, the alloy also exhibits an oxygen-enriched region ahead of the oxide scale, which can lead to hardening of the material and may also embrittle the alloy.

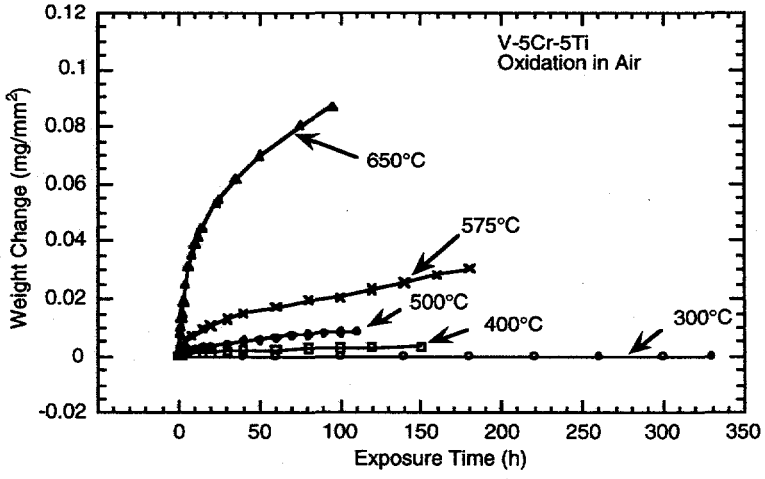

Fig. 1. Weight change data for oxidation of V-5Cr-5Ti alloy in air at several test temperatures.

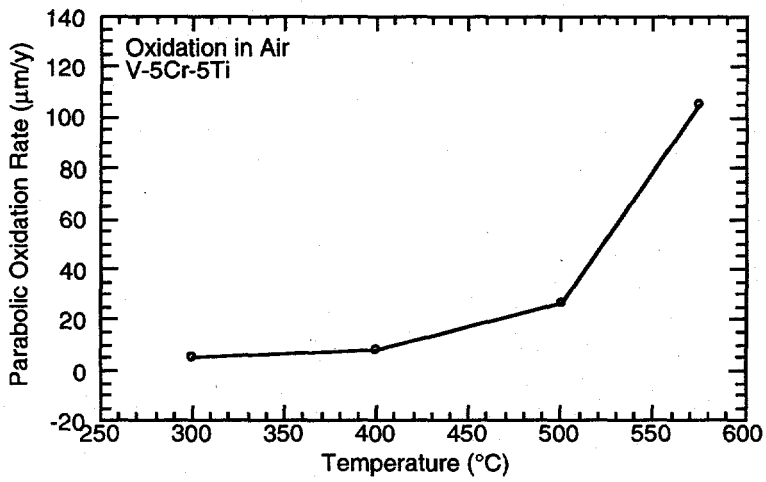

Fig. 2. Parabolic rate (for first year) for oxidation of V-5Cr-5Ti alloy in air as a function of exposure temperature.

To evaluate the effect of oxidation and oxide penetration into the substrate alloy, several tests are in progress to examine the tensile behavior of the alloy as a function of oxygen ingress and oxide scale formation. In the first series of tests, tensile specimens were exposed to air for 24-1000 h in air at 500°C and then tensile-tested in air at the same temperature. Most of the tests were conducted at a strain rate of 1.75×10^{-4} s^{-1}, while a few specimens were tested at lower strain rates to evaluate the strain rate effect on tensile properties. Figure 3 shows the Vickers hardness profile of the specimens exposed to air for various times at 500°C. Oxide scale thickness is ≈10 μm but a hardness increase is noted to a depth of 50-70 μm, indicating an oxygen-enriched zone ahead of the oxide scale. Detailed analysis of this oxygen-enriched zone is in progress.

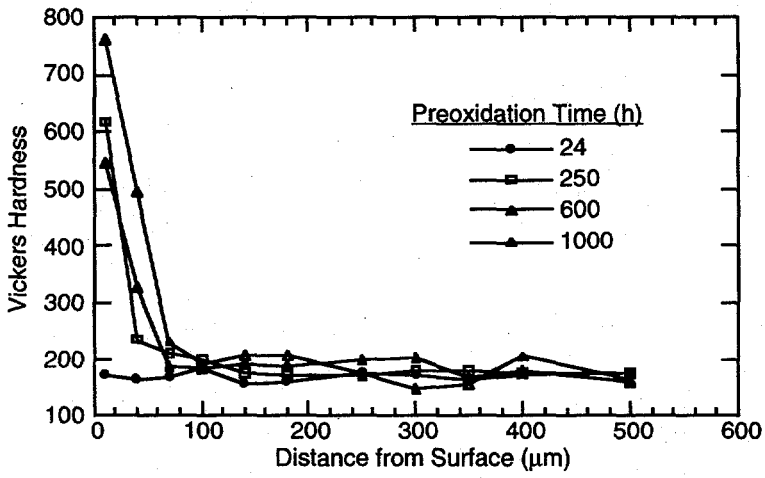

Fig. 3. Vickers hardness data for specimens of V-5Cr-5Ti alloy oxidized at 500°C in air for various times.

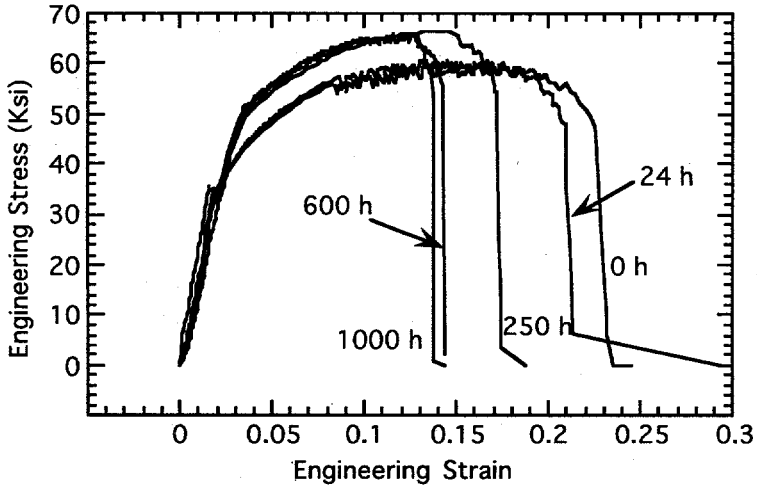

Fig. 4. Effect of preoxidation at 500°C on stress-strain behavior of V-5Cr-5Ti alloy tested at 500°C in air at a strain rate of 1.75 x 10^{-4} s^{-1}.

Figure 4 shows the engineering stress/engineering strain curves for specimens in the oxidized condition and after preoxidation for 24, 250, 600, and 1000 h in air at 500°C. The results show that air exposure for 24 h at 500°C has a negligible effect on tensile properties. The ultimate tensile strength value was ≈60 ksi for the specimens with and without 24 h exposure. Tensile strain decreased from 0.23 to 0.21 as a result of the 24-h oxidation treatment. Air exposures of 250, 600, and 1000 h resulted in some increase in ultimate tensile strength of the material, but strength seemed to saturate at 67 ksi after 1000 h. Tensile strain decreased to 0.175, 0.145, and 0.14 after 250, 600, and 1000 h, respectively. Results to date indicate that the material is not subject to catastrophic embrittlement due to oxygen ingress. Additional exposures as a function of oxygen partial pressure in the exposure environment, as well as tensile tests at lower temperatures, are in progress to establish the performance envelope for the alloy in an oxygenated environment.

Subtask 12F1: EFFECT OF NEUTRON IRRADIATION ON SWELLING OF VANADIUM-BASE ALLOYS, H. M. Chung, B. A. Loomis, and D. L. Smith (Argonne National Laboratory)

OBJECTIVE

The objective of this work is to determine the effects of neutron irradiation on the density change, void distribution, and microstructural evolution of vanadium–base alloys.

SUMMARY

Swelling behavior and microstructural evolution of V-Ti, V-Cr-Ti, and V-Ti-Si alloys were investigated after irradiation at 420-600°C up to 114 dpa. The alloys exhibited swelling maxima between 30 and 80 dpa and swelling decreased on irradiation to higher dpa. This is in contrast to the monotonically increasing swelling of binary alloys that contain Fe, Ni, Cr, Mo, W, and Si. Precipitation of dense Ti_5Si_3 promotes good resistance to swelling of the Ti-containing alloys, and it was concluded that Ti of >3 wt.% and 400-1000 wppm Si are necessary to effectively suppress swelling. Swelling was minimal in V-4Cr-4Ti, identified as the most promising alloy based on good mechanical properties and superior resistance to irradiation embrittlement.

INTRODUCTION

Vanadium-base alloys have significant advantages over other candidate alloys (such as austenitic and ferritic steels) for use as structural materials in fusion devices, e.g., in the International Thermonuclear Experimental Reactor (ITER) and in magnetic fusion reactors (MFRs).[1–5] As part of a program to screen candidate alloys and develop an optimal alloy, extensive investigations have been conducted on the swelling behavior, tensile properties, impact toughness, and microstructural evolution of V alloys after irradiation by fast neutrons.[6–14] From these investigations, V-Cr-Ti alloys containing 5-7 wt.% Cr, 3-5 at.% Ti, 400-1000 wt. ppm Si, and <1000 wt. ppm O+N+C were identified as most desirable alloys that exhibit superior resistance to swelling, embrittlement, and hydrogen-induced effects during fast-neutron irradiation in lithium.[6–10] As a result, recent attention has focused primarily on V-4Cr-4Ti, V-5Cr-5Ti, V-5Cr-3Ti, and V-5Ti. Recent studies on tensile properties,[11] impact toughness,[12] and ductile-brittle transition temperature (DBTT)[12,13] of unirradiated[13] and irradiated[11,12] specimens showed excellent mechanical properties and superior resistance to irradiation-induced embrittlement of some of these alloys, in particular V-4Cr-4Ti and V-5Ti. Thermal creep behavior of V-4Cr-4Ti has been also reported to be superior to those of austenitic and ferritic steels.[14] For these alloys, however, no data base has been reported on irradiation-induced swelling. In the work reported here, irradiation-induced density change and microstructural evolution of a number of the promising binary and ternary alloys were investigated after irradiation at 420-600°C up to 114 dpa in the Fast Flux Test Facility (FFTF).

MATERIALS AND PROCEDURES

Density measurements and transmission electron microscopy (TEM) were conducted on standard-size disk specimens irradiated in the FFTF. The chemical composition of the alloys is given in Table 1. The disks were irradiated at 425, 520, and

600°C to neutron fluences (E > 0.1 MeV) of 7.8 x 10^{22} n cm^{-2} (≈44 dpa) and 1.9 x 10^{23} n cm^{-2} (≈114 dpa). They were sealed in TZM capsules filled with 99.99%-enriched ^{7}Li during irradiation to prevent contamination with O, N, and C impurities dissolved in the Na coolant of the FFTF and formation of unacceptable levels of He and T from ^{6}Li.

Table 1. Composition of vanadium alloys irradiated in fast flux test facility materials open test assembly

ANL ID	Nominal Composition (wt.%)	Concentration (wt. ppm) O	N	C	Si
BL-11	4.9Ti	1820	530	470	220
BL-46	4.6Ti	305	53	85	160
BL-34	8.6Ti	990	180	420	290
BL-12	9.8Ti	1670	390	450	245
BL-13	14.4Ti	1580	370	440	205
BL-15[a]	17.7Ti	830	160	380	480
BL-16	20.4Ti	390	530	210	480
BL-21	13.7Cr-4.8Ti	340	510	180	1150
BL-22	13.4Cr-5.1Ti	300	52	150	56
BL-23	12.9Cr-5.9Ti	400	490	280	1230
BL-24	13.5Cr–5.2Ti	1190	360	500	390
BL-40	10.9Cr-5.0Ti	470	80	90	270
BL-43	9.2Cr-4.9Ti	230	31	100	340
BL-44	9.9Cr-9.2Ti	300	87	150	270
BL-47	4.1Cr-4.3Ti	350	220	200	870
BL-27	3.1Ti–0.25Si	210	310	310	2500
BL-42	3.1Ti–0.5Si	580	190	140	5400
BL-45	2.5Ti-1Si	345	125	90	9900

[a]Contains a significant level of boron as impurity.

RESULTS AND DISCUSSION

Density Change

Swelling of V-Ti, V-Cr-Ti, and V-Ti-Si alloys, determined from density measurements after irradiation at 420 and 600°C, is shown as a function of irradiation damage (dpa) in Figs. 1-3, respectively. Most of the Ti-containing alloys exhibited swelling maxima in the damage range of 30-80 dpa. When irradiated to higher dpa, swelling in these alloys decreased monotonically. For irradiation at 600°C, sufficient data for higher dpa were not available for some of the alloys, and it was not possible to verify whether swelling actually decreased or saturated at higher dpa. The anomalous behavior that exhibited actual decrease of swelling (i.e., increase of density) is in distinct contrast to the normal swelling of other binary alloys of V containing Fe, Ni, Cr, Mo, W, and Si, which increases monotonically for increasing dpa.[7,10] Closer examination of Figs. 1 and 2 indicates the tendency for a higher content of Ti to lower maximum swelling in the V-Ti binary alloys,

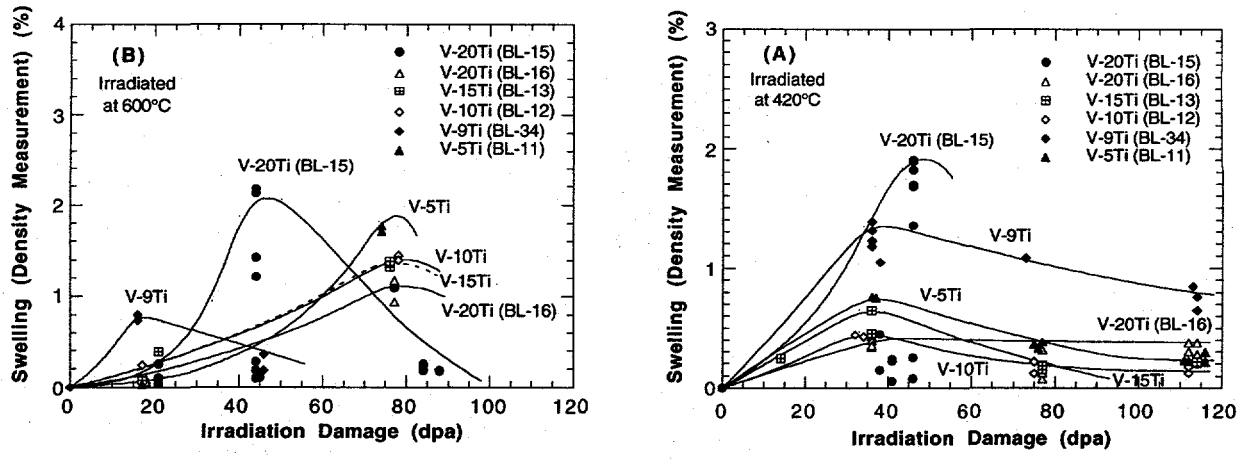

Fig. 1. Density change of V-Ti alloys as function of dose (dpa) after irradiation at 420 (A) and 600°C (B)

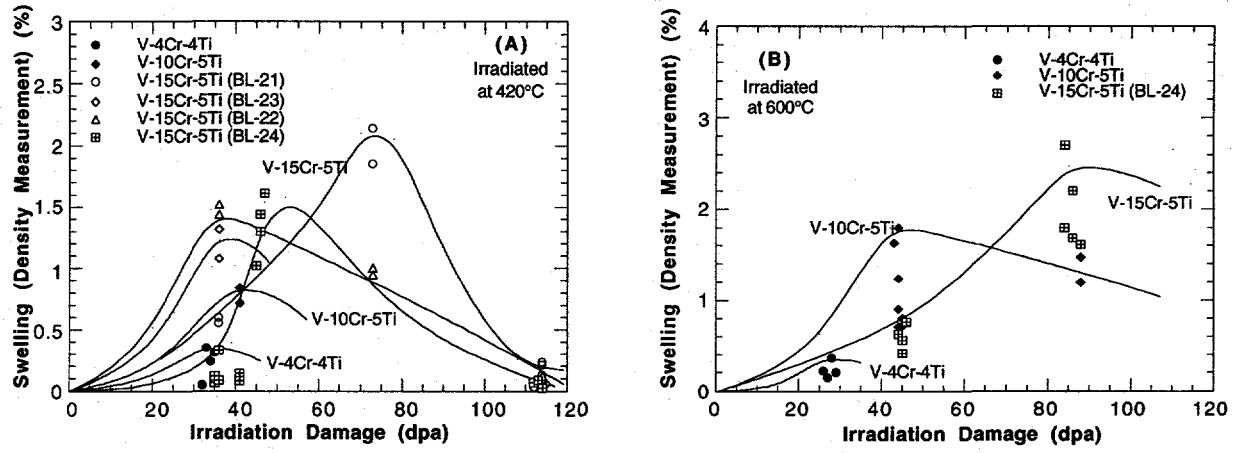

Fig. 2. Density change of V-Cr-Ti alloys as function of dose (dpa) after irradiation at 420 (A) and 600°C (B)

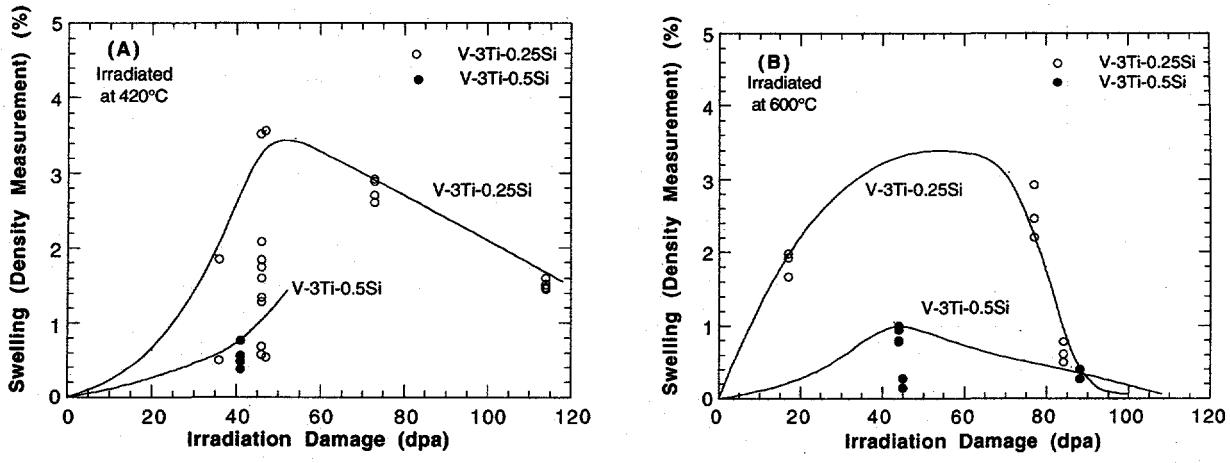

Fig. 3. Density change of V-3Ti-Si alloys as function of dose (dpa) after irradiation at 420 (A) and 600°C (B).

whereas a higher content of Cr is conducive to a higher level of swelling maxima in the V-Cr-Ti ternary alloys. Therefore, Cr addition >9 wt.% in the ternary alloys is not desirable from the standpoint of not only irradiation embrittlement but also of irradiation-induced swelling.

Swelling of the V-3Ti-0.25Si and V-3Ti-0.5Si alloys was relatively higher despite the high level of Si. These alloys are known to exhibit relatively higher yield[13] and creep[15] strengths, which have been attributed to a tendency to form a relatively high density of Ti(O,N,C) precipitates.[13] Therefore, unless the combined impurity level of O, N, C, S, and P is extremely low, virtually all of the Ti solutes in the alloys could be tied up in Ti-based precipitates. This will prevent dense precipitation of ultrafine Ti_5Si_3 particles, to which the resistance to swelling of Ti-containing alloys has been attributed.[9] In V-3Ti-0.25Si, Ti_5Si_3 precipitates were not observed.[16] Ti(O,N,C) precipitates were reported to be absent in Ti-containing vanadium alloys when O+N+C content is <400 wppm.[17] Therefore, it is expected that, by limiting the impurity content of the V-3Ti-Si alloys to below <400 wppm, swelling can be suppressed in the alloys. However, Loomis et al have reported that high Si content in the V-3Ti-Si alloys is conducive to higher DBTT and increased effects of H.[12]

Swelling resistance of the V-4Cr-4Ti alloy was excellent (<0.4% for <35 dpa). This is shown in Fig. 4. V-4Cr-4Ti, designated as one the primary candidate alloys, also exhibited an excellent resistance to irradiation embrittlement; after irradiation to ≈34 dpa at 420, 520, and 600°C, DBTT remained below -196°C.[12] Uniform and total elongations of the alloy, when measured at room temperature after the same irradiations, were 8.1 and 10.2%, respectively.[11] Thermal creep behavior of the alloy was also excellent compared with those of austenitic and ferritic/martensitic steels.[14]

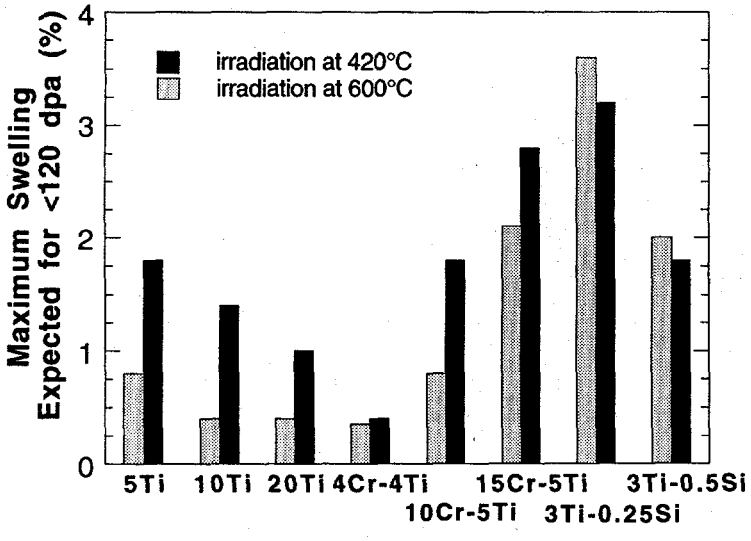

Fig. 4.

Maximum swelling (density change) of several vanadium-base alloys for irradiation at 420-600°C to ≈35–120 dpa

Model of swelling kinetics

The Ti-containing alloys that exhibited relatively low swelling contained high-density ultrafine precipitates of Ti_5Si_3. Some of the examples of the dark-field images of Ti_5Si_3 precipitates are shown in Fig. 5. Swelling in the specimens containing dense Ti_5Si_3 was

relatively low except for the B-containing V-20Ti (BL-15) irradiated at 420°C to 46 dpa. In V-3Ti-0.25Si, which produced dense microvoids upon irradiation at 420°C to 114 dpa (density change ≈1.6%), precipitation of Ti_5Si_3 was negligible. Void swelling and density change in Ti-containing alloys were generally consistent and could be correlated well with the number density of the ultrafine Ti_5Si_3 precipitates. That is, a greater number density of the precipitates is conducive to lower swelling during irradiation. This could be attributed to the large interface area generated between the matrix and high-density precipitates of Ti_5Si_3. This interface area is believed to act as an efficient sink for vacancies and thereby inhibits nucleation and growth of voids.

Anomalous swelling behavior has also been reported by Maziasz[18] for some heats of 14Cr-16Ni-2.5Mo-2Mn austenitic stainless steels stabilized by addition of ≈0.25% Ti with and without P doping. In these steels, swelling reached maxima of ≈2% at ≈34 dpa and decreased to 0.6-1.1% at 57 dpa. The decrease of swelling was accompanied by high-density precipitation of ultrafine MC carbides. According to Maziasz, such profound microstructural changes could disrupt the balance between sink strengths of dislocations, voids, and precipitates, so that MC precipitates and voids now become the dominant sinks for vacancies and interstitials. The breakdown of the steady-state biased partitioning of defects then would lead to increased defect recombination at the large interface area between matrix and precipitates, which would lead to reduction or elimination of the vacancy supersaturation. Dramatic changes in microstructure, defect partitioning, and recombination behavior could cause the critical radius of voids (necessary to maintain stability) to increase enough so that small existing voids would become unstable. When this occurs, existing subcritical-size voids will stop growing or actually begin shrinking with increasing damage level, and further nucleation of voids will be prevented.

The anomalous swelling maxima of the V-base alloys could be explained in a similar manner, with the high-density ultrafine precipitates of Ti_5Si_3 playing a role similar to that of MC carbide in the steels. Apparently, the dramatic changes in microstructure, sink density, and upset of the steady-state biased partitioning of defects are produced only when the size of the ultrafine precipitates is comparable to those of critical-size microvoids and precipitation occurs in very high density, e.g., those in Fig. 5. According to this model, the dependence of swelling on damage level is expected to be strongly influenced by the kinetics of the irradiation-induced precipitation of Ti_5Si_3 phase, as illustrated in Fig. 6.

CONCLUSIONS

1. Resistance to irradiation-induced swelling of V-4Cr-4Ti, identified as the most promising candidate alloy primarily on the basis of good mechanical properties and superior resistance to irradiation embrittlement and creep, was excellent. Swelling of the alloy is expected to be minimal (<0.4%) for the design life of ITER.

2. Ti-containing alloys exhibited anomalous swelling maxima in the damage range of 30-80 dpa. When irradiated to higher dpa, swelling in these alloys decreased monotonically.

3. Dense precipitation of ultrafine Ti_5Si_3 is conducive to low swelling. The anomalous swelling behavior seems to be caused by the profound microstructural evolution associated with the dense precipitation of ultrafine Ti_5Si_3.

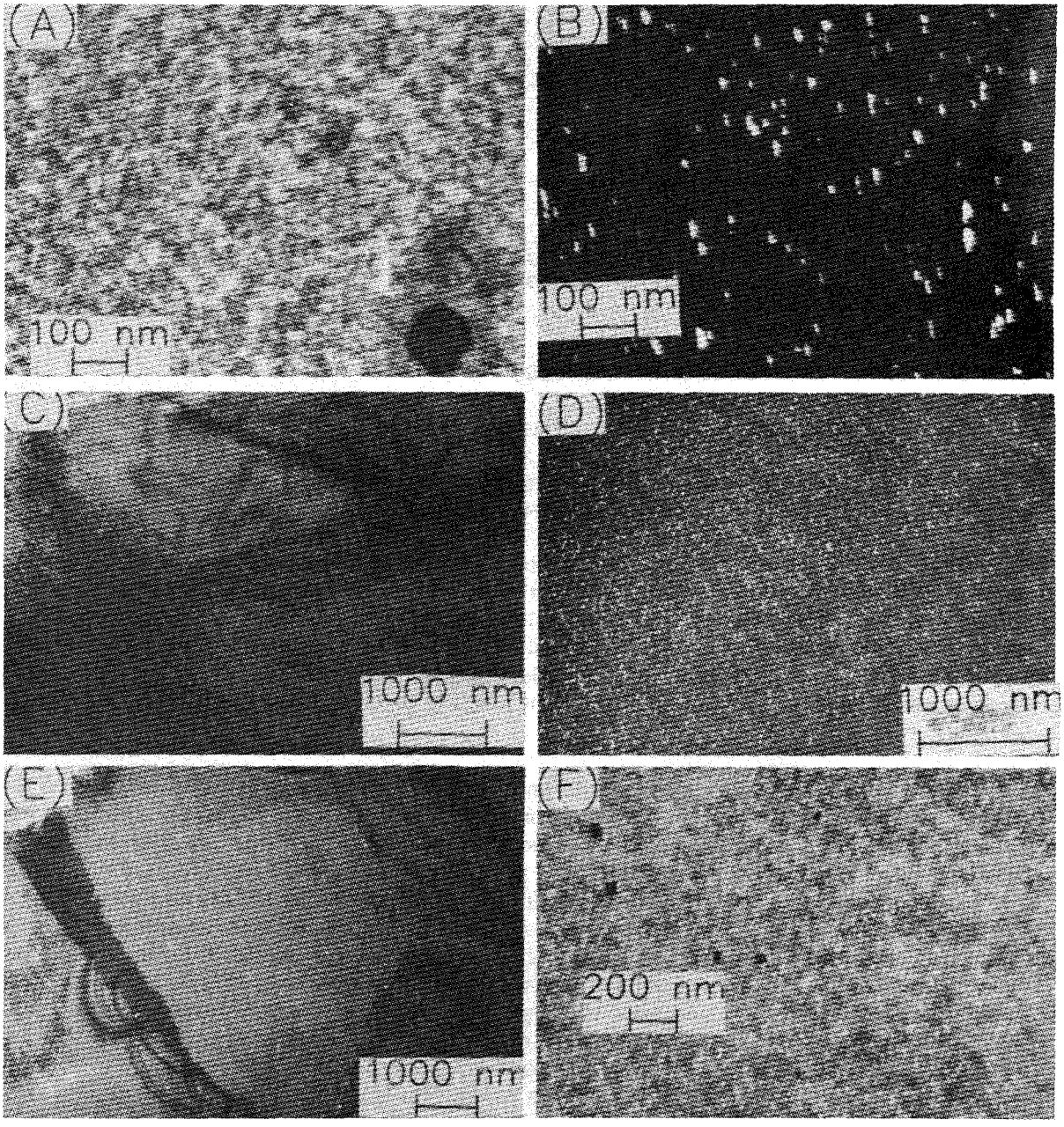

Fig. 5. Bright- (BF) and dark-field (DF) microstructures of vanadium-base alloys showing voids and Ti_5Si_3 distributions: (A) BF and (B) DF of Ti_5Si_3 in V-4Cr-4Ti irradiated to ≈34 dpa at 420 and 600°C, respectively; (C) BF of voids and (D) DF of Ti_5Si_3 in V-20Ti irradiated at 420°C to 114 dpa; (E) BF of voids and (F) DF of Ti_5Si_3 in V-18Ti irradiated at 420°C to 46 dpa.

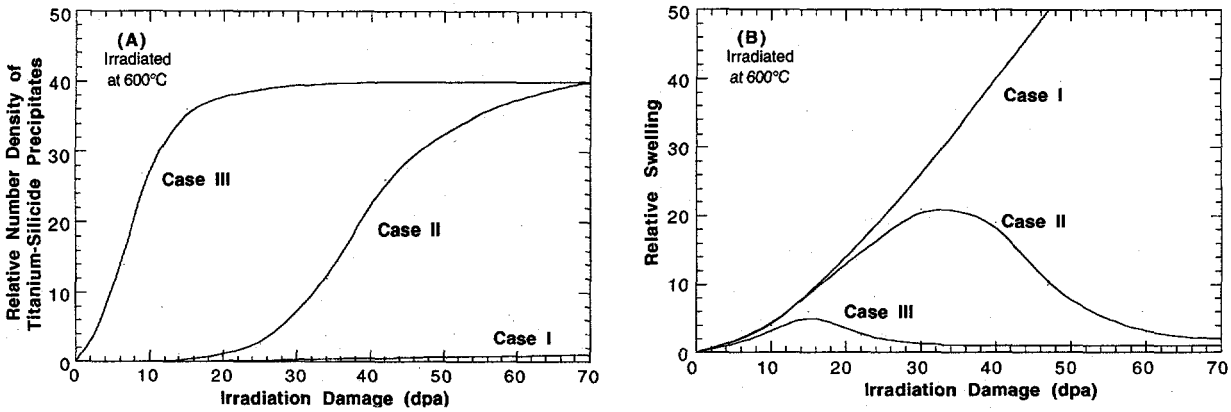

Fig. 6. Schematic illustration of relationship between kinetics of Ti_5Si_3 precipitation (A) and swelling (B) as function of irradiation damage in Ti-containing vanadium alloys

ACKNOWLEDGMENTS

The authors are grateful to L. J. Nowicki and J. Gazda for their contributions to experimental efforts.

REFERENCES

1. T. Noda, F. Abe, H. Araki, and M. Okada, J. Nucl. Mater. 155-157 (1988) 581.
2. R. Santos, J. Nucl. Mater. 155-157 (1988) 589.
3. S. J. Piet et al., J. Nucl. Mater. 141-143 (1986) 24.
4. F. L. Yaggee, E. R. Gilbert, and J. W. Styles, J. Less-Comm. Met. 19 (1969) 39.
5. D. L. Smith, B. A. Loomis, and D. R. Diercks, J. Nucl. Mater. 135 (1985) 125.
6. B. A. Loomis, A. B. Hull, and D. L. Smith, J. Nucl. Mater. 179-181 (1991) 148-154.
7. B. A. Loomis and D. L. Smith, J. Nucl. Mater. 191-194 (1992) 84-91.
8. H. M. Chung and D. L. Smith, J. Nucl. Mater. 191-194 (1992) 942-947.
9. H. M. Chung, B. A. Loomis, and D. L. Smith, in: Effects of Radiation on Materials: 16th International Symposium, ASTM STP 1175, A. S. Kumar, D. S. Gelles, R. K. Nanstad, and T. A. Little, eds. (American Society for Testing and Materials, Philadelphia, 1993, PP. 1185–1200.
10. D. L. Smith, B. A. Loomis, and H. M. Chung, Plasma Devices and Operations, Vol 3, 1994, 167–179.
11. B. A. Loomis, L. J. Nowicki, and D. L. Smith, J. Nucl. Mater. 212–215 (1994) 790–793.
12. B. A. Loomis, H. M. Chung, L. J. Nowicki, and D. L. Smith, ibid., 799–803.
13. B. A. Loomis, J. Gazda, and D. L. Smith, in Fusion Reactor Materials, Semiannual. Prog. Report. DOE/ER-0313/15, Oak Ridge National Laboratory, Oak Ridge, TN (1993), 232–239.
14. H. M. Chung, B. A. Loomis, and D. L. Smith, J. Nucl. Mater. 212–215 (1994) 772–777.

15. D. Harrod and R. Gold, Int. Met. Rev. 25 (1980) 163-221.

16. H. M. Chung, L. J. Nowicki, and D. L. Smith, in: Fusion Reactor Materials Semiannual. Prog. Report. DOE/ER-0313/11, Oak Ridge National Laboratory, Oak Ridge, TN (1992) 215-226.

17. M. Satou and H. M. Chung, in: Fusion Reactor Materials Semiannual. Prog. Report. DOE/ER-0313/13, Oak Ridge National Laboratory, Oak Ridge, TN (1993) 227-234.

18. P. J. Maziasz, in: Fusion Reactor Materials Semiannual. Prog. Report. DOE/ER-0313/12, Oak Ridge National Laboratory, Oak Ridge, TN (1992), 163-174.

Subtask 12F2: MICROSTRUCTURAL EVOLUTION OF V-4Cr-4Ti DURING NEUTRON IRRADIATION,

H. M. Chung, J. Gazda and B. A. Loomis (Argonne National Laboratory)

OBJECTIVE

The objective of this work is to characterize the microstructural evolution of V-4Cr-4Ti alloy during irradiation by fast neutrons, and thereby to provide a better understanding of long-term performance of the alloy under fusion conditions.

SUMMARY

Microstructural evolution of V-4Cr-4Ti, an alloy recently shown to exhibit excellent tensile and creep properties, virtual immunity to irradiation embrittlement, and good resistance to swelling, was characterized after irradiation in a lithium environment in the Fast Flux Test Facility (FFTF) (a sodium-cooled fast reactor located in Richland, Washington) at 420, 520, and 600°C to 24-34 dpa. The primary feature of microstructural evolution during irradiation at 520 and 600°C was high-density formation of ultrafine Ti_5Si_3 precipitates and short dislocations. For irradiation at 420°C, precipitation of Ti_5Si_3 was negligible, and "black-dot" defects and dislocations were observed in significantly higher densities. In spite of their extremely high densities, neither the "black-dot" defects nor Ti_5Si_3 precipitates are overly detrimental to ductility and toughness of the alloy, yet they very effectively suppress irradiation-induced swelling. Therefore, these features, normally observed in V-base alloys containing Ti and Si, are considered stable. Unstable microstructural modifications that are likely to degrade mechanical properties significantly were not observed, e.g., irradiation-induced formation of fine oxides, carbides, nitrides, or Cr-rich clusters.

INTRODUCTION

Vanadium-base alloys have significant advantages over other candidate alloys (such as austenitic and ferritic steels) for use as structural materials in fusion devices, e.g., in the International Thermonuclear Experimental Reactor (ITER) and in magnetic fusion reactors. These advantages include intrinsically lower levels of long-term activation, irradiation afterheat, neutron-induced helium- and hydrogen-transmutation rates, biological hazard potential, and thermal stress factor.

As part of a program to screen candidate alloys and develop an optimal alloy, extensive investigations have been conducted on the swelling behavior, tensile properties, impact toughness, and microstructural evolution of V, V-Ti, V-Cr, V-Cr-Ti, and V-Ti-Si alloys after irradiation by fast neutrons at 420, 520, and 600°C up to ≈120 dpa. From these investigations, V-Cr-Ti alloys containing ≈4-5 wt.% Cr, 3-5 wt.% Ti, 400-1000 wt. ppm Si, and <1000 wt. ppm O+N+C were identified as the most desirable alloys that exhibit superior resistance to swelling, embrittlement, and hydrogen-induced effects during fast-neutron irradiation in Li.[1-5] Of these alloys, V-4Cr-4Ti has been shown recently to exhibit the most attractive combination of mechanical properties,[6-12] i.e., tensile properties,[7] impact energy,[8,11] and ductile-brittle-transition temperature (DBTT) before[6,11] and after irradiation[8] in the FFTF. In these investigations, it was shown that V-4Cr-4Ti is virtually immune to irradiation-induced embrittlement, a property very remarkable for a body-centered-cubic or hexagonal-close-packed alloy. Thermal creep

behavior of V-4Cr-4Ti has also been reported to be superior to that of austenitic and ferritic steels,[10] and resistance of the alloy to irradiation-induced density change was also reported to be very good.[9]

In view of the excellent performance of the V-4Cr-4Ti alloy during fission-neutron irradiation, it was considered important that we understand the nature of the irradiation-induced microstructural evolution and thereby provide a sound basis for predicting the alloy performance during irradiation under fusion-neutron conditions to higher damage levels. Therefore, microstructural evolution of the alloy was investigated in this work after irradiation at 420-600°C up to 34 dpa under the fission-neutron spectrum of the FFTF.

MATERIALS AND PROCEDURES

The elemental composition of the V-4Cr-4Ti alloy is given in Table 1. Microstructural characterization of the alloy was conducted on standard transmission electron microscopy (TEM) disks after irradiation in the FFTF. TEM disks were irradiated at 420, 520, and 600°C to neutron fluences (E > 0.1 MeV) of 6.0 x 10^{22} n cm^{-2} (≈34 dpa), 4.3 x 10^{22} n◊cm^{-2} (≈24 dpa), and 5.0 x 10^{22} n cm^{-2} (≈28 dpa), respectively. The disks were sealed in TZM capsules filled with 99.99%-enriched ^{7}Li during irradiation to prevent contamination with O, N, and C impurities dissolved in the Na coolant of the FFTF and formation of unacceptable levels of He and tritium from transmutation of ^{6}Li.

After irradiation, the specimens were thoroughly cleaned of Li and annealed at 400°C for 1 h in a vacuum of 2.6 x 10^{-7} Pa to expel residual H and tritium. The irradiated specimens were jet-thinned in a solution of 15% sulfuric acid-72% methanol-13% butyl cellosolve maintained at -5°C. TEM was conducted with a JEOL 100CX-II scanning transmission electron microscope operating at 100 keV or with a Philips CM-30T transmission electron microscope operating at 200 keV.

Table 1. Elemental composition and irradiation conditions of V-4Cr-4Ti alloy (ANL ID BL-47) in FFTF

Cr (wt.%)	Ti (wt.%)	O (wppm)	N (wppm)	C (wppm)	Si (wppm)	DBTT before irradiation (°C)	Irradiation temperature (°C)	Damage level (dpa)	DBTT after irradiation (°C)
4.1	4.3	350	220	200	870	<-190	420	34	<-190
–	–	–	–	–	–	–	520	24	<-190
–	–	–	–	–	–	–	600	28	<-190

MICROSTRUCTURAL EVOLUTION

Structure of Unirradiated Material

An ingot of V-4Cr-4Ti was produced by vacuum arc melting. The ingot was extruded at 1150°C, followed by several repeated steps of rolling (at 400°C) and annealing (at 1100°C) to produce sheets 3.80 and 0.89 mm thick.[12] These sheets were then annealed and recrystallized at 1125°C for 1 h in a vacuum of 2.6 x 10^{-7} Pa before they were machined into TEM disks and tensile specimens. Subsequently, the specimens were encapsulated for irradiation. A typical TEM microstructure of the alloy after the final anneal at 1125°C is shown in Fig. 1. In the figure, Ti(O,N,C) precipitates, 200-600 nm in size, were observed in a number density of ≈3 x 10^{18} m^{-3} and a volume fraction of ≈10%.

The Ti(O,N,C) phase has been observed to precipitate in most of the V-base alloys containing Ti during ingot melting and solidification.[4,13] A few titanium phosphide precipitates in the form of Ti_5Si_3 (hcp structure, a_o = 0.7234 nm, c_o = 0.5090 nm) were also observed in a number density approximately one order of magnitude lower than that of the Ti(O,N,C). The phosphides, shaped as stretched ellipsoids, were ≈200-400 nm thick and 400-800 nm long (see Fig. 2).

Specimens Irradiated at 600°C

An example of typical microstructures of specimens irradiated at 600°C is shown in Fig. 2. In the bright-field micrograph of Fig. 2A, images of nearly spherical Ti(O,N,C), large elongated-ellipsoid-shaped Ti_5Si_3 (denoted "P"), dislocation loops, and short dislocations are visible. In addition to these features, ultrafine precipitates ≈1 nm thick and 2-10 nm long are visible in high density. From dark-field imaging and indexing of selected-area diffraction (SAD) patterns, these fine precipitates were identified as Ti_5Si_3 (hcp structure, a_o = 0.7463 nm, c_o = 0.5165 nm).[4] A dark-field image produced with (210) reflection of the titanium silicide is shown in Fig. 2B. In previous investigations, good resistance to swelling of V-Ti and V-Cr-Ti alloys was attributed to dense precipitation of Ti_5Si_3.[3,4]

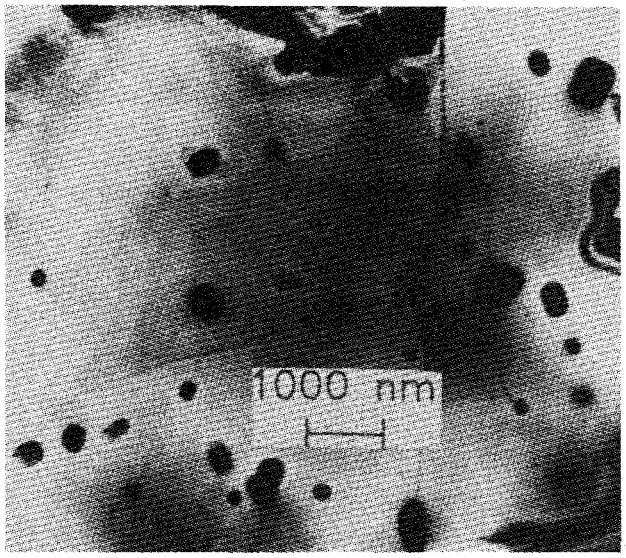

Fig. 1.

TEM microstructure of unirradiated V-4Cr-4Ti showing a normal distribution of Ti(O,N,C)

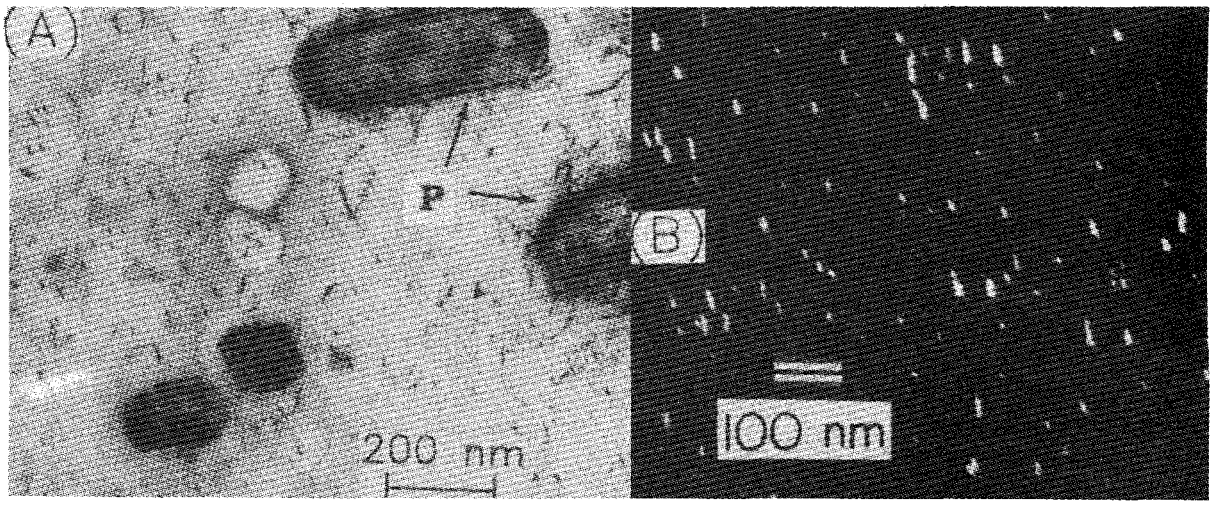

Fig. 2. Microstructure of V-4Cr-4Ti irradiated at 600°C to ≈28 dpa; (A) bright-field image of large Ti(O,N,C) and Ti_5Si_3 (denoted "P"), dislocation loops, short dislocations, and ultrafine Ti_5Si_3 in high density; (B) dark-field image produced with (210) reflection of Ti_5Si_3.

The average size of the Ti(O,N,C) precipitates in the irradiated material (Fig. 2A) was considerably smaller than that of unirradiated material (Fig. 1), i.e., ≈130 nm vs. ≈250 nm. This is probably because of transfer of O atoms from the V-alloy matrix to Li during irradiation, which, consequently, resulted in partial dissolution of Ti(O,N,C) precipitates.

Specimens Irradiated at 520°C

Microstructures of the specimens irradiated at 520°C were similar to those of specimens irradiated at 600°C. Examples of bright- and dark-field images of the alloy irradiated at 520°C to ≈24 dpa are shown in Figs. 3A and 3B, respectively. The density of short dislocations was higher in this material than in the specimens irradiated at 600°C. The precipitation behavior of Ti_5Si_3 at both 600 and 520°C seemed to be similar, although size was somewhat smaller after irradiation at 520°C (Fig. 3B). The dark-field micrograph (Fig. 3B), produced with (110) reflection of V (d-spacing 0.218 nm) superimposed on (300) reflection of Ti_5Si_3 (d-spacing 0.215 nm), shows images of short line dislocations, Ti_5Si_3 precipitates, and "black-dot" defects (clusters of vacancy or interstitial defects) <1 nm in size. Although care must be exercised to discern "black-dot"

defects (spherical dots) and Ti_5Si_3 precipitates (small platelets), the density of "black-dot" defects seems to be higher in specimens irradiated at 520°C (Fig. 3A) than in specimens irradiated at 600°C (Fig. 2A).

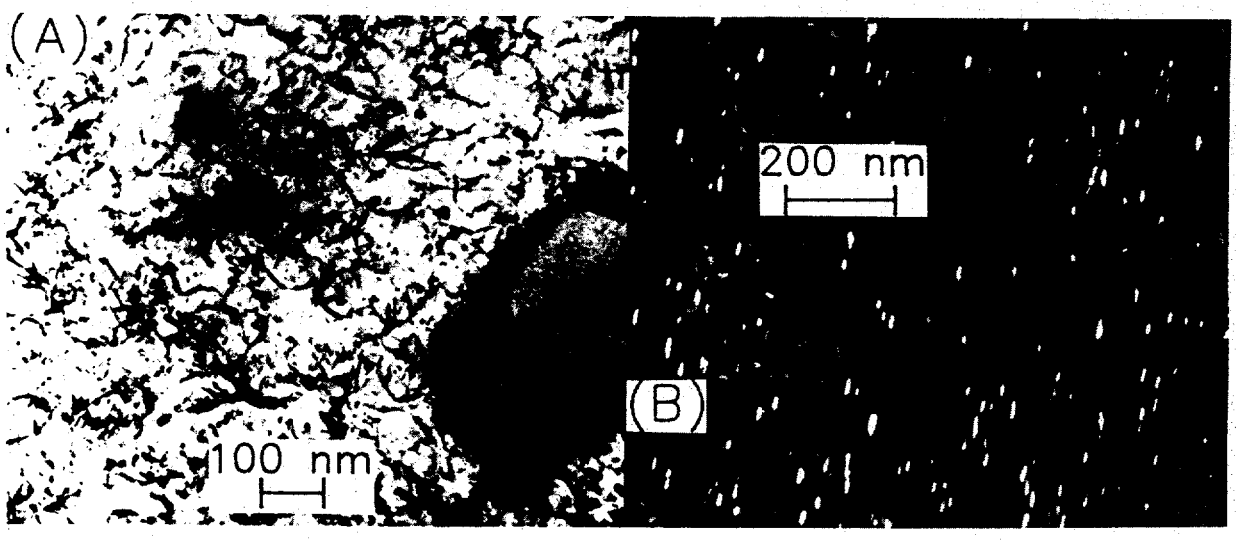

Fig. 3. Microstructure of V-4Cr-4Ti irradiated at 520°C to ≈24 dpa; (A) bright-field image of large Ti(O,N,C), "black-dot" defects, short dislocations, and Ti_5Si_3 in high density; (B) dark-field image of dislocations and Ti_5Si_3 produced with (110) reflection of V superimposed on (300) reflection of Ti_5Si_3

Specimens Irradiated at 420°C

Examples of typical microstructures of specimens irradiated at 420°C to ≈34 dpa are shown in Fig. 4. In the low-magnification micrograph (Fig. 4A), the overall grain size and phase structure are shown. In this micrograph, most of the Ti(O,N,C) precipitates 100-200 nm in size are surrounded by concentric shells of distinct contrast, indicating that larger original Ti(O,N,C) precipitates, 200-500 nm in size, dissolved partially in the matrix during the irradiation in Li. This feature is visible more clearly in the high-magnification micrograph of Fig. 4B.

High-magnification micrographs, such as Fig. 4B, were characterized by "black-dot" defects in extremely high density. This is shown in a more direct manner in the dark-field image, Fig. 4C. The image, produced with (110) reflection of the V matrix superimposed on the (300) reflection of a Ti_5P_3 precipitate, shows line dislocations, as well as "black-dot" defects, concentrated in higher density around a Ti_5P_3 precipitate. However, in contrast to irradiation at 520 and 600°C, no evidence of irradiation-induced precipitation

of the Ti_5Si_3 phase was observed at 420°C. The density of dislocation loops was also negligible at this temperature.

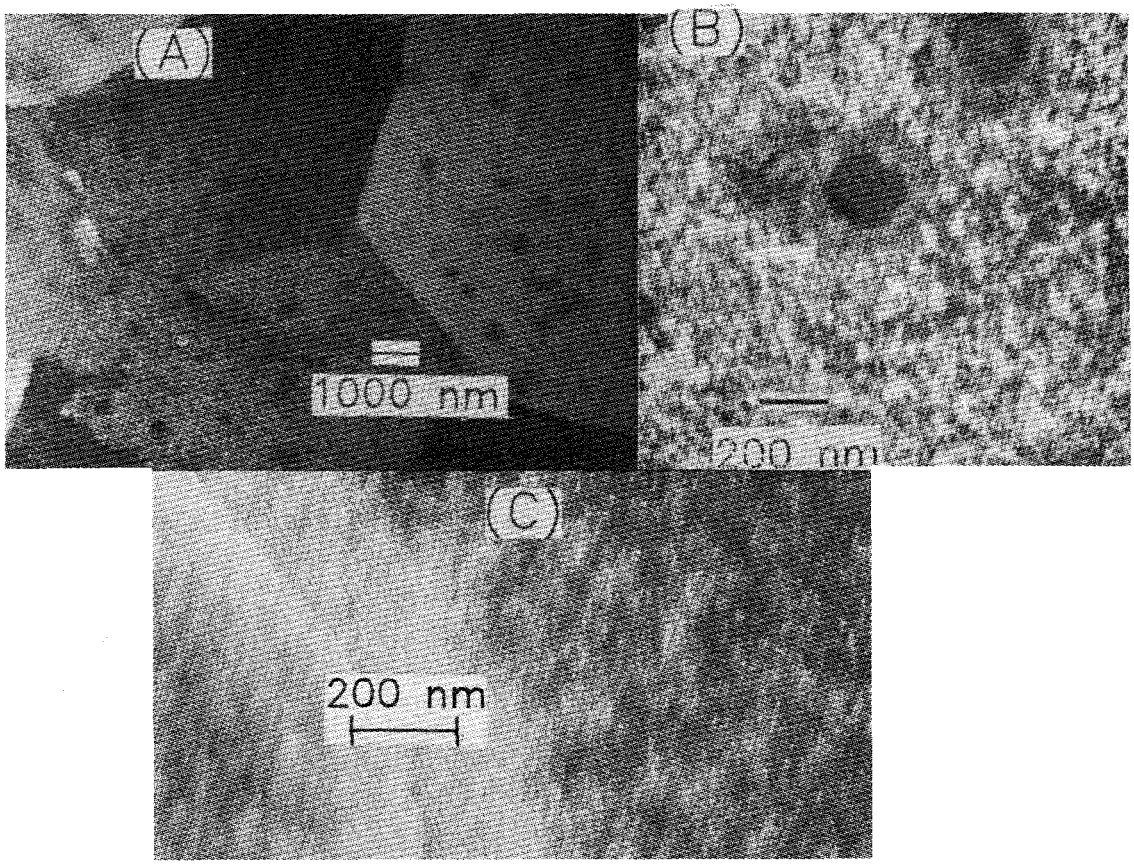

Fig. 4. Microstructure of V-4Cr-4Ti irradiated at 420°C to ≈34 dpa; (A) low-magnification bright-field image showing size and distribution of Ti(O,N,C); (B) higher-magnification of (A) showing distinct darker contrast surrounding Ti(O,N,C); and (C) dark-field image of dislocations and "black-dot" defects in higher density, surrounding a large Ti_5P_3 precipitate

DISCUSSION

In view of the results from previous investigations on irradiation-induced microstructural evolution of V-Ti, V-Cr-Ti, and V-3Ti-1Si alloys,[4,6,15] no surprising microstructural features were found in V-4Cr-4Ti after irradiation at 420-600°C up to 34 dpa. The characteristic partial dissolution of Ti(O,N,C) precipitates, precipitates normally present in as-fabricated alloys in significant number density, is apparently due to O transfer from the matrix to Li during irradiation. Any effect of this process on the reduction of alloy strength seems to have been more than compensated for by the hardening effect of displacement damage.

Precipitation of the ultrafine Ti_5Si_3 precipitates was observed, as expected, after irradiation at 520 and 600°C. However, in contrast to V-20Ti, in which high-density Ti_5Si_3 precipitated during irradiation at 420°C to ≈114 dpa,[15] no precipitation of Ti_5Si_3 was observed in V-4Cr-4Ti after irradiation at the same temperature to ≈34 dpa. In a similar recrystallized material of V-5Cr-5Ti alloy doped with Si, Al, and Y, precipitation of Ti_5Si_3

was reported to be negligible after irradiation at 406°C to ≈51 dpa but significant after irradiation at 600°C to 31 dpa.[14] In view of these observations, it is not quite clear if the absence of Ti_5Si_3 precipitates in the present V-4Cr-4Ti is due to the lower dose or to inherently slower kinetics of precipitation in V-(4-5)Cr-(4-5)Ti alloys than in V-20Ti. On the other hand, one cannot rule out the possibility that clusters of Ti and Si atoms, precursors of Ti_5Si_3, formed in the V-4Cr-4Ti and V-5Cr-5Ti alloys during the low-temperature irradiation, most likely in association with "black-dot" defects. Such clusters would be too small to be detected by TEM.

Similar to V-4Cr-4Ti irradiated at 420°C, the V-5Cr-5Ti-1Si-1Al-1Y alloy irradiated at 406°C contained "black-dot" defects in extremely high density. In spite of the negligible precipitation of Ti_5Si_3, swelling both in V-4Cr-4Ti[9] and V-5Cr-5Ti-1Si-1Al-1Y[16,17] was negligible after irradiation at 406-420°C to 34-40 dpa. This indicates that high-density precipitation of ultrafine Ti_5Si_3 produces good resistance to swelling, but it is not necessarily the only condition that is conducive to low swelling.

Despite the formation of ultrafine "black-dot" damage and/or Ti_5Si_3 precipitates in high density, Charpy impact and tensile specimens irradiated under the three irradiation conditions exhibited excellent toughness (DBTT <-190°C and Charpy energy ≈140 J/cm^2)[8] and tensile ductility (uniform and total elongation ≈8 and ≈10 %, respectively, at 25°C).[7] Comparable tensile properties (total elongation of 8-16 % at 25°C) have been reported for the V-5Cr-5Ti-1Si-1Al-1Y alloy, which exhibited similar microstructures characterized by high-density "black-dot" damage and Ti_5Si_3 precipitates.[18] Based on these observations, it is concluded that neither the high-density "black-dot" defects nor Ti_5Si_3 precipitates are overly detrimental, and a sufficient level of ductility and toughness is retained in V-(4-5)Cr-(4-5)Ti-type alloys.

CONCLUSIONS

1. Microstructural evolution of V-4Cr-4Ti alloy was characterized after irradiation in a lithium environment in FFTF at 420, 520, and 600°C to 24-34 dpa. Thermally formed Ti(O,N,C) precipitates were found to dissolve partially in the matrix, probably because of oxygen transfer from the alloy to Li during irradiation.

2. The primary feature of microstructural evolution during irradiation at 520 and 600°C is high-density formation of ultrafine Ti_5Si_3 precipitates and short dislocations. For irradiation at 420°C, precipitation of Ti_5Si_3 was negligible, and "black-dot" defects and dislocations were observed in significantly higher density.

3. In spite of their extremely high densities, neither the high-density "black-dot" defects nor the Ti_5Si_3 precipitates are sufficiently detrimental to significantly degrade material ductility and toughness, yet they effectively suppress irradiation-induced swelling. Therefore, these features of microstructural evolution are considered stable. No unstable microstructural modifications that are likely to degrade mechanical properties significantly were observed in V-4Cr-4Ti, e.g., irradiation-induced formation of fine oxides, carbides, nitrides, or Cr-rich clusters.

4. Void formation was negligible in V-4Cr-4Ti for all the irradiated conditions.

ACKNOWLEDGMENTS

The authors are grateful to L. J. Nowicki for his contributions to the preparation of the irradiated specimens.

REFERENCES

1. B. A. Loomis, A. B. Hull, and D. L. Smith, J. Nucl. Mater., 179-181 (1991) 148-154.
2. B. A. Loomis and D. L. Smith, J. Nucl. Mater., 191-194 (1992) 84-91.
3. H. M. Chung and D. L. Smith, J. Nucl. Mater. ibid., 942-947.
4. H. M. Chung, B. A. Loomis, and D. L. Smith, "Irradiation-Induced Precipitation in Vanadium-Base Alloys Containing Titanium," Effects of Radiation on Materials: 16th International Symposium, ASTM STP 1175, A. S. Kumar, D. S. Gelles, R. K. Nanstad, and T. A. Little, eds., American Society for Testing and Materials, Philadelphia, 1993, pp. 1185–1200.
5. D. L. Smith, B. A. Loomis, and H. M. Chung, Plasma Devices and Operations, Vol. 3, 1994, pp. 167–179.
6. B. A. Loomis, J. Gazda, L. J. Nowicki, and D. L. Smith, J. Nucl. Mater., 191-194 (1992) 84-91.
7. B. A. Loomis, L. J. Nowicki, and D. L. Smith, J. Nucl. Mater., 212–215 (1994) 790–793.
8. B. A. Loomis, H. M. Chung, L. J. Nowicki, and D. L. Smith, J. Nucl. Mater., 212–215 (1994) 799–803.
9. H. M. Chung, B. A. Loomis, and D. L. Smith, J. Nucl. Mater., 212–215 (1994) 804–812.
10. H. M. Chung, B. A. Loomis, and D. L. Smith, J. Nucl. Mater., 212–215 (1994) 772–777.
11. B. A. Loomis, L. J. Nowicki, J. Gazda, and D. L. Smith, "Ductile-Brittle Transition Temperatures of Unirradiated Vanadium Alloys Based on Charpy-Impact Testing," Fusion Reactor Materials Semiannual Progress Report for Period Ending March 31, 1993, DOE/ER-0313/14, Oak Ridge National Laboratory, Oak Ridge, TN, pp. 318-325.
12. H. M. Chung, L. J. Nowicki, J. E. Sanecki, J. Gazda, and D. L. Smith,"Effects of Fabrication Variables on the Impact Properties and Microstructure of V-Cr-Ti Alloys," Fusion Reactor Materials Semiannual Progress Report for Period Ending September 30, 1993, DOE/ER-0313/15, Oak Ridge National Laboratory, Oak Ridge, TN, pp. 207–218.
13. T. Schober and D. N. Braski, Met. Trans. 20A (1989) 1927-1932.
14. M. Satou and H. M. Chung, in Fusion Reactor Materials Semiannual Progress Report for Period Ending September 30, 1992, DOE/ER-0313/13, Oak Ridge National Laboratory, Oak Ridge, TN, (1993) pp. 227-234.
15. H. M. Chung "Effects of Irradiation-Induced Precipitation on Properties of Vanadium Alloys," ibid., pp. 194-202.
16. M. Satou, K. Abe, and H. Matsui, J. Nucl. Mater. 191-194 (1992) 938-941.
17. M. Satou, K. Abe, H. Kayano, and H. Takahashi, J. Nucl. Mater. 191-194 (1992) 956-959.
18. M. Satou, K. Abe, and H. Kayano, J. Nucl. Mater., 212–215 (1994) 794–798.

Subtask 12F3: EFFECTS OF NEUTRON IRRADIATION ON TENSILE PROPERTIES OF VANADIUM-BASE ALLOYS

B. A. Loomis, H. M. Chung, and D. L. Smith (Argonne National Laboratory)

OBJECTIVE

The objective of this work is to determine the effects of neutron irradiation on the tensile properties of candidate vanadium–base alloys.

SUMMARY

Vanadium-base alloys of the V-Cr-Ti system are attractive candidates for use as structural materials in fusion reactors. The current focus of the U.S. program of research on these alloys is on the V-(4-6)Cr-(3-6)Ti-(0.05-0.1)Si (in wt.%) alloys. In this paper, we present experimental results on the effects of neutron irradiation on tensile properties of selected candidate alloys after irradiation at 400°C–600°C in lithium in fast fission reactors to displacement damages of up to ≈120 displacement per atom (dpa). Effects of irradiation temperature and dose on yield and ultimate tensile strengths and uniform and total elongations are given for tensile test temperatures of 25°C, 420°C, 500°, and 600°C. Effects of neutron damage on tensile properties of the U.S. reference alloy V–4Cr–4Ti are examined in detail.

INTRODUCTION

Vanadium-base alloys have significant advantages over other candidate alloys (such as austenitic and ferritic steels) for use as structural materials in fusion devices, e.g., in the international thermonuclear experimental reactor (ITER) and in magnetic fusion reactors (MFRs). These advantages include intrinsically lower levels of long-term activation, irradiation afterheat, neutron-induced helium- and hydrogen-transmutation rates, biological hazard potential, and thermal stress factor.[1–5] However, to make use of these favorable neutronic and physical properties of structural materials in fusion systems, the alloys must retain adequate tensile strength and ductility and be resistant to neutron-induced swelling, creep, and embrittlement, and they must also be compatible with the reactor coolant.

In this paper, we report a comprehensive database on the effects of neutron irradiation on tensile strengths and ductilities of several major alloys including the U. S. reference alloy V–4Cr–4Ti after irradiation at 400°C–600°C in lithium environment in fast fission reactors to ≈120 dpa. Effects of irradiation temperature and dose on yield and ultimate tensile strengths and uniform and total elongations are given for tensile test temperatures of 25°C, 420°C, 500°, and 600°C.

MATERIALS AND IRRADIATION

The chemical compositions of as-fabricated alloys, typically annealed and recrystallized at 1050°C-1125°C for 1 h in high–quality vacuum, are given in Table 1. The alloys were irradiated in the Fast Flux Test Facility (FFTF), a fission test reactor located in Richland, Washington, at 420°C, 520°C, and 600°C to neutron fluences (E > 0.1 MeV) ranging from 3×10^{22} n/cm^2 [17 displacements per atom (dpa)] to 1.9×10^{23} n/cm^2 (114 dpa). The specimens were sealed in TZM/Mo capsules filled with 99.99%-enriched Li^7 during irradiation to prevent contamination by oxygen, nitrogen, and carbon impurities dissolved in the sodium coolant of the FFTF and formation of unacceptable levels of

Table 1. Composition of Vanadium Alloys Irradiated in Various Fission Reactors

Heat ID	Nominal Comp. (wt.%)	Impurity Concentration (wt. ppm) O	N	C	Si
BL-19	V	1101	161	360	-
BL-20	V	570	110	120	325
BL-36	V	810	86	250	<50
BL-51	V	570	49	56	370
820626	V	260	75	28	260
820630	V	200	62	75	780
BL-35	9.5Cr	340	45	120	<50
BL-4	10.0Cr	530	76	240	<50
BL-5	14.1Cr	330	69	200	<50
BL-50	1.0Ti	230	130	235	1050
BL-52	3.1Ti	210	310	300	500
BL-46	4.6Ti	305	53	85	160
BL-11	4.9Ti	1820	530	470	220
BL-34	8.6Ti	990	180	420	290
BL-12	9.8Ti	1670	390	450	245
BL-13	14.4Ti	1580	370	440	205
BL-15	17.7Ti	830	160	380	480
BL-16	20.4Ti	390	530	210	480
BL-10	7.2Cr-14.5Ti	1110	250	400	400
BL-21	13.7Cr-4.8Ti	340	510	180	1150
BL-22	13.4Cr-5.1Ti	300	52	150	56
BL-23	12.9Cr-5.9Ti	400	490	280	1230
BL-24	13.5Cr-5.2Ti	1190	360	500	390
BL-25	14.4Cr-0.3Ti	390	64	120	<50
BL-26	14.1Cr-1.0Ti	560	86	140	<50
BL-40	10.9Cr-5.0Ti	470	80	90	270
BL-41	14.5Cr-5.0Ti	450	120	93	390
BL-43	9.2Cr-4.9Ti	230	31	100	340
BL-44	9.9Cr-9.2Ti	300	87	150	270
BL-49	7.9Cr-5.7Ti	400	150	127	360
BL-54	5.1Cr-3.0Ti	480	82	133	655
BL-63	4.6Cr-5.1Ti	440	28	73	310
BL-62	3.1Ti-0.1Si	320	86	109	660
BL-27	3.1Ti-0.25Si	210	310	310	2500
BL-42	3.1Ti-0.5Si	580	190	140	5400
BL-45	2.5Ti-1Si	345	125	90	9900
QN74[a]	4.0Cr-4.1Ti	480	79	54	350
BL-47	4.1Cr-4.3Ti	350	220	200	870
T87	4.9Cr-5.1Ti	380	89	109	545
932665	3.8Cr-3.9Ti	310	85	80	783

helium and tritium from Li^6. Tensile tests of irradiated specimens were conducted in hot cells in Argonne National Laboratory at room temperature and temperatures same as the irradiation temperatures (i.e., 420°C to 600°C). The high–temperature tests were conducted in a quartz cylinder evacuated and continuously flushed with flowing argon or helium.

RESULTS AND DISCUSSION

The present study focused on effects of neutron irradiation on tensile properties of V–Cr–(4–5)Ti alloys containing Cr contents of 0, 4–5, 9–10, and 14–15 wt.% and Si contents of 200–900 wppm. Baseline tensile properties of these alloys have been documented in this report.[6] Particular emphasis was placed on the effects of neutron damage on tensile properties of the U.S. reference alloy V–4Cr–4Ti containing 500–1000 wppm Si.[7]

Effects of irradiation and test temperature on yield strength, ultimate tensile strength, uniform elongation, and total elongation of V–5Ti (BL–46, Table 1), V–4Cr–4Ti (BL–47), V–9Cr–5Ti (BL–43), and V–14Cr–5Ti (BL–24) alloys, determined after irradiation in lithium to 28–46 dpa at 420°C–600°C, are shown in Figs. 1–4, respectively. In most of these tests, irradiation and tensile test temperature were the same. However, some of the irradiated (at 420°C) specimens were tested at room temperature to obtain database that will be needed to evaluate component performance during reactor shutdown.

Effects of damage level (dpa) on the yield strength and the total elongation of the same four alloys, determined after irradiation at 420°C, 520°C, and 600°C up to ≈120 dpa, are plotted in Figs. 5 and 6, respectively. The yield strength data presented in Fig. 5 show that the alloys undergo maximum irradiation–induced hardening (i.e., increase of yield stress) on irradiation to ≈40 dpa; then this is followed by a decrease of hardening on further irradiation to >50 dpa. The exact mechanism of the decrease of hardening is not understood, although oxygen transfer from alloy matrix to lithium is speculated to be a factor. The tensile data also show that the total elongation (Fig. 6) of the alloys decreases with dose to ≈30 dpa and does not decrease further on irradiation to >50 dpa.

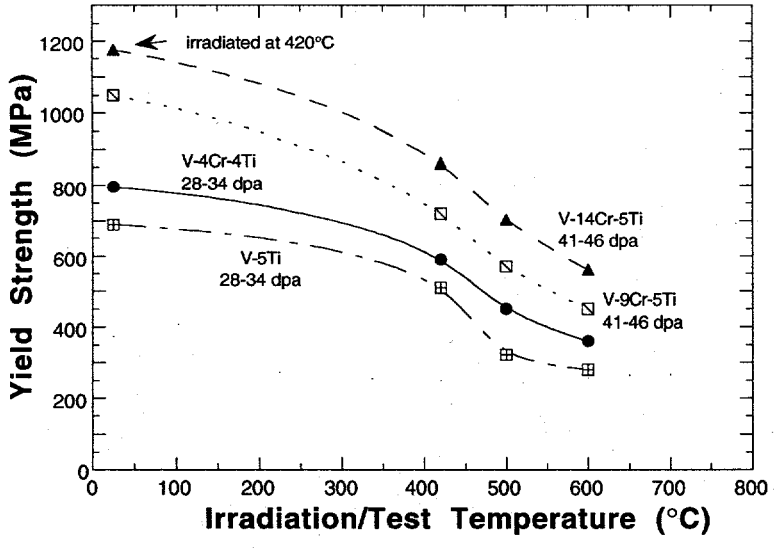

Fig. 1. Yield strength of V–(0–15)Cr–(4–5)Ti alloys irradiated at 420°C–600°C to 24–46 dpa as function of irradiation and test temperature.

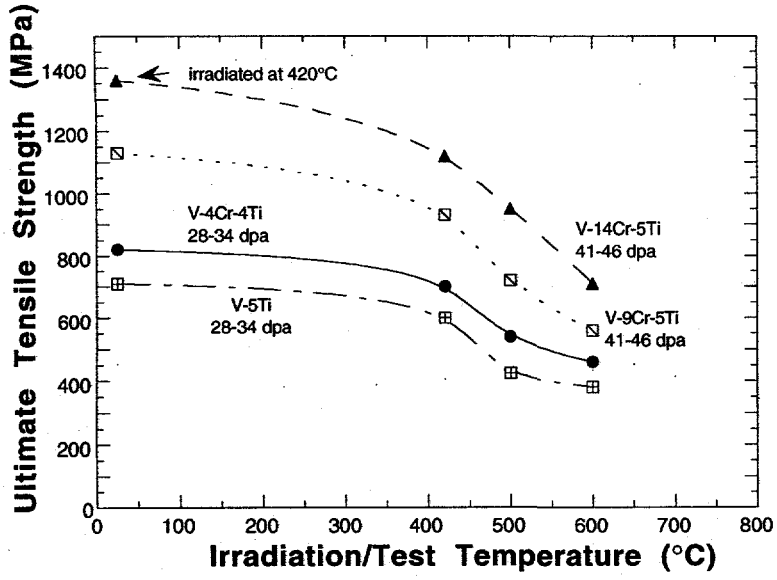

Fig. 2.
Ultimate tensile strength of V–(0–15)Cr–(4–5)Ti alloys irradiated at 420°C–600°C to 24–46 dpa as function of irradiation and test temperature.

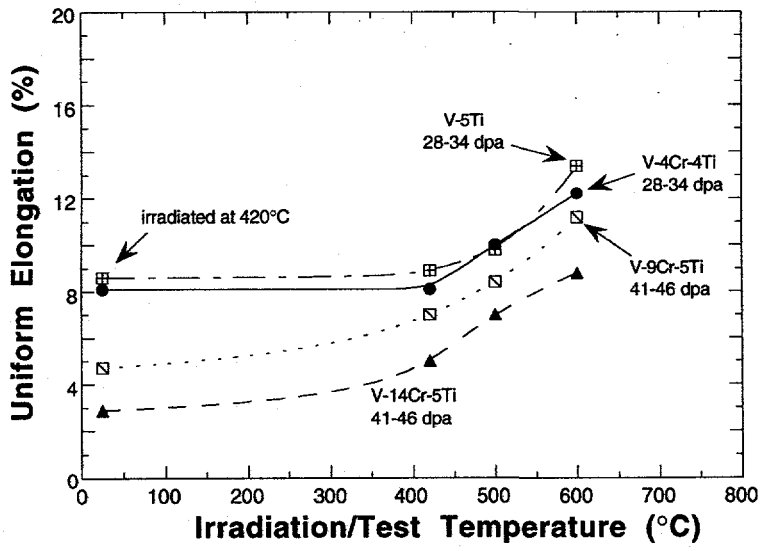

Fig. 3.

Uniform elongation of V–(0–15)Cr–(4–5)Ti alloys irradiated at 420°C–600°C to 24–46 dpa as function of irradiation and test temperature.

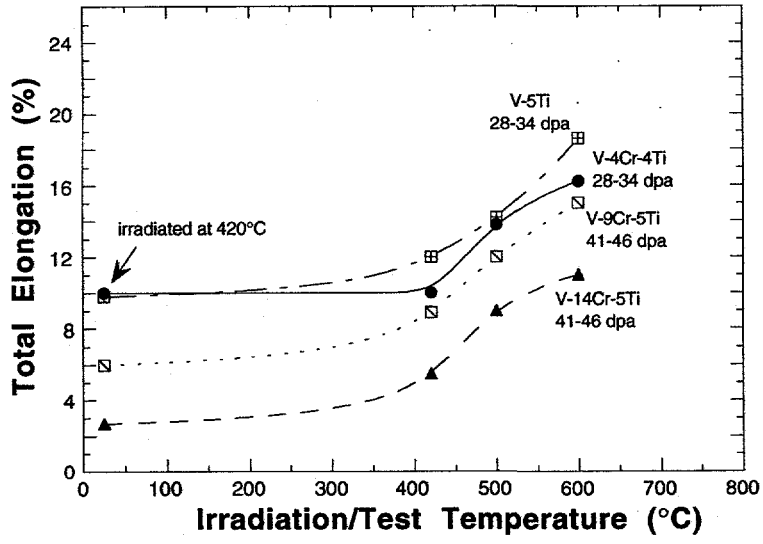

Fig. 4.

Total elongation of V–(0–15)Cr–(4–5)Ti alloys irradiated at 420°C–600°C to 24–46 dpa as function of irradiation and test temperature.

With the exception of V-14Cr-5Ti irradiated at 420°C, total elongation of the alloys exceeds ≈5% at the relatively high fluence of 1.7 x 10^{23} n/cm^2, or ≈100 dpa. The uniform elongation of the alloys, corresponding to ≈80% of the total elongation,[6] exceeds ≈3.7%, showing significant level of ductility retained after the high–dose irradiation.

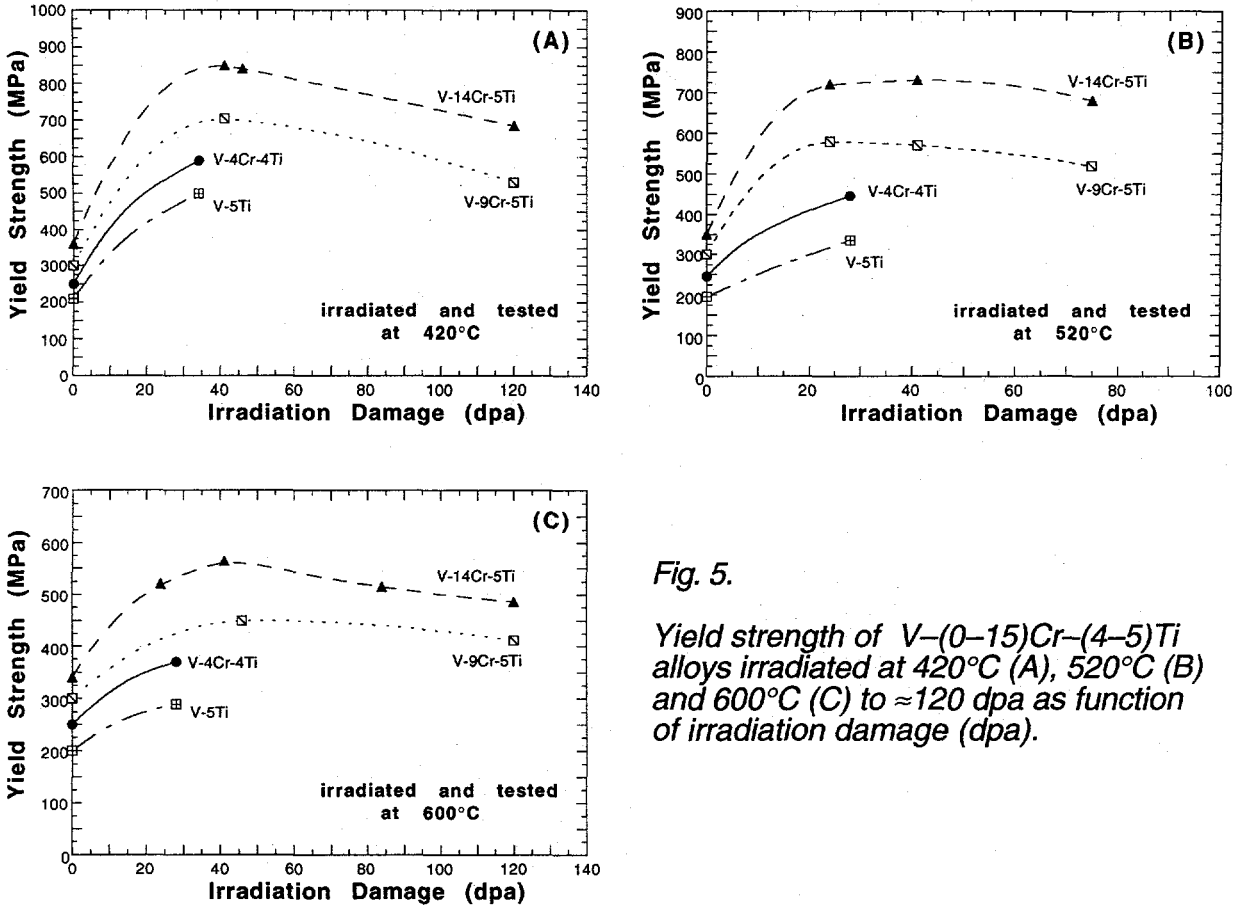

Fig. 5.

Yield strength of V–(0–15)Cr–(4–5)Ti alloys irradiated at 420°C (A), 520°C (B) and 600°C (C) to ≈120 dpa as function of irradiation damage (dpa).

Cr plays the most significant role in influencing the tensile properties of these alloys (containing a constant content of Ti of ≈4–5 wt.%) both in unirradiated and irradiated conditions. Out of these alloys, V–4Cr–4Ti has been identified as the most promising candidate alloy on the basis of its excellent resistance to irradiation–induced embrittlement, swelling, creep, and microstructural instability.[7] To show the effects of neutron irradiation (helium generation negligible) on the tensile properties of this alloy in a more direct manner, comparative tensile properties of unirradiated and irradiated V–4Cr–4Ti are also plotted as function of irradiation temperature in Figs. 7–10.

For irradiation at >600°C, irradiation–induced hardening of the alloy is insignificant (Figs. 7 and 8). As expected, effect of neutron irradiation on ductility is more pronounced for lower irradiation temperature. However, after irradiation to 28–34 dpa at 420°C–600°C, the alloy still retained excellent ductility regardless of irradiation and test temperature, i.e., uniform and total elongation of ≈8 and 10%, respectively.

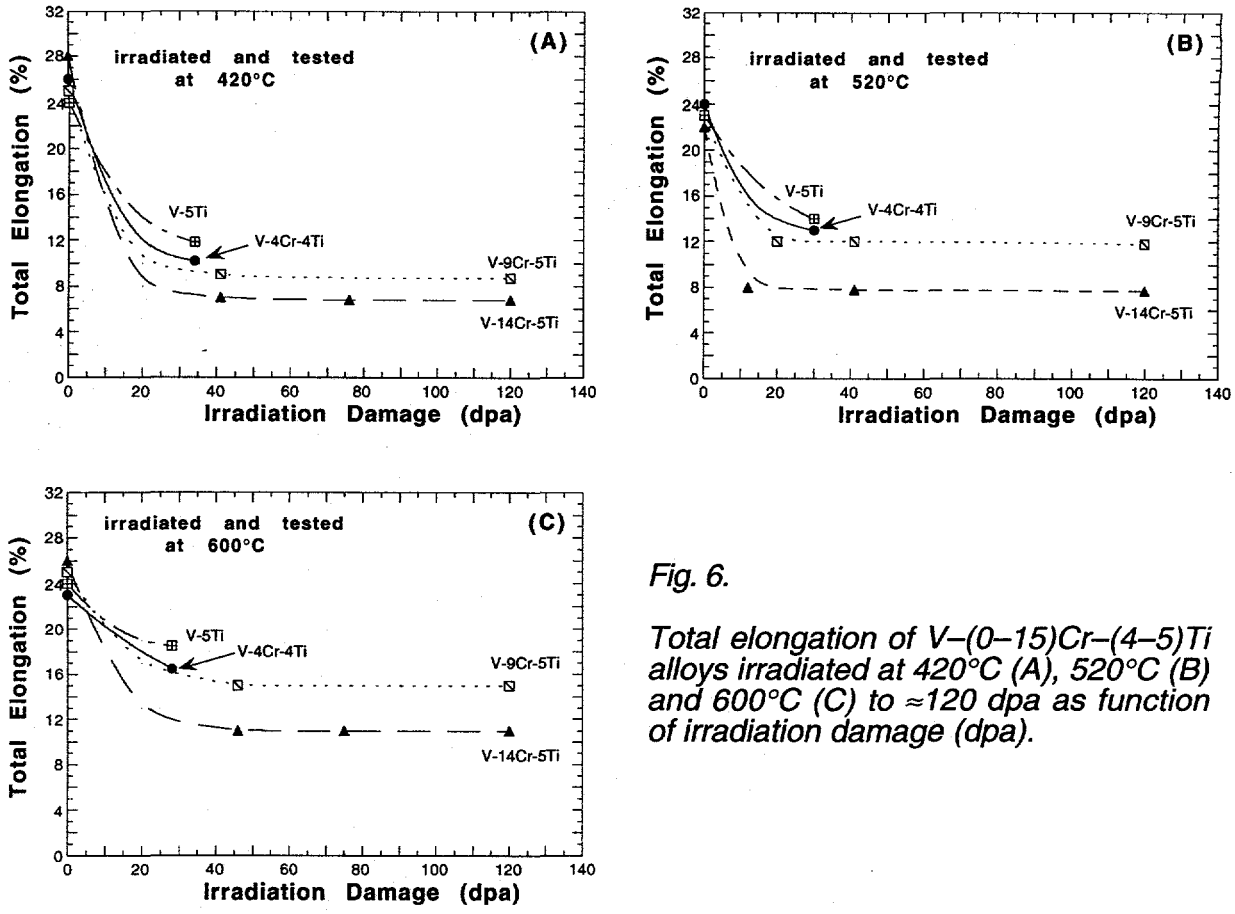

Fig. 6.

Total elongation of V–(0–15)Cr–(4–5)Ti alloys irradiated at 420°C (A), 520°C (B) and 600°C (C) to ≈120 dpa as function of irradiation damage (dpa).

CONCLUSIONS

1. Tensile properties of V–Cr–Ti alloys containing 0–15 wt.% Cr, 4–5 wt.% Ti, and 200–1000 wppm Si have been determined at 23°C and at 420°–600°C after irradiation at 420°C, 520°C, and 600°C up to ≈120 dpa in lithium environment in fast reactors. Cr plays the most significant role in influencing the irradiation hardening of the alloys, probably in association with irradiation–induced clustering of Cr atoms.

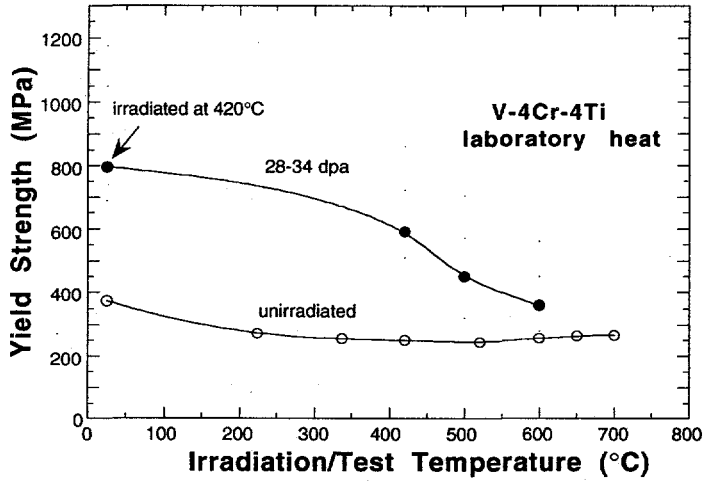

Fig. 7.

Yield strength of V–4Cr–4Ti before and after irradiation at 420°C–600°C in lithium to 24–34 dpa as function of irradiation and test temperature.

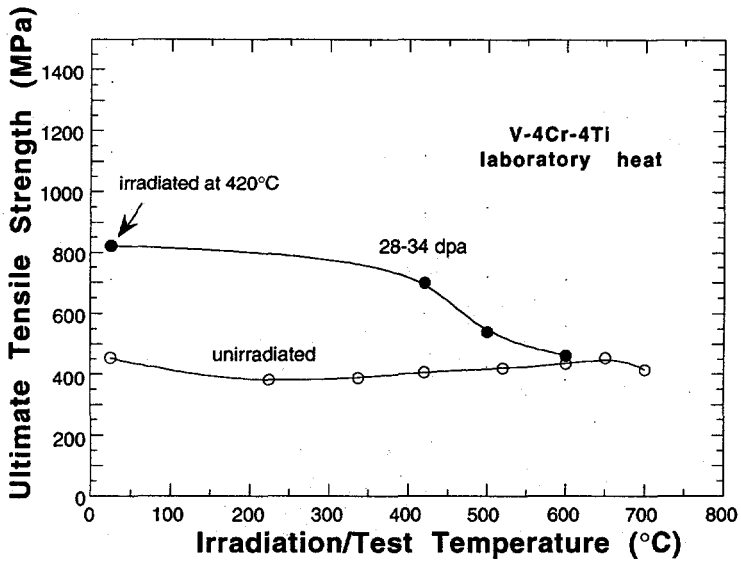

Fig. 8.

Ultimate tensile strength of V–4Cr–4Ti before and after irradiation at 420°C–600°C in lithium to 24–34 dpa as function of irradiation and test temperature.

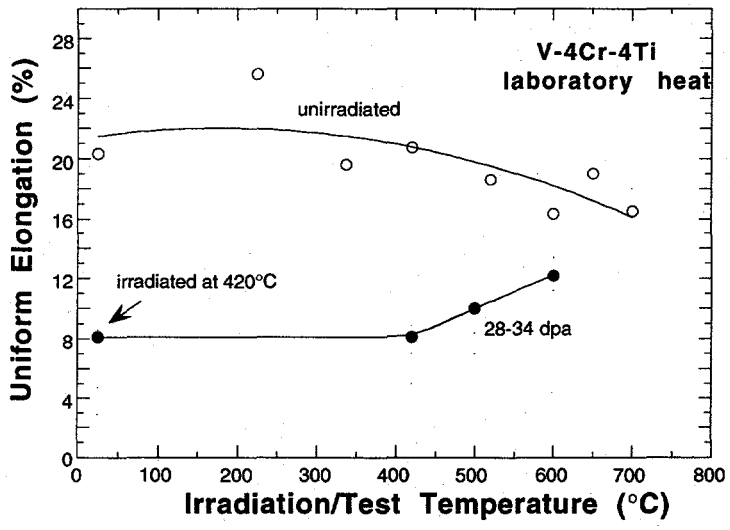

Fig. 9.

Uniform elongation of V–4Cr–4Ti before and after irradiation at 420°C–600°C in lithium to 24–34 dpa as function of irradiation and test temperature.

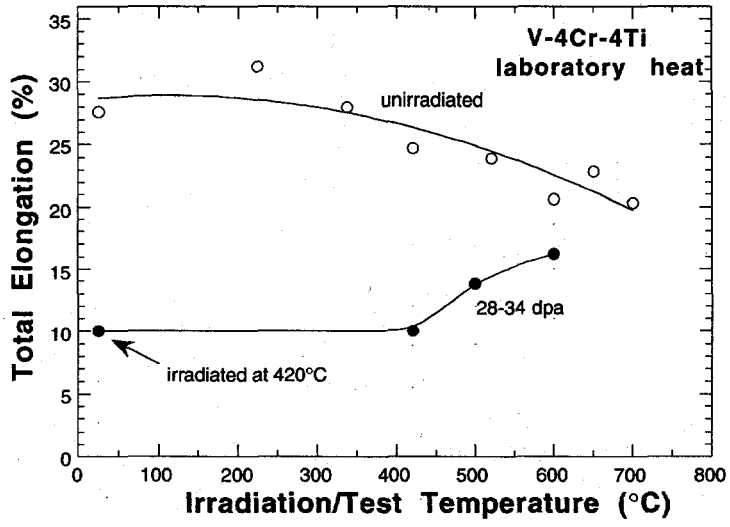

Fig. 10

Total elongation of V–4Cr–4Ti before and after irradiation at 420°C–600°C in lithium to 24–34 dpa as function of irradiation and test temperature.

2. Irradiation–induced hardening is more pronounced for lower irradiation temperature. For irradiation at >600°C irradiation hardening of the alloys is insignificant. The alloys undergo maximum irradiation hardening on irradiation to ≈30–40 dpa; then this is followed by a decrease of hardening on further irradiation to >50 dpa.

3. Irradiation–induced ductility degradation is more pronounced for lower irradiation temperature. Total elongation of the alloys decreases with damage level to ≈30–40 dpa and does not decrease further on irradiation to >50 dpa up to ≈120 dpa.

4. After irradiation to 28–34 dpa, the U.S. reference alloy V–4Cr–4Ti retained sufficient strength and excellent ductility regardless of irradiation (420°C–600°C) and test temperature (23°C–600°C), i.e., uniform and total elongation of ≥8 and ≥10%, respectively.

ACKNOWLEDGMENTS

The authors are grateful to L. J. Nowicki and J. Gazda for their contributions to experimental efforts.

REFERENCES

1. T. Noda, F. Abe, H. Araki, and M. Okada, J. Nucl. Mater. 155-157 (1988) 581.
2. R. Santos, J. Nucl. Mater. 155-157 (1988) 589.
3. S. J. Piet, H. G. Kraus, R. M. Neilson, Jr. and J. L. Jones, J. Nucl. Mater. 141-143 (1986) 24.
4. F. L. Yaggee, E. R. Gilbert and J. W. Styles, J. Less-Comm. Met. 19 (1969) 39.
5. D. L. Smith, B. A. Loomis, and D. R. Diercks, J. Nucl. Mater. 135 (1985) 125.
6. B. A. Loomis, H. M. Chung, and D. L. Smith, "Baseline Tensile Properties of V–Cr–Ti Alloys," in this report.
7. H. M. Chung, B. A. Loomis, and D. L. Smith, "Properties of V–4Cr–4Ti for Application as Fusion Reactor Structural Components," Fusion Eng. Design, 1995, in press.

Subtask 12F4: EFFECTS OF NEUTRON IRRADIATION ON THE IMPACT PROPERTIES AND FRACTURE BEHAVIOR OF VANADIUM-BASE ALLOYS,

H. M. Chung, B. A. Loomis, and D. L. Smith (Argonne National Laboratory)

SUMMARY

Up–to–date results on the effects of neutron irradiation on the impact properties and fracture behavior of V, V–Ti, V-Cr-Ti and V–Ti–Si alloys are presented in this paper, with an emphasis on the behavior of the U.S. reference alloys V–4Cr–4Ti containing 500–1000 wppm Si. Database on impact energy and ductile–brittle transition temperature (DBTT) has been established from Charpy impact tests of one–third–size specimens irradiated at 420°C–600°C up to ≈50 dpa in lithium environment in fast fission reactors. To supplement the Charpy impact tests fracture behavior was also characterized by quantitative SEM fractography on miniature tensile and disk specimens that were irradiated to similar conditions and fractured at –196°C to 200°C by multiple bending. For similar irradiation conditions irradiation–induced increase in DBTT was influenced most significantly by Cr content, indicating that irradiation–induced clustering of Cr atoms takes place in high–Cr (Cr ≥ 7 wt.%) alloys. When combined contents of Cr and Ti were ≤10 wt.%, effects of neutron irradiation on impact properties and fracture behavior were negligible. For example, from the Charpy–impact and multiple–bend tests there was no indication of irradiation–induced embrittlement for V–5Ti, V–3Ti–1Si and the U.S. reference alloy V–4Cr–4Ti after irradiation to ≈34 dpa at 420°C to 600°C, and only ductile fracture was observed for temperatures as low as –196°C.

INTRODUCTION

Vanadium-base alloys have significant advantages over other candidate alloys (such as austenitic and ferritic steels) for use as first wall and blanket structural materials in fusion devices, e.g., the International Thermonuclear Experimental Reactor (ITER) and magnetic fusion reactors.[1–5] As part of a program to screen candidate alloys and develop an optimal alloy, extensive investigations have been conducted on V, V-Ti, V-Cr, V-Cr-Ti, and V-Ti-Si alloys after irradiation to ≈120 dpa by fast neutrons at 420, 520, and 600°C.[6–14] These investigations indicated that V–(4–5)Cr–(3–5)Ti alloys exhibited in particular excellent baseline creep properties,[11] impact behavior[13] and superior resistance to irradiation–induced density change,[12] microstructural instability,[7] and degradation of impact toughness,[10] which cannot be matched by other candidate materials such as austenitic and ferritic/martensitic alloys. This paper presents an overview of up–to–date results on the effects of neutron irradiation on the impact properties and fracture behavior of V–Ti, V-Cr-Ti and V–Ti–Si alloys, with an emphasis on the behavior of the U.S. reference alloys V–4Cr–4Ti containing 500–1000 wppm Si. Database on impact energy and ductile–brittle transition temperature (DBTT) has been established from Charpy impact tests of one–third–size specimens irradiated at 420°C–600°C to ≈43 dpa, and to supplement the Charpy impact tests, fracture behavior was also characterized by quantitative SEM fractography on irradiated miniature tensile and disk specimens fractured by multiple bending.

MATERIALS, IRRADIATION, AND TEST PROCEDURES

The elemental composition of the alloys is given in Table 1. The alloy ingots were melted from low–chlorine titanium and low–impurity vanadium raw materials by multiple

Table 1. Chemical Composition of Vanadium–Base Alloys

ANL ID	Alloy Composition (wt.%)	Impurity Concentration (wt. ppm) O	N	C	Si
BL-19	V	1101	161	360	–
BL-20	V	570	110	120	325
BL-36	V	810	86	250	<50
BL-51	V	570	49	56	370
840626	V	260	75	28	260
820630	V	200	62	75	780
BL-35	9.5Cr	340	45	120	<50
BL-4	10.0Cr	530	76	240	<50
BL-5	14.1Cr	330	69	200	<50
BL-50	1.0Ti	230	130	235	1050
BL-52	3.1Ti	210	310	300	500
BL-46	4.6Ti	305	53	85	160
BL-11	4.9Ti	1820	530	470	220
BL-34	8.6Ti	990	180	420	290
BL-12	9.8Ti	1670	390	450	245
BL-13	14.4Ti	1580	370	440	205
BL-15	17.7Ti	830	160	380	480
BL-16	20.4Ti	390	530	210	480
BL-10	7.2Cr-14.5Ti	1110	250	400	400
BL-21	13.7Cr-4.8Ti	340	510	180	1150
BL-22	13.4Cr-5.1Ti	300	52	150	56
BL-23	12.9Cr-5.9Ti	400	490	280	1230
BL-24	13.5Cr–5.2Ti	1190	360	500	390
BL-25	14.4Cr-0.3Ti	390	64	120	<50
BL-26	14.1Cr-1.0Ti	560	86	140	<50
BL-40	10.9Cr-5.0Ti	470	80	90	270
BL-41	14.5Cr-5.0Ti	450	120	93	390
BL-43	9.2Cr-4.9Ti	230	31	100	340
BL-44	9.9Cr-9.2Ti	300	87	150	270
BL-49	7.9Cr-5.7Ti	400	150	127	360
BL-62	3.1Ti–0.1Si	320	86	109	660
BL-27	3.1Ti–0.25Si	210	310	310	2500
BL-42	3.1Ti–0.5Si	580	190	140	5400
BL-45	2.5Ti-1Si	345	125	90	9900
BL-47	4.1Cr-4.3Ti	350	220	200	870
832665	3.8Cr–3.9Ti	310	85	80	783
T87	4.9Cr–5.1Ti	380	89	109	545

vacuum–arc melting process. Typically, Charpy–impact, tensile, and disk specimens were machined out of the alloy plates and sheets 3.8, 1.0, and 0.25 mm in thickness; then the machined specimens were cleaned and annealed at 1050°C to 1125°C in high vacuum before encapsulation for irradiation. Orientation of Charpy–impact specimens, relative to

the rolling direction of the 3.8–mm–thick plates, was the same as that of the unirradiated specimens reported elsewhere.[13] Dimensions of the 45°–notched specimens were 3.33 x 3.33 x 25.4 in mm, with a notch depth of 0.61 mm and a root radius of 0.25 mm.

The alloys were irradiated in the Materials Open Test Assembly (MOTA) in the Fast Flux Test Facility (FFTF), a fast fission reactor located in Richland, Washington, at 420°C, 520°C, and 600°C to neutron fluences (E > 0.1 MeV) ranging from 3 x 10^{22} n/cm^2 [≈17 displacements per atom (dpa)] to 1.9 x 10^{23} n/cm^2 (≈114 dpa). Because of the insignificant thermal neutron spectrum in the FFTF, transmutation of vanadium to Cr was negligible. The specimens were sealed in TZM/Mo capsules filled with 99.99%-enriched Li^7 during irradiation to prevent contamination by oxygen, nitrogen, and carbon impurities dissolved in the sodium coolant of the FFTF and formation of unacceptable levels of helium and tritium from Li^6.

After irradiation, Li in the capsules were dissolved in liquid ammonia in hot cell to free the specimens from capsule, then each specimen was cleaned further in liquid ammonia and acetone. Prior to impact or bend testing, the irradiated specimens were annealed carefully at 400°C for 1 h to expel hydrogen or tritium that were introduced into the specimen during irradiation, retrieval from irradiated capsules, or subsequent cleaning.

Charpy–impact tests were performed with an instrumented Dynatup Drop–Weight Test machine. Impact velocity and load for these tests were 2.56 m/s and 14.995 kg, respectively. Energy absorption during impact was determined automatically by computer from applied load vs. time data acquired during the impact. Typical impact time for a ductile condition was 3–4 ms. The specimen surface temperature at the instant of impact was determined from a thermocouple spot–welded near the notch and was displayed digitally during the test. The lowest attainable specimen temperature was –196°C, the temperature of liquid–nitrogen bath. A test specimen with thermocouple attached was soaked in the bath to reach an equilibrated temperature of –196°C and quickly transferred to test position in <2 s. When the specimen surface temperature increased to a desired impact–test temperature (e.g., –110°C), the tup was then released instantaneously. For specimen surface temperatures of ≈–170°C to ≈–70°C in which the temperature increase is rapid, inside temperature below the notch is believed to be somewhat lower than the recorded surface temperature. This corresponds to somewhat conservative determination of absorbed energy as a function of impact temperature reported in this study, in particular for the above range of test (surface) temperatures. Test temperatures above room temperature were controlled by heating the specimen by a blowing heat gun.

Fracture behavior was also determined by repeatedly bending a TEM disk (0.25–mm thick) or a piece of the shoulder region of a fractured tensile (0.76– to 1.0–mm thick) specimen in low–temperature bath of liquid nitrogen or mixtures of dry ice and acetone. Tensile specimens fractured in gauge section at room temperature were selected for this bending test. Temperature of the surrounding liquid was measured with a calibrated thermocouple. Specimen constraint during the bending test was similar to that in a four–point bend test. At a given test temperature, cold–work accumulated in the specimen as the number of bends increased, thereby hardening the material progressively. After fracture, morphology of the fracture surface was examined quantitatively by SEM. A few dozen SEM fractographs were taken at ≈300X, and a composite of the whole fracture surface was made. Four types of fracture morphology were observed: cleavage, quasi–

cleavage, ductile-dimple, and fibrous ductile fracture. From the fracture surface composite, the percentage of ductile-fracture morphology was measured for each specimen with a planimeter. Ductile–brittle–transition temperature (DBTT) was then determined from a plot of fracture appearance (i.e., percentage of ductile-fracture morphology) vs. specimen bending temperature.

RESULTS AND DISCUSSION

Examples of impact data showing the effects of neutron irradiation relative to baseline impact properties of unirradiated specimens are shown in Figs. 1–6 for six typical alloys, i.e., two heats of V–15Cr–5Ti, V–9Cr–5Ti, the US reference alloy V–4Cr–4Ti, V–5Ti, and V–3Ti–1Si, respectively. Also shown in Figs. 2 (V–15Cr–5Ti) and 4 (V–4Cr–4Ti) are examples of the results of the quantitative fractography of tensile and disk specimens that were fractured by multiple bending. This same technique was utilized to investigate the fracture behavior of disk and tensile specimens that were irradiated in the Dynamic Helium Charging Experiment, in which no Charpy impact specimens could be accommodated because of severe limitation in available irradiation space.[14] Although it is rather time–consuming to construct a sufficiently detailed fracture surface map, ductile–brittle transition behavior determined from the technique seems to be consistent with and complementary to that determined from the instrumented impact tests. For example, it was conclusively shown that no brittle fracture could be produced in the US reference alloy V–4Cr–4Ti for >–196°C (Fig. 4) after irradiation to 24–34 dpa at 425°C–600°C. This was verified from three different types of testing, i.e., Charpy–impact testing of one–third–size specimens, multiple–bend testing of 1.0–mm–thick tensile sheet specimens, and

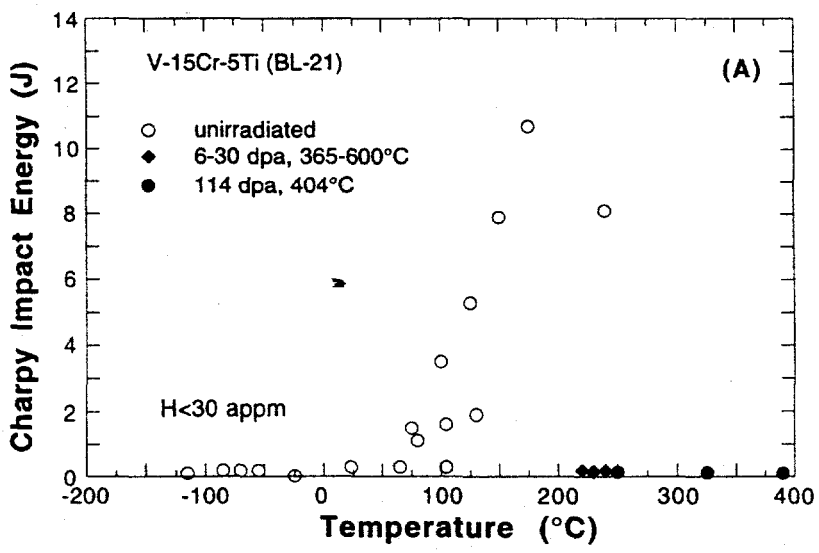

Fig. 1.

Impact properties of V–15Cr–5Ti (BL–21) before and after neutron irradiation.

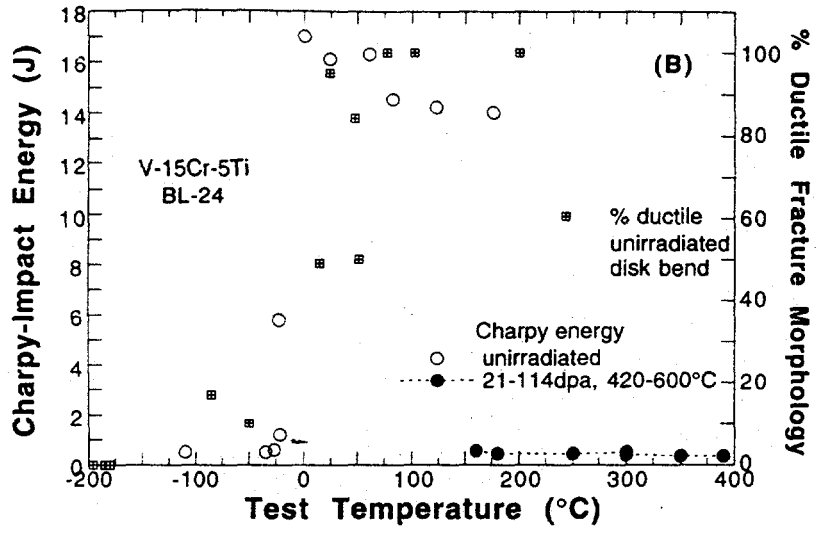

Fig. 2.

Impact properties and fracture behavior of V–15Cr–5Ti (BL–24) before and after neutron irradiation.

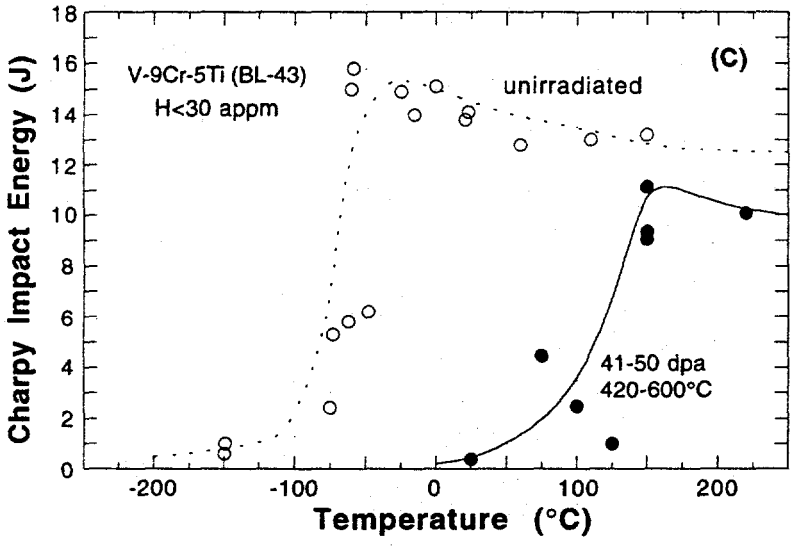

Fig. 3.

Impact properties of V–9Cr–5Ti (BL–43) before and after neutron irradiation.

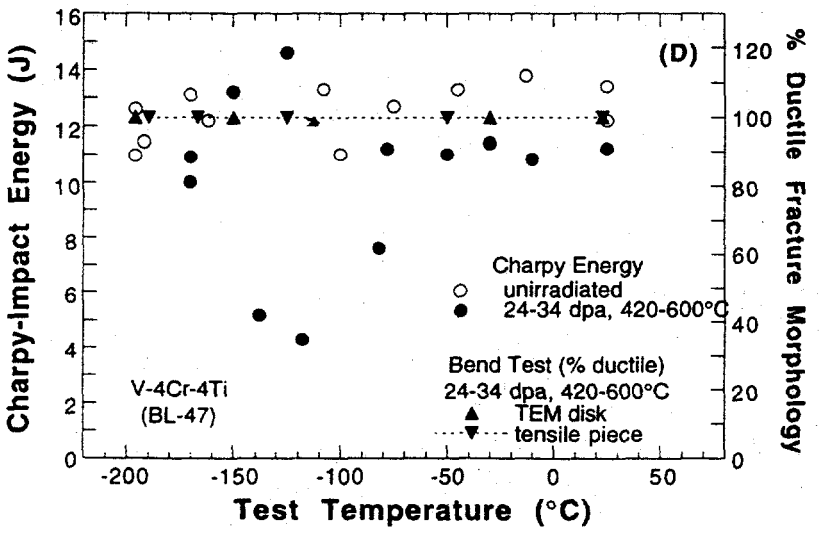

Fig. 4.

Impact properties and fracture behavior of V–4Cr–4Ti (BL–47) before and after neutron irradiation.

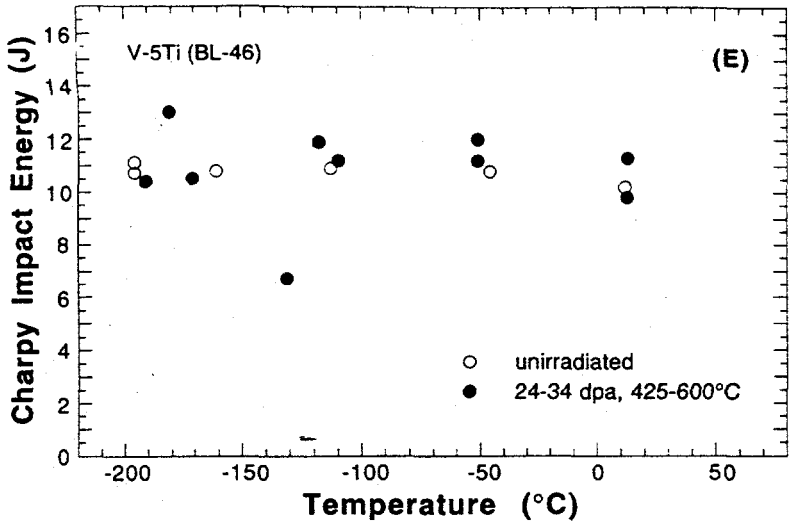

Fig. 5.

Impact properties of V–5Ti (BL–46) before and after neutron irradiation.

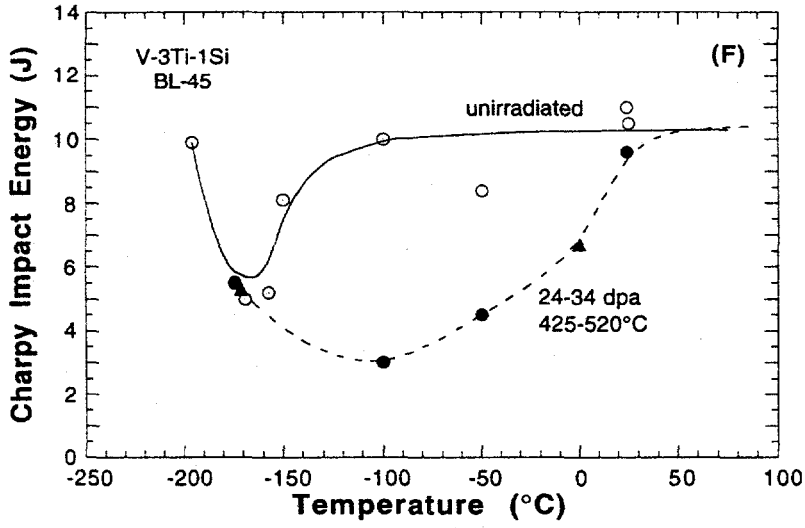

Fig. 6.

Impact properties of V–3Ti–1Si (BL–45) before and after neutron irradiation.

multiple–bend testing of 0.25–mm–thick TEM disks. This means that the US reference alloy V–4Cr–4Ti is virtually immune to neutron displacement damage, at least for the irradiation temperatures of 425°C–600°C. This is a remarkable property considering the BCC structure of the refractory alloy. Virtual immunity to neutron displacement damage is also evident for V–5Ti (Fig. 5), and to a lesser extent, for V–3Ti–1Si (Fig. 6).

V–3Ti–0.5Si (BL–42), an alloy similar to V–3Ti–1Si (BL–45), exhibited DBTTs of –50°C to –85°C after irradiation to 45–50 dpa at 425°C–600°C, indicating that V–3Ti–Si family of alloys are not as excellent as the V–(4–5)Cr–(3–5)Ti alloys. Both V–3Ti–0.5Si and V–3Ti–1Si alloys seem to retain considerable amount of hydrogen or tritium after irradiation that were not expelled completely by the post–irradiation annealing at 400°C for 1 h. During impact testing, the residual hydrogen or tritium atoms will diffuse rapidly from the warmer surface region of the specimen to the relatively colder inner region (i.e., in front of the notch root). This will be most pronounced for the range of test (surface) temperatures of –170°C to –70°C in which increase in specimen surface temperature from

the equilibrated temperature of −196°C is fastest. Therefore, the compounded effects of residual hydrogen and thermal stress are expected to be most pronounced for this range of impact temperature (i.e., specimen surface temperature of −170°C to −70°C). It seems that the Charpy energy minima, observed at −120°C, −130°C, and −100°C for V–4Cr–4Ti (Fig. 4), V–5Ti (Fig. 5), and V–3Ti–1Si (Fig. 6), respectively, are manifestation of these compounded effects.

Effects of neutron irradiation on DBTT shift and upper shelf energy were very significant for high–Cr alloys of V–15Cr–5Ti (Figs. 1 and 2) and V–9Cr–5Ti (Fig. 3). Therefore, these high–Cr alloys are simply unacceptable from the standpoint of irradiation embrittlement alone. To better define the effect of Cr, DBTTs of the V–Cr–(4–5)Ti alloys, determined before and after irradiation to 24–43 dpa at 420°C–600°C, have been plotted in Fig. 7 as function of Cr concentration. A Ti content of 4–5 wt.% has been considered most desirable in V–Cr–Ti ternary alloys primarily from the standpoint of irradiation–induced density change and tensile and creep strength. That is, to assure good resistance to swelling, Ti content must be kept ≥ 3 wt.%,[12] whereas Ti content ≥8 wt. % is conducive to

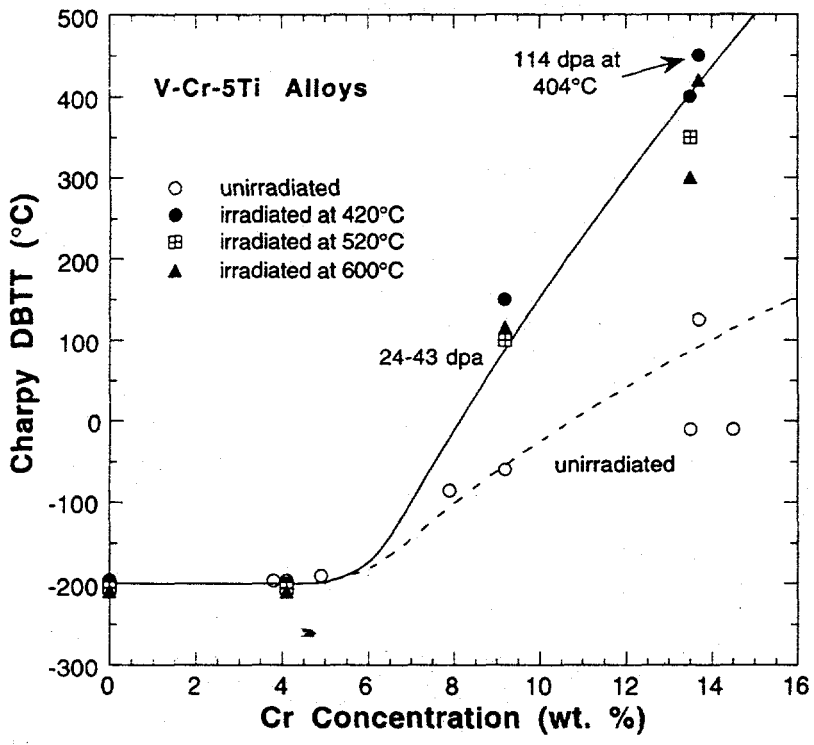

Fig. 7.

DBTT as a function of Cr content measured on one–third–size Charpy specimens of V–Cr–5Ti alloys before and after irradiation to 24–43 dpa at 420°C–600°C.

lower tensile strength[9] and higher creep rate.[11] The results in Fig. 7 clearly show that Cr content must be limited to <6 wt.% in order to ensure excellent impact properties (i.e., virtual immunity to irradiation embrittlement). Given a similar irradiation condition, DBTT shift is obviously more pronounced for increasing Cr content in the alloy.

Although some effect of irradiation temperature is evident for high–Cr alloys in Fig. 7, DBTT of V–Cr–5Ti alloys with Cr < 6 wt.% is so low (<–200°C) that the effect seems to be inconsequential for this range of irradiation temperature.

In Fig. 8, DBTTs of all the irradiated V–Ti, V–Ti–Si, and V–Cr–Ti alloys are plotted as a function of combined concentrations of Cr and $Ti^{0.95}$. A good correlation is evident between DBTT and the combined contents. The figure also demonstrates that excellent resistance to irradiation–induced embrittlement is assured by limiting combined contents of Cr and Ti to ≤10 wt.% and Si content to ≤1000 wppm (e.g., as in the U. S. reference alloy V–4Cr–4Ti).

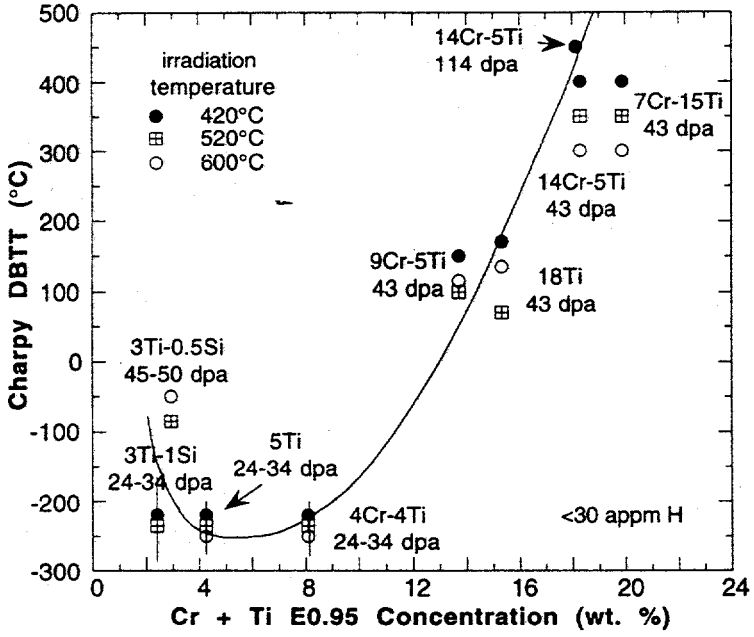

Fig. 8.

DBTT as a function of combined Cr and Ti contents measured on one–third–size Charpy specimens of V–Ti, V–Cr–Ti, and V–Ti–Si alloys after irradiation.

CONCLUSIONS

(1) Impact tests were conducted on V–Ti, V–Ti–Si, and V-Cr-Ti alloys after neutron irradiation to ≈50 dpa at 400°C to 600°C in lithium environment in fast reactors. Irradiation–induced shift of ductile–brittle transition temperature (DBTT) is significant for Ti ≥ 10 wt.% in V–Ti alloys and for Cr ≥ 6 wt.% for V–Cr–5Ti alloys. Therefore, these high–Ti binary and high–Cr ternary alloys are not acceptable simply from the standpoint of irradiation embrittlement alone.

(2) A good correlation was observed between DBTT and Cr content of V–Cr–(4–5)Ti alloys, irradiated to 24–43 dpa at 420°C to 600°C. For Cr ≤ 6 wt.%, irradiation–induced embrittlement of these alloys was negligible regardless of the irradiation temperature. Impact properties of V–3Ti–(0.5–1)Si alloys irradiated to similar conditions were not as good as those of V–(3–5)Cr–(4–5)Ti alloys.

(3) To assure excellent impact properties in V–Cr–Ti alloys, combined contents of Cr and Ti must be limited to ≤10 wt.% and Si content to ≤1000 wppm. For example, the U.S. reference alloy V–4Cr–4Ti containing 500–1000 wppm Si was virtually immune to neutron–irradiation damage; after irradiation to 24–34 dpa at 420°C–600°C, the alloy exhibited DBTT<–200°C and an upper–shelf energy of ≈120–140 J/cm^{-2}. This remarkable property was also verified from quantitative analysis of fracture

appearance of irradiated specimens that were fractured by multiple bending; only ductile fracture morphology was observed for all temperatures as low as –196°C.

ACKNOWLEDGMENTS

The authors are grateful to L. Nowicki, J. Gazda, D. Donahue, and D. Busch for many experimental contributions.

REFERENCES

1. T. Noda, F. Abe, H. Araki, and M. Okada, J. Nucl. Mater. 155-157 (1988) 581.
2. R. Santos, J. Nucl. Mater. 155-157 (1988) 589.
3. S. J. Piet, et al., J. Nucl. Mater. 141-143 (1986) 24.
4. F. L. Yaggee, E. R. Gilbert, and J. W. Styles, J. Less-Comm. Met. 19 (1969) 39.
5. D. L. Smith, B. A. Loomis, and D. R. Diercks, J. Nucl. Mater. 135 (1985) 125.
6. H. M. Chung and D. L. Smith, J. Nucl. Mater. 191–194 (1992) 942–947.
7. H. M. Chung, B. A. Loomis, and D. L. Smith, ASTM STP 1175, American Society for Testing and Materials, Philadelphia, 1993, pp. 1185–1200.
8. D. L. Smith, B. A. Loomis, and H. M. Chung, Plasma Devices and Operations, Vol. 3, 1994, pp. 167–179.
9. B. A. Loomis, L. Nowicki, and D. L. Smith, J. Nucl. Mater. 212–215 (1994) 790.
10. B. A. Loomis, H. M. Chung, L. Nowicki, and D. L. Smith, J. Nucl. Mater. 212–215 (1994) 799.
11. H. M. Chung, B. A. Loomis, and D. L. Smith, J. Nucl. Mater. 212–215 (1994) 772.
12. H. M. Chung, B. A. Loomis, and D. L. Smith, J. Nucl. Mater. 212–215 (1994) 804.
13. H. M. Chung, B. A. Loomis, and D. L. Smith, "Baseline Impact Properties of Vanadium Alloys," in this report.
14. H. M. Chung, L. J. Nowicki, D. E. Busch, and D. L. Smith, "Fracture Properties of V–4Cr–4Ti Irradiated in the Dynamic Helium Charging Experiment," in this report.

Subtask 12G1: EFFECTS OF DYNAMICALLY CHARGED HELIUM ON SWELLING AND MICROSTRUCTURE OF VANADIUM-BASE ALLOYS,

H. M. Chung, L. Nowicki, J. Gazda, and D. L. Smith (Argonne National Laboratory)

OBJECTIVE

The objective of this work is to determine void structure, distribution, and density changes of several promising vanadium–base alloys irradiated in the Dynamic Helium Charging Experiment (DHCE).

SUMMARY

Combined effects of dynamically charged helium and neutron damage on density change, void distribution, and microstructural evolution of V–4Cr–4Ti alloy have been determined after irradiation to 18–31 dpa at 425–600°C in the DHCE, and the results compared with those from a non–DHCE in which helium generation was negligible. For specimens irradiated to ≈18–31 dpa at 500–600°C with a helium generation rate of 0.4–4.2 appm He/dpa, only a few helium bubbles were observed at the interface of grain matrices and some of the Ti(O,N,C) precipitates, and no microvoids or helium bubbles were observed either in grain matrices or near grain boundaries. Under these conditions, dynamically produced helium atoms seem to be trapped in the grain matrix without significant bubble nucleation or growth, and in accordance with this, density changes from DHCE and non–DHCE (negligible helium generation) were similar for comparable fluence and irradiation temperature. Only for specimens irradiated to ≈31 dpa at 425°C, when helium was generated at a rate of 0.4–0.8 appm helium/dpa, were diffuse helium bubbles observed in limited regions of grain matrices and near ≈15% of the grain boundaries in densities significantly lower than those in the extensive coalescences of helium bubbles typical of other alloys irradiated in tritium–trick experiments. Density changes of specimens irradiated at 425°C in the DHCE were significantly higher than those from non–DHCE irradiation. Microstructural evolution in V–4Cr–4Ti was similar for DHCE and non–DHCE except for helium bubble number density and distribution. As in non–DHCE, the irradiation–induced precipitation of ultrafine Ti_5Si_3 was observed for DHCE at >500°C but not at 425°C.

INTRODUCTION

Recent attention in the development of vanadium–base alloys for application in fusion reactor first wall and blanket structure has focused on V-4Cr-4Ti, an alloy reported to exhibit an excellent combination of mechanical and physical properties before and after irradiation.[1–6] One unresolved issue in the performance of the alloy, however, has been the effect of fusion–relevant simultaneous generation of helium and neutron damage (at a ratio of 4–5 appm helium/displacement per atom [dpa]) on density change and void swelling. Helium effects determined for other vanadium–base alloys by means of less fusion–relevant simulation approaches such as tritium-trick,[7–13] cyclotron-injection,[14–18] and boron-doping[18–21] techniques have been inconsistent with regard to concentration of helium bubbles on grain boundaries and the concomitant propensity for intergranular fracture. In the unique DHCE, the fusion–relevant helium–to–dpa ratio is simulated realistically by utilizing transmutation of controlled amounts of ^6Li and a predetermined amount of tritium–doped mother alloy immersed in $^6Li + {}^7Li$.[22–24] This report describes

results of microstructural characterization and density measurement, primarily of V–4Cr–4Ti alloy specimens irradiated to 18–31 dpa at 425–600°C in the DHCE.

MATERIALS AND PROCEDURES

The elemental composition of the 30–kg heat of V–4Cr–4Ti alloy (ANL Identification BL–47), determined prior to irradiation, is given in Table 1. Postirradiation examination of other alloys listed in Table 1 (i.e., V–5Ti, V–3Ti–1Si, and V–8Cr–6Ti) was limited; unless pointed out specifically, all results reported in this study refer to V–4Cr–4Ti. Fabrication procedures of the alloy ingots and annealed plates and sheets have been reported elsewhere.[25] TEM disks, punched from 0.3–mm–thick cold–worked sheets for use in *investigating* density change, void swelling behavior, and microstructural characteristics, were annealed at 1050°C in an ion–pumped high–vacuum system. The annealed material was ≈95% recrystallized and exhibited an average grain size of ≈14 mm. Phase structures of the alloy, characterized before and after irradiation in a non–DHCE (negligible helium generation), have been described in detail elsewhere.[4] The only secondary phase present in the as–annealed specimens was Ti(O,N,C), which is normally observed in titanium–containing vanadium alloys with O+N+C > 400 wppm.[26]

Table 1. Chemical composition of vanadium–base alloys

ANL ID	Nominal Composition (wt.%)	Impurity Composition (wppm) O	N	C	Si	S	P	Nb	Mo
BL-47	V–4.1Cr–4.3Ti	350	220	200	870	20	<40	<100	<100
BL-46	V–4.6Ti	305	53	85	160	10	<100	<100	–
BL-45	V–2.5Ti–1.0Si	345	125	90	9900	30	–	200	140
BL-49	V–7.9Cr–5.7Ti	400	150	127	360	20	–	<100	170

The alloy specimens were irradiated in the Fast Flux Test Facility (FFTF), a fast reactor located in Richland, Washington, at 420, 520, and 600°C to neutron fluences (E > 0.1 MeV) ranging from 3.7 x 10^{22} n/cm^2 (≈18 displacements per atom, or dpa) to 6.4 x 10^{23} n/cm^2 (≈31 dpa). Helium in the alloy specimens was produced by utilizing transmutation of controlled amounts of ^{6}Li and a predetermined amount of tritium–doped vanadium mother alloy immersed in ^{6}Li + ^{7}Li.[22–24] Table 2 summarizes the actual postirradiation parameters determined from tensile and disk specimens of the V–4Cr–4Ti alloy, i.e., fast neutron fluence, dose, and helium and tritium content measured shortly after the postirradiation tests. Helium and tritium were determined by mass spectrometry at Rockwell International Inc., Canoga Park, California.

The retrieved TEM specimens, which contained helium, tritium, and neutron displacement damage, were cleaned ultrasonically in alcohol prior to density measurement and microstructural analysis. Most of the examined TEM disks were not degassed at 400°C for 1 h, a customary procedure to expel tritium and hydrogen from Charpy–impact and tensile specimens. Several TEM disks were examined after degassing, but none indicated an appreciable difference in void or helium bubble distribution and microstructure from undegassed specimens that should contain tritium and hydrogen in addition to helium. The irradiated specimens were jet–thinned for TEM in a solution of 15% sulfuric acid-72% methanol-13% butyl cellosolve maintained at -5°C.

TEM was conducted with a JEOL 100CX-II scanning transmission electron microscope operating at 100 keV, or with a Philips CM-30 analytical electron microscope operating at 200 keV. Density change was determined from specimen weights measured in air and in research–grade CCl_4.

VOID STRUCTURE AND DISTRIBUTION

A summary of microstructural characterization of voids in the DHCE specimens is given in Table 3. Appreciable numbers of voids in the DHCE specimens were absent, except for specimens retrieved from Capsules 4D1 and 4D2, which were irradiated at 425°C. In specimens irradiated at 600°C and retrieved from Capsules 5C1 and 5C2, only a few helium bubbles were observed at interfaces between the grain matrix and a limited number of Ti(O,N,C) precipitates. TEM images of these microstructural characteristics were reported previously.[27]

Specimens irradiated to 18–31 dpa at 425°C–600°C in the other three capsules (Capsule 5E2, helium generation rate of 0.11 appm He/dpa; 5D1, 0.83 appm He/dpa; and 5E1, 0.36 appm He/dpa) exhibited microstructural characteristics essentially similar to those of specimens from Capsule 5C1 and 5C2, i.e., no helium bubbles either in the grain matrix or on grain boundaries, a few helium bubbles on the interface between the grain matrix and a limited number of Ti(O,N,C) precipitates, and ultrafine Ti_5Si_3 precipitates in high density (only in specimens irradiated at 500°C–600°C). In these specimens, virtually all of the dynamically produced helium atoms seem to have been trapped in the grain matrix without significant bubble nucleation or growth.

Table 2. Summary of irradiation parameters of Dynamic Helium Charging Experiment and helium and tritium contents measured in V–4Cr–4Ti specimens

Capsule ID No.	Irradiation Temp. (°C)	Fluence (E >0.1 MeV) (10^{22} n cm^{-2})	Total Damage (dpa)	Calculated Helium (appm) to dpa Ratio[a] at EOI[b] (Assumed k_a or k_W)[c] k_a=0.073 (k_W=0.01)	Measured Helium Content[d] (appm)	Actual Helium to dpa Ratio (appm/dpa)	Measured Tritium Content[e] (appm)
4D1	425	6.4	31	3.8	11.2–13.3	0.39	27
4D2	425	6.4	31	2.8	22.4–22.7	0.73	39
5E2	425	3.7	18	2.1	3.3–3.7	0.11	2
5D1	500	3.7	18	4.4	14.8–15.0	0.83	4.5
5E1	500	3.7	18	3.1	6.4–6.5	0.36	1.7
5C1	600	3.7	18	1.1	8.4–11.0	0.54	20
5C2	600	3.7	18	1.1	74.9–75.3	4.17	63

[a] L. R. Greenwood "Revised Calculations for the DHCE," April 30, 1993.

[b] Beginning of irradiation (BOI) May 27, 1991; end of irradiation (EOI) March 19, 1992; 203.3 effective full power days (EFPD), hot standby at ≈220°C until November 1992.

[c] Equilibrium ratio (k_a by atom, k_W by weight) of tritium in V alloy to that in the surrounding liquid lithium.

[d] Measured June 1994.

[e] Measured August 1994.

Table 3. Summary of void distribution in V–4Cr–4Ti irradiated in the DHCE.

Capsule ID No.	Irradiation Temp (°C)	Fluence (E >0.1 MeV) (10^{22} n cm^{-2})	Total Damage (dpa)	Helium–to–dpa Ratio (appm/dpa)	Voids in Grain Matrix	Voids on Boundary of Grain Matrix and Ti(O,N,C)	Voids on Grain Boundaries
non–DHCE	425, 500, 600°C	–	24–34	≈0.01	none	none	none
4D1	425	6.4	31	0.39	some	some	some
4D2	425	6.4	31	0.73	some	some	some
5E2	425	3.7	18	0.11	none	none	none
5D1	500	3.7	18	0.83	none	some	none
5E1	500	3.7	18	0.36	none	some	none
5C1	600	3.7	18	0.54	none	some	none
5C2	600	3.7	18	4.17	none	some	none

For DHCE specimens irradiated to 31 dpa at 425°C in high–tritium capsules 4D1 (helium generation rate ≈0.4 He/dpa) and 4D2 (helium generation rate of ≈0.73 He/dpa), helium bubbles (≈5 nm in diameter) were observed in the grain matrix and on ≈15% of the grain boundaries. Helium bubbles observed near grain boundaries in these specimens were characterized by (a) diffuse bubbles in a number density significantly lower than that of the compact coalescences of helium bubbles observed in other alloys irradiated in tritium–trick experiments;[7–12] (b) discontinuous (≈15% of grain boundaries), in contrast to continuous (≈100% of grain boundaries) coalescence observed in tritium–trick experiments;[7–12] and (c) more or less similar bubble distribution in the grain matrix and near grain boundaries, in contrast to virtual concentration of all helium bubbles on grain boundaries in tritium–trick experiments. These observations seem to indicate that most of the helium atoms produced dynamically at 425°C were trapped in the grain matrix, preventing extensive formation of a continuous coalescence of helium bubbles on grain boundaries. Figure 1 shows typical microstructures of the diffuse helium bubbles in the grain matrix and near grain boundaries and helium shells surrounding Ti(O,N,C) precipiates in specimens irradiated at 425°C (helium generation rates 0.4–0.8 appm He/dpa).

As in non–DHCEs,[4] Ti_5Si_3 did not precipitate during irradiation at 425°C in the DHCEs. If Ti_5Si_3 precipitation was indeed significant for 425°C irradiation, void swelling at that temperature would have been suppressed significantly, as in other alloys irradiated at 420°C in non–DHCEs.[28]

DENSITY CHANGE

Results of density measurements for specimens irradiated at 600 (18 dpa in Capsule 5C1) and 425°C (18 dpa in Capsule 5E2, 31 dpa in Capsules 4D1 and 4D2) are given in Figs. 2A and 2B, respectively. The helium generation rates in the DHCE specimens are also given in the figure (see Table 2). For comparison, density changes determined for similar irradiation conditions in non–DHCEs[3] are also shown in the figures.

Density changes in the non–DHCE and DHCE specimens irradiated at 500°C and 600°C were low (<0.6 %). The small density change seems to be consistent with the negligible number density of voids or helium bubbles (Table 3).[27] However, density

changes in the DHCE specimens irradiated at 425°C (Capsules 4D1, helium generation rate ≈0.4 He/dpa and 4D2, helium generation rate ≈0.73 He/dpa) were somewhat higher than those of the non–DHCE specimens. The relatively large density changes measured for these specimens seem also to be consistent with the relatively higher number density of helium bubbles (Fig. 1).

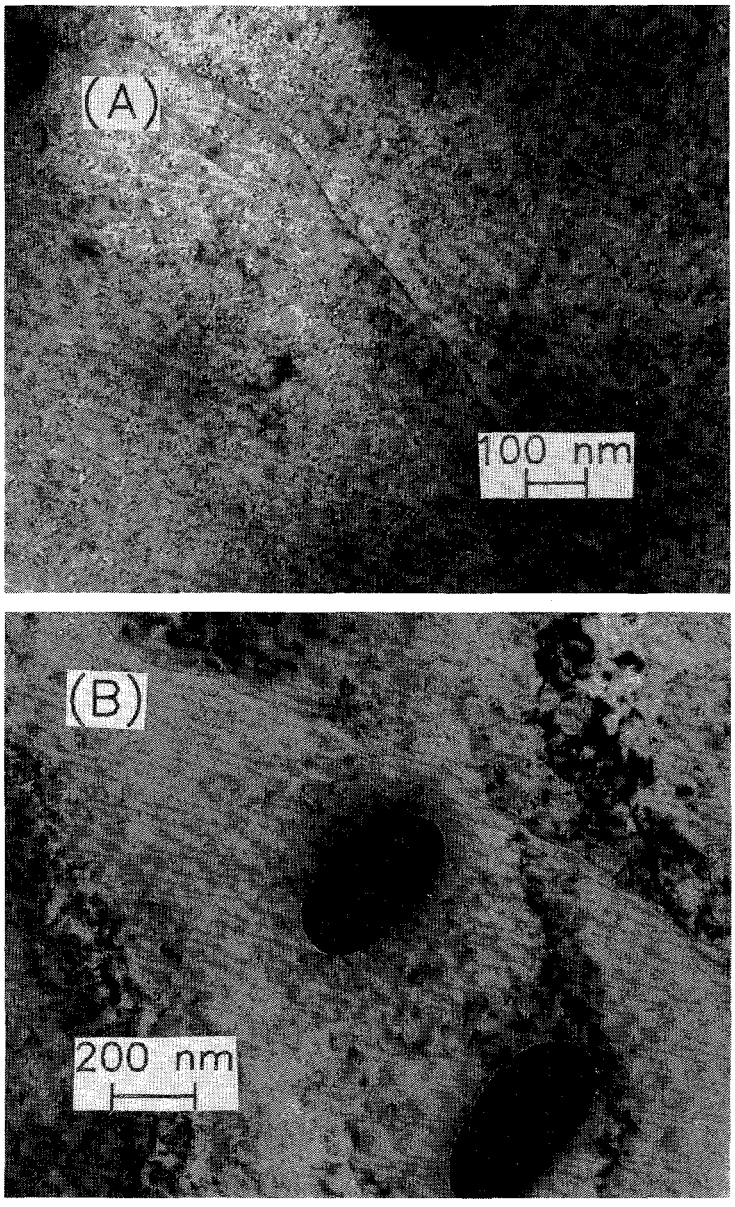

Figure 1. Void microstructure of V-4Cr-4Ti irradiated at 425°C to ≈31 dpa in DHCE (Capsules 4D2 and 4D1): (A) similar distribution of diffuse voids in grain matrices and near grain boundary; and (B) limited number of voids near grain boundary and void shells surrounding Ti(O, N, C).

Density changes measured in disk specimens of V–5Ti, V–3Ti–1Si, and V–8Cr–6Ti, irradiated to ≈18 dpa at 425°C in a DHCE in Capsule 5E2, are shown in Fig. 3. In the figure, density changes in the DHCE are compared with those obtained on similar specimens irradiated to ≈34 dpa in a non–DHCE. Although the helium content of these alloy specimens was not measured, the actual helium generation rate was expected to be low and similar to that of V–4Cr–4Ti (i.e., 0.11 appm He/dpa). Effects of helium on density changes in these alloy specimens were insignificant.

DISCUSSION

Microvoids or helium bubbles were absent from all of the specimens of V–4Cr–4Ti irradiated in the DHCE at 500–600°C, except for a few helium bubbles at interfaces between the grain matrix and some Ti(O,N,C) precipitates that are normally present in V–Ti and V–Cr–Ti alloys. Preferential formation of voids near blocky precipitates [presumably Ti(O,N,C) precipitates] was also reported by Braski in V–3Ti–1Si specimens that were preimplanted with 82 appm helium by the tritium–trick technique and then irradiated to 40 dpa at 600°C.[8]

Buitenhuis et al. proposed that interfaces between the grain matrix and Ti(O,N,C) precipitates act as preferential sinks for helium.[29] From a series of thermal desorption analyses by mass spectroscopy, these authors have identified a helium desorption peak at the surprisingly low temperature of ≈280°C in V–5Ti specimens that were irradiated and implanted with helium ions. Some of the desorption peaks were sharp and narrow and some were weak and broad below and above ≈280°C. Furthermore, Buitenhuis et al. attributed the former and the latter types of peaks to helium–vacancy–impurity (O, N, and C) complexes that are produced in the grain matrix and near the interfaces between the grain matrix and Ti(O,N,C) precipitates, respectively, and are subsequently dissociated into helium and vacancy–impurity complexes upon heating to ≈280°C or higher. During our degassing treatment in which DHCE specimens were heated to ≈405°C at a linear rate of 0.2°C/s in high vacuum in the present study, desorption peaks were observed consistently at ≈280°C. However, a positive identification of helium desorption was not made from a mass spectroscopic analysis.

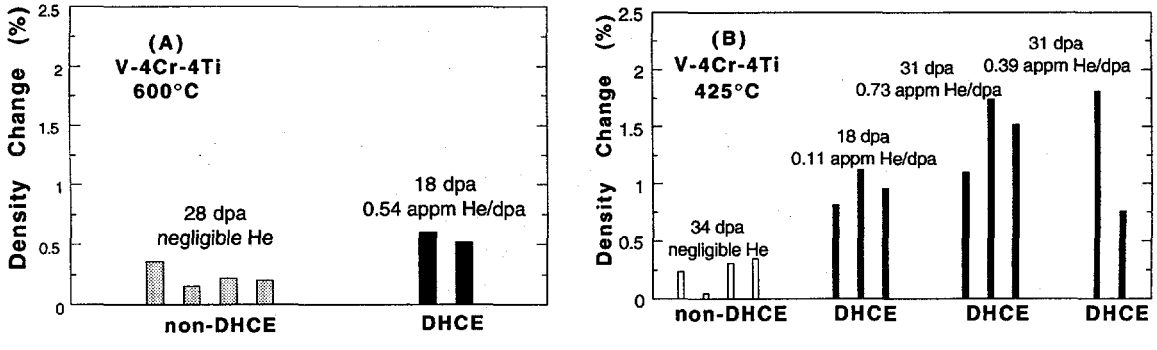

Figure 2. Comparison of density changes of V–4Cr–4Ti from DHCE and non–DHCE experiments: (A) 600°C and (B) 425°C.

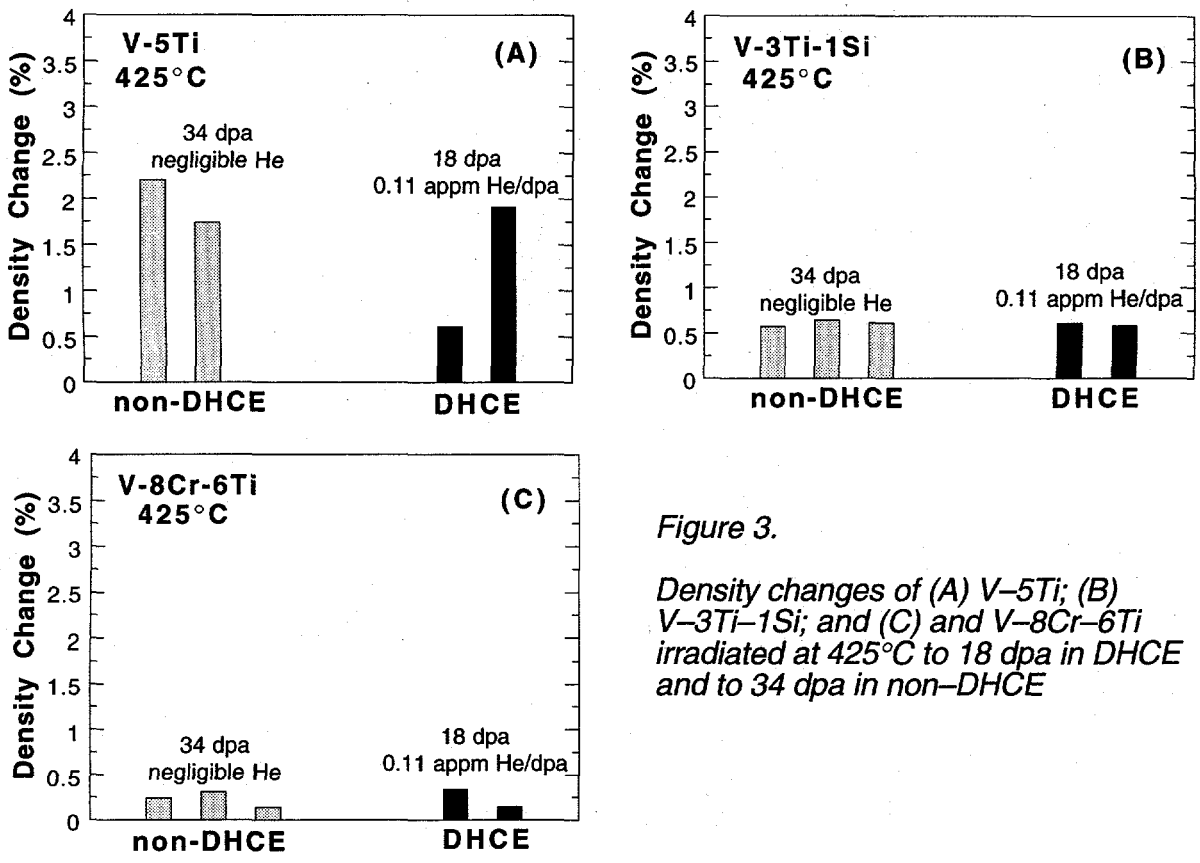

Figure 3.

Density changes of (A) V–5Ti; (B) V–3Ti–1Si; and (C) and V–8Cr–6Ti irradiated at 425°C to 18 dpa in DHCE and to 34 dpa in non–DHCE

One of the important findings from the DHCE was that the actual (measured) helium and tritium content of V–4Cr–4Ti specimens was significantly lower than that calculated on the basis of the assumed equilibrium ratio (k_W = 0.01) of tritium in the alloy to that in the liquid lithium (Table 2). This could be interpreted to indicate that k_W is significantly lower than previously thought, in particular for irradiations at 425 and 500°C.

Microvoids or helium bubbles were absent in the grain matrix and on grain boundaries in all of the specimens irradiated at 500–600°C, in which ultrafine Ti_5Si_3 precipitated in high density. Even in specimens irradiated at 600°C at the highest helium generation rate of ≈4.2 appm helium/dpa (Capsule 5C2), no microvoids could be detected either in the grain matrix or on grain boundaries. This correlation between the high–density precipitation of ultrafine Ti_5Si_3 and negligible void swelling seems to be consistent with similar observations reported previously for non–DHCE conditions.[28] Conversely, the relatively higher void swelling and larger density change observed in specimens irradiated at 425°C (in Capsule 4D1 and 4D2) seems to be associated with an absence of precipitation of ultrafine Ti_5Si_3 at the low irradiation temperature.

As pointed out above, the characteristics of grain–boundary helium bubbles observed in the specimens irradiated to 31 dpa at 425°C were in distinct contrast to those observed in specimens from tritium–trick experiments, i.e., diffuse bubbles in significantly lower number density than those of the compact coalescences of helium bubbles in tritium–trick experiments; discontinous (on ≈15% of grain boundaries), in contrast to continuous

(≈100% of grain boundaries) coalescences in tritium–trick experiments; and similar bubble distribution in the grain matrix and near grain boundaries, in contrast to virtual concentration of all helium bubbles on grain boundaries in tritium–trick experiments. These characteristics seem to indicate that most of the helium atoms produced at 425°C in DHCEs were trapped by vacancies or vacancy–impurity complexes, a finding that is in accordance with the findings of Buitenhuis et al.[29]

Intergranular fracture morphology was not observed in any of the specimens irradiated in the DHCE and subsequently tested by uniaxial tensile tests at 23 to 600°C and multiple bending tests at –196 to 50°C. Even in specimens irradiated at 425°C and fractured in brittle manner during multiple bending tests at –196°, only cleavage and ductile tearing were observed, i.e., intergranular fracture morphology was absent. These observations, consistent with the characteristics of helium bubble distribution described above, are in distinct contrast to the propensity to intergranular fracture that is commonly observed in tritium–trick experiments.

CONCLUSIONS

(1). For specimens irradiated to ≈18 dpa at 500–600°C in the Dynamic Helium Charging Experiment (DHCE) with helium generation rates of ≈0.4–4.2 appm He/dpa, void swelling was negligible, and density changes from the DHCE and non–DHCE (negligible helium generation) were similar (<0.6%). Only limited number of voids or helium bubbles were observed at the interface of the grain matrix and some of the Ti(O,N,C) precipitates. Neither helium bubbles nor voids were observed either in the grain matrix or near grain boundaries. Under irradiation at these temperatures, ultrafine Ti_5Si_3 precipitated in high density and most of the dynamically produced helium atoms seem to be trapped in the grain matrix and at the interface between the matrix and Ti_5Si_3 precipitates, without a significant chance for bubble nucleation or growth.

(2). For DHCE specimens irradiated to 31 dpa at 425°C at helium generation rates of ≈0.4–0.73 appm He/dpa, helium bubbles ≈5 nm in diameter were observed in localized regions of the grain matrix as well as on limited portions (≈15%) of grain boundaries. Grain–boundary helium bubbles in these specimens were diffuse, in contrast to the compact coalescences of helium bubbles observed from tritium–trick experiments; discontinous (near ≈15% of grain boundaries), in contrast to continuous (on ≈100% grain boundaries) coalescence observed in tritium–trick experiments; and more or less evenly distributed in the grain matrix and near grain boundaries, in contrast to virtual concentration of all helium bubbles on grain boundaries in tritium–trick experiments. These observations indicate that most of the helium atoms that were produced dynamically at 425°C were trapped in the grain matrix, preventing formation of continuous coalescence of compact bubbles on grain boundaries. As in non–DHCE, the irradiation–induced precipitation of ultrafine Ti_5Si_3 was not observed after irradiation at 425°C.

(3) Intergranular fracture morphology was not observed in any of the specimens irradiated in DHCEs and subsequently fractured during uniaxial tensile tests at 23 to 600°C and multiple bending tests at –196 to 50°C. This observation, consistent with the characteristic helium bubble distribution, is in distinct contrast to the propensity to

intergranular fracture commonly observed in tritium–trick experiments.

(4) The actual measured helium and tritium content of V–4Cr–4Ti was significantly lower than that calculated with an assumed equilibrium ratio (≈0.01 by weight) of tritium in the alloy to that in the liquid lithium. This indicates that the tritium equilibrium ratio is significantly lower than previously assumed, in particular, for irradiations at <500°C. It also indicates that the tritium level in lithium–cooled V–4Cr–4Ti first wall/blanket structures, and hence the effect of tritium on the fracture toughness, will be significantly lower than previously thought.

ACKNOWLEDGMENTS

The successful completion of the complex and difficult Dynamic Helium Charging Experiment was possible through many years of contributions from F. W. Wiffen, H. Matsui, K. Abe, C. E. Johnson, R. G. Clemmer, J. P. Kopasz, L. R. Greenwood, M. L. Hamilton, K. L. Pearce, R. Ermi, A. Ermi, H.–C. Tsai, and R. V. Strain. The authors are grateful to L. R. Greenwood and B. M. Oliver for calculation and measurement, respectively, of helium and tritium contents.

REFERENCES

[1] B. A. Loomis, L. Nowicki, and D. L. Smith, "Effect of Neutron Irradiation on Tensile Properties of V–Cr–Ti Alloys," in Fusion Reactor Materials, Semiannual. Prog. Report, DOE/ER-0313/15, Oak Ridge National Laboratory, Oak Ridge, TN (1994), pp. 219–222.

[2] B. A. Loomis, H. M. Chung, L. Nowicki, and D. L. Smith, "Effects of Neutron Irradiation and Hydrogen on Ductile-Brittle Transition Temperatures of V–Cr–Ti Alloys," ibid., pp. 253–257.

[3] H. M. Chung, B. A. Loomis, L. Nowicki, J. Gazda, and D. L. Smith, "Irradiation-Induced Density Change and Microstructural Evolution of Vanadium-Base Alloys," ibid., pp. 223–231.

[4] H. Matsui, M. Tanno, J. Gazda, and H. M. Chung, "Microstructural Stability of V-4Cr-4Ti During Neutron Irradiation," ibid., pp. 240–246.

[5] H. M. Chung, J. Gazda, L. Nowicki, J. E. Sanecki, and D. L. Smith, "Effects of Fabrication Variables on Impact Properties and Microstructure of V–Cr–Ti Alloys," ibid., pp. 207–218.

[6] H. M. Chung, B. A. Loomis, and D. L. Smith, "Thermal Creep Behavior of V–5Cr–5Ti and V–10Cr–5Ti Alloys," in Fusion Reactor Materials, Semiannual. Prog. Report, DOE/ER-0313/14, Oak Ridge National Laboratory, Oak Ridge, TN (1993), pp. 309-317.

[7] D. N. Braski and D. W. Ramey, in Effects of Radiation on Material Properties, ASTM-STP 870, F. A. Garner and J. S. Perrin, eds., American Society for Testing and Materials, Philadelphia, 1985, pp. 1211–1224.

[8] D. N. Braski, in Influence of Radiation on Material Properties, ASTM-STP 956, F. A. Garner, C. H. Henager, and N. Igata, Eds., American Society for Testing and Materials, Philadelphia, 1987, pp. 271-290.

[9] D. N. Braski, J. Nucl. Mater. 141-143 (1986) 1125.

[10] D. N. Braski, in Reduced Activation Materials for Fusion Reactors, ASTM-STP 1047,

Philadelphia (1988) pp. 161-178.

[11] H. Matsui, M. Tanaka, M. Yamamoto, and M. Tada, J. Nucl. Mater. 191-194 (1992) 919.

[12] M. Satou, K. Abe, and H. Matsui, J. Nucl. Mater. 191-194 (1992) 938.

[13] M. Tanaka and H. Matsui, Mater. Trans., JIM, 34 (1993) 1083.

[14] W. van Witzenburg, A. Mastenbroek, and J. D. Ellen, J. Nucl. Mater. 103-104 (1981) 1187.

[15] M. P. Tanaka, E. E. Bloom, and J. A. Horak, J. Nucl. Mater. 114 (1981) 895.

[16] M. L. Grossbeck and J. A. Horak, in Influence of Radiation on Material Properties, ASTM-STP 956, Philadelphia (1986) 291.

[17] J. M. Vitek, D. N. Braski, and J. A. Horak, J. Nucl. Mater. 141-143 (1986) 982.

[18] W. van Witzenburg and E. de Vries, in Effects of Radiation on Materials, ASTM-STP 1125, Philadelphia (1990).

[19] L. L. Horton and K. Farrell, J. Nucl. Mater. 122-123 (1984) 687.

[20] H. Kawanishi and S. Ishino, in Reduced Activation Materials for Fusion Reactors, ASTM-STP 1047, Philadelphia (1988) pp. 179-189.

[21] H. Kawanishi, Y. Arai, and S. Ishino, J. Nucl. Mater. 191-194 (1992) 933.

[22] D. L. Smith, H. Matsui, L. R. Greenwood, and B. A. Loomis, J. Nucl. Mater. 155-157 (1988) 1359.

[23] D. L. Smith, B. A. Loomis, H. Matsui, M. L. Hamilton, K. L. Pearce, J. P. Kopasz, C. E. Johnson, R. G. Clemmer, and L. R. Greenwood, in Fusion Reactor Materials, Semiannual. Prog. Report. DOE/ER-0313/10, Oak Ridge National Laboratory, Oak Ridge, TN (1991), p. 159.

[24] H. Tsai, H. M. Chung, B. A. Loomis, and D. L. Smith, "Status of Dynamic Helium Charging Experiment (DHCE)," in Fusion Reactor Materials, Semiannual. Prog. Report. DOE/ER-0313/15, Oak Ridge National Laboratory, Oak Ridge, TN (1994), p. 247.

[25] H. M. Chung, B. A. Loomis, L. Nowicki, and D. L. Smith, "Effect of Dynamically Charged Helium on Tensile Properties of V–4Cr–4Ti," in this report.

[26] M. Satou and H. M. Chung, in Fusion Reactor Materials, Semiannual Prog. Rep. DOE/ER-0313/13, Oak Ridge National Laboratory, Oak Ridge, TN (1993), p. 227.

[27] H. M. Chung, B. A. Loomis, H. Tsai, L. Nowicki, J. Gazda, and D. L. Smith, "Swelling and Structure of Vanadium Alloys Irradiated in the Dynamic Helium Charging Experiment," in Fusion Reactor Materials, Semiannual. Prog. Report, DOE/ER-0313/16, Oak Ridge National Laboratory, Oak Ridge, TN (1994), p. 204.

[28] H. M. Chung, B. A. Loomis, and D. L. Smith, in Effects of Radiation on Materials, ASTM-STP 1175, A. S. Kumar, D. S. Gelles, R. K. Nanstad, and T. A. Little, Eds., American Society for Testing and Materials, Philadelphia, 1993, pp. 1185–1200.

[29] T. Buitenhuis, A. Fedorov, and A. van Veen, "Thermal Desorption Investigation of V–5Ti Alloy," IRI–131–94–005, Delft University of Technology Report, The Netherlands, 1994.

Subtask 12G2: EFFECTS OF DYNAMICALLY CHARGED HELIUM ON TENSILE PROPERTIES OF V–4Cr–4Ti, H. M. Chung, B. A. Loomis, L. Nowicki, and D. L. Smith (Argonne National Laboratory)

OBJECTIVE

The objective of this work is to determine the effect of displacement damage and dynamically charged helium on tensile properties of V–4Cr–4Ti alloy irradiated to 18–31 dpa at 425–600°C in the Dynamic Helium Charging Experiment (DHCE).

SUMMARY

One property of vanadium-base alloys that is not well understood in terms of their potential use as fusion reactor structural materials is the effect of simultaneous generation of helium and neutron damage under conditions relevant to fusion reactor operation. In the present Dynamic Helium Charging Experiment (DHCE), helium was produced uniformly in the specimen at linear rates of ≈0.4 to 4.2 appm helium/dpa by the decay of tritium during irradiation to 18–31 dpa at 425–600°C in the Li-filled DHCE capsules in the Fast Flux Test Facility. This report presents results of postirradiation tests of tensile properties of V-4Cr-4Ti, an alloy identified as the most promising vanadium–base alloy for fusion reactors on the basis of its superior baseline and irradiation properties. Effects of helium on tensile strength and ductility were insignificant after irradiation and testing at >420°C. Contrary to initial expectation, room–temperature ductilities of DHCE specimens were higher than those of non–DHCE specimens (in which there was negligible helium generation), whereas strengths were lower, indicating that different types of hardening centers are produced during DHCE and non–DHCE irradiation. In strong contrast to tritium–trick experiments in which dense coalescence of helium bubbles is produced on grain boundaries in the absence of displacement damage, no intergranular fracture was observed in any tensile specimens irradiated in the DHCE.

INTRODUCTION

Vanadium-base alloys have significant advantages over other candidate alloys (such as austenitic and ferritic steels) for use as structural materials in fusion devices, e.g., the International Thermonuclear Experimental Reactor (ITER) and magnetic fusion reactors. These advantages include intrinsically lower levels of long-term activation, irradiation afterheat, neutron-induced helium- and hydrogen-transmutation rates, biological hazard potential, and thermal stress factor. Recent attention has focused on V-4Cr-4Ti for fusion reactor structural components because of its excellent combination of mechanical and physical properties before and after irradiation.[1–6] One property of vanadium–base alloys that is not well understood is the effect of helium; no tensile data have been reported on effects of simultaneous generation of helium and neutron displacement damage under fusion–relevant conditions (i.e., ≈5 appm He/dpa ratio), although helium effects on other vanadium alloys have been investigated by less–than–prototypical simulation techniques such as tritium-trick,[7–11] cyclotron-injection,[12–16] and boron-doping.[16–19] In the DHCE,[20–22] the fusion–relevant helium–to–dpa damage ratio is closely simulated by utilizing slow transmutation of controlled amounts of ^{6}Li and a tritium–doped mother alloy immersed in $^{6}Li + ^{7}Li$. This report presents results of postirradiation examination of mechanical properties of V-4Cr-4Ti alloy, which has been identified as the most promising candidate alloy on the basis of its superior baseline and irradiation properties.

MATERIALS AND PROCEDURES

The elemental composition of the 30–kg heat of V–4Cr–4Ti alloy, determined prior to irradiation, is given in Table 1. An alloy ingot, melted from low–chlorine titanium and high–purity vanadium, was extruded at 1150°C and annealed at 1050°C *several times* after 8–10 passes of warm (400°C) rolling between the annealings. Final forms of the product were annealed plates and sheets 3.8–, 1.0–, and 0.3–mm in thickness. SS–3 tensile specimens with a gauge length of 7.62 mm and a gauge width of 1.52 mm were machined from 1.0–mm–thick annealed (1050°C) sheets. The specimens were ≈95% recrystallized and exhibited an average grain size of ≈14 mm. The only secondary phase in the as–annealed specimen was Ti(O,N,C), which is normally observed in titanium–containing vanadium alloys with O+N+C > 400 wppm. Tensile properties were measured at 23°C and at irradiation temperatures in flowing argon at a strain rate of 0.0011 s^{-1}. The thickness and gauge width of each specimen were measured individually after irradiation and before each tensile test.

Table 1. Chemical composition of V–4Cr–4Ti

	Nominal Composition	Impurity Composition (wppm)							
ANL ID	(wt.%)	O	N	C	Si	S	P	Nb	Mo
BL-47	V–4.1Cr–4.3Ti	350	220	200	870	20	<40	<100	<100

The alloy specimens were irradiated in the Fast Flux Test Facility (FFTF), a fast reactor located near Richland, Washington, at 420, 520, and 600°C to neutron fluences (E > 0.1 MeV) ranging from 3.7 x 10^{22} n/cm^2 (≈18 displacements per atom, or dpa) to 6.4 x 10^{23} n/cm^2 (≈31 dpa). Helium in the alloy specimens was produced by utilizing transmutation of controlled amounts of ^{6}Li and predetermined amounts of tritium–doped vanadium mother alloy immersed in ^{6}Li + ^{7}Li.[20–22] Table 2 summarizes the irradiation temperature, weight of the mother alloy, fraction of ^{6}Li, and tritium and lithium inventory charged in each of the seven DHCE capsules before irradiation.

Table 3 summarizes actual postirradiation parameters determined from tensile and TEM disk specimens of the V–4Cr–4Ti alloy, i.e., fast neutron fluence, dose, and helium and tritium contents measured ≈20–25 days after the postirradiation tests.

Table 2. Summary of capsule–loading parameters of DHCE.

Capsule ID No.	Irradiation Temp. (°C)	Total Weight (g)			Fraction of ^{6}Li (%)	Initial Tritium Charged[a]	
		Vanadium[a]	Specimen[b]	Lithium		(Ci)	(mmol)
4D1	425	1.5468	5.86	0.765	5.0	99	1.70
4D2	425	1.5536	5.38	0.765	4.5	70	1.20
5E2	425	1.5657	5.38	0.670	1.0	26	0.45
5D1	500	1.5727	5.77	0.938	6.5	73.5	1.26
5E1	500	1.5651	5.82	0.952	1.0	57	0.98
5C1	600	1.5656	5.82	0.808	8.0	16.4	0.28
5C2	600	1.5466	5.95	0.955	8.0	18	0.31

[a] Letter from C. E. Johnson to K. Pearce, April 23, 1991; 1 mmol = 58.3 Ci.

[b] Excluding tritium–charged mother alloy.

Helium and tritium contents were determined by mass spectrometry at Rockwell International Inc., Canoga Park, California. Two TEM disk or broken tensile specimens were selected from each capsule after multiple–bending (at –196°C to 50°C) or tensile tests (at room temperature) and analyzed to determine helium and tritium contents. For each specimen, four separate analyses of ^{3}He and ^{4}He were conducted. The tritium contents were determined on the basis of analysis of ^{3}He decay measured on the same specimens ≈50 days apart.

RESULTS

Yield strength, ultimate tensile strength, uniform elongation, and total elongation measured on tensile specimens irradiated at 425°C–600°C to 18–34 dpa in the DHCE are summarized in Fig. 1. For comparison, similar properties measured on irradiated non–DHCE specimens are also plotted as a function of irradiation temperature.

Table 3. Summary of irradiation parameters of Dynamic Helium Charging Experiment and helium and tritium contents measured in V–4Cr–4Ti specimens

Capsule ID No.	Irradiation Temp. (°C)	Fluence (E >0.1 MeV) (10^{22} n cm^{-2})	Total Damage (dpa)	Calculated Helium (appm) to dpa Ratio[a] at EOI[b] (Assumed k_a or k_w)[c] k_a=0.073 (k_w=0.01)	Measured Helium Content[d] (appm)	Actual Helium to dpa Ratio (appm/dpa)	Measured Tritium Content[e] (appm)
4D1	425	6.4	31	3.8	11.2–13.3	0.39	27
4D2	425	6.4	31	2.8	22.4–22.7	0.73	39
5E2	425	3.7	18	2.1	3.3–3.7	0.11	2
5D1	500	3.7	18	4.4	14.8–15.0	0.83	4.5
5E1	500	3.7	18	3.1	6.4–6.5	0.36	1.7
5C1	600	3.7	18	1.1	8.4–11.0	0.54	20
5C2	600	3.7	18	1.1	74.9–75.3	4.17	63

[a] L. R. Greenwood "Revised Calculations for the DHCE," April 30, 1993.
[b] Beginning of irradiation (BOI) May 27, 1991; end of irradiation (EOI) March 19, 1992; 203.3 effective full power days (EFPD), hot standby at ≈220°C until November 1992.
[c] Equilibrium ratio (k_a by atom, k_w by weight) of tritium in V alloy to that in the surrounding liquid lithium.
[d] Measured June 1994.
[e] Measured August 1994.

After irradiation to ≈30 dpa in either a DHCE or a non–DHCE, ductility of the alloy remained significantly high, i.e., >8% uniform elongation and >10% total elongation. Tensile properties measured at 425°C, 500°C, and 600°C (the same as the irradiation temperatures) were essentially the same as those measured on non–DHCE specimens, showing that the effect of helium was insignificant. Room–temperature ductilities of the DHCE specimens (irradiated at 425°C, 500°C, and 600°C) were higher than those of the similar non–DHCE specimens, whereas strengths were lower. This was an unexpected finding. Although the mechanisms leading to the higher ductility and lower strength of the DHCE specimens are not understood at this time, the consistent observations indicate that different types of hardening centers are produced during DHCE and non–DHCE.

The dependence of uniform and total elongation on irradiation and test temperature, shown in Figs. 1C and ID, respectively, is in sharp contrast to similar results obtained on specimens in which helium atoms were produced by the tritium–trick method. In the latter

type of experiments, total elongation measured at room temperature and at 700–800°C was significantly lower than that measured at 500–600°C because of the strong susceptibility to intergranular cracking associated with extensive formation of grain-boundary helium bubbles.[10] However, no intergranular fracture surface morphology was observed in the tensile specimens irradiated in the DHCE and tested at 25–600°C (including the specimen irradiated in Capsule 5C2 at 600°C at a helium generation rate of 4.2 appm He/dpa), and no ductility degradation similar to that in tritium–trick experiments was observed. This is shown in Fig. 2, where the ratio of total strain in specimens with and without helium is plotted as a function of irradiation and test temperature for tritium–trick and dynamic helium charging experiments.

DISCUSSION

An important finding from the DHCE was that the actual (measured) contents of helium and tritium in the V–4Cr–4Ti specimens were significantly lower than those calculated previously (see Table 3) on the basis of assumed equilibrium ratio (k_W = 0.01) of tritium in the alloy to that in the liquid lithium (Table 2). Except for specimens iradiated in Capsule 5C1 and 5C2 at 600°C, actual helium/dpa ratios (i.e., 0.36–0.83) were several times lower than those calculated on the basis of an equilibrium ratio of k_W = 0.01 (i.e.,

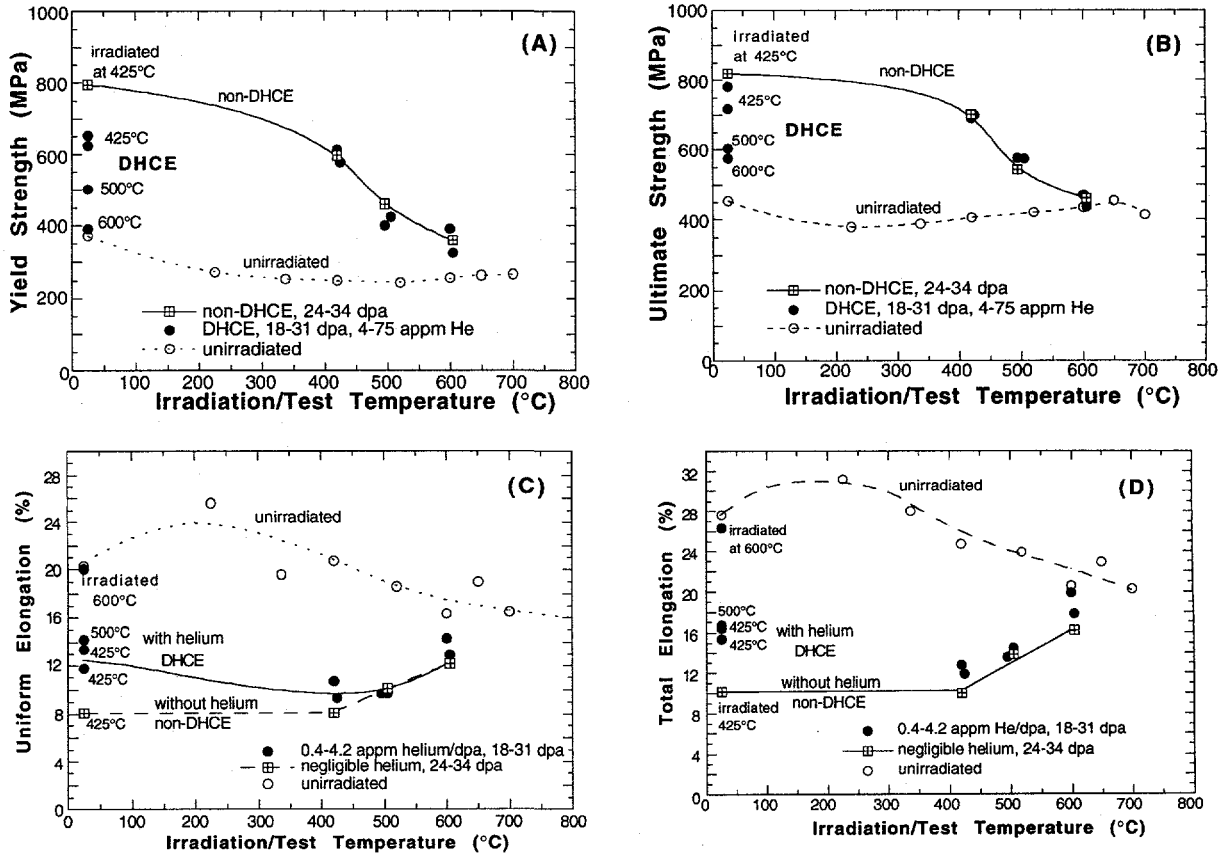

Fig. 1. Yield strength (A), ultimate tensile strength (B), uniform elongation (C), and total elongation (D) of V–4Cr–4Ti after irradiation at 420–600°C to 18–34 dpa in DHCE and non–DHCE conventional irradiation (negligible helium generation).

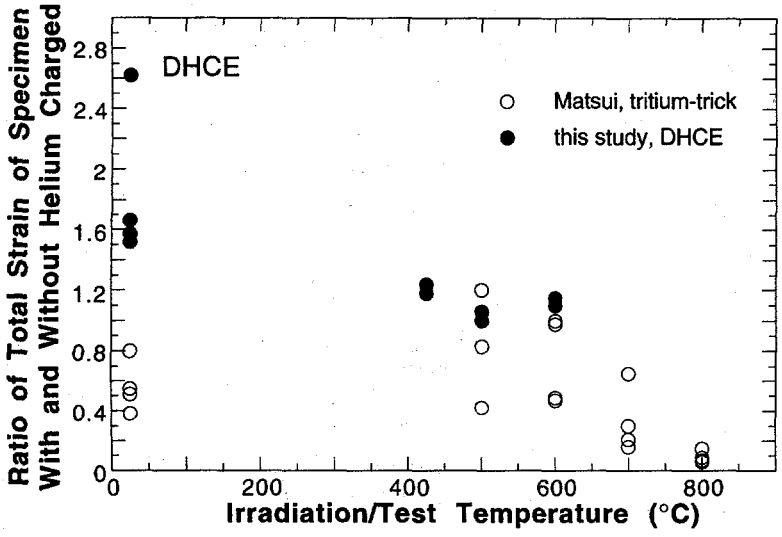

Fig. 2.
Ratio of total strain in specimens with and without helium as a function of irradiation and test temperature. Results obtained from tritium–trick experiment and DHCE are shown for comparison.

2.1–4.4). This indicates that the level of hydrogen and tritium in the Li–cooled V–4Cr–4Ti first wall/blanket structure, and hence the effect of hydrogen and tritium on fracture toughness, will be significantly lower than previously assumed.

As described in a separate report,[23] helium microvoids were negligible in all specimens irradiated in DHCE except for those irradiated at 425°C and retrieved from Capsule 4D1 and 4D2; only a few helium bubbles were observed at the interface between the grain matrix and some Ti(O,N,C) precipitates that are normally present in V–Ti and V–Cr–Ti alloys. Even in specimens irradiated at 600°C at the highest helium generation rate of ≈4.2 appm helium/dpa (Capsule 5C2), no microvoids could be detected in either grain matrix or grain boundaries. For specimens irradiated to 31 dpa at 425°C (retrieved from Capsules 4D1, ≈0.4 appm helium/dpa and 4D2, ≈0.73 appm helium/dpa), moderate number densities of diffuse helium bubbles were observed in localized grain matrix and near a limited fraction (≈15–20%) of grain boundaries.[23] The number density of helium bubbles, observed near the limited region of grain boundaries, was significantly lower than those in other alloys tested in the tritium–trick experiments, where extensive coalescence of helium bubbles occurred on all grain boundaries.[7–11] The absence of intergranular fracture morphology in any of the tensile specimens irradiated in the present DHCE seems to be consistent with the microstructural characteristics described above. However, a more comprehensive data base is needed for irradiation at <400°C to determine the effects of higher helium–dpa ratio (i.e., the fusion–relevant ratio of 4–5 appm helium/dpa) at the lower temperatures.

The uniform and total elongations determined from the room–temperature tensile tests on DHCE specimens were significantly greater than similar room–temperature elongations measured on specimens irradiated in either non–DHCE (Fig. 1) or tritium–trick experiments (Fig. 2). This is also consistent with the absence of continuous aggregation of helium bubbles on grain boundaries in the specimens irradiated in DHCE. In addition, the observation indicates that different types of hardening centers are produced in the alloy during DHCE and non–DHCE irradiation at 425–600°C.

Although the nature of the hardening centers produced during DHCE is not understood at this time, helium atoms are believed to be associated with them. In a series

of studies on thermal desorption behavior of helium from unalloyed vanadium and V–5Ti irradiated with helium ions of various energy levels, van Veen et al.[24] and Buitenhuis et al.[25] concluded that helium–oxygen–vacancy and helium–nitrogen–vacancy (and probably helium–vacancy–carbon as well) complexes formed in the irradiated material. These investigators further deduced that the complexes are stable at low temperatures (<230°C) but dissociate into helium atoms and oxygen–vacancy and nitrogen–vacancy complexes at 270–310°C, leading to a prominent helium desorption peak at ≈290°C that was observed consistently in their experiments. Desorption peaks at ≈770°C and ≈1250°C, observed only after irradiation with helium ion to higher doses, were attributed to clusters of helium atoms and helium bubbles, respectively. The clusters and bubbles of helium are believed to be unstable only at the high temperatures. During the degassing treatment in the present study in which DHCE specimens were heated to 400°C at a rate of ≈0.2°C/s, desorption peaks were observed consistently at ≈290°C,[23] although helium desorption was not positively identified by mass spectroscopy, as done by van Veen et al. and Buitenhuis et al.

Based on these observations, it is likely that stable helium–vacancy–impurity complexes are also present in the specimens irradiated in DHCE during tensile tests at room temperature. In contrast, in specimens irradiated in non–DHCE under similar conditions, vacancies and impurities (such as oxygen, nitrogen, and carbon) are not expected to form complexes in the absence of appreciable helium atoms. Rather, the impurity atoms in solution and vacancies or vacancy clusters will be scattered more or less randomly in interstitial and vacancy sites, respectively. Dislocation motion would then be more difficult, and hence ductility would be lower in the non–DHCE than in the DHCE specimens; this is in accordance with the results shown in Fig. 1.

CONCLUSIONS

1. Tensile ductility of the V–4Cr–4Ti alloy, irradiated to 18–31 dpa at 425°C to 600°C in the Dynamic Helium Charging Experiment (DHCE) at helium generation rates of 0.4–4.2 appm helium/dpa, remained significantly high at 25–600°C, i.e., >8% uniform elongation and >10% total elongation. Tensile properties measured at >400°C were essentially the same as those measured on non–DHCE specimens (negligible helium), showing that effects of helium were insignificant. Room–temperature ductilities of the DHCE specimens (irradiated at 425, 500, and 600°C) were higher than those of the similar non–DHCE specimens, whereas strengths were lower. These observations indicate that different types of hardening centers are present at room temperature in the DHCE specimens (helium–vacancy–impurities complex, impurities being oxygen, nitrogen, and carbon) and in non–DHCE specimens (defects and defect clusters, impurities in interstitial sites).

2. The dependence of uniform and total elongation on irradiation and test temperature and fracture morphology were in sharp contrast to similar results obtained on specimens in which helium atoms were produced by the tritium–trick method. Neither partial nor predominantly intergranular fracture was observed in tensile specimens irradiated in the DHCE and tested at 23 to 600°C.

ACKNOWLEDGMENTS

Successful completion of the Dynamic Helium Charging Experiment, a complex and difficult irradiation test, was possible only through many years of effort and contributions from many investigators in the United States and Japan: F. W. Wiffen, H. Matsui, K. Abe, C.

E. Johnson, R. G. Clemmer, J. P. Kopasz, L. R. Greenwood, M. L. Hamilton, K. L. Pearce, R. Ermi, A. Ermi, H.–C. Tsai, R. V. Strain, and D. Donahue. The authors are grateful in particular to L. R. Greenwood and B. M. Oliver for their calculation and measurement, respectively, of helium and tritium contents.

REFERENCES

[1] B. A. Loomis, L. Nowicki, and D. L. Smith, "Effect of Neutron Irradiation on Tensile Properties of V–Cr–Ti Alloys," in Fusion Reactor Materials, Semiannual Prog. Report, DOE/ER-0313/15, Oak Ridge National Laboratory, Oak Ridge, TN (1994), pp. 219–222.

[2] B. A. Loomis, H. M. Chung, L. Nowicki, and D. L. Smith, "Effects of Neutron Irradiation and Hydrogen on Ductile-Brittle Transition Temperatures of V–Cr–Ti Alloys," ibid., pp. 253–257.

[3] H. M. Chung, B. A. Loomis, L. Nowicki, J. Gazda, and D. L. Smith, "Irradiation-Induced Density Change and Microstructural Evolution of Vanadium-Base Alloys," ibid., pp. 223–231.

[4] H. Matsui, M. Tanno, J. Gazda, and H. M. Chung, "Microstructural Stability of V-4Cr-4Ti During Neutron Irradiation," ibid., pp. 240–246.

[5] H. M. Chung, J. Gazda, L. Nowicki, J. E. Sanecki, and D. L. Smith, "Effects of Fabrication Variables on Impact Properties and Microstructure of V–Cr–Ti Alloys," ibid., pp. 207–218.

[6] H. M. Chung, B. A. Loomis, and D. L. Smith, "Thermal Creep Behavior of V–5Cr–5Ti and V–10Cr–5Ti Alloys," in Fusion Reactor Materials, Semiannual Prog. Report, DOE/ER-0313/14, Oak Ridge National Laboratory, Oak Ridge, TN (1993), pp. 309-317.

[7] D. N. Braski, in Influence of Radiation on Material Properties, ASTM-STP 956 (1986), pp. 271-290.

[8] D. N. Braski, J. Nucl. Mater. 141-143 (1986) 1125.

[9] D. N. Braski, in Reduced Activation Materials for Fusion Reactors, ASTM-STP 1047 (1988), pp. 161-178.

[10] H. Matsui, M. Tanaka, M. Yamamoto, and M. Tada, J. Nucl. Mater. 191-194 (1992) 919.

[11] M. Satou, K. Abe, and H. Matsui, J. Nucl. Mater. 191-194 (1992) 938.

[12] W. van Witzenburg, A. Mastenbroek, and J. D. Ellen, J. Nucl. Mater. 103-104 (1981) 1187.

[13] M. P. Tanaka, E. E. Bloom, and J. A. Horak, J. Nucl. Mater. 114 (1981) 895.

[14] M. L. Grossbeck and J. A. Horak, in Influence of Radiation on Material Properties, ASTM-STP 956 (1986), p. 291.

[15] J. M. Vitek, D. N. Braski, and J. A. Horak, J. Nucl. Mater. 141-143 (1986) 982.

[16] W. van Witzenburg and E. de Vries, in Effects of Radiation on Materials, ASTM-STP 1125 (1990).

[17] L. L. Horton and K. Farrell, J. Nucl. Mater. 122-123 (1984) 687.

[18] H. Kawanishi and S. Ishino, in Reduced Activation Materials for Fusion Reactors, ASTM-STP 1047 (1988), pp. 179-189.

[19] H. Kawanishi, Y. Arai, and S. Ishino, J. Nucl. Mater. 191-194 (1992) 933.

[20] D. L. Smith, H. Matsui, L. R. Greenwood, and B. A. Loomis, J. Nucl. Mater. 155-157 (1988) 1359.

[21] D. L. Smith, B. A. Loomis, H. Matsui, M. L. Hamilton, K. L. Pearce, J. P. Kopasz, C. E. Johnson, R. G. Clemmer, and L. R. Greenwood, in Fusion Reactor Materials, Semiannual. Prog. Rep. DOE/ER-0313/10, Oak Ridge National Laboratory, Oak Ridge, TN (1991), p. 159.

[22] H. Tsai, H. M. Chung, B. A. Loomis, and D. L. Smith, "Status of Dynamic Helium Charging Experiment (DHCE)," in Fusion Reactor Materials, Semiannual Prog. Report, DOE/ER-0313/15, Oak Ridge National Laboratory, Oak Ridge, TN (1994), pp. 247–252.

[23] H. M. Chung, B. A. Loomis, L. Nowicki, J. Gazda, and D. L. Smith, "Effects of Dynamically Charged Helium on Swelling and Microstructure of Vanadium–Base Alloys," in this report.

[24] A. van Veen, H. Eleveld, and M. Clement, "Helium Impurity Interactions in Niobium and Vanadium," in Proc. 6th Intl. Conf. on Fusion Reactor Materials, September 27–October 1, 1993, Stresa, Italy, in press.

[25] T. Buitenhuis, A. Fedorov, and A. van Veen, "Thermal Desorption Investigation of V–5Ti Alloy," IRI–131–94–005, Delft University of Technology, The Netherlands, 1994.

Subtask 12G3: FRACTURE PROPERTIES OF V–4Cr–4Ti IRRADIATED IN THE DYNAMIC HELIUM CHARGING EXPERIMENT, H. M. Chung, L. J. Nowicki, D. E. Busch, and D. L. Smith (Argonne National Laboratory)

OBJECTIVE

The objective of this work is to determine the effect of simultaneous displacement damage and dynamically charged helium on the ductile–brittle transition behavior of V–4Cr–4Ti specimens irradiated to 18–31 dpa at 425–600°C in the Dynamic Helium Charging Experiment (DHCE).

SUMMARY

One property of vanadium-base alloys that is not well understood in terms of their potential use as fusion reactor structural materials is the effect of simultaneous generation of helium and neutron damage under conditions relevant to fusion reactor operation. In the present DHCE, helium was produced uniformly in the specimen at linear rates ranging from ≈0.4 to 4.2 appm helium/dpa by the decay of tritium during irradiation to 18–31 dpa at 425–600°C in Li-filled DHCE capsules in the Fast Flux Test Facility. Ductile–brittle transition behavior of V–4Cr–4Ti, recently identified as the most promising vanadium–base alloy for fusion reactor use, was determined from multiple–bending tests (at –196°C to 50°C) and quantitative SEM fractography on TEM disks (0.3–mm thick) and broken tensile specimens (1.0–mm thick). No brittle behavior was observed at temperatures >–150°C, and predominantly brittle–cleavage fracture morphologies were observed only at –196°C in some specimens irradiated to 31 dpa at 425°C during DHCE. Ductile–brittle transition temperatures (DBTTs) were –200°C to –175°C for both types of specimens. In strong contrast to tritium–trick experiments in which dense coalescence of helium bubbles is produced on grain boundaries in the absence of displacement damage, no intergranular fracture was observed in the bend–tested specimens irradiated in the DHCE.

INTRODUCTION

Vanadium-base alloys have significant advantages over other candidate alloys (such as austenitic and ferritic steels) for use as structural materials in fusion devices, e.g., the International Thermonuclear Experimental Reactor (ITER) and DEMO reactor. These advantages include intrinsically low long-term activation, low decay heat, low neutron-induced helium- and hydrogen-transmutation rates, low biological hazard, and high thermal stress factor. Recently, V-4Cr-4Ti has been identified as the most promising vanadium–base alloy for fusion reactor structural components because of its excellent combination of mechanical and physical properties before and after irradiation.[1–6] One property of the alloy that is not well understood is the effect of helium on ductile–brittle transition behavior; no data on impact properties or ductile–brittle transition behavior have been reported on effects of simultaneous generation of helium and neutron displacement damage under fusion–relevant conditions (i.e., ≈5 appm He/dpa ratio), although helium effects on other vanadium alloys have been investigated by less–than–prototypical simulation techniques such as tritium-trick,[7–11] cyclotron-injection,[12–16] and boron-doping.[16–19] In the DHCE,[20–22] the fusion–relevant helium–to–dpa damage ratio is closely simulated by utilizing slow transmutation of controlled amounts of ^{6}Li and a tritium–doped mother alloy immersed in $^{6}Li + ^{7}Li$. Effects of the fusion–relevant generation of helium on tensile properties have been investigated on specimens irradiated in the DHCE to 18–31 dpa at 425°C–600°C and are reported elsewhere.[23]

However, no Charpy–impact specimens were included in the DHCE capsules because of severe limitations on irradiation space. Therefore, the important information on ductile–brittle transition behavior of the alloy could be extracted only from miniature specimens such as TEM disks and broken tensile specimens. This paper presents results of multiple–bending tests of V-4Cr-4Ti alloy and quantitative SEM fractography of the fracture surface morphologies conducted subsequently to determine ductile–brittle transition behavior.

MATERIALS AND PROCEDURES

The elemental composition of the 30–kg heat of V–4Cr–4Ti alloy, determined prior to irradiation, is given in Table 1. Information on fabrication, phase structure, grain size, and other microstructural characteristics of the alloy has been given elsewhere.[4,5,23] The tensile and TEM disk specimens were irradiated in the Fast Flux Test Facility (FFTF) at 420, 520, and 600°C to neutron fluences (E > 0.1 MeV) ranging from 3.7 x 10^{22} n/cm^2 (≈18 displacements per atom, or dpa) to 6.4 x 10^{23} n/cm^2 (≈31 dpa). Helium in the specimens was produced by utilizing transmutation of controlled amounts of ^{6}Li and predetermined amounts of tritium–doped vanadium mother alloy immersed in ^{6}Li + ^{7}Li.[20–22]

Table 1. Chemical composition of V–4Cr–4Ti (ANL ID BL–47)

	Nominal	Impurity Composition (wppm)							
ANL ID	Composition (wt.%)	O	N	C	Si	S	P	Nb	Mo
BL-47	V–4.1Cr–4.3Ti	350	220	200	870	20	<40	<100	<100

Table 2 summarizes actual postirradiation parameters determined from tensile and TEM disk specimens of the V–4Cr–4Ti alloy, i.e., fast neutron fluence, dose, and helium and tritium contents measured shortly (≈20–25 days) after the post–irradiation tests. Helium and tritium contents were determined by mass spectrometry at Rockwell International Inc., Canoga Park, California. Two TEM disk or broken tensile specimens were selected from each capsule after multiple–bending (at –196°C to 50°C) or tensile tests (at room–temperature) and analyzed to determine helium and tritium contents. For each disk or broken tensile specimen, four separate analyses of ^{3}He and ^{4}He were conducted. The tritium contents were determined on the basis of analysis of ^{3}He decay measured on the same specimens ≈50 days apart.

Fracture behavior was determined by repeatedly bending a TEM disk (thickness 0.25–0.3 mm) or a piece of the shoulder region of a fractured tensile (thickness 1.0 mm) specimen[23] in low–temperature baths of liquid nitrogen or mixtures of dry ice and acetone. Tensile specimens fractured in gauge section only at room temperature were selected for this bending tests. The tensile specimens, irradiated at 425°C, 500°C, and 600°C and recovered from four capsules, were not heat treated (at 400°C for 1 h), which has been a customary procedure to expel hydrogen or tritium. Temperature of the surrounding liquid was measured with a calibrated thermocouple. Approximately one–third of each side of a bend specimen was firmly held by two grips in the test bath and the middle portion of the disk was bent repeatedly until fracture. Thus, specimen constraint was similar to that in a four–point bend test.

Depending on irradiation conditions and test temperature, 3 to 62 bends were required to produce fracture in the specimens at –196°C to 50°C. At a given test temperature, cold–work accumulated in the specimen as the number of bends increased, thereby hardening the material near the bend progressively. After fracture, morphology of the fracture surface was examined quantitatively by SEM. A few dozen SEM fractographs were taken at ≈300X, and a composite of the whole fracture surface was made. Four types of fracture morphology were observed: cleavage, quasicleavage, ductile-dimple, and fibrous ductile fracture. From the fracture surface composite, the percentage of ductile-fracture morphology was measured for each specimen with a planimeter.

Table 2. Summary of irradiation parameters of DHCE and helium and tritium contents measured in V–4Cr–4Ti specimens

Capsule ID No.	Irradiation Temp. (°C)	Fluence (E >0.1 MeV) (10^{22} n cm^{-2})	Total Damage (dpa)	Calculated Helium (appm) to dpa Ratio[a] at EOI[b] (Assumed k_a or k_W)[c] k_a=0.073 (k_W=0.01)	Measured Helium Content[d] (appm)	Actual Helium to dpa Ratio (appm/dpa)	Measured Tritium Content[e] (appm)
4D1	425	6.4	31	3.8	11.2–13.3	0.39	27
4D2	425	6.4	31	2.8	22.4–22.7	0.73	39
5E2	425	3.7	18	2.1	3.3–3.7	0.11	2
5D1	500	3.7	18	4.4	14.8–15.0	0.83	4.5
5E1	500	3.7	18	3.1	6.4–6.5	0.36	1.7
5C1	600	3.7	18	1.1	8.4–11.0	0.54	20
5C2	600	3.7	18	1.1	74.9–75.3	4.17	63

[a] L. R. Greenwood "Revised Calculations for the DHCE," April 30, 1993.

[b] Beginning of irradiation (BOI) May 27, 1991; end of irradiation (EOI) March 19, 1992; 203.3 effective full power days (EFPD), hot standby at ≈220°C until November 1992.

[c] Equilibrium ratio (k_a by atom, k_W by weight) of tritium in V alloy to that in the surrounding liquid lithium.

[d] Measured June 1994.

[e] Measured August 1994.

RESULTS AND DISCUSSION

As reported previously,[2,5] brittle (impact) fracture of V–4Cr–4Ti (BL–47) did not occur at temperatures >–196°C either in the nonirradiated condition or after irradiation to 24–34 dpa at 425–600°C in non–DHCE (i.e., negligible helium/dpa ratio). Consistent with this behavior, only ductile fracture was observed from the present multiple–bend tests in a similar temperature range on disk and broken tensile specimens of the alloy either unirradiated or irradiated in non–DHCE. This is shown in Figs. 1 and 2, respectively.

The percentage of fracture surface of disk and broken tensile specimens (irradiated at 425–600°C to 18–31 dpa) with ductile–fracture morphology is plotted as a function of test temperature in Fig. 3. The figure shows combined effects of simultaneous displacement damage (18–31 dpa, Table 2), helium generation (0.4–4.2 appm helium/dpa), and tritium (2–63 appm) uptake on ductile–brittle transition behavior. For comparison, similar results obtained for nonirradiated and irradiated non–DHCE specimens (containing negligible amounts of helium) are also shown in Fig. 3. Despite the difference in thickness, ductile–brittle transition behaviors of the disk and broken tensile specimens were similar.

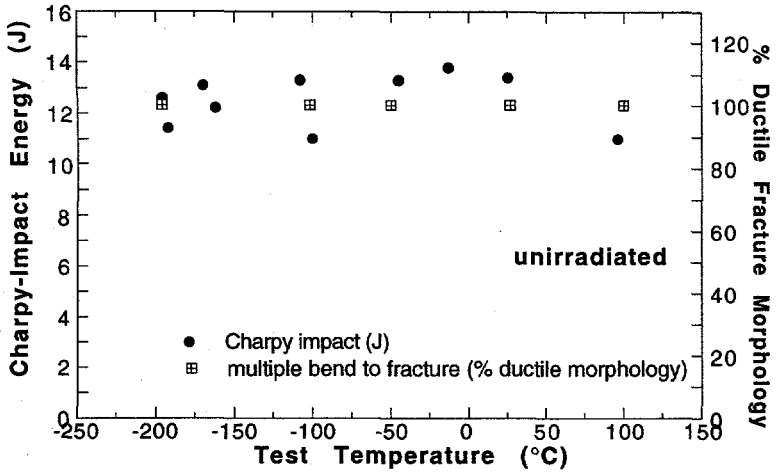

Fig. 1.

Comparison of Charpy–impact energy and percentage of ductile fracture surface morphology of TEM disks (determined after multiple bend until fracture) of unirradiated V–4Cr–4Ti, plotted as a function of test temperature.

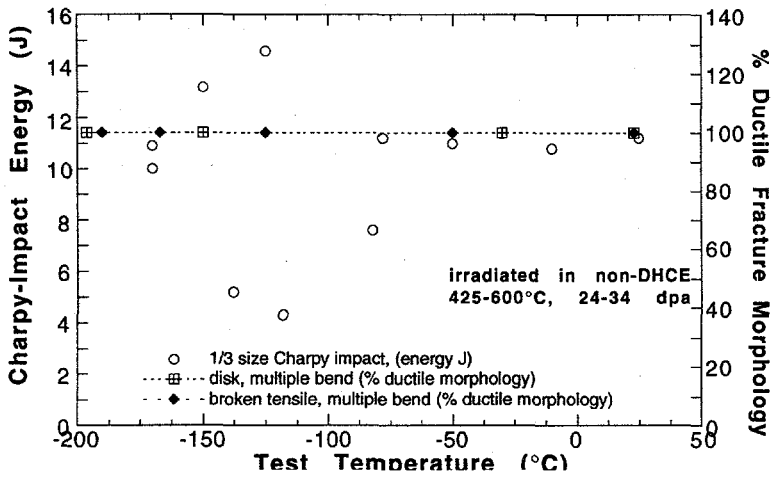

Fig. 2.

Comparison of Charpy–impact energy and percentage of ductile fracture surface morphology of TEM disks and broken pieces of tensile specimens (determined after multiple bend until fracture) of V–4Cr–4Ti irradiated in non–DHCE, plotted as a function of test temperature.

The results in Fig. 3 show that the percentage of brittle cleavage measured from fracture surfaces produced near –190°C was more pronounced in specimens irradiated at 425°C and retrieved from high–tritium capsules (e.g., 4D1 and 4D2) than in specimens irradiated at 500–600°C and retrieved from low–tritium capsules (e.g., 5E1 and 5C2). As in non–DHCE irradiation, no brittle behavior was observed at temperatures >–150°C in DHCE specimens in which the helium generation rate was ≈0.4–4.2 appm helium/dpa (Table 2). Predominantly brittle–cleavage fracture morphologies were observed only at –196°C in some specimens irradiated to 31 dpa at 425°C during DHCE. Figure 3 indicates that DBTTs of specimens irradiated at 425°C and 500–600°C are –175°C and –200°C, respectively. As in the tensile tests at 25–600°C, no intergranular fracture was observed in any specimens fractured at –196 to 50°C by multiple bending.

As described in a separate article,[24] helium microvoids were negligible in all specimens irradiated in DHCE except those irradiated at 425°C and retrieved from Capsules 4D1 and 4D2; only a few helium bubbles were observed at the interface between the grain matrix and some Ti(O,N,C) precipitates that are normally present in V–Ti and V–Cr–Ti alloys. Even in specimens irradiated at 600°C at the highest helium generation rate of ≈4.2 appm helium/dpa (Capsule 5C2), no microvoids could be detected in either grain matrix or grain boundaries. In specimens irradiated to 31 dpa at 425°C

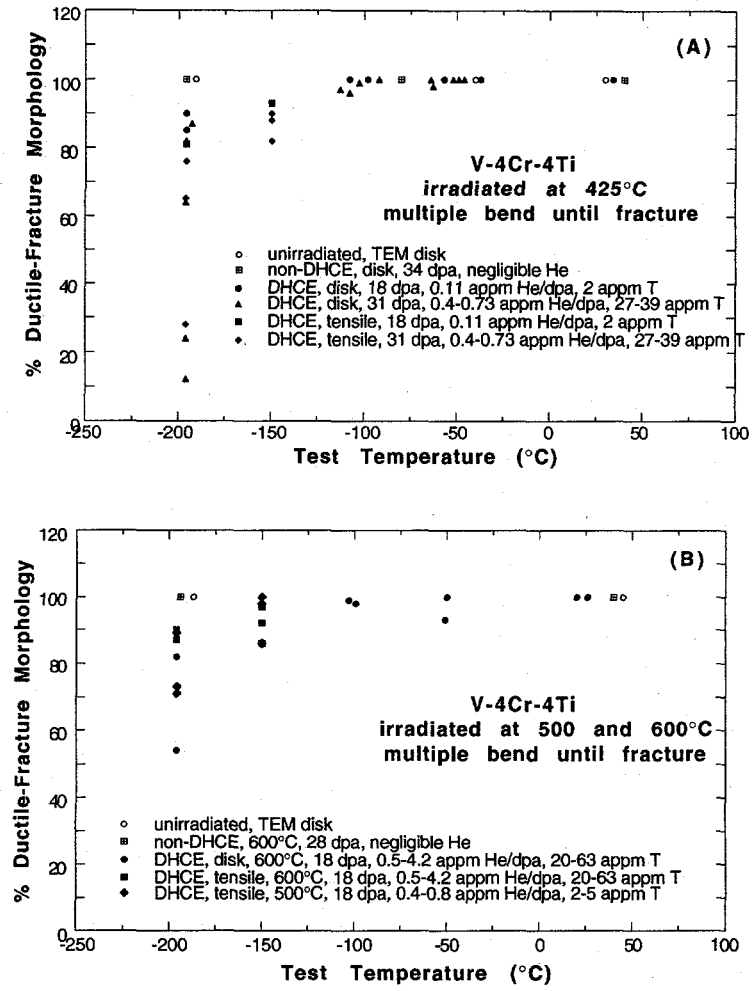

Fig. 3. Percent ductile–fracture morphology vs. test temperature of V–4Cr–4Ti disks and tensile specimens irradiated at (A) 425°C and (B) 600°C and fractured by multiple bending.

(retrieved from Capsules 4D1, ≈0.4 appm helium/dpa and 4D2, ≈0.73 appm helium/dpa), moderate number densities of diffuse helium bubbles were observed in localized grain matrix and near a limited fraction (≈15–20%) of grain boundaries.[24] The number density of helium bubbles, observed near the limited region of grain boundaries, was significantly lower than those in other alloys tested in the tritium–trick experiments, where extensive coalescence of helium bubbles occurred on all grain boundaries.[7–11] The absence of intergranular fracture morphology in any of the present specimens seems consistent with the negligible or insignificant coalescence of helium bubbles on grain boundaries.

CONCLUSIONS

1. Effects of dynamically charged helium, neutron damage, and retained tritium on DBTT of V–4Cr–4Ti alloy were determined after irradiation in the Dynamic Helium Charging Experiment (DHCE). TEM disks and broken pieces of tensile specimens, irradiated at 425–600°C to 18–31 dpa and at helium generation rates of 0.4–4.2 appm helium/dpa, were fractured by repeated bending while submerged in low–temperature baths. Ductile–brittle transition behaviors of both types of specimens were similar. Ductile–

brittle transition temperatures, based on quantitative SEM fractography of ductile and brittle fracture surface morphologies, were –175°C and –200°C, respectively, in specimens irradiated at 425°C and 500°C–600°C.

2. Neither partial nor predominantly intergranular fracture was observed in multiple–bending tests at –196 to 50°C. Predominantly brittle–cleavage fracture morphologies were observed only at –196°C in some specimens irradiated to 31 dpa at 425°C in the DHCE. Cleavage fracture was negligible during tests at >–150°C regardless of irradiation temperature, dose, and helium generation rate.

ACKNOWLEDGMENTS

Many investigators in the United States and Japan have contributed over a period of several years to the successful completion of the Dynamic Helium Charging Experiment: F. W. Wiffen, H. Matsui, K. Abe, C. E. Johnson, R. G. Clemmer, J. P. Kopasz, L. R. Greenwood, M. L. Hamilton, K. L. Pearce, R. Ermi, A. Ermi, H.–C. Tsai, R. V. Strain, and D. Donahue. The authors are grateful in particular to L. R. Greenwood and B. M. Oliver for their calculation and measurement, respectively, of helium and tritium contents.

REFERENCES

[1] B. A. Loomis, L. Nowicki, and D. L. Smith, "Effect of Neutron Irradiation on Tensile Properties of V–Cr–Ti Alloys," in Fusion Reactor Materials, Semiannual. Prog. Report, DOE/ER-0313/15, Oak Ridge National Laboratory, Oak Ridge, TN (1994), pp. 219–222.

[2] B. A. Loomis, H. M. Chung, L. Nowicki, and D. L. Smith, "Effects of Neutron Irradiation and Hydrogen on Ductile-Brittle Transition Temperatures of V–Cr–Ti Alloys," ibid., pp. 253–257.

[3] H. M. Chung, B. A. Loomis, L. Nowicki, J. Gazda, and D. L. Smith, "Irradiation-Induced Density Change and Microstructural Evolution of Vanadium-Base Alloys," ibid., pp. 223–231.

[4] H. Matsui, M. Tanno, J. Gazda, and H. M. Chung, "Microstructural Stability of V-4Cr-4Ti During Neutron Irradiation," ibid., pp. 240–246.

[5] H. M. Chung, J. Gazda, L. Nowicki, J. E. Sanecki, and D. L. Smith, "Effects of Fabrication Variables on Impact Properties and Microstructure of V–Cr–Ti Alloys," ibid., pp. 207–218.

[6] H. M. Chung, B. A. Loomis, and D. L. Smith, "Thermal Creep Behavior of V–5Cr–5Ti and V–10Cr–5Ti Alloys," in Fusion Reactor Materials, Semiannual Prog. Report, DOE/ER-0313/14, Oak Ridge National Laboratory, Oak Ridge, TN (1993), pp. 309-317.

[7] D. N. Braski, in Influence of Radiation on Material Properties, ASTM-STP 956 (1986), pp. 271-290.

[8] D. N. Braski, J. Nucl. Mater. 141-143 (1986) 1125.

[9] D. N. Braski, in Reduced Activation Materials for Fusion Reactors, ASTM-STP 1047 (1988), pp. 161-178.

[10] H. Matsui, M. Tanaka, M. Yamamoto, and M. Tada, J. Nucl. Mater. 191-194 (1992) 919.

[11] M. Satou, K. Abe, and H. Matsui, J. Nucl. Mater. 191-194 (1992) 938.

[12] W. van Witzenburg, A. Mastenbroek, and J. D. Ellen, J. Nucl. Mater. 103-104 (1981) 1187.

[13] M. P. Tanaka, E. E. Bloom, and J. A. Horak, J. Nucl. Mater. 114 (1981) 895.

[14] M. L. Grossbeck and J. A. Horak, in Influence of Radiation on Material Properties, ASTM-STP 956 (1986), p. 291.

[15] J. M. Vitek, D. N. Braski, and J. A. Horak, J. Nucl. Mater. 141-143 (1986) 982.

[16] W. van Witzenburg and E. de Vries, in Effects of Radiation on Materials, ASTM-STP 1125 (1990).

[17] L. L. Horton and K. Farrell, J. Nucl. Mater. 122-123 (1984) 687.

[18] H. Kawanishi and S. Ishino, in Reduced Activation Materials for Fusion Reactors, ASTM-STP 1047 (1988), pp. 179-189.

[19] H. Kawanishi, Y. Arai, and S. Ishino, J. Nucl. Mater. 191-194 (1992) 933.

[20] D. L. Smith, H. Matsui, L. R. Greenwood, and B. A. Loomis, J. Nucl. Mater. 155-157 (1988) 1359.

[21] D. L. Smith, B. A. Loomis, H. Matsui, M. L. Hamilton, K. L. Pearce, J. P. Kopasz, C. E. Johnson, R. G. Clemmer, and L. R. Greenwood, in Fusion Reactor Materials, Semiannual Prog. Rep. DOE/ER-0313/10, Oak Ridge National Laboratory, Oak Ridge, TN (1991), p. 159.

[22] H. Tsai, H. M. Chung, B. A. Loomis, and D. L. Smith, "Status of Dynamic Helium Charging Experiment (DHCE)," in Fusion Reactor Materials, Semiannual. Prog. Report, DOE/ER-0313/15, Oak Ridge National Laboratory, Oak Ridge, TN (1994), pp. 247–252.

[23] H. M. Chung, B. A. Loomis, L. J. Nowicki, and D. L. Smith, "Effect of Dynamically Charged Helium on Tensile Properties of V–4Cr–4Ti," in this report.

[24] H. M. Chung, L. J. Nowicki, J. Gazda, and D. L. Smith, "Effect of Dynamically Charged Helium on Swelling and Microstructure of Vanadium–Base Alloys," in this report.

Subtask 12H1: VANADIUM ALLOY IRRADIATION EXPERIMENT X530 IN EBR-II, H. Tsai, R. V. Strain, A. G. Hins, H. M. Chung, L. J. Nowicki, and D. L. Smith (Argonne National Laboratory)

OBJECTIVE

The objective of the X530 experiment in EBR-II was to obtain early irradiation performance data, particularly the fracture properties, on the new 500-kg production heat of V-4Cr-4Ti material before the scheduled reactor shutdown at the end of September 1994.

SUMMARY

To obtain early irradiation performance data on the new 500-kg production heat of the V-4Cr-4Ti material before the scheduled EBR-II shutdown, an experiment, X530, was expeditiously designed and assembled. Charpy, compact tension, tensile and TEM specimens with different thermal mechanical treatments (TMTs), were enclosed in two capsules and irradiated in the last run of EBR-II, Run 170, from August 9 through September 27. For comparison, specimens from some of the previous heats were also included in the test. The accrued exposure was 35 effective full power days, yielding a peak damage of ≈4 dpa in the specimens. The irradiation is now complete and the vehicle is awaiting to be discharged from EBR-II for postirradiation disassembly.

PROGRESS AND STATUS

Introduction

V-4 wt.%Cr-4 wt.%Ti has been identified as the most promising vanadium-based alloy for application in fusion reactor first wall and blanket structures. A 500-kg production heat of the V-4Cr-4Ti alloy was recently produced (see accompanying article in this report) as part of the developmental effort. It is important to confirm at an early date the performance of this new heat with irradiation in a fast flux environment. A decision was made in June 1994 to test this material in an irradiation experiment in EBR-II before the scheduled reactor shutdown at the end of September 1994.

In addition to the production heat V-4Cr-4Ti material, several earlier heats of ternary and binary vanadium alloys, and a Russian heat of V-4Cr-4Ti, were included in the experiment for comparison. A ^{10}B-doped V-4Cr-4Ti material was included to study the effect of helium generation on mechanical properties. The irradiation temperature for the test was ≈375-400°C, the lowest attainable in EBR-II, because of the importance of low-temperature data for ITER.

Thermal mechanical treatments are known to have significant effects on the mechanical properties of body-center-cubic metals, e.g., the vanadium alloys. One of the objectives of the experiment was to investigate these effects. The production heat and a V-5Cr-5Ti material were given different heat treatments before irradiation for this study.

Experiment Description

Hardware

The irradiation consisted of two Mark B7 (0.807-in. diameter) capsules with six subcapsules in each capsule. Near the top and bottom end of the capsules, holes were drilled through the capsule walls so that reactor coolant sodium could flow between the capsule and the subcapsules to provide heat transfer. Lithium was used as a heat transfer medium for the specimens in the sealed subcapsules. All capsule and subcapsule components were fabricated from Type 316 stainless steel.

The specimens were machined from either sheets or plates of the specified heats of material. The as-machined specimens were polished and then given a heat treatment in a vacuum to remove any hydrogen that may have been adsorbed during these procedures.

An important aspect of the fabrication of the subcapsules was the handling, purification, and loading of the lithium. Primary operations were performed in an ultra-high-purity helium glovebox (oxygen level ≈30 ppb). Prior to introducing lithium into the helium glovebox, an initial purification step was removal of the outer rind from the lithium ingots that were stored in oil. This operation was performed in a small argon-atmosphere glovebox. The interstitial content of the lithium was reduced by heating it with SAES getter pellets at 650°C for about 22 h. During this process, the nitrogen content was reduced from ≈400 ppm to ≈10 ppm. After the purification, the lithium was poured into tantalum trays at a temperature of 250°C. The lithium was prepared for loading into the subcapsules by cutting 0.625-in.-diameter pellets from the 0.5-in.-thick sheets in the tantalum trays with a "cork borer." The Li pellets were cut to length and loaded into the bottom of the subcapsules. The specimens were then placed on top of the Li-pellet (a typical loading is shown in Fig. 1). The subcapsules were capped with a tight-fitting lid and transferred to another He-atmosphere glovebox for welding.

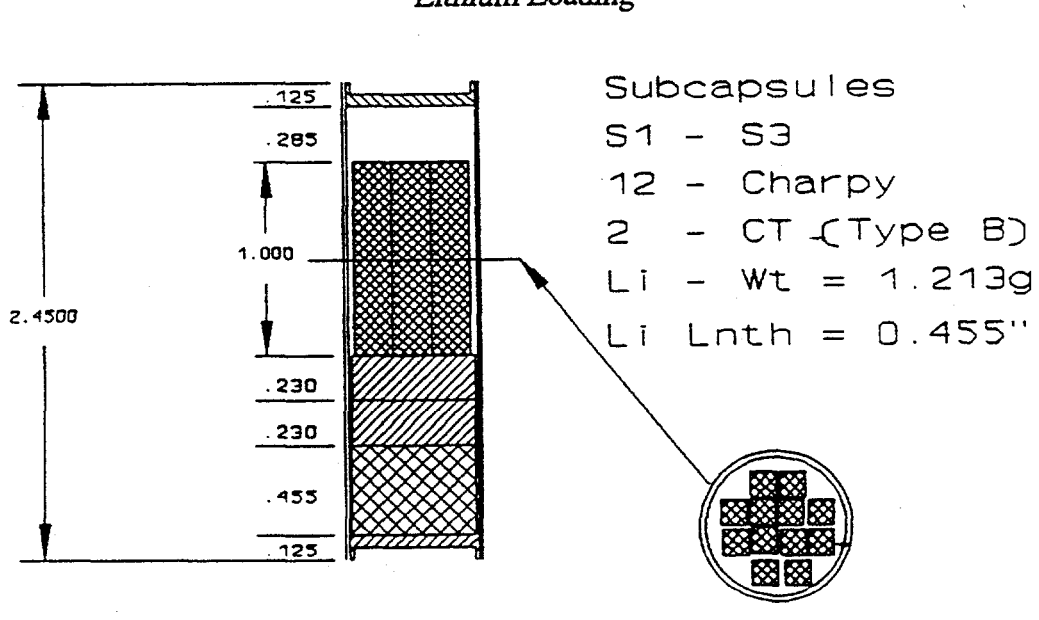

Fig. 1. Typical Subcapsule Loading for the X530 Irradiation.

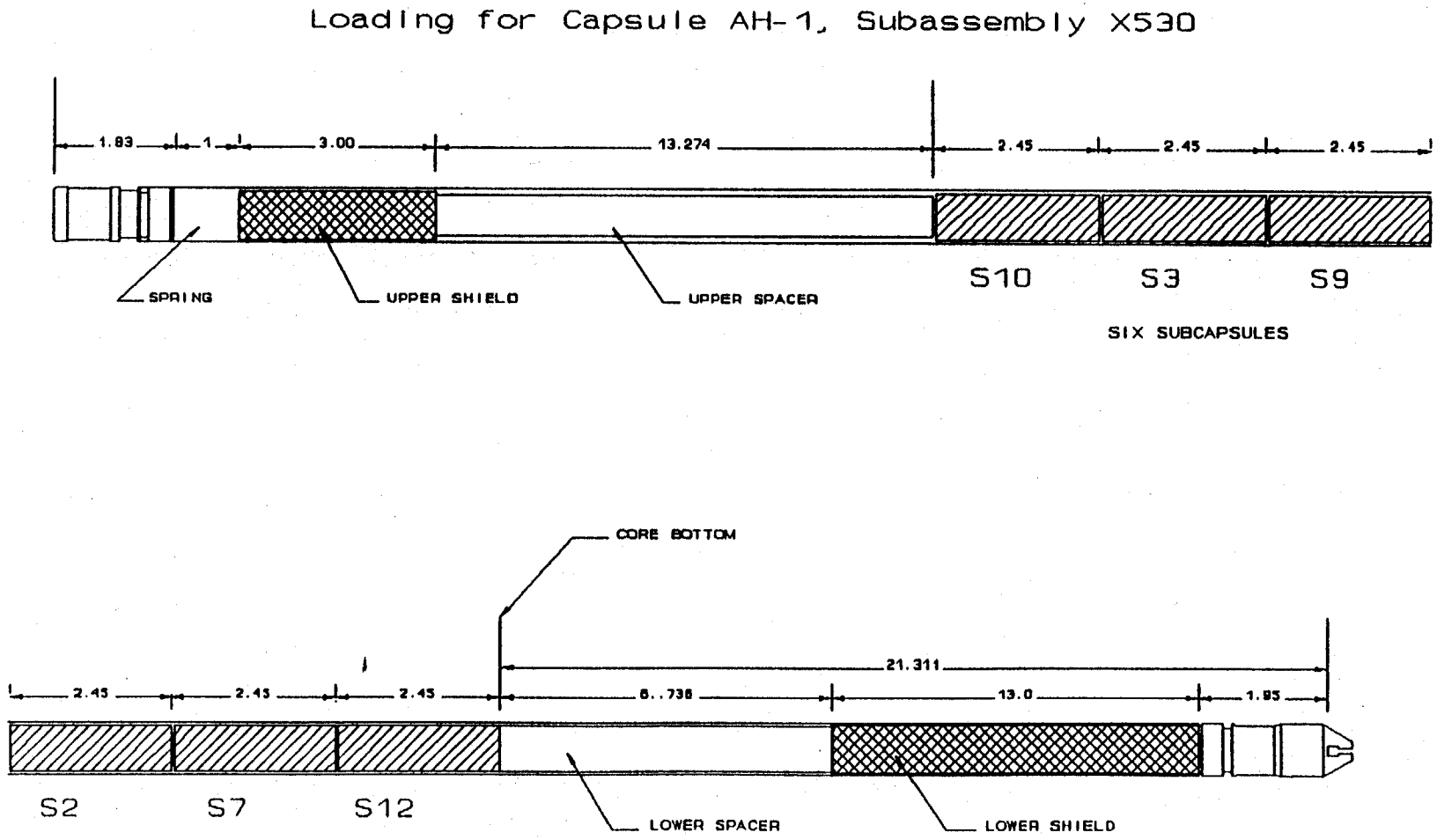

Fig. 2. Loading of Capsule AH-1 for X530.

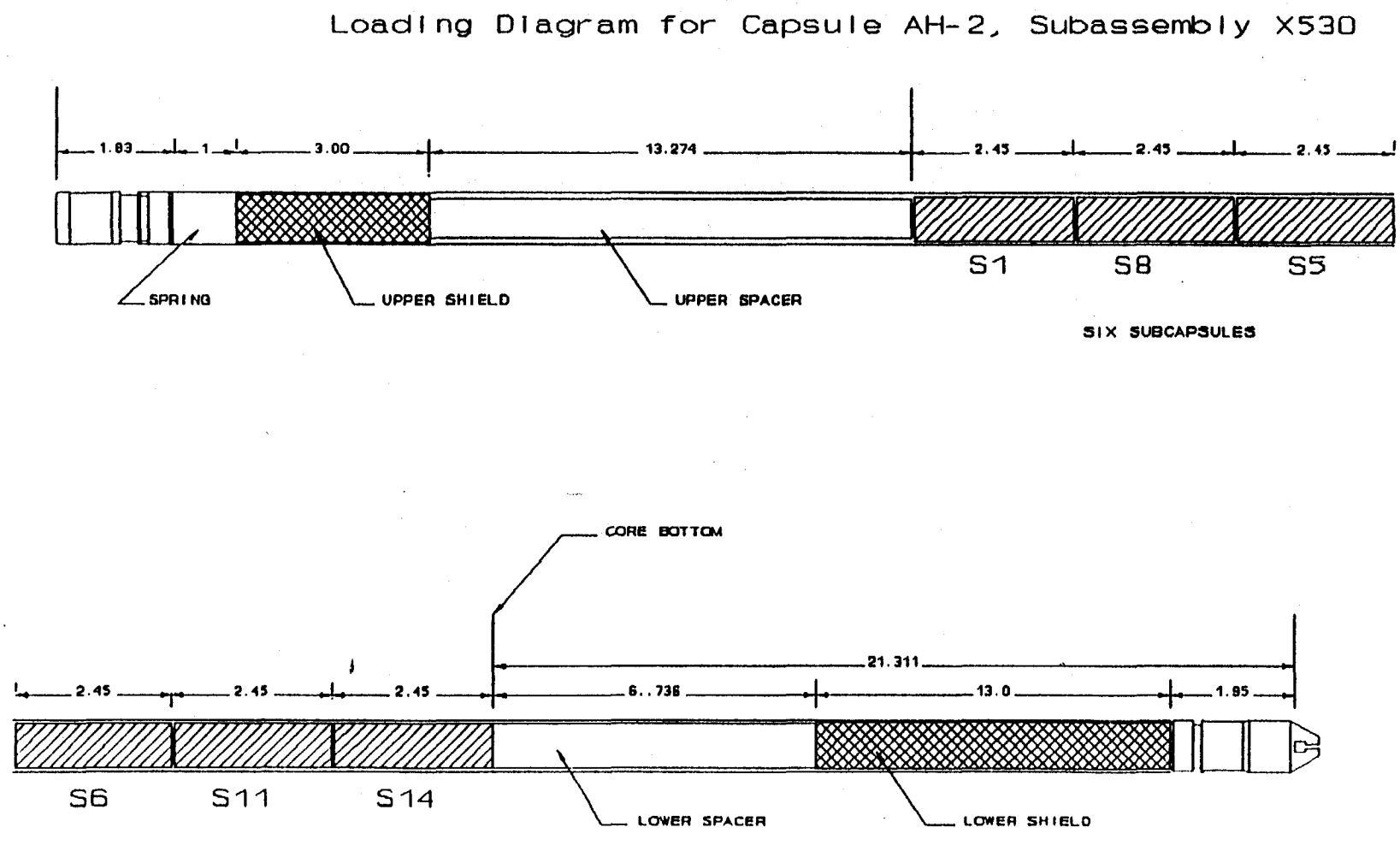

Fig. 3. Loading of Capsule AH-2 for X530.

The subcapsules and appropriate spacers and shields were then loaded into the capsules as shown in Figs. 2 and 3. These two capsules, four dummy rods, and a capsule containing samples of yttria (for the National Institute of Standards and Technology) were assembled in a Mark B7A subassembly and placed in Row 2 of EBR-II. The surface temperatures for the subcapsules were calculated using the HECTIC heat transfer code. Heat transfer from the adjacent subassemblies was important in this low-power, low-flow subassembly. The temperature calculations indicated that specimen temperatures differed with their axial positions in the subassembly (Fig. 4) and were between 370 and 410°C.

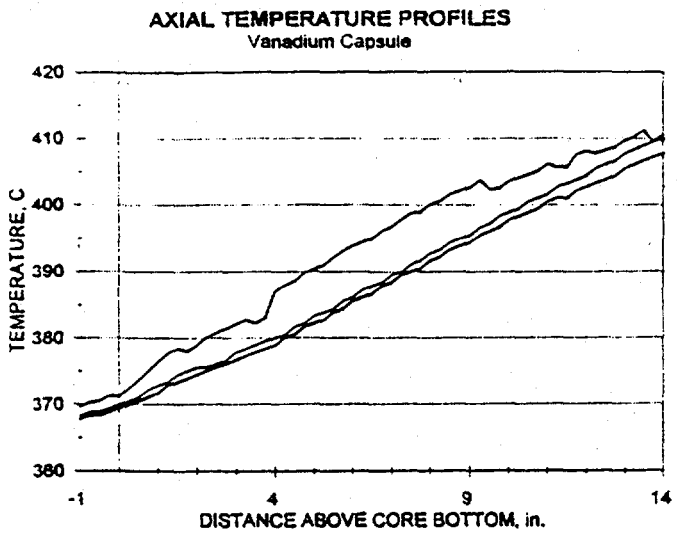

Fig. 4. Calculated Axial Temperature Profile for Capsule AH–1.

Test Matrix

The list of specimens included in the X530 experiment is shown in Table 1, and specimen loadings in the subcapsules are summarized in Table 2.

The most important, and hence most extensively tested, material in the X530 experiment was the 500-kg production heat V-4Cr-4Ti material (Heat No. 832665, also designated BL-71). The test specimens consisted of disk compact tension, 1/3-size Charpy, SS-3 tensile, and transmission electron microscopy disks. These specimens were prepared from sheets/plates that were hot rolled at ≈400°C, followed by a vacuum annealing at 950, 1050, or 1125°C. The purpose of the different annealing temperatures was to yield data on the effects of TMT on mechanical properties.

The other materials included in the X530 test were

- A 250 ppm-^{10}B-doped V-4Cr-4Ti material (BL-70) to study the effect of helium generation,
- A Russian Federation heat of V-4Cr-4Ti material (BL-69),
- A V-5Cr-5Ti material (BL-63) whose original fracture properties were marginal and that was modified for this test by additional TMTs, i.e., either cold rolling or warm rolling at 400°C, then annealing at 950 or 1050°C, and
- Several other earlier heats of materials with different binary or ternary compositions.

Depending on emphasis and material availability, as shown in Table 1, not all forms of specimens were prepared for all materials.

Irradiation History

Subassembly X530 was loaded into EBR-II core position 2F1 (with a fast flux of 2.4×10^{15} $n \cdot cm^{-2} \cdot s^{-1}$, E>0.11 MeV) and irradiated for the entire 170A run from August 19 until the final reactor shutdown on September 27. The accrued exposure was 35 effective full power days, yielding a peak damage of ≈4 dpa in the vanadium specimens.

For Run 170A, the reactor inlet temperature was lowered from the nominal 371 to 366°C. The flow rate for the subassembly was 13.3 gpm, within the requested range.

Table 1. Types and Numbers of Specimens Irradiated in the X530 Experiment

Composition, wt.%	ANL ID Number	DCT-A, 0.140 in.	DCT-B, 0.230 in.	1/3-size Charpy	SS-3 Tensile	TEM
V-3Ti-1Si	BL-45	-	-	5	2	-
V-5Ti	BL-46	3	-	5	2	5
V-4Cr-4Ti	BL-74	-	4	6	-	-
V-7Cr-5Ti	BL-49	3	-	5	2	5
V-5Cr-3Ti	BL-54	-	-	5	-	-
V-3Ti	BL-62	3	-	5	2	4
V-5Cr-5Ti	BL-63	-	2	5	2	-
V-5Cr-5Ti	BL-63-CR950	1	-	5	2	3
V-5Cr-5Ti	BL-63-CR1050	1	-	5	2	3
V-5Cr-5Ti	BL-63-WR950	1	-	5	2	3
V-5Cr-5Ti	BL-63-WR1050	1	-	5	2	3
V-4Cr-4Ti-RF	BL-69	-	-	-	5	5
V-4Cr-4Ti-B	BL-70	4	4	6	5	5
V-4Cr-4Ti	BL-71-WR950	4	-	6	5	5
V-4Cr-4Ti	BL-71-WR1050	4	-	6	5	5
V-4Cr-4Ti	BL-71-WR1125	3	-	6	5	5
SUBTOTAL		28	10	80	43	51

B = Boron doped (250 appm ^{10}B)
RF = Russian Federation
CR950 = Cold roll and final anneal at 950°C
CR1050 = Cold roll and final anneal at 1050°C
WR950 = Warm roll and final anneal at 950°C
WR1050 = Warm roll and final anneal at 1050°C
WR1125 = Warm roll and final anneal at 1125°C

FUTURE ACTIVITIES

X530 has successfully completed the planned irradiation in EBR-II Run 170. Instructions have been given to EBR-II personnel to discharge and disassemble the test vehicle. Nondestructive examination, including neutron radiography, is scheduled for the two capsules before their return to ANL-East for disassembly and specimen retrieval.

Initial results on specimen examination and testing are expected to be available in the next reporting period.

Table 2. Subcapsule Specimen Loading for X530

Capsule	Specimen Type	Material Composition	Quantity	Capsule	Specimen Type	Material Composition	Quantity
S1	DCT-B	V-4Cr-4Ti (BL-74)	2	S8	Tensile	V-3Ti (BL-62)	2
	Charpy	V-3Ti-1Si (BL-45)	5		Tensile	V-5Ti (BL-46)	2
	Charpy	V-5Ti (BL-46)	5		Tensile	V-7Cr-5Ti (BL-49)	2
	Charpy	V-7Cr-5Ti (BL-49)	2		Tensile	V-3Ti (BL-62)	2
					Tensile	V-5Cr-5Ti (BL-63	2
S2	DCT-B	V-4Cr-4Ti (BL-74)	2		Tensile	V-5Cr-5Ti (BL-63)	2
	Charpy	V-4Cr-4Ti (BL-74)	6		Tensile	V-5Cr-5Ti (BL-63)	2
	Charpy	V-7Cr-5Ti (BL-49)	1		Tensile	V-5Cr-5Ti (BL-63)	2
	Charpy	V-5Cr-3Ti (BL-54)	5		Tensile	V-5Cr-5Ti (BL-63)	2
					Tensile	V-4Cr-4Ti (RF)	3
S3	DCT-B	V-5Cr-5Ti (BL-63)	2		TE	V-5Ti (BL-46)	5
	Charpy	V-7Cr-5Ti (BL-49)	2		TE	V-7Cr-5Ti (BL-49)	5
	Charpy	V-3Ti (BL-62)	5		TE	V-3Ti (BL-62)	4
	Charpy	V-5Cr-5Ti (BL-63)	5		TE	V-5Cr-5Ti (BL-63)	3
					TE	V-5Cr-5Ti (BL-63)	3
S14	DCT-B	V-4Cr-4Ti-B (BL-70)	2		TE	V-5Cr-5Ti (BL-63)	3
	Charpy	V-5Cr-5Ti (BL-63)	5		TE	V-5Cr-5Ti (BL-63)	3
	Charpy	V-4Cr-4Ti-B (BL-70)	6				
				S9	Tensile	V-4Cr-4Ti (RF)	2
S4	DCT-B	V-4Cr-4Ti-B (BL-70)	2		Tensile	V-4Cr-4Ti-B (BL-70)	5
	Charpy	V-5Cr-5Ti (BL-63)	5		Tensile	V-4Cr-4Ti (BL-71)	5
	Charpy	V-4Cr-4Ti (BL-71)	6		Tensile	V-4Cr-4Ti (BL-71)	5
					Tensile	V-4Cr-4Ti (BL-71)	5
S6	DCT-A	V-5Ti (BL-46)	2		TE	V-4Cr-4Ti (RF)	5
	Charpy	V-5Cr-5Ti (BL-63)	5		TE	V-4Cr-4Ti-B (BL-70)	5
	Charpy	V-4Cr-4Ti (BL-71)	6		TE	V-4Cr-4Ti (BL-71)	5
					TE	V-4Cr-4Ti (BL-71)	5
S7	DCT-A	V-5Ti (BL-46)	1		TE	V-4Cr-4Ti (BL-71)	5
	DCT-A	V-7Cr-5Ti (BL-49)	1				
	Charpy	V-5Cr-5Ti (BL-63)	5	S10	DCT-A	V-7Cr-5Ti (BL-49)	2
	Charpy	V-4Cr-4Ti (BL-71)	6		DCT-A	V-3Ti (BL-62)	3
					DCT-A	V-4Cr-4Ti (BL-71)	3
				S11	DCT-A	V-5Cr-5Ti (BL-63)	1
					DCT-A	V-5Cr-5Ti (BL-63)	1
					DCT-A	V-5Cr-5Ti (BL-63)	1
					DCT-A	V-5Cr-5Ti (BL-63)	1
					DCT-A	V-4Cr-4Ti-B (BL-70)	4
				S12	DCT-A	V-4Cr-4Ti (BL-71)	4
					DCT-A	V-4Cr-4Ti (BL-71)	4

Subtask 12H2: STATUS OF THE DYNAMIC HELIUM CHARGING EXPERIMENT

H. Tsai, R. V. Strain, H. M. Chung, and D. L. Smith (Argonne National Laboratory)

OBJECTIVE

The objective of the dynamic helium charging experiment (DHCE) is to investigate the effects of concurrent helium production and fast-neutron irradiation on the physical and mechanical properties of vanadium-based alloys for fusion blanket applications. A major task in this reporting period was to disassemble the tritium-bearing DHCE capsules to retrieve irradiated specimens for examination and testing.

SUMMARY

Seven DHCE capsules containing vanadium-alloy specimens were irradiated in the MOTA-2B vehicle in FFTF to ≈20-29 dpa. In this and the previous reporting periods, equipment and procedures were developed at Argonne National Laboratory-East to disassemble these capsules. Six of the seven capsules have been disassembled. (The seventh capsule was processed in April 1994, immediately following this reporting period.) Effluence of tritium into the cell exhaust was <2% of the total inventory. No contamination incidents occurred during the DHCE disassembly work. Initial testing of the retrieved specimens is under way.

PROGRESS AND STATUS

Introduction

Because helium generated in vanadium-based structural materials from (n,a) reactions may affect the physical and mechanical properties of these materials for fusion reactor applications, the potential effects of enhanced helium generation to levels comparable in fusion reactors must be studied. This was achieved in the DHCE in the FFTF MOTA-2B by doping the lithium bond in the capsules with tritium, which diffused into the specimens and subsequently decayed in-situ into helium. Tritium doping was performed by placing a piece of tritiated vanadium foil in the capsule during assembly. Additional tritium generation from the (n,T) reactions with ^{6}Li in the lithium bond replenished the tritium lost to diffusion leakage through the capsule wall. A detailed description of the DHCE capsules is provided in Refs. 1–3.

In processing the irradiated DHCE capsules to retrieve the specimens, the main challenge was to contain the tritium, which ranged between 17 and 99 Ci per capsule, in the capsules. Because of the induced radioactivity in the capsule material (molybdenum-based TZM alloy), capsule disassembly was performed remotely in a hot cell.

System Description

The basic approach adopted for capsule disassembly was to use liquid ammonia (-33°C bp) to dissolve the lithium bond, alcohol to rinse the retrieved specimens, and chemical getters (containing a reactive metal alloy) to trap the released tritium gas. The system, built specifically for these tasks, consisted of a capsule–puncture jig, a chamber for ammonia dissolution and alcohol rinsing, two stages of cold traps at liquid-nitrogen

temperature to remove (by condensation) the ammonia and alcohol vapors from the process gas stream, and two or three chemical getters in series. The capsules were processed one at a time. Except during capsule loading and unloading, the entire system was isolated from the cell atmosphere and maintained under a purge of high-purity (99.999%) nitrogen gas. Nitrogen was selected mainly for its compatibility with the tritium detectors because, unexpectedly, helium gas, the first choice, caused the ionization chambers in the tritium detectors to arc. The puncture jig and the dissolution chamber were located inside the hot cell; the remainder of the system was out-of-cell in a nearby vented cabinet. Flow meters, pressure gauges, thermometers, and tritium monitors were deployed at various locations in the system to provide operational data. A schematic representation of the system, showing two getters, is shown in Fig. 1.

The equipment most critical to successful operation was the remotely operated dissolution chamber. The final design incorporated a counterbalanced top cover capable of maintaining hermeticity up to $\approx 3 \times 10^4$ Pa (5 psi) positive pressure, a translucent (for viewing purposes) chamber body that could be slid back and forth to facilitate removal/replacement of used ammonia and alcohol beakers, a feed line that permitted the loading of liquid ammonia directly from a supply cylinder without breaking the hermeticity, a heater in the base to evaporate excess liquid ammonia, and all necessary purge lines.

Procedures

The major steps used for the disassembly of the capsules were as follows:

1. Puncture the capsule in the puncture jig and sweep the released gas to the tritium getters before venting.
2. Open the capsule with a tubing cutter to expose the contents inside.
3. Load the opened capsule into a wire-mesh specimen basket and attach the specimen basket to a support rod in the dissolution chamber.
4. After thoroughly purging the chamber, load liquid ammonia directly from a supply cylinder into a beaker in the chamber. Lower the specimen basket into the ammonia to dissolve the lithium bond that encased the specimens. Condense all evaporated ammonia in the gas stream with the cold traps and send the swept gas to the tritium getters.
5. When lithium dissolution is complete, raise the specimen basket above the ammonia and evaporate the residual ammonia in the beaker. Condense the ammonia vapor and trap the tritium gas as in Step 4.
6. Open the dissolution chamber and remove the used ammonia beaker with the reaction residues (a thin crust possibly containing azide, amide, and hydroxide).
7. In the same enclosed chamber but with a new beaker, load alcohol into the beaker and use alcohol to remove the surface residues on the specimens. Condense the evaporated alcohol as in Step 4 and send the swept gas to the tritium getters.
8. Repeat the rinsing of specimens in clean alcohol in the open atmosphere of the cell.
9. Completely evaporate the residual alcohol remaining in the beakers from Steps 7 and 8.

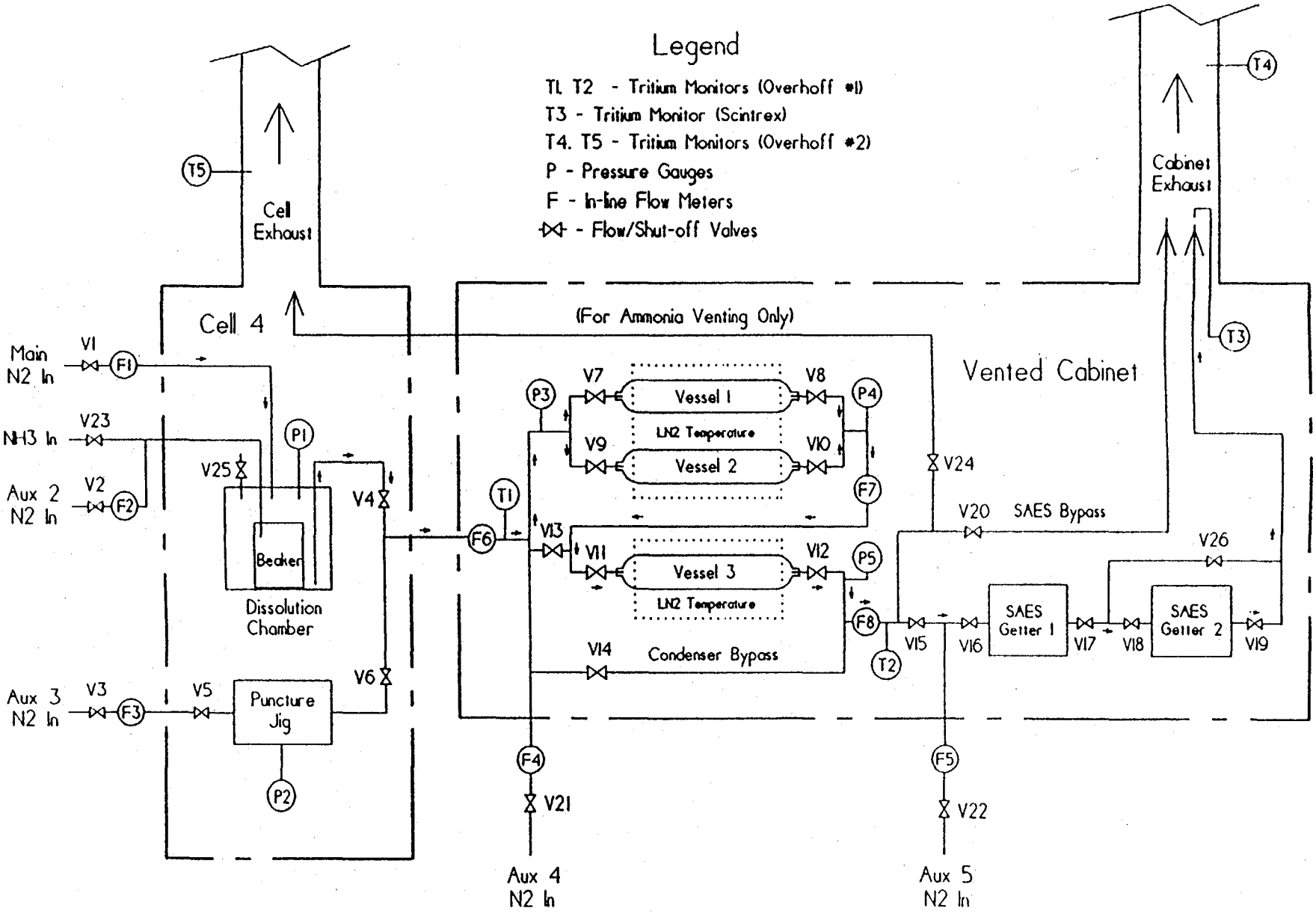

Figure 1. Schematic representation of DHCE capsule disassembly system.

10. Allow the cold traps to return to room temperature and vent the contents (condensed ammonia and alcohol) in preparation for the next capsule.

Steps 2, 3, 6, 8, and 9 involved operations in the open atmosphere of the cell. Tritium releases during these operations were monitored with a monitor located in the cell exhaust duct (T5, see Fig. 1). The releases were found to be small and well within the allowable limits. Step 10 was also performed under fully monitored conditions, with monitors T2 and T4, shown in Fig. 1. Because tritiation of ammonia or alcohol was minimal, the releases were also small and well within allowable exhaust limits. The total tritium release from these operations to the cell exhaust was <2% of the tritium content of the capsules.

Prior to the processing of the DHCE capsules, two dry runs, with low-tritium capsules (COBRA-1A capsules V575 and V680 for the first and MOTA capsule V673 for the second) were completed. In the first dry run, the second-stage tritium getter overheated, evidently because the portable tritium monitor was deployed between the two tritium getters to monitor the performance of the first getter. The monitor had a built-in recirculating pump to sample the process gas in the line. Apparently, the recirculating system contained an unforeseen air leak, which introduced oxygen to the line and caused an excessive reaction with the getter alloy. This situation was rectified by relocating the tritium monitor downstream of all getters, and the affected getter was replaced before the second dry run. The relocated monitor is shown as T3 in Fig. 1. After this modification, no further overheating occurred. The overheating did not cause a tritium release because the structural integrity of the affected getter was not breached. Any tritium release would have been small because of the insignificant tritium content of V575 and V680 capsules.

RESULTS AND CONCLUSIONS

Six of the seven DHCE capsules were processed in this reporting period. The seventh, i.e., capsule 4D1, was processed immediately after this reporting period, on April 4, 1994. The sequence of processing was generally in ascending order of tritium content of the capsules to gain experience and avoid a large inadvertent tritium release should an error develop in either the hardware or the procedures during the processing of the first capsules.

Tritium removal for the first DHCE capsule, 5C1, was substantially more difficult than the dry runs. The cause of the difficulty was apparently an insufficient opening of the capsule for the ammonia to dissolve the lithium. In the interest of protecting the test specimens to the maximum extent possible, only two cuts, one at each end of the capsule, were made. The elongated capsule geometry (120 mm long x 9 mm ID) and the tightness of specimen packing in the capsule were such that prolonged and repeated rinsing was necessary to remove the lithium bond. Although all specimens were eventually successfully retrieved, the strain on the equipment and operators was substantial. After the 5C1 operation, the procedure was modified to include a third cut, near the middle of the capsule, where the specimens were still protected by the coiled vanadium mother alloy. A further advantage of this third cut was that the brittle TZM capsule would invariably split longitudinally and create more contact surfaces for

dissolution. With this modification, all remaining capsules were processed with minimal difficulties.

It was necessary to replace the reactive metal cartridges in the tritium getters twice during the experiment. The apparent lack of capacity of the cartridges was possibly the result of contamination of the reactive metal by ammonia and alcohol vapors that escaped the cold traps upstream of the getters. In any future work, a third-stage cold trap will be added to improve condensation efficiency. Replacement of the tritium-bearing reactive-metal getter cartridges in a fume hood was straightforward and caused no contamination.

Tritium concentrations in the process gas were measured by tritium monitors in the system. The recorded data were integrated to yield the estimated quantities of gaseous tritium released during each of the major steps of the operation. The results are summarized in Table 1. In all cases, most of the tritium release (up to ≈50-60% of the total inventory in the capsule) occurred during the ammonia dissolution process (Step 4). All other releases, such as those from plenum gas venting, alcohol rinsing, or venting of the condensers, were substantially smaller. Much of the unaccounted-for tritium activity is apparently contained in the reaction residues formed at the bottom of the ammonia beaker after evaporation. These beakers will be carefully disposed of by approved procedures in the near future.

Radiographs of the assembled capsules before irradiation show that some of the tensile specimens in the DHCE capsules were not fully immersed in the lithium bond, apparently because of interference with the tritiated mother alloy coil, and jam-packing of the specimens. During capsule disassembly, the elevated positions of these specimens were generally confirmed visually. For future in-reactor experiments, both specimen packing density and internal capsule design should be reviewed to ensure proper lithium bonding of all specimens.

Table 1. Integrated tritium activity measured during the processing of DHCE capsules

		Tritium Activity (Ci)						
Capsule No.[1]	Irrad. Temp. (°C)	Tritium Content	Capsule Puncture	Ammonia Dissolved	Ammonia Evaporated	Alcohol Rinse	Ammonia Venting	Total
5C1	600	16	<0.001	2.0	1.1	1.4	0.03	4.5
5E2	425	26	<0.001	1.7	0.4	1.2	0.06	3.4
5C2	600	18	<0.001	11.4	0.6	0.2	0.1	12.3
5E1	500	57	<0.001	≈19.5	1.1	3.4	0.1	≈24.1
4D2	425	70	<0.001	33.0	2.8	2.3	0.3	38.4
5D1	500	74	<0.001	ND[2]	ND	ND	ND	ND
4D1	425	99	<0.001	37.3	5.9	2.8	0.3	46.3

[1]The order of the processing sequence.

[2]ND: No data, due to malfunctioning of the tritium detector.

REFERENCES

1. D. L. Smith, et al., *Status of the Dynamic Helium Charging Experiment (DHCE) in FFTF/MOTA,* Fusion Reactor Materials Semiannual Progress Report DOE/ER-0313/10, March 31, 1991, pp. 159-163.
2. L. R. Greenwood, *Revised Calculations for the Dynamic Helium Charging Experiment in FFTF/MOTA 2B,* Fusion Reactor Materials Semiannual Progress Report DOE/ER-0313/10,
   March 31, 1991, pp. 156-158.
3. H. Tsai, et al., *Status of the Dynamic Helium Charging Experiment (DHCE),* Fusion Reactor Materials Semiannual Progress Report DOE/ER-0313/15, September 30, 1993, pp. 247–252.

DISTRIBUTION LIST FOR ANL/FPP/TM-287

Internal

H. Attaya
M. Billone
H. Chung
D. Ehst
Y. Gohar
I. Gomes
A. Hassanein
T. Hua
T.F. Kassner
M.J. Lineberry
B. Loomis
S. Majumdar
R. Mattas
K. Natesan
J.-H. Park
R. Poeppel
W. Shack
D.K. Sze
C. E. Till
H. Tsai
R. W. Weeks

FPP Files (15)
TIS Files

External

DOE/OSTI for distribution per UC-424 (41)
Manager, Chicago Operations Office
ANL-E Libraries (2)
ANL-W Library
K. Abe, Tohoku University, Japan
M. Abdou, University of California, Los Angeles
C. Baker, University of California, San Diego
S. Berk, U.S. Department of Energy
E.E. Bloom, Oak Ridge National Laboratory
H. Borgstedt, Forschungszentrum Karlsruhe, Germany
R. Causey, Sandia National Laboratories, Livermore
M. Cohen, U.S. Department of Energy
W. Daenner, ITER, Germany
J. Davis, McDonnell Douglas Astronautics Company
J. Doggett, Lawrence Livermore National Laboratory
L. El-Guebaly, University of Wisconsin
S. Fabritsiev, D.V. Efremov Institute, Russia
F. Garner, Pacific Northwest Laboratories
D. Gelles, Pacific Northwest Laboratories
N. Ghoneim, University of California, Los Angeles
L. Greenwood, Battelle Pacific Northwest Laboratory
M. Grossbeck, Oak Ridge National Laboratory
D. R. Harries, Cumnor Hill, UK
A. Hishinuma, Tokai Research Establishment, Japan
S. Ishino, Tokaki University, Japan
T. James, University of California, Los Angeles
R. Johnson, General Atomics
R.H. Jones, Pacific Northwest Laboratory, Richland, WA
G. Kalinin, ITER Garching Joint Work Site, Germany
A. Kohyama, Kyoto University, Japan
T. Kondo, Japan Atomic Energy Research Institute, Japan
G. Kulcinski, University of Wisconsin, Madison
D. Lousteau, Fusion Engineering Design Center, Oak Ridge, TN
E. Lucas, University of California, Santa Barbara

K. McCarthy, EG&G Idaho, Inc.
H. Maekawa, Japan Atomic Energy Research Institute, Japan
S. Malang, Forschungszentrum Karlsruhe, Germany
R. Matera, ITER Garching Joint Work Site, Germany
H. Matsui, Tohoku University, Japan
G. Odette, University of California, Santa Barbara
A. Opdenaker, U.S. Department of Energy
R. Parker, ITER JCT, Garching, Germany
D. Petti, EG&G Idaho, Inc.
Y. Prokofiev, Argonne National Laboratory
S. Piet, ITER JCT, San Diego, California
R. Price, U.S. Department of Energy
H. Rohrig, Forschungszentrum Karlsruhe, Germany
A. Rowcliffe, Oak Ridge National Laboratory
M. Sawan, University of Wisconsin
M. Seki, Japan Atomic Energy Research Institute, Japan
J. Smith, General Atomics
D. Steiner, Rensselaer Polytechnic Institute
I. Sviatoslavsky, University of Wisconsin
F. Tavassoli, CEA-CE/Saclay, France
M. Tillack, University of California, San Diego
W. Van Witzenburg, ECN, Petten, The Netherlands
J. Vetter, Forschungszentrum Karlsruhe, Germany
G. Vieider, ITER, Germany
S. Votinov, Institute of Inorganic Materials (VNIINM), Russia
R. Watson, Sandia National Laboratories, Albuquerque
F.W. Wiffen, U.S. Department of Energy
K. Wilson, Sandia National Laboratories, Livermore
C. Wong, General Atomics
Bibliothek, Max-Planck-Institute fur Plasmaphysik, Germany
C.E.A. Library, Fontenay-aux-Roses, France
Librarian, Culham Laboratory, England
Thermonuclear Library, Japan Atomic Energy Research Institute, Japan